DYNAMICS, CONTROL AND SIMULATION
OF FLEXIBLE ROBOTIC SYSTEMS

by

ALCY RODOLFO DOS SANTOS CARRARA,
B.Sc.(Mech.Eng.),M.Sc.(Aerospace Eng./Orbit.Mech.)

A Thesis

Submitted to the School of Graduate Studies

In Partial Fulfillment of the Requirements

for the Degree

Doctor of Philosophy

McMaster University

DYNAMICS, CONTROL AND SIMULATION OF

FLEXIBLE ROBOTIC SYSTEMS

Doctor Of Philosophy (1995)
(Mechanical Engineering)

McMaster University
Hamilton, Ontario

Title: Dynamics, Simulation and Control of Flexible Robotic Systems

Author: Alcy Rodolfo dos Santos Carrara,
B.Eng. (State University of Rio de Janeiro),
M.Sc.Aerosp.Eng./Orbit. Mech. (Brazilian Inst. for Space
Research)

Supervisor: Professor Mohamed A. Dokainish
Co-Supervisor: Professor William M. Mansour

Number Of Pages: xvii, 207

To My Wife Ana

ACKNOWLEDGEMENTS

ABSTRACT

This research develops a new methodology for the control of two link flexible arms. The methodology is referred to here as "Nonlinear Integrated Tabular" NIT Control. Starting with a new trajectory, the inverse kinematic problem is solved and adequate algorithms are presented to evaluate the commanding voltages to guarantee that the wrist point will track the desired trajectory. Continuous and discontinuous paths are tried with models which were developed to account for the flexibility in the joints and the flexibility in the links. Lagrange's equation and finite element formulation were used to construct realistic models. Computer simulations were conducted to assess the control qualities for tracking using NIT. The accuracy, smoothness as well as the levels of the command signals during tracking were quantified to serve as criteria to evaluate the quality of tracking.

A number of classical controls were developed and applied to the elbow arm to compare NIT with the current available approaches. A proportional plus derivative plus gravity, a feedback linearization as well as a VEE-MOD-VEE controllers were tried. It was shown that NIT compares well with the most successful conventional methods. In addition, it was found to offer simple, smooth, robust, computationally economic controls. NIT compares well with the majority of the conventional methods.

An experimental setup was constructed with the objectives of verifying the analytical predictions. It was built in a modular form to allow continuity of research in this

area at McMaster's laboratories. Great care and long hours were spent in the design, fabrication, assembly, debugging of the hardware for the mechanical parts. The setup is referred to here as FLEXROD. The up-to-date technologies available today were implemented in the design of FLEXROD which include Harmonic Drives for speed reduction and transputers for the controller. Enormous efforts went into streamlining the software and in developing the interfaces between the sensory system and the controller. Experiments were conducted to validate the transient dynamics of the elbow arm when the motors are brought to a sudden stop by applying the brakes simultaneously. Reasonable agreement was found between the analysis and the experiment. The thesis is concluded with recommendations for future research in this area to implement and develop NIT using FLEXROD.

TABLE OF CONTENTS

LIST OF FIGURES

(xi)

LIST OF NOMENCLATURE

τ_m = Torque exerted on J_m.

J_m = Mass moment of inertia of rotor about axis of rotation.

K_1, K_2, K_m = Constant coefficients with $K_m = K_1 \phi_f = K_1 K_2 i_f$

i_a, i_f = Armature and field currents respectively with i_f constant.

ϕ_f = Magnetic field in gap,

      $= K_2 i_f$

t   = Time

R_a, L_a = Resistance (ohms) and inductance (henries) of armature windings.

u(t)   = Input voltage to D.C. motor (control input).

v_b = Back electromotive force (e.m.f.).

K_b = Back e.m.f. constant.

ϕ = Angular displacement of output shaft of motor, just before the harmonic drive.

b_m = Damping coefficient on the motor side.

τ_m^{*} = Net torque through shaft, just before the harmonic drive.

ϕ^{*} = Angular displacement of output shaft just before speed reduction.

Ψ = Angular displacement of driven link immediately after harmonic drive.

b_L = Damping coefficient on link side.

τ = Torque delivered to link less friction in the revolute.

T	= Dimensionless time.
ω_0	= Time scaling coefficient
$\tau_i^{\bullet}$	= Dimensionless torque applied to i'th link = $\tau_i / (m_i a_i g)$
m_i, a_i	= Mass and length of link.
g	= Gravitational acceleration
$u_i^{\bullet}$	= Dimensionless control signal = u_i / E_0
E_0	= Reference voltage = 100 V
E	= Young's modulus
ρ	= mass density of the material.
x_0, y_0	= coordinates of the center of the square
η	= Tilt angle
Np	= Number of points on the trajectory.
$[K_p]$	= A diagonal (2 x 2) position gain matrix.
$[K_d]$	= A diagonal (2 x 2) velocity gain matrix.
$\underline{r}, \underline{q}$	= (2 x 2) Vectors for the desired and actual positions of the wrist point.
I	= Mass-moment of inertia,
a_c	= Distance from the motor to the center of mass of the link respectively.
ξ, η	= Longitudinal coordinates and lateral deflections of a point on the centre level beam.

CHAPTER 1

INTRODUCTION

1.1 BACKGROUND

Space shuttle programs prompted the need for using large flexible manipulators of the slave-master type which are used by the astronauts through joy-sticks and vision cameras. CANADARM was designed and built by Canadian SPAR where simple proportional and derivative (PD) controls were used for the actuators of the joints. The design was done successfully and the overall performance of the manipulator was satisfactory. However, the unwanted oscillations are adding to a high cost because of the waiting time required for the transient vibrations to die out.

Today there is an ever increasing demand for robots which have lighter structure, faster response and higher payload to weight ratio. The future generation of robots will have more compliant structures to allow the manipulators to work together in a "cooperative mode" and to ensure safer operation when impact loadings occur.

This research is a contribution to a better understanding and use of the dynamics and controls of flexible robots which are at the heart of "fixtureless assembly" lines.

1.2 RELEVANCE

The robots which are currently in use have their parts oversized to achieve some degree of rigidity and consequently are slow. They have high operational cost because most of the energy is consumed to overcome the inertial forces of the oversized links. There is a need for light, fast and precise robots to meet the industrial demands. Reduction of weight induces flexibility which has to be treated with care.

Such flexible robots are in demand by space programs as well as by production lines in automotive industry. There is also an incresing demand for these robots in assembly lines for computer, electronic equipment, eletrodomestic appliances and textile industries.

1.3 LINES OF CURRENT RESEARCH IN ROBOTICS

There are two basic lines of research in robotics: namely, dynamics and controls.

The first line of research is essentially related to the dynamic modelling and simulation of the manipulator with the objectives of predicting the instantaneous position, velocity and acceleration of the wrist point or the gripper given a set of input torques and forces at the joints and hand. Evaluation of natural frequencies and their associated modes is an important part in this line of investigation.

The second line of research is associated with developing adequate control strategies to guarantee that the manipulator will perform given movements and/or will exert given forces and torques on the ambient. This line of investigation normally assumes that an adequate dynamic model of the system is available a priori.

In most cases it is difficult to distinguish which line of investigation a given paper is aiming at. Quite often a paper starts with dynamics and ends up with recommendations for controls.

1.4 REVIEW OF LITERATURE (DYNAMICS OF MANIPULATOR)

The dynamics of robotic systems attracted the attention of several researchers in the past. Today, a wealth of information exists in the literature in this area. The following is a brief summary of the significant work which was reported recently.

Luh et al [29] and Carrara [7] used the Newton-Euler approach to develop simple models to describe the dynamics of a manipulator assuming that the links are rigid. The models were found adequate to size up the motors and the components of the system. Hollerbach and Sahar [20] partitioned the inverse kinematic problem into a "wrist" problem and a "link" problem.

Maizza-Neto [30] and Book et al [6] employed Transfer Matrices to conduct a modal analysis for a flexible manipulator. Finite Element methods were applied to robotics with Hurty [23] who established the theoretical fundamentals for the "component mode synthesis" approach.

Bathe and Bolourchi [3] and [4], Mattiasson et al [33], Berkkan [5] and Low [27] emphasized the need for adequate description of the dynamics to be able to evaluate the associated large displacements. Hsiao et al [21], [22] obtained an efficient Finite Element model for the beam element by using co-rotational formulation. They applied the method to

flexible mechanisms but not to robots. Gandhi and Thompson [15] and Thompson and Gandhi [48] developed design strategies for flexible arms which use composite material. Hsiao et al [21] and [22] and Sunada and Dubowsky [44], [45], [46] showed that Hurty's method can be adapted for robotics to reduce the number of degrees of freedom , and consequently the computational cost. Dado and Soni [13] and Naganathan and Soni [36] and [37] developed complicated Finite Element models which account for the actuators. The models were not validated. Hallauer and Wagie [17] validated a Finite Element model using an experimental setup and used the results to design the controller. Alves et al [1] were able to perform finite element computations using transputers and they obtained encouraging results. Tzou et al [51] and [52] applied and developed the idea of using distributed sensors and actuators to control the transient vibrations of the manipulator. Meirovitch and Kwak [35] compared the convergence of the Finite Element method compared with conventional approaches. Chang and Hamilton [11] and [12] investigated the dynamics of the manipulator taking into account the flexibility in the links . They combined the Finite Element method with Lagrange's equations. The approach was computationally costly.

Recently Seering [42] assessed the vibration behavior of a larger and complicated 22 degrees of freedom (d.o.f.) model representing the arm of the Space Shuttle and the Shuttle itself using a software model developed at the Draper Laboratory. He proved that the free vibrations change drastically with the configuration of the arm. The arm tends to be stiffer in the retracted compared to its extended position. A very unique and outstanding work from Sakawa and Matsuno [32] is reported where they used perturbation methods to analyze the

dynamics of flexible robots.

Harmonic Drive Reducers were the center of attraction of many investigations. Marilier and Richard [31], Cetinkunt and Book [9], Nikolic [40], Yang and Donath [55], Hewit [19], Nicosia and Tomei [39], Tomei [49], Good et al [16] and De Luca [14] investigated different aspects of the Harmonic Drives and evaluated their effect on the dynamics of the links of the manipulator. Good et al [16] pointed out that including joint flexibility caused by Harmonic Drives in the dynamic model would suppress large errors caused by unmodelled dynamics. Nikolic [40] focused his investigation on prismatic joints Yang and Donath [55] took into account the results obtained by Good et al [16] when they conducted dynamic simulation of a one-link flexible arm with joint flexibility.

Marilier and Richard [31] studied the Harmonic Drive reducers and proposed a stick-slip nonlinear model for the friction. Cetinkunt and Book [9] used symbolic computation software to develop the dynamic model of a two-link flexible-joint flexible-link robot. The equations were simulated in a microcomputer and also in parallel computation using transputers.

Hastings and Book [18] investigated one-link flexible arms using linear models. The arm was modelled as a (pinned-free) and as a (clamped-free) cantilever beam. The results were compared with the experimental findings. It was found that pinned-free boundary conditions do not explain the frequency response as measured experimentally. Unless there is significant backlash in the gears, the clamped-free boundary conditions are the ones that best reproduce the experimental frequency response.

1.5 REVIEW OF LITERATURE (CONTROLS OF MANIPULATORS)

The available research related to controls of manipulators addresses a wide spectrum of topics. After reviewing the most significant publications, it was obvious that the most crucial part of control development is the control design strategy itself rather than developing the control theory.

Conventional PD controllers were applied by Nicosia and Tomei [39] for a manipulator with flexible joints. They confirmed the difficulties encountered in achieving acceptable performance in the presence of compliance in the joints. Lin et al [26] investigated simple control strategies for a 6 d.o.f. flexible robot.

Distributed-parameter controls are reported by Balas [2] and Meirovitch et al [34] for large flexible structures as encountered in spacecrafts. The proposed strategies called for the use of estimators such as Kalman filters, sophisticated observers and optimal controls which require the repeated solution of Ricatti's equation in real-time. Although it is tempting to implement these strategies for the control of flexible arms, yet the computation cost is prohibitive and impractical at the moment.

Takegaki and Arimoto [47] reported a generalized method of control using output feedback. Koivo [25] and Spong and Vidyasagar [43] reviewed the available methodologies for the control of the position of the tip point of the manipulator. Pfeiffer and Gebler [41] introduced a multistage concept where the system is driven to its nominal motion first and then controlled around the equilibrium position. They conducted experimental investigations using the multistage-approach and compared their findings with some published analytical

results. Wells et al [54] used feedforward and feedback controls to achieve better results.

Hewit [19] applied multistage control concepts to control a SCARA robot with flexible joints. Tomei [49] investigated a simple PD and gravity controller for a 3 d.o.f. arm with elasticity in the joint and showed that the controller is robust. De Luca [14] established theoretical models for the controls of robots with flexibility in the joints. Adaptive control was used to construct control strategies for a one-link manipulator with flexibility in the joint where the parameters of the link itself are unknown.

Carusone and D'Eleuterio [8] used a linear optimal regulator and a linearized control system for tracking a predetermined trajectory. No experimental validation was reported.

A strong school in the early years in robotics pursued controls through Model Identification. With the advent of adaptive control that approach gained incredible importance. However, physical limitations of the hardware and software slowed down its evolution. The linear speed of the wrist point is approximately 1 m/s or more and sampling rates necessary for the controllers are about 7 msec. That does not leave room for adequate estimation in real-time. Tzes and Yurkovich [50], Yurkovich et al [58] and Cetinkunt and Wu [10], contributed a great deal for that area.

The Variable Structure Control is by far the most outstanding school in the control of robots because it respects the inherent nonlinear behaviour of the robot and still keeps the control design simple and consistent. The concept was established by Vadim I. Utkin [53] and later developed by Yeung and Chen [56], and by Young [57]. Nathan and Singh [38]

suggested a SLIDING MODE control formulation based on the theory of variable structure systems. However this formulation was general and cannot be implemented for practical systems. The approach does not lead to unique control policies.

It is known that nonlinear controls are generally accompanied by chatter. The current efforts are aimed at minimizing chatter improving the model which describes the interaction of the controller with the structure.

Luecke and Gardner [28] reported on the recent trends on cooperative robots . They established conditions for the stability of the operation. No analytical or experimental simulation was given. The most recent work on the control of flexible robots was reported by Khorrami and Jain [24]. The experimental setup was designed in such a way that the two links were driven in a horizontal plane. The arms were supported on air film to minimize the friction and were commanded by a 486 PC. The actuators were chosen to be DC-motors. One motor drove one link directly and the other drove the other link through an antibacklash gearing. The use of linearization feedback control gave satisfactory results.

1.6 OBJECTIVES AND ORGANIZATION OF THESIS

The main objective of this thesis is to develop a new methodology for the control of flexible robots which is referred to in this thesis as the "Nonlinear Integrated Tabular" NIT Control. The algorithms are developed using adequate models which can take into account the flexibility in the joints as well as the flexibility in the links. NIT was tested and simulated to assess its scope and its limitations. To be able to compare it with coventional controls,

elaborate models were developed for the two-link elbow arm. Comparisons between NIT and some of the conventional controls showed that NIT offers a simple, low cost, robust and smooth controller which compares well with other available strategies. Tracking of continuous and discontinuous trajectories was attempted with satisfactory results.

An experimental setup was built to verify some of the analytical results obtained in the previous part. It was not just a setup which would be scrapped at the termination of the investigation. Guided by the designs of CRS Plus Corp., it was built in a modular form which allows its adaptation and extension to conduct these investigations as well as future ones in the area of flexible manipulators. Up-to-date technologies were implemented in its making: Harmonic Drives, transputers and advanced sensory systems are but a few. Hundreds of hours were spent in designing the parts and subsystems using AUTOCAD, machining and milling, assembly and debugging the mechanical parts. Tremendous effort went in streamlining, extending and debugging the software package for the industrial controller. Some simple experiments were conducted to check the interfaces which are developed between the sensory system and the controller. Another series of experiments were conducted to validate the dynamic prediction of a flexible arm when the brakes of the motors are applied suddenly. Reasonable agreement was found between theory and experiment. The experimental setup was given the name "FLEXROD" which stands for FLEXible RObot Device. It will remain and will be used in the labs of McMaster for sometime to come to conduct further experiments and to implement NIT and other strategies of control on flexible robots. "FLEXROD" is a reality which is structured along the most advanced designs of robots in its category.

The thesis is organized as follows:

1. Chapter 1 contains the literature review, objectives and scope of thesis.

2. Three mathematical models were developed in Chapter 2 from basic principles using Lagrange's equation and finite element formulation. The first model is termed "RAM" assumes that there is no flexibility anywhere in the two link arm. Gravity terms are included. The Coriolis components were suppressed from the model because of choice of drives used. However the nonlinearities due to the centrifugal forces and due to the gravity terms stayed with the model. The second model is termed "FJM". In that model we assumed that the flexibility of the elbow arm is basically due to the harmonic drives at the joints. The degrees of freedom doubled in number and the model became more complex. The third model is termed "FLM" and the flexibility is assumed to be dominated by the links themselves. Finite element formulation was used to develop the model and special care was given to the nature of transmission of forces and torques at the revolutes when assembling the global stiffness and mass matrices. The three models are realistic representations of actual systems encountered in practice.

3. The NIT control strategy is developed in Chapter 3. Solving the inverse kinematic problem one can evaluate the derivatives of the variables of the joint. Adequate and numerically stable algorithms are developed and tested. The command voltages are systematically evaluated and stored in a TABULAR form. Tracking of continuous as well as discontinuous trajectories was tried. Criteria for comparisons were established. Computer simulations for NIT are presented and analyzed.

4. Conventional methodologies of control were developed using "RAM", "FJM" and "FLM".

In particular, the proportional plus derivative plus gravity control required high levels for the command voltages. With the feedback linearization, the performance improved a little but the controller was found highly sensitive to the variations of parameters. The "Sliding Mode Control", and in particular the VEE-MOD-VEE was developed and simulated for a single arm. In that case, tracking was found to be smooth in spite of the violent oscillations (chatter) noticed in the command voltage. In all this chapter showed that NIT compares well with the best conventional strategy.

5. Capter 5 covers the methodologies in designing, manufacturing and assembling the mechanical parts of FLEXROD. Chapter 6 describes the acrchitecture of the industrial controler and the details of the interface unit which was developed between the sensory system and the controler. Experimental results are presented, compared and the motors were activated suddenly.

6. Chapter 7 gives a summary and recommendations for future research.

CHAPTER 2

GENERALIZED DIMENSIONLESS MODELS

FOR THE DYNAMICS OF THE ELBOW ARM

2.1 OBJECTIVES

The main objective of this chapter is to develop mathematical models which adequately describe the dynamics of the elbow arm. The models are used in the subsequent chapters for the proper simulation and control of the manipulator. The models are rendered dimensionless to cover a wide class of elbow arms.

The actuators are considered as armature-controlled D.C. motors with linear damping in the revolutes. The forearm is assumed to be remotely driven as shown in Figure (2.1). This architecture is typical of the arrangement used in a wide class of industrial manipulators. The main advantage of such architecture is that it yields a dynamic model which is free from Coriolis forces. However the centrifugal forces appear in the models.

Three models are developed in this chapter which are described briefly as follows:

(a) The Rigid Arm Model "RAM"

This model does not account for flexibility in the joints or links. It is simple and describes the dynamics of the two-link elbow arm together with the associated actuators. The model

12

is reported here because it is used as a basis for future comparisons. The model is casted in

the form of two coupled (nonlinear second order) differential equations.

(a)   **(b)**
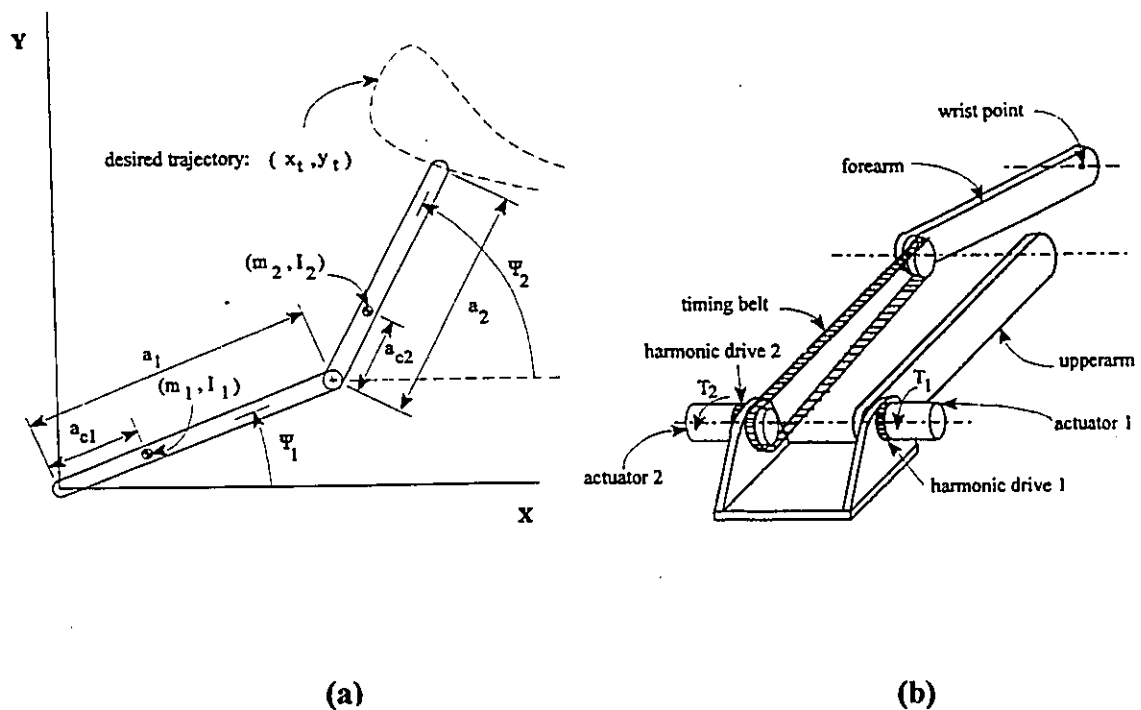
Figure 2.1: Elbow arm with remotely controlled forearm.

(b) The Flexible Joint Model "FJM"

The FJM model assumes that the flexibility is due to the presence of the "HARMONIC

DRIVES". The Harmonic Drives are speed-reducing elements implemented between the

output shaft of the D.C. motor and the driven link. The model, is shown to be expressed by

four coupled second order nonlinear differential equations.

(c) The Flexible Link Model "FLM"

The FLM model assumes that the flexibility of the links are dominant. The flexibility in the joints is ignored in comparison with the flexibility in the links. A finite element modelling is developed where each link is considered as a structural beam element with the end nodes coinciding with the revolutes. The model is shown to be given by eight second order differential equations which are nonlinear and coupled.

In the analysis that follows new quantities are always defined as soon as they appear the first time. Some of these quantities are included in the list of NOMENCLATURE to facilitate future cross-reference. The S.I. system of units is used throughout the thesis.

2.2 THE ACTUATOR AND THE HARMONIC DRIVE

The actuator is considered to be an armature-controlled D.C. motor as shown in Figure(2.2). A torsional spring K_h is placed between the motor and the gear train to represent the torsional stiffness of the HARMONIC DRIVE. The latter achieves a speed reduction N from the D.C. motor to the associated link (normally N ≈ 100).

The field-armature interaction is described by:

$$\tau_m = K_1 \, \phi_f \, i_a = K_m \, i_a \tag{2.1.a}$$
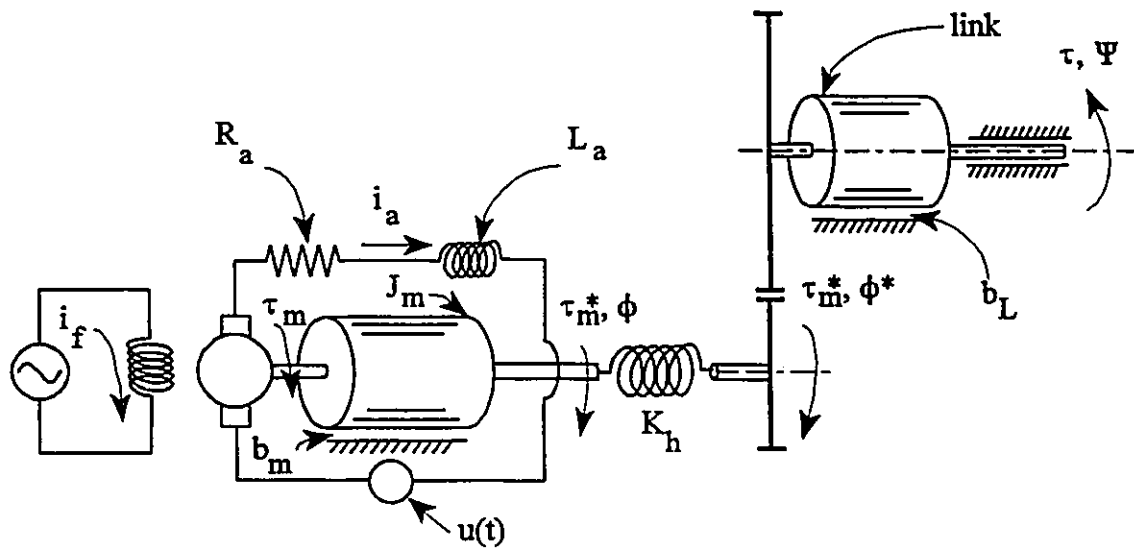
Figure 2.2: The actuator.

where:

τ_m = Torque exerted on J_m .

J_m = Mass moment of inertia of rotor about axis of rotation.

K_1, K_2, K_m = Constant coefficients with $K_m = K_1 \phi_f = K_1 K_2 i_f$

i_a, i_f = Armature and field currents respectively with i_f constant.

ϕ_f = Magnetic field in gap,

         $= K_2 i_f$

Applying Kirchoff's law to the armature circuit, one obtains:

$$R_a i_a + L_a \frac{di_a}{dt} + v_b = u(t) \qquad\qquad \text{(2.1.b)}$$

where:

t   = Time

R_a, L_a = Resistance (ohms) and inductance (henries) of armature windings.

u(t)   = Input voltage to D.C. motor (control input).

v_b = Back electromotive force (e.m.f.).

K_b = Back e.m.f. constant.

ϕ = Angular displacement of output shaft of motor, just before the harmonic drive.

One can thus write

$$v_b = K_b \, \dot{\phi} \qquad\qquad \text{(2.1.c)}$$

The following relation describes the dynamic equilibrium of the rotating parts on the motor's side:

$$J_m \ddot{\phi} + b_m \dot{\phi} + \tau_m^{'} = \tau_m \qquad\qquad \text{(2.1.d)}$$

where:

b_m = Damping coefficient on the motor side.

$\tau_m^{'}$ = Net torque through shaft, just before the harmonic drive.

For the speed reducer one can write:

$$N \ \Psi = \phi^*$$
(2.1.e)

$$\tau = N \ \tau_m^{\cdot} - b_L \dot{\Psi}$$
(2.1.f)

where:

ϕ^* = Angular displacement of output shaft just before speed reduction.

Ψ = Angular displacement of driven link immediately after harmonic drive.

b_L = Damping coefficient on link side.

τ = Torque delivered to link less friction in the revolute.

Assuming no flexibility in the joints, one can write

$$\phi^* = \phi$$
(2.1.g)

Laplace transforming and rearranging (2.1.a) to (2.1.g) inclusive and eliminating $V_b(s)$ and $\tau_m(s)$ one obtains:

$$(R_a + L_a s) \ I_a(s) + K_b \ s \ \phi(s) = U(s)$$

$$(J_m \ s^2 + b_m \ s) \ \phi(s) + \tau_m^{\cdot}(s) = K_m \ I_a(s)$$

$$N \ \tau_m^{\cdot}(s) - b_L \ s \ \Psi(s) = \tau(s)$$
(2.2.a,b,c)

where s is the Laplace variable.

Visualizing the dynamics of the links, reflected by the term $\tau(s)$ as noise imposed

on the system then relations (2.2.a,b,c) can be represented by the block diagram shown in Figure (2.3). The output $\phi(s)$ is considered as the superposition of an excitation due to U(s) and another due to $-1/N$ $\tau(s)$. The response due to the first is denoted by $\phi_{(1)}(s)$ and the response due to the second is denoted by $\phi_{(2)}(s)$. One can thus write:

$$\frac{\phi_{(1)}(s)}{U(s)} = \frac{K_m}{(R_a + L_a s)\left[J_m s^2 + b_m s + \dfrac{b_L s}{N^2}\right] + K_m K_b s}$$

and

$$\frac{\phi_{(2)}(s)}{-\dfrac{1}{N}\tau(s)} = \frac{R_a + L_a s}{(R_a + L_a s)\left[J_m s^2 + b_m s + \dfrac{b_L s}{N^2}\right] + K_m K_b s}$$

From which one obtains

$$\phi(s) = \phi_{(1)} + \phi_{(2)} = \frac{K_m U(s) - \dfrac{1}{N}\tau(s)\cdot[R_a + L_a s]}{(R_a + L_a s)\left[J_m s^2 + b_m s + \dfrac{b_L s}{N^2}\right] + K_m K_b s}$$

Taking the view that the contribution of (L_a) to the time constant is negligible compared to that due to (R_a), one can replace L_a by 0 in the previous expression to obtain:
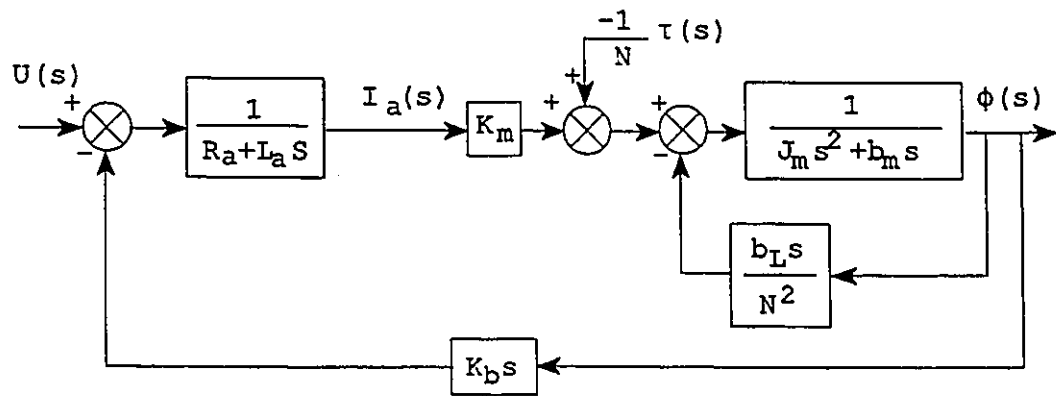
Figure 2.3: Link dynamics as noise.

$$\phi(s) = \frac{\left(\dfrac{K_m}{R_a}\right) U(s) - \dfrac{1}{N}\,\tau(s)}{[J_m]\,s^2 + \left[\, b_m + \dfrac{b_L}{N^2} + \dfrac{K_b\,K_m}{R_a}\,\right] s}$$

The equation of the actuator of the i'th link in terms of the link's angular displacement Ψ_i, is thus given by:

$$(N_i \, J_{m,i}) \, \ddot{\Psi}_i + N_i \left(b_{m,i} + \frac{b_{L,i}}{N_i^2} + \frac{K_{b,i} \, K_{m,i}}{R_{a,i}} \right) \dot{\Psi}_i$$

$$= \left(\frac{K_{m,i}}{R_{a,i}} \right) u_i(t) - \left(\frac{1}{N_i} \right) \tau_i(t) \tag{2.2.d}$$

where i=1,2.

Introducing the dimensionless time T given by:

$$T = \omega_0 \, t \tag{2.3}$$

where

ω_0 = time scaling coefficient

relation (2.2.d) can be written in the following dimensionless form:

$$\Psi_i'' + \alpha_i \, \Psi_i' = \beta_i \, u_i^*(T) - \gamma_i \, \tau_i^*(T) \tag{2.4}$$

where

τ_i^* = Dimensionless torque applied to i'th link = $\tau_i \, / \, (m_i a_i g)$

m_i, a_i = Mass and length

g = Gravitational acceleration

u_i^* = Dimensionless control signal = $u_i \, / \, E_0$

E_0 = Reference voltage = 100 V

$$\alpha_i = \left[b_{m,i} + \frac{b_{L,i}}{N_i^2} + \frac{K_{b,i} K_{m,i}}{R_{a,i}} \right] \Big/ \left[\omega_0 J_{m,i} \right]$$

$$\beta_i = \left[\frac{E_0 K_{m,i}}{R_{a,i}} \right] \Big/ \left[N_i \, \omega_0^2 J_{m,i} \right]$$

$$\gamma_i = \left[m_i \, g \, a_i \right] \Big/ \left[N_i^2 \, \omega_0^2 J_{m,i} \right] \tag{2.5}$$

Primes on the variables refer to differentiation with respect to the dimensionless time T.

In case the flexibility of the joint has to be taken into account and assuming a linear spring for the harmonic drive one replaces Eq.(2.1.g) by:

$$\tau_m^{\cdot} = K_h \left(\phi - N \, \Psi \right) \tag{2.6.a}$$

where

K_h = Torsional stiffness of the harmonic drive.

Relations (2.1.f) and (2.6.a) then relation (2.6.a) can be rearranged for the i'th link to read:

$$\tau_i = - b_{L,i} \, \dot{\Psi}_i + N_i \, K_{h,i} \, \phi_i - N_i^2 \, K_{h,i} \, \Psi_i$$

which can be written in the following dimensionless form

$$\tau_i^{\cdot} = - \alpha_i^{\cdot} \, \psi_i' + \beta_i^{\cdot} \, \Psi_i^{\cdot} - \gamma_i^{\cdot} \, \Psi_i \tag{2.6.b}$$

where

$$\alpha_i^{\cdot} = \frac{b_{L,i} \, \omega_0}{m_i \, g \, a_i} \; ; \; \beta_i^{\cdot} = \frac{K_{h,i} \, N_i}{m_i \, g \, a_i} \; ; \; \gamma_i^{\cdot} = \frac{K_{h,i} \, N_i^2}{m_i \, g \, a_i} \tag{2.7}$$

The dynamics of the actuator with harmonic drive are constructed by substituting (2.6.a) in (2.1.d) to obtain

$$J_m \ \ddot{\phi} + b_m \ \dot{\phi} + K_h \ (\phi - N \ \Psi) = \tau_m \qquad \qquad \text{(2.8.a)}$$

Recalling that L_a=0, then relations (2.1.a), (2.1.b) and (2.1.c) can be combined to read:

$$\tau_m = \frac{K_m}{R_a} \ [u - K_b \ \dot{\phi}] \qquad \qquad \text{(2.8.b)}$$

Substituting (2.8.b) in (2.8.a) and rearranging one obtains:

$$J_m \ \ddot{\phi} + \left(b_m + \frac{K_m K_b}{R_a} \right) \ \dot{\phi} + K_h \ \phi - (K_h \ N) \ \Psi = \left(\frac{K_m}{R_a} \right) \ u$$

The previous relation can be written for the i'th link in a dimensionless form as follows:

$$\phi_i'' + \alpha_i^0 \ \phi_i' + \beta_i^0 \ \phi_i - \gamma_i^0 \ \Psi_i = \mu_i^0 \ u_i^. \qquad \qquad \text{(2.8.c)}$$

where

$$\alpha_i^0 = \left[b_{m,i} + \frac{K_{b,i} K_{m,i}}{R_{a,i}} \right] \Big/ \ [J_{m,i} \ \omega_0]$$

$$\beta_i^0 = K_{h,i} \ \Big/ \ [J_{m,i} \ \omega_0^2]$$

$$\gamma_i^0 = [K_{h,i} \ N_i] \ \Big/ \ [J_{m,i} \ \omega_0^2]$$

$$\mu_i^0 = \left(\frac{K_{m,i} E_0}{R_{a,i}} \right) \ \Big/ \ [J_{m,i} \ \omega_0^2] \qquad \qquad \text{(2.9)}$$

Equations (2.4), (2.6.b) and (2.8.b) are used in future sections to construct the "RAM", the

"FJM" and the "FLM" models.

2.3 THE RIGID ARM MODEL "RAM"

The model to describe the dynamics of the arm is constructed using Lagrange's equation which reads:

$$\frac{d}{dt}\left(\frac{\partial L}{\partial \dot{q}_k}\right) - \frac{\partial L}{\partial q_k} = \tau_k \qquad\qquad ; k = 1,2,...n \qquad\qquad (2.10.a)$$

where

L $\qquad$ = Lagrangian of system.

n $\qquad$ = Number of generalized coordinates.

q_k $\qquad$ = k'th generalized coordinate.

T_E $\qquad$ = Total kinetic energy stored $\qquad = \sum_{i=1}^{n} (T_E)_i$

V_E $\qquad$ = Total potential energy stored $\qquad = \sum_{i=1}^{n} (V_E)_i$

τ_k $\qquad$ = k'th generalized force.

One can write

$$L = T_E - V_E \qquad\qquad (2.10.b)$$

The potential energy of the i'th link is given by:

$$(V_E)_i = m_i \{\underline{g}\}^T \{\underline{r}_{c,i}\} \tag{2.10.c}$$

where bars underneath the variables indicate vector quantities and the superscript T indicates

the transpose of the vector and;

m_i = Mass of i'th link.

g = Gravity vector in world coordinates $= [0,-g]^T$

$r_{c,i}$ = Position vector of center of mass of i'th link in world coordinates.

The kinetic energy of the i'th link is given by:

$$(T_E)_i = \frac{1}{2} m_i \{\underline{v}_{c,i}\}^T \{\underline{v}_{c,i}\} + \frac{1}{2} \{\underline{\omega}\}^T [I_m] \{\underline{\omega}\} \tag{2.10.d}$$

where

$v_{c,i}$ = Velocity of the center of mass of i'th link in world coordinates.

ω_i = Angular velocity of i'th link in link-fixed frame.

$[I_m]_i$ = Mass moment of inertia matrix about center of mass of i'th link.

The kinetic energy T_E of the system can be expressed as follows:

$$T_E = \frac{1}{2} \{\dot{q}\}^T [D(q)] \{\dot{q}\} \tag{2.10.e}$$

where

q   = (n × 1) vector of generalized coordinates.

[D(q)] = (n × n) symmetric positive definite inertia matrix.

Substituting (2.10.c) and (2.10.e) in Lagrange's equations (2.10.a) one can show that the

governing relations are given by:

$$\sum_{j\text{-}1}^{n} d_{kj} \ddot{q}_j + \sum_{i,j\text{-}1}^{n} c_{ijk} \dot{q}_i \dot{q}_j + b_k = \tau_k$$

$$i,j,k = 1,2..,n$$

(2.11)

or in the more compact form

$$[D(q)] \{\ddot{q}\} + [C(q,\dot{q})] \{\dot{q}\} + \{b(q)\} = \{\tau(t)\}$$

(2.12)

where

$c_{i,j,k}$ = Christoffel symbols of first kind.

$$= \frac{1}{2} \left\{ \frac{\partial d_{kj}}{\partial q_i} + \frac{\partial d_{kj}}{\partial q_j} - \frac{\partial d_{ij}}{\partial q_k} \right\}$$

(2.13.a)

b_k $= \dfrac{\partial V_E}{\partial q_k}$

(2.13.b)

$d_{u,v}$ = The (u,v) element of [D(q)] matrix.

$C_{k,j}$ = The (k,j) element of [C(q,q̇)] matrix.

$$= \sum_{i\text{-}1}^{n} c_{ijk} q_i$$

(2.13.c)

It can be shown that for a constant k, the Christoffel symbols $c_{i,j,k} = c_{j,i,k}$. Referring to Figure (2.1.b) and assuming no flexibility in the joints or the links, one can see that Ψ_1 and Ψ_2 are natural choice for the generalized coordinates. One can thus write the following relations

$$\underline{r}_{c1} = [a_{c1}\, c_1 \,,\, a_{c1}\, s_1]^T$$

$$\underline{r}_{c2} = [a_1\, c_1 + a_{c2}\, c_2 \,,\, a_1\, s_1 + a_{c2}\, s_2]^T$$

$$\underline{v}_{c1} = [-\, a_{c1}\, s_1\, \dot{\Psi}_1 \,,\, a_{c1}\, c_1\, \dot{\Psi}_1]^T$$

$$\underline{v}_{c2} = [-\, a_1\, s_1\, \dot{\Psi}_1 - a_{c2}\, s_2\, \dot{\Psi}_2 \,,\, a_1\, c_1\dot{\Psi}_1 + a_{c2}\, c_2\, \dot{\Psi}_2]^T$$

$$\underline{\omega}_1 \,,\, \underline{\omega}_2 = angular \quad velocities \quad of \quad links \quad 1 \quad and \quad 2.$$

$$= [0\,,\,0\,,\,\dot{\Psi}_1]^T,\, [0\,,\,0\,,\,\dot{\Psi}_2]^T$$

$$c_1\,,\,c_2\,,\,s_1\,,\,s_2 = \cos\,\Psi_1\,,\,\cos\,\Psi_2\,,\,\sin\,\Psi_1\,,\,\sin\Psi_2$$

$$c_{21}\,,\,s_{21} = \cos\,(\Psi_2 - \Psi_1)\,,\,\sin\,(\Psi_2 - \Psi_1)$$

$$a_{c1}\,,\,a_{c2} = distances \quad as \quad shown \quad in \quad Fig.2.1.b. \tag{2.13.d}$$

The potential and kinetic energy of the elbow arm are obtained from relations (2.10.c) and (2.10.e) as follows:

$$V_E = m_1 \ g \ (a_{cl} \ s_1) + m_2 \ g \ (a_1 \ s_1 + a_{c2} \ s_2)$$

$$T_E = \frac{1}{2} \ [\dot{\Psi}_1 \ , \ \dot{\Psi}_2] \ [D(q)] \ \begin{Bmatrix} \dot{\Psi}_1 \\ \dot{\Psi}_2 \end{Bmatrix}$$

where

$$[D] = \begin{bmatrix} m_1 \ a_{cl}^2 + m_2 \ a_1^2 + I_1 & \vdots & m_2 \ a_1 \ a_{c2} \ c_{21} \\ ----------- & \vdots & ----------- \\ m_2 \ a_1 \ a_{c2} \ c_{21} & \vdots & m_2 \ a_{c2}^2 + I_2 \end{bmatrix} \qquad (2.13.e)$$

where I_1, I_2 are the mass moments of inertia of links 1 and 2 about axes through their

respective centers of mass and normal to the plane of motion. Using the [D] matrix as defined

by (2.13.e) and the definition of the Christoffel symbols as given by (2.13.a) one can write:

$$\frac{\partial d_{11}}{\partial \Psi_1} = \frac{\partial d_{11}}{\partial \Psi_2} = 0 \ ; \ \frac{\partial d_{22}}{\partial \Psi_1} = \frac{\partial d_{22}}{\partial \Psi_2} = 0$$

$$\frac{\partial d_{12}}{\partial \Psi_1} = \frac{\partial d_{21}}{\partial \Psi_1} = m_2 \ a_1 \ a_{c2} \ s_{21} \ ; \ \frac{\partial d_{12}}{\partial \Psi_2} = \frac{\partial d_{21}}{\partial \Psi_2} = - \ m_2 \ a_1 \ a_{c2} \ s_{21}$$

from which one obtains:

$$c_{111} = 0 \ ; \ c_{121} = c_{211} = 0 \ ; \ c_{221} = - \ m_2 \ a_1 \ a_{c2} \ s_{21}$$

$$c_{112} = m_2 \ a_1 \ a_{c2} \ s_{21} \ ; \ c_{122} = c_{212} = 0 \ ; \ c_{222} = 0$$

The [C] matrix as given by equation (2.13.c) is

$$[C] = \begin{bmatrix} 0 & - \ m_2 \ a_1 \ a_{c2} \ s_{21} \ \dot{\Psi}_2 \\ m_2 \ a_1 \ a_{c2} \ s_{21} \ \dot{\Psi}_1 & 0 \end{bmatrix} \qquad (2.13.f)$$

The $\{\underline{b}\}$ vector in equation(2.12) is obtained by using relation (2.13.b) which yields:

$$\{\underline{b}\} = \left\{ \begin{array}{c} (m_1\, a_{cl} + m_2\, a_1\,)\, g\, c_1 \\ m_2\, a_{c2}\, g\, c_2 \end{array} \right\} \tag{2.13.g}$$

The equations describing the dynamics of the links of the "RAM", i.e. with no flexibility in the jints or in the links are constructed by substituting (2.13.e), (2.13.f) and (2.13.g) in (2.12). One thus obtains:

$$\begin{bmatrix} m_1\, a_{cl}^2 + m_2\, a_1^2 + I_1 & \vdots & m_2\, a_1\, a_{c2}\, c_{21} \\ \hline m_2\, a_1\, a_{c2}\, c_{21} & \vdots & m_2\, a_{c2}^2 + I_2 \end{bmatrix} \left\{ \begin{array}{c} \ddot{\Psi}_1 \\ \ddot{\Psi}_2 \end{array} \right\} +$$

$$\begin{bmatrix} 0 & \vdots & - m_2\, a_1\, a_{c2}\, s_{21}\, \dot{\Psi}_2 \\ \hline m_2\, a_1\, a_{c2}\, s_{21}\, \dot{\Psi}_1 & \vdots & 0 \end{bmatrix} \left\{ \begin{array}{c} \dot{\Psi}_1 \\ \dot{\Psi}_2 \end{array} \right\} +$$

$$\left\{ \begin{array}{c} (m_1\, a_{cl} + m_2\, a_1\,)\, g\, c_1 \\ m_2\, a_{c2}\, g\, c_2 \end{array} \right\} = \left\{ \begin{array}{c} \tau_1 \\ \tau_2 \end{array} \right\} \tag{2.14}$$

where τ_1 and τ_2 are control torques which are applied by the actuators to the respective links. The previous relations can be written in the following dimensionless form:

$$\Psi_1'' + \alpha_1'\, c_{21}\, \Psi_2'' - \alpha_1'\, s_{21}\, (\Psi_2')^2 + \beta_1'\, c_1 = \gamma_1'\, \tau_1'$$

$$\Psi_2'' + \alpha_2'\, c_{21}\, \Psi_1'' + \alpha_2'\, s_{21}\, (\Psi_1')^2 + \beta_2'\, c_2 = \gamma_2'\, \tau_2' \tag{2.15}$$

where

$$\alpha_1^\bullet = \frac{m_2 \, a_1 \, a_{c2}}{m_1 \, a_{c1}^2 + m_2 \, a_1^2 + I_1} \qquad ; \; \alpha_2^\bullet = \frac{m_2 \, a_1 \, a_{c2}}{m_2 \, a_{c2}^2 + I_2}$$

$$\beta_1^\bullet = \frac{(m_1 \, a_{c1} + m_2 \, a_1) \, g}{(m_1 \, a_{c1}^2 + m_2 \, a_1^2 + I_1) \, \omega_0^2} \qquad ; \; \beta_2^\bullet = \frac{m_2 \, a_{c2} \, g}{(m_2 a_{c2}^2 + I_2) \, \omega_0^2}$$

$$\gamma_1^\bullet = \frac{m_1 \, g \, a_1}{(m_1 \, a_{c1}^2 + m_2 \, a_1^2 + I_1) \, \omega_0^2} \qquad ; \; \gamma_2^\bullet = \frac{m_2 \, g \, a_2}{(m_2 \, a_{c2}^2 + I_2) \, \omega_0^2} \qquad (2.16)$$

The rest of the variables and parameters are as defined before.

The required "RAM" is obtained by eliminating $\tau_1^\bullet$ and $\tau_2^\bullet$ between equations (2.4) and equations (2.15). One thus obtains:

$$\Psi_1'' + a_{11} \, \Psi_1' + a_{12} \, c_{21} \, \Psi_2'' - a_{12} \, s_{21} \, (\Psi_2')^2 + a_{13} \, c_1 = \mu_1 \, u_1^\bullet$$

$$\Psi_2'' + a_{21} \, \Psi_2' + a_{22} \, c_{21} \, \Psi_1'' + a_{22} \, s_{21} \, (\Psi_1')^2 + a_{23} \, c_2 = \mu_2 \, u_2^\bullet$$

$$(2.17)$$

where:

$$a_{11} = \frac{\alpha_1\,\dot{\gamma_1}}{\gamma_1 + \dot{\gamma_1}} \qquad ; a_{12} = \frac{\dot{\alpha_1}\,\gamma_1}{\gamma_1 + \dot{\gamma_1}}$$

$$a_{13} = \frac{\dot{\beta_1}\,\gamma_1}{\gamma_1 + \dot{\gamma_1}} \qquad ; \mu_1 = \frac{\beta_1\,\dot{\gamma_1}}{(\gamma_1 + \dot{\gamma_1})\,N_1}$$

$$a_{21} = \frac{\alpha_2\,\dot{\gamma_2}}{\gamma_2 + \dot{\gamma_2}} \qquad ; a_{22} = \frac{\dot{\alpha_2}\,\gamma_2}{\gamma_2 + \dot{\gamma_2}}$$

$$a_{23} = \frac{\dot{\beta_2}\,\gamma_2}{\gamma_2 + \dot{\gamma_2}} \qquad ; \mu_2 = \frac{\beta_2\,\dot{\gamma_2}}{(\gamma_2 + \dot{\gamma_2})\,N_2} \qquad\qquad (2.18)$$

2.4 THE FLEXIBLE JOINT MODEL "FJM"

The model is constructed using relations (2.8.c), (2.15) and (2.6.b) . It is written in the following form:

$$\phi_1'' + \alpha_1^0\,\phi_1' + \beta_1^0\,\phi_1 - \gamma_1^0\,\Psi_1 = \mu_1^0\,\dot{u_1}$$

$$\Psi_1'' + \dot{\alpha_1}\,c_{21}\,\Psi_2'' - \dot{\alpha_1}\,s_{21}\,(\Psi_2')^2 + \dot{\beta_1}\,c_1 = \dot{\gamma_1}\,\dot{\tau_1}$$

$$\phi_2'' + \alpha_2^0\,\phi_2' + \beta_2^0\,\phi_2 - \gamma_2^0\,\Psi_2 = \mu_2^0\,\dot{u_2}$$

$$\Psi_2'' + \dot{\alpha_2}\,c_{21}\,\Psi_1'' + \dot{\alpha_2}\,s_{21}\,(\Psi_1')^2 + \dot{\beta_2}\,c_2 = \dot{\gamma_2}\,\dot{\tau_2}$$

$$\dot{\tau_1} = -\dot{\alpha_1}\,\Psi_1' + \dot{\beta_1}\,\phi_1 - \dot{\gamma_1}\,\Psi_1$$

$$\dot{\tau_2} = -\dot{\alpha_2}\,\Psi_2' + \dot{\beta_2}\,\phi_2 - \dot{\gamma_2}\,\Psi_2$$

Eliminating $\dot{\tau_1}$ and $\dot{\tau_2}$ from the previous equations and rearranging, one obtains the "FJM" in the following form:

$$\phi_1'' + b_{11}\,\phi_1' + \omega_1^2\,\phi_1 - b_{12}\,\Psi_1 = \mu_1^0\,u_1^{\cdot}$$

$$\Psi_1'' + b_{21}\,\Psi_1' + \omega_2^2\,\Psi_1 + b_{22}\,c_{21}\,\Psi_2'' - b_{22}\,s_{21}\,(\Psi_2)^2 - b_{23}\,\phi_1 + b_{24}\,c_1 = 0$$

$$\phi_2'' + b_{31}\,\phi_2' + \omega_3^2\,\phi_2 - b_{32}\,\Psi_2 = \mu_2^0\,u_2^{\cdot}$$

$$\Psi_2'' + b_{41}\,\Psi_2' + \omega_4^2\,\Psi_2 + b_{42}\,c_{21}\,\Psi_1'' + b_{42}\,s_{21}\,(\Psi_1)^2 - b_{43}\,\phi_2 + b_{44}\,c_2 = 0$$

$$(2.19.a)$$

where:

$$b_{11} = \alpha_1^0 \qquad\qquad ;\ \omega_1^2 = \beta_1^0 \qquad\qquad ;\ b_{12} = \gamma_1^0$$

$$b_{21} = \alpha_1^{\cdot}\gamma_1^{\cdot} \qquad\quad ;\ \omega_2^2 = \gamma_1^{\cdot}\gamma_1^{\cdot} \qquad\quad ;\ b_{22} = \alpha_1^{\cdot}$$

$$b_{23} = \beta_1^{\cdot}\gamma_1^{\cdot} \qquad\quad ;\ b_{24} = \beta_1^{\cdot}$$

$$b_{31} = \alpha_2^0 \qquad\qquad ;\ \omega_3^2 = \beta_2^0 \qquad\qquad ;\ b_{32} = \gamma_2^0$$

$$b_{41} = \alpha_2^{\cdot}\gamma_2^{\cdot} \qquad\quad ;\ \omega_4^2 = \gamma_2^{\cdot}\gamma_2^{\cdot} \qquad\quad ;\ b_{42} = \alpha_2^{\cdot}$$

$$b_{43} = \beta_2^{\cdot}\gamma_2^{\cdot} \qquad\quad ;\ b_{44} = \beta_2^{\cdot}$$

$$(2.20)$$

Relations (2.19) can be written in the following matrix form:

$$[M\ (\underline{X})]\ \underline{X}'' + [C\ (\underline{X}\ ,\ \underline{X}')]\ \underline{X}' + [G]\ \underline{X} + \underline{b}\ (\underline{X}) = [B]\ \underline{u} \qquad\qquad (2.21.a)$$

where:

$$X = [\phi_1, \Psi_1, \phi_2, \Psi_2]^T \qquad ; \underline{u} = [u_1^{\cdot}, u_2^{\cdot}]^T$$

$$[M] = \begin{bmatrix} 1 & 0 & 0 & 0 \\ 0 & 1 & 0 & (b_{22}\,c_{21}) \\ 0 & 0 & 1 & 0 \\ 0 & (b_{42}\,c_{21}) & 0 & 1 \end{bmatrix} \qquad ; [B] = \begin{bmatrix} \mu_1^0 & 0 \\ 0 & 0 \\ 0 & \mu_2^0 \\ 0 & 0 \end{bmatrix}$$

$$[C] = \begin{bmatrix} (b_{11}) & 0 & 0 & 0 \\ 0 & (b_{21}) & 0 & (-b_{22}\,s_{21}\,\Psi_2) \\ 0 & 0 & (b_{31}) & 0 \\ 0 & (b_{42}\,s_{21}\,\Psi_1) & 0 & (b_{41}) \end{bmatrix} \qquad ; \underline{b} = \begin{Bmatrix} 0 \\ b_{24}c_{21} \\ 0 \\ b_{44}\,c_2 \end{Bmatrix}$$

$$[G] = \begin{bmatrix} \omega_1^2 & -b_{12} & 0 & 0 \\ -b_{23} & \omega_2^2 & 0 & 0 \\ 0 & 0 & \omega_3^2 & -b_{32} \\ 0 & 0 & -b_{43} & \omega_4^2 \end{bmatrix}$$

(2.21.b)

The derivation of relations (2.19) was obtained by combining a "Lagrangian" approach for the dynamics of the links with a "Newton-Euler" approach for the actuator. It can be shown that an "all-Lagrangian approach" can be used to obtain relations (2.19). In this case the expressions for V_E and T_E given by (2.10.c) and (2.10.d) are replaced by:

$$V_E^{\cdot} = V_E + \Delta V_E \quad ; \quad T_E^{\cdot} = T_E + \Delta T_E$$

and

$$\Delta V_E = \frac{1}{2} K_{h,1} (\phi_1 - N_1 \Psi_1)^2 + \frac{1}{2} K_{h,2} (\phi_2 - N_2 \Psi_2)^2$$

$$\Delta T_E = \frac{1}{2} J_{m,1} (\dot{\phi})^2 + \frac{1}{2} J_{m,2} (\dot{\phi}_2)^2$$

The presence of ΔV_E will contribute with four more terms to Lagrange's equations due to the partial derivatives:

$$\frac{\partial V_E}{\partial \Psi_k} = - N_k K_{h,k} (\phi_k - N_k \Psi_k) \qquad ; k = 1,2$$

$$\frac{\partial V_E}{\partial \phi_k} = K_{h,k} (\phi_k - N_k \Psi_k) \qquad ; k = 1,2$$

Similarly, the presence of ΔT_E will contribute with two more terms due to the partial derivatives:

$$\frac{d}{dt} \left(\frac{\partial T_E}{\partial \dot{\Psi}_k} \right) - \frac{\partial T_E}{\partial \Psi_k} = J_{m,k} \ddot{\phi}_k \qquad ; k = 1,2$$

The generalized forces will receive four more terms due to the virtual work of the friction forces: $(b_{m,k} \dot{\phi}_k)$ and $(b_{L,k} \dot{\Psi}_k)$ for $k = 1,2$.

The model given by (2.19) is a full representation of the dynamics of the elbow arm in the presence of the flexibility in the joints. The model consists of four second order differential equations which are nonlinear and coupled.

2.5 FINITE ELEMENT IDEALIZATION OF FLEXIBLE LINKS

Each link of the arm is idealized as one dimensional finite element capable of withstanding lateral forces in the form of shear forces and moments. These are associated with lateral displacements and small rotations.

The nodes of each element are chosen to coincide with the joints themselves. Conditions of compatibility are enforced at the nodes. A local set of axes (x_e, y_e, z_e) is chosen for the i'th link with the origin at the i'th joint, i.e. at the inboard joint of the link.

Figure 2.4 depicts the forces, torques, displacements and rotations of the i'th link. The world frame frame is denoted by X, Y, Z and its origin at the base of the manipulator.
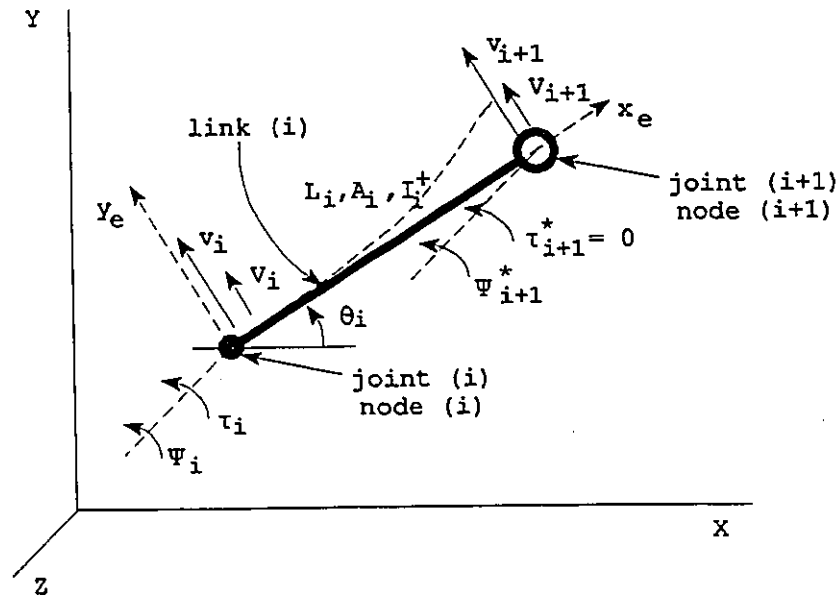
Figure 2.4: Flexible link.

L_i, A_i, I_i^* refer to the length, cross sectional area and area moment of inertia of the i'th link about the neutral axis. The nodal displacement vector q_e^* of the i'th link is given by:

$$q_e^* = [\ v_i\ ,\ \Psi_i\ ,\ v_{i\cdot1}\ ,\ \Psi_{i\cdot1}^{\cdot}\ ]^T \qquad (2.22)$$

The vector of generalized forces p_e^* is given by

$$p_e^* = [\ V_i\ ,\ \tau_i\ ,\ V_{i\cdot1}\ ,0\ ]^T \qquad (2.23)$$

It should be noticed that the fourth entry of p_e^* is zero which implies that the frictional moments at the outboard joint of the i'th link are ignored. The second entry τ_i represents the driving moment of the i'th link. q_e^* and p_e^* are expressed in the local x_e, y_e, z_e frame. The superscript * is used as a reminder that the quantities are expressed in the local frame.

The i'th link is governed by

$$[M^*]\ \ddot{q}_e^* + [K^*]\ q_e^* = p_e^*(t) + p_{be}^*(t) \qquad (2.24)$$

where $p_{be}^*(t)$ is the vector representing the equivalent body forces acting at the joints. $[K_e^*]$ and $[M_e^*]$ are the i'th link stiffness and consistent-mass matrix respectively expressed in the local frame. The $[K_e^*]$ and $[M_e^*]$ are given by:

$$[\ K_e^*\ ] = \frac{2EI^*}{L^3} \begin{bmatrix} 6 & 3L & -6 & 3L \\ 3L & 2L^2 & -3L & L^2 \\ -6 & -3L & 6 & -3L \\ 3L & L^2 & -3L & 2L^2 \end{bmatrix} \qquad (2.25)$$

where E is the Young's modulus and

$$[M_e^*] = \frac{\rho A L}{420} \begin{bmatrix} 156 & 22L & 54 & -13L \\ 22L & 4 L^2 & 13 L & -3 L^2 \\ 54 & 13L & 156 & -22L \\ -13 L & -3 L^2 & -22 L & 4 L^2 \end{bmatrix} \qquad (2.26)$$

where ρ is the mass density of the material.

One then seeks a rotation matrix [R] for the i'th link such that it satisfies the following relation

$$\underline{r} = [R] \, \underline{r}^* \qquad (2.27.a)$$

where $\underline{r}$ and $\underline{r}^*$ represent the components of the same position vector of a generic point in the world and the local frames respectively. It is noticed that the (4×1) nodal displacement vector q_e^* in the local frame will transform into a (6×1) augmented vector q_e in the world frame as shown symbolically after.

$$\underline{q}_e = [X_1 , X_2 , X_3 , X_4 , X_5 , X_6]^T$$

For this reason, one should rewrite the q_e^* the displacement vector, in the following form:

$$\underline{q}_e^* = [0 , v_i , \Psi_i , 0 , v_{i-1} , \Psi_{i-1}^*]^T$$

to be able to perform the proper transformation to the world frame. The same strategy applies for the vector p_e which should be written in the following form:

$$\underline{p}_e^* = [0 , V_i , \tau_i , 0 , V_{i-1} , 0]^T$$

The $[K_e^*]$ and $[M_e^*]$ (4×4) matrices have to be expanded as shown symbolically after:

$$
\begin{bmatrix}
X_{11} & X_{12} & X_{13} & X_{14} \\
X_{21} & X_{22} & X_{23} & X_{24} \\
X_{31} & X_{32} & X_{33} & X_{34} \\
X_{41} & X_{42} & X_{43} & X_{44}
\end{bmatrix}
\Longrightarrow
\left[\begin{array}{ccc|ccc}
0 & 0 & 0 & 0 & 0 & 0 \\
0 & X_{11} & X_{12} & 0 & X_{13} & X_{14} \\
0 & X_{21} & X_{22} & 0 & X_{23} & X_{24} \\
\hline
0 & 0 & 0 & 0 & 0 & 0 \\
0 & X_{31} & X_{32} & 0 & X_{33} & X_{34} \\
0 & X_{41} & X_{42} & 0 & X_{43} & X_{44}
\end{array}\right]
$$

where X_{ij} represents the (i,j)'th element of the $[K_e^*]$ or the $[M_e^*]$ matrices.

It can be shown that the rotation matrix $[R]$ is given by:

$$
[R_0^i] = \begin{bmatrix} [R] & [0] \\ [0] & [R] \end{bmatrix} = \left[\begin{array}{ccc|ccc}
c_i & -s_i & 0 & 0 & 0 & 0 \\
s_i & c_i & 0 & 0 & 0 & 0 \\
0 & 0 & 1 & 0 & 0 & 0 \\
\hline
0 & 0 & 0 & c_i & -s_i & 0 \\
0 & 0 & 0 & s_i & c_i & 0 \\
0 & 0 & 0 & 0 & 0 & 1
\end{array}\right]
$$

(2.27.b)

where

$$ s_i = \sin \theta_i \; ; \; c_i = \cos \theta_i \tag{2.27.c} $$

where θ_i is the angle between the x_e axis and the horizontal axis of the world system.

Premultiplying (2.24) by $[R_0^i]$ and recalling that $[R_0^i]^{-1} = [R_0^i]^T$, one obtains:

$$([R_0^i]\ [M_e^\cdot]\ [R_0^i]^T)\ ([R_0^i]\ \ddot{q}_e^\cdot)\ +\ ([R_0^i]\ [K_e^\cdot]\ [R_0^i]^T)\ ([R_0^i]q_e^\cdot)$$

$$=\ [R_0^i]\ p_{be}^\cdot\ +\ [R_0^i]\ p_e^\cdot$$

which can be written in the following compact form:

$$[M_e]\ \ddot{q}_e\ +\ [K_e]\ q_e\ =\ p_{be}\ +\ p_e \qquad (2.28)$$

where:

$$[M_e]\ =\ [R_0^i]\ [M_e^\cdot]\ [R_0^i]^T$$

$$[K_e]\ =\ [R_0^i]\ [K_e^\cdot]\ [R_0^i]^T$$

$$p_{be}\ =\ [R_0^i]\ p_{be}^\cdot$$

$$p_e\ =\ [R_0^i]\ p_e^\cdot \qquad (2.29)$$

Now $[M_e]$, $[K_e]$, p_e and p_{be} for the i'th link are all expressed in the world's frame.

They are given by:

$$[M_e] = \begin{bmatrix}
s_i^2\,Y_{1,j} & -s_i\,c_i\,Y_{1,j} & -s_i\,Y_{2,j} & s_i^2\,Y_{4,j} & -s_i\,c_i\,Y_{4,j} & s_i\,Y_{5,j} \\
-s_i\,c_i\,Y_{1,j} & c_i^2\,Y_{1,j} & c_i\,Y_{2,j} & -s_i\,c_i\,Y_{4,j} & c_i^2\,Y_{4,j} & -c_i\,Y_{5,j} \\
-s_i\,Y_{2,j} & c_i\,Y_{2,j} & Y_{3,j} & -s_i\,Y_{5,j} & c_i\,Y_{5,j} & -Y_{6,j} \\
s_i^2\,Y_{4,j} & -s_ic_iY_{4,j} & -s_iY_{5,j} & s_i^2Y_{1,j} & -s_ic_iY_{1,j} & s_iY_{2,j} \\
-s_ic_iY_{4,j} & c_i^2Y_{4,j} & c_iY_{5,j} & -s_ic_iY_{1,j} & c_i^2Y_{1,j} & -c_iY_{2,j} \\
s_iY_{5,j} & -c_iY_{5,j} & -Y_{6,j} & s_iY_{2,j} & -c_iY_{2,j} & Y_{3,j}
\end{bmatrix}$$

$$(2.30.a)$$

where

$$Y_{1,i} = \frac{156 \ \rho \ A_i \ a_i}{420} \quad ; \ Y_{2,i} = \frac{22 \ \rho \ A_i \ a_i^2}{420} \quad ; \ Y_{3,i} = \frac{4 \ \rho \ A_i \ a_i^3}{420}$$

$$Y_{4,i} = \frac{54 \ \rho \ A_i \ a_i}{420} \quad ; \ Y_{5,i} = \frac{13 \ \rho \ A_i \ a_i^2}{420} \quad ; \ Y_{6,i} = \frac{3 \ \rho \ A_i \ a_i^3}{420}$$

$$(\ i = 1,2 \ )$$

(2.30.b)

and

$$[K_e] = \begin{bmatrix} s_i^2 X_{1,i} & -s_i c_i X_{1,i} & -s_i X_{2,i} & -s_i^2 X_{1,i} & s_i c_i X_{1,i} & -s_i X_{2,i} \\ -s_i c_i X_{1,i} & c_i^2 X_{1,i} & c_i X_{2,i} & s_i c_i X_{1,i} & -c_i^2 X_{1,i} & c_i X_{2,i} \\ -s_i X_{2,i} & c_i X_{2,i} & X_{3,i} & s_i X_{2,i} & -c_i X_{2,i} & X_{4,i} \\ -s_i^2 X_{1,i} & s_i c_i X_{1,i} & s_i X_{2,i} & s_i^2 X_{1,i} & -s_i c_i X_{1,i} & s_i X_{2,i} \\ s_i c_i X_{1,i} & -c_i^2 X_{1,i} & -c_i X_{2,i} & -s_i c_i X_{1,i} & c_1^2 X_{1,i} & -c_i X_{2,i} \\ -s_i X_{2,i} & c_i X_{2,i} & X_{4,i} & s_i X_{2,i} & -c_i X_{2,i} & X_{3,i} \end{bmatrix}$$

(2.31.a)

where

$$X_{1,i} = \frac{12 \ E \ I_i^+}{a_i^3} \quad ; \quad X_{2,i} = \frac{6 \ E \ I_i^+}{a_i^2} \quad ; \quad X_{3,i} = \frac{4 \ E \ I_i^+}{a_i} \quad ; \quad X_{4,i} = \frac{2 \ E \ I_i^+}{a_i}$$

$$(i = 1,2)$$

(2.31.b)

s_i and c_i are as defined in (2.27.c)

The q_e and p_e vectors take the form:

$$\underline{q}_e = [\ x_i\ ,\ y_i\ ,\ \Psi_i\ ,\ x_{i+1}\ ,\ y_{i+1}\ ,\ \Psi_{i+1}^{\cdot}\ ]^T$$

$$\underline{p}_e = [\ p_{x,i}\ ,\ p_{y,i}\ ,\ \tau_i\ ,\ p_{x,i+1}\ ,\ p_{y,i+1}\ ,\ 0\ ]^T$$

where x_i, y_i, Ψ_i represent the x-displacement, the y-displacement and the element's rotation

at the i'th node. $p_{x,i}$, $p_{y,i}$ and τ_i are the external x-force, y-force and the moment applied to the

i'th node. All expressed in the world's frame.

The body forces vector p_{be} takes the form:

$$\underline{p}_{b_e} = m_i\ g\ [\ g_{x,i}\ ,\ g_{y,i}\ ,\ g_{z,i}\ ,\ g_{x,i+1}\ ,\ g_{y,i+1}\ ,\ g_{z,i+1}\ ]^T \qquad (2.32)$$

where:

$$g_{x,i} = 0 \qquad ;\ g_{y,i} = \frac{a_i}{2} \qquad ;\ g_{z,i} = \frac{a_i^2}{12}$$

$$g_{x,i+1} = 0 \qquad ;\ g_{y,i+1} = \frac{a_i}{2} \qquad ;\ g_{z,i+1} = \frac{-\ a_i^2}{12}$$

Relations (2.28) represent the governing equation of the i'th element in the world frame. It

is obvious that the overall "structural mass" and "stiffness" matrices cannot be assembled

directly using the conventional "direct stiffness" method. This is due to the fact that the

moments applied on an element are not transmitted in full to the adjacent element because of

the nature of the revolutes. The only constraints enforced at a common junction pertain to the

linear displacements (x_i, y_i) and to the internal reactions ($p_{x,i}$, $p_{y,i}$) at the common node. Only

these have to be equal in magnitude and opposite in direction for the two adjacent links.

2.6 THE FLEXIBLE LINK MODEL "FLM"

The consistent mass matrix $[M_e]_i$ for the i'the link is given by equations (2.30). It can be partitioned in the following form:

$$[M_e]_i = \begin{bmatrix} [M_{11,i}] & [M_{12,i}] & [M_{13,i}] & [M_{14,i}] \\ [M_{21,i}] & (m_{22,i}) & [M_{23,i}] & (m_{24,i}) \\ [M_{31,i}] & [M_{32,i}] & [M_{33,i}] & [M_{34,i}] \\ [M_{41,i}] & (m_{42,i}) & [M_{43,i}] & (m_{44,i}) \end{bmatrix}$$

(2.33.a)

The stiffness matrix $[K_e]_i$ for the i'th link is given by relations (2.31). It can be also partitioned in a similar manner

$$[K_e]_i = \begin{bmatrix} [K_{11,i}] & [K_{12,i}] & [K_{13,i}] & [K_{14,i}] \\ [K_{21,i}] & (k_{22,i}) & [K_{23,i}] & (k_{24,i}) \\ [K_{31,i}] & [K_{32,i}] & [K_{33,i}] & [K_{34,i}] \\ [K_{41,i}] & (k_{42,i}) & [K_{43,i}] & (k_{44,i}) \end{bmatrix}$$

(2.33.b)

The submatrices of $[M_{jk,i}]$ and $[K_{jk,i}]$ are obtained from (2.30.a) and (2.31.a) respectively. The vectors for nodal displacements, external and body forces are also partitioned as follows:

$$\begin{bmatrix} u_i \\ v_i \\ \Psi_i \\ u_{i+1} \\ v_{i+1} \\ \Psi_{i+1}^{\cdot} \end{bmatrix} = \begin{bmatrix} d_i \\ \Psi_i \\ d_{i+1} \\ \Psi_{i+1}^{\cdot} \end{bmatrix} \quad ; \quad \begin{bmatrix} P_{x,i} \\ P_{y,i} \\ \tau_i \\ P_{x,i+1} \\ P_{y,i+1} \\ 0 \end{bmatrix} = \begin{bmatrix} P_i \\ \tau_i \\ P_{i+1} \\ 0 \end{bmatrix} \quad ; \quad P_{bi} = \begin{bmatrix} P_{bi} \\ 0 \\ P_{b,i+1} \\ 0 \end{bmatrix}$$

(2.33.c)

The vectors $\underline{d}_i$, $\underline{p}_i$ and $\underline{p}_{bi}$ are given by:

$$\underline{d}_i = [\; x_i \;,\; y_i \;]^T \quad ; \quad \underline{p}_i = [\; p_{xi} \;,\; p_{yi} \;]^T \quad ; \quad \underline{p}_{bi} = [\; p_{bx} \;,\; p_{by} \;]^T \qquad \text{(2.33.d)}$$

Node 1 on link 1 is restrained in the x and y directions in the world frame, i.e. $\underline{d}_1 = \underline{0}$. The vector $\underline{p}_1$ associated with node 1 represents the reaction components at joint 1. The equations governing the dynamics of link 1 are thus given by:

$$
\begin{bmatrix}
(m_{22,1}) & [M_{23,1}] & (m_{24,1}) \\
[M_{32,1}] & [M_{33,1}] & [M_{34,1}] \\
(m_{42,1}) & [M_{43,1}] & (m_{44,1})
\end{bmatrix}
\begin{bmatrix}
\ddot{\Psi}_1 \\
\ddot{\underline{d}}_2 \\
\ddot{\Psi}_2^{\bullet}
\end{bmatrix}
+
$$

$$
\begin{bmatrix}
(k_{22,1}) & [K_{23,1}] & (k_{24,1}) \\
[K_{32,1}] & [K_{33,1}] & [K_{34,1}] \\
(k_{42,1}) & [K_{43,1}] & (k_{44,1})
\end{bmatrix}
\begin{bmatrix}
\Psi_1 \\
\underline{d}_2 \\
\Psi_2^{\bullet}
\end{bmatrix}
=
\begin{bmatrix}
\tau_1 \\
\underline{p}_2 + \underline{p}_{b2} \\
0
\end{bmatrix}
\qquad \text{(2.34.a.b.c)}
$$

These are four relations in seven variables, namely,

$$\Psi_1 \;,\; \underline{d}_2 \;,\; \Psi_2^{\bullet} \;,\; \underline{p}_2, \; \tau_1$$

where $\underline{p}_2$ represents the components of the unknown reactions exerted by link 2 on link 1 at node 2. The equilibrium of link 2 contributes four additional relations. Node 2, considered as a point on link 2, will be subjected to a force given by ($-\underline{p}_2$) and will have the same displacement vector $\underline{d}_2$. The rotation associated with that point is Ψ_2 which is different from $\Psi_2^{\bullet}$. Assuming zero external loads at node 3, one can write:

$$
\begin{bmatrix}
[M_{11,2}] & [M_{12,2}] & [M_{13,2}] & [M_{14,2}] \\
[M_{21,2}] & (m_{22,2}) & [M_{23,2}] & (m_{24,2}) \\
[M_{31,2}] & [M_{32,2}] & [M_{33,2}] & [M_{34,2}] \\
[M_{41,2}] & (m_{42,2}) & [M_{43,2}] & (m_{44,2})
\end{bmatrix}
\begin{bmatrix}
\ddot{d}_2 \\
\ddot{\Psi}_2 \\
\ddot{d}_3 \\
\ddot{\Psi}_3^{\cdot}
\end{bmatrix} +
$$

$$
\begin{bmatrix}
[K_{11,2}] & [K_{12,2}] & [K_{13,2}] & [K_{14,2}] \\
[K_{21,2}] & (k_{22,2}) & [K_{23,2}] & (k_{24,2}) \\
[K_{31,2}] & [K_{32,2}] & [K_{33,2}] & [K_{34,2}] \\
[K_{41,2}] & (k_{42,2}) & [K_{43,2}] & (k_{44,2})
\end{bmatrix}
\begin{bmatrix}
d_2 \\
\Psi_2 \\
d_3 \\
\Psi_3^{\cdot}
\end{bmatrix} =
\begin{bmatrix}
-p_2 + p_{b2}^{\cdot} \\
\tau_2 \\
p_{b3} \\
0
\end{bmatrix}
$$

(2.34.d,e,f,g)

These represent six additional relations in five additional variables, namely:

$$
\Psi_2 \,,\, d_3 \,,\, \Psi_3^{\cdot} \,,\, \tau_2
$$

Relations (2.34.a) to (2.34.g) represent a total of ten equations in twelve variables. Two variables, namely τ_1 and τ_2 are known inputs. Thus relations (2.34) represent the required finite element model; ten independent relations in ten unknowns. However, relations (2.34) can be reduced to eight equations in the variables by eliminating the internal reactions p_2 at joint 2. This is achieved by adding (2.34.b) and (2.34.d) and rearranging. One obtains the following matrix relation:

$$
\begin{bmatrix}
m_{22,1} & M_{23,1} & m_{24,1} & 0 & 0 & 0 \\
M_{32,1} & M_{33,1} + M_{11,2} & M_{34,1} & M_{12,2} & M_{13,2} & M_{14,2} \\
m_{42,1} & M_{43,1} & m_{44,1} & 0 & 0 & 0 \\
0 & M_{21,2} & 0 & m_{22,2} & M_{23,2} & m_{24,2} \\
0 & M_{31,2} & 0 & M_{32,2} & M_{33,2} & M_{34,2} \\
0 & M_{41,2} & 0 & m_{42,2} & M_{43,2} & m_{44,2}
\end{bmatrix}
\begin{bmatrix}
\ddot{\Psi}_1 \\
\ddot{d}_2 \\
\ddot{\Psi}_2^{\cdot} \\
\ddot{\Psi}_2 \\
\ddot{d}_3 \\
\ddot{\Psi}_3
\end{bmatrix}
+
$$

$$
\begin{bmatrix}
k_{22,1} & K_{23,1} & k_{24,1} & 0 & 0 & 0 \\
K_{32,1} & K_{33,1} + K_{11,2} & K_{34,1} & K_{12,2} & K_{13,2} & K_{14,2} \\
k_{42,1} & K_{43,1} & k_{44,1} & 0 & 0 & 0 \\
0 & K_{21,2} & 0 & k_{22,2} & K_{23,2} & k_{24,2} \\
0 & K_{31,2} & 0 & K_{32,2} & K_{33,2} & K_{34,2} \\
0 & K_{41,2} & 0 & k_{42,2} & K_{43,2} & k_{44,2}
\end{bmatrix}
\begin{bmatrix}
\Psi_1 \\
d_2 \\
\Psi_2^{\cdot} \\
\Psi_2 \\
d_3 \\
\Psi_3
\end{bmatrix}
=
\begin{bmatrix}
\tau_1 \\
0 \\
(0) \\
\tau_2 \\
0 \\
(0)
\end{bmatrix}
+
\begin{bmatrix}
(0) \\
P_{b2} + P_{b2}^{\cdot} \\
(0) \\
(0) \\
P_{b3} \\
(0)
\end{bmatrix}
$$

$$(2.35.a)$$

The required "FLM" is given by (2.35.a) together with the following two relations governing the actuators which are obtained from (2.2.d):

$$
\tau_i = \left(\frac{N_i \, K_{m,i}}{R_{a,i}} \right) u_i - (N_i^2 \, J_{m,i}) \, \ddot{\Psi}_i - N_i^2 \left(b_{m,i} + \frac{b_{L,i}}{N_i^2} + \frac{K_{b,i} \, K_{m,i}}{R_{a,i}} \right) \Psi_i
$$

$$(2.35.b)$$

$$i = 1,2$$

The dimensionless form of "FLM" is obtained from (2.35.a) by substituting for the torques (τ_1, τ_2) from (2.35.b). One can define the dimensionless coordinates (X_2, Y_2) for joint 2 and (X_3, Y_3) for the wrist point as follows:

$$X_2 = \left(\frac{x_2}{a_1}\right) \; ; \; Y_2 = \left(\frac{y_2}{a_1}\right) \; ; \; X_3 = \left(\frac{x_3}{a_1}\right) \; ; \; Y_3 = \left(\frac{y_3}{a_1}\right) \qquad (2.36)$$

The dimensionless "FLM" is given by:

$$[M] \, \underline{U}'' + [C] \, \underline{U}' + [K] = \underline{R} \qquad\qquad (2.37)$$

where each of [M], [C] and [K] is an (8×8) symmetric matrix. The vector $\underline{U}$ reads:

$$\underline{U} = [\; \Psi_1 \, , X_2 \, , Y_2 \, , \Psi_2^{\cdot} \, , \Psi_2 \, , X_3 \, , Y_3 \, , \Psi_3^{\cdot} \;]^T \qquad (2.38.a)$$

The nonzero coefficients of the symmetric [M] matrix are denoted by m_{ij} ; i=1,2,...,8 and

j=i,i+1,...,8 and are given by:

$$m_{11} = Y_{31} + N_1^2 \, J_{m,1} \qquad\qquad ; m_{12} = - \, a_1 \, (s_1 \, Y_{51}) \qquad ; m_{13} = a_1 \, (c_1 \, Y_{51})$$

$$m_{14} = - \, a_1 \, (Y_{61})$$

$$m_{22} = a_1 \, (s_1^2 \, Y_{11} + s_2^2 \, Y_{12}) \qquad ; m_{23} = - \, a_1 \, (s_1 \, c_1 \, Y_{11} + s_2 \, c_2 \, Y_{12})$$

$$m_{24} = s_1 \, Y_{21} \quad ; m_{25} = - \, s_2 \, Y_{22} \quad ; m_{26} = a_1 \, (s_2^2 \, Y_{42})$$

$$m_{27} = - \, a_1 \, (s_2 \, c_2 \, Y_{42}) \qquad\qquad ; m_{28} = s_2 \, Y_{52}$$

$$m_{33} = a_1 \, (c_1^2 \, Y_{11} + c_2^2 \, Y_{12}) \qquad ; m_{34} = - \, c_1 \, Y_{21} \qquad\qquad ; m_{35} = c_2 \, Y_{22}$$

$$m_{36} = - \, a_1 (s_2 \, c_2 \, Y_{42}) \qquad\qquad ; m_{37} = a_1 \, (c_2^2 \, Y_{42}) \qquad ; m_{38} = - \, c_2 \, Y_{52}$$

$$m_{44} = Y_{31}$$

$$m_{55} = Y_{32} + N_2^2 \, J_{m,2} \qquad\qquad ; m_{56} = - \, a_1 \, (s_2 \, Y_{52}) \qquad ; m_{57} = a_1 \, (c_2 \, Y_{52})$$

$$m_{58} = - \, Y_{62}$$

$$m_{66} = a_1 \, (s_2^2 \, Y_{12}) \qquad\qquad\qquad ; m_{67} = - \, a_1 \, (s_2 \, c_2 \, Y_{12}) \quad ; m_{68} = s_2 \, Y_{22}$$

$$m_{77} = a_1 \, (c_2^2 \, Y_{12}) \qquad\qquad\qquad ; m_{78} = - \, c_2 \, Y_{22}$$

$$m_{88} = Y_{32}$$

<div align="right">(2.38.b)</div>

The [C] matrix is an all zero matrix except for two diagonal elements given by:

$$c_{1,1} = N_1^2 \left(b_{m,1} + \frac{b_{L,1}}{N_1^2} + \frac{k_{b,1} \, k_{m,1}}{k_{a,1}} \right) \Big/ \, \omega_o$$

$$c_{5,5} = N_2^2 \left(b_{m,2} + \frac{b_{L,2}}{N_2^2} + \frac{k_{b,2} \, k_{m,2}}{k_{a,2}} \right) \Big/ \, \omega_o$$

<div align="right">(2.38.c)</div>

The non-zero coefficients of the symmetric [K] matrix are denoted by k_{ij}; i=1,2,...8 and

j = i,i+1,...8 and are given by:

$$k_{11} = X_{31} / \omega_o^2 \qquad\qquad ; k_{12} = a_1 (s_1 X_{21} / \omega_o^2)$$

$$k_{13} = - a_1 (c_1 X_{21} / \omega_o^2) \qquad ; k_{14} = - X_{41} / \omega_o^2$$

$$k_{22} = a_1 (s_1^2 X_{11} + s_2^2 X_{12}) / \omega_o^2 \quad ; k_{23} = - a_1 (s_1 c_1 X_{11} + s_2 c_2 X_{12}) / \omega_o^2$$

$$k_{24} = (s_1 X_{21}) / \omega_o^2 \qquad\qquad ; k_{25} = - s_2 X_{22} / \omega_o^2$$

$$k_{26} = - a_1 (s_2^2 X_{12}) / \omega_o^2 \qquad ; k_{27} = a_1 (s_2 c_2 X_{12}) / \omega_o^2$$

$$k_{28} = - s_2 X_{22} / \omega_o^2$$

$$k_{33} = a_1 (c_1^2 X_{11} + c_2^2 X_{12}) / \omega_o^2 \quad ; k_{34} = - c_1 X_{21} / \omega_o^2$$

$$k_{35} = c_2 X_{22} / \omega_o^2 \qquad\qquad ; k_{36} = a_1 (s_2 c_2 X_{12}) / \omega_o^2$$

$$k_{37} = - a_1 (c_2^2 X_{12}) / \omega_o^2 \qquad ; k_{38} = c_2 X_{22} / \omega_o^2$$

$$k_{44} = X_{31} / \omega_o^2$$

$$k_{55} = X_{32} / \omega_o^2 \qquad\qquad ; k_{56} = a_1 (s_2 X_{22}) / \omega_o^2$$

$$k_{57} = - a_1 (c_2 X_{22}) / \omega_o^2$$

$$k_{66} = a_1 (s_2^2 X_{12}) / \omega_o^2 \qquad ; k_{67} = - a_1 (s_2 c_2 X_{132}) / \omega_o^2$$

$$k_{68} = s_2 X_{22} / \omega_o^2$$

$$k_{77} = a_1 (c_2^2 X_{12}) / \omega_o^2 \qquad ; k_{78} = - c_2 X_{22} / \omega_o^2$$

$$k_{88} = X_{32} / \omega_o^2 \qquad\qquad\qquad\qquad\qquad (2.38.d)$$

The vector $\underline{R}$ in (2.37) reads:

$$\underline{R} \equiv [(r_1 \ u_1^{\cdot}) \ , \ 0 \ , \ (r \ P_2) \ , \ 0 \ , \ (r_2 \ u_2^{\cdot}) \ , \ 0 \ , \ (r \ P_3) \ , 0 \ ]^T$$

where $u_1^{\cdot}$ and $u_2^{\cdot}$ are defined in (2.4) and

$$P_2 = \frac{p_{b2} + \dot{p}_{b2}}{m_1 \ g} \qquad ; \quad P_3 = \frac{p_{b3}}{m_1 \ g}$$

$$r_1 = \frac{N_1 \ K_{m,1} \ E_0}{R_{a,1} \ \omega_o^2} \qquad ; \quad r = \frac{m_1 \ g}{\omega_o^2} \qquad ; \quad r_2 = \frac{N_2 \ k_{m,2} \ E_0}{R_{a,2} \ \omega_o^2} \qquad (2.38.e)$$

2.7 SUMMARY

In this chapter, the RAM, the FJM and the FLM models have been developed and casted in compact dimensionless forms. The models can be used for future investigations pertaining to the dynamics and the controls of the elbow arm. Considerable care was taken to define each coefficient in the models in terms of the physical parameters of the manipulator. This makes the model reliable and realistic.

CHAPTER 3

THE NONLINEAR INTEGRATED TABULAR

(NIT) CONTROL

3.1 OBJECTIVES

In this chapter, a new strategy is developed for tracking continuous and discontinuous trajectories. The method is based on adequate algorithms for the evaluation of the command voltages, in tabular form, which guarantee that the wrist point will follow a prescribed trajectory. The control strategy takes into account the nonlinearities inherent in the model as well as the flexibility of the joints or the links. For this reason, the new strategy is referred to as the NONLINEAR INTEGRATED TABULAR (NIT) Control. The NIT Control is simple, accurate, stable, computationally economical and can be easily implemented in practical systems in the real-time.

Realistic mathematical models for the elbow arm were established in the previous chapter. Some of these models are used here to develop the NIT Control. To that end the elbow arm is treated as open loop system, i.e. the command voltages are constructed from the sole knowledge of the desired trajectory and its kinematics and without taking into account the actual outputs of the elbow arm. The transient response of the wrist point is also assessed in this chapter by considering the case when the brakes are applied to bring the

motors to a sudden stop during tracking.

3.2 REFERENCE PARAMETERS

The reference parameters, used to test NIT Control, are chosen as close as possible to the parameters of the experimental setup described in a later chapter. The stiffness-coefficients of the harmonic drives are deliberately varied around their nominal values to study their role in the dynamics of the elbow arm. The reference parameters are:

$$g = 9.81 \ m/s^2$$
$$a_1 = a_2 = 0.305 \ m \qquad ; a_{c1} = a_{c2} = 0.145 \ m$$
$$m_1 = m_2 = 4.803 \ kg \qquad ; I_1 = I_2 = 0.025 \ kg.m^2$$
$$A_1 = A_2 = 0.001 \ m^2 \qquad ; I_1^{\cdot} = I_2^{\cdot} = 0.4996 \times 10^{-7} \ m^4$$
$$E = 0.68 \times 10^{11} \ N/m^2 \qquad ; \rho = 2700 \ kg/m^3$$
$$N_1 = N_2 = 100 \qquad ; K_{h1} = K_{h2} = 209.8 \ N.m/rad$$
$$J_{m1} = J_{m2} = 0.9532 \times 10^{-4} \ kg.m^2$$
$$b_{m1} = b_{L1} = 0.687 \ N.m/rad/s \qquad ; b_{m2} = b_{L2} = 0.687 \ N.m/rad/s$$
$$K_{m1} = K_{m2} = 0.142 \ N.m/amps \qquad ; K_{b1} = K_{b2} = 0.3952 \ V/rad/s$$
$$R_{a1} = R_{a2} = 0.84 \ ohms \qquad ; E_0 = 100 \ V$$

$$(3.1)$$

The values of K_{h1} and K_{h2} are selected much lower than the stiffness of the actual harmonic drives used today. This choice is deliberately made to amplify the effect of the compliance of the joint which have to be faced in future designs of the elbow arm.

3.3 METHODOLOGY OF NIT CONTROL

The diagram in Figure (3.1) depicts the basic steps which are followed in this chapter to develop NIT controls for the elbow arm. Each step is discussed in some details in the sections that follow:
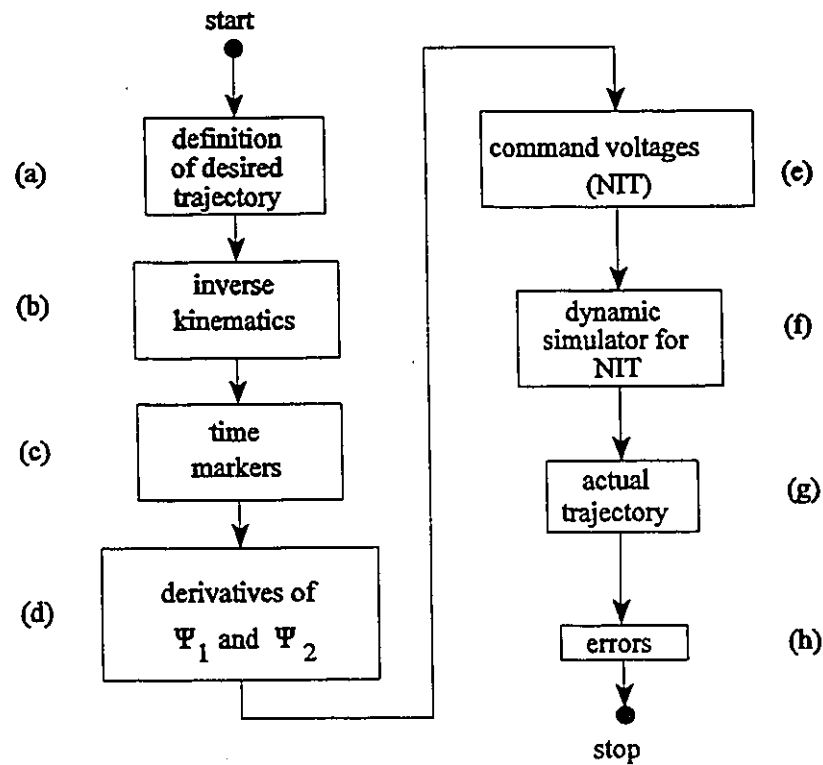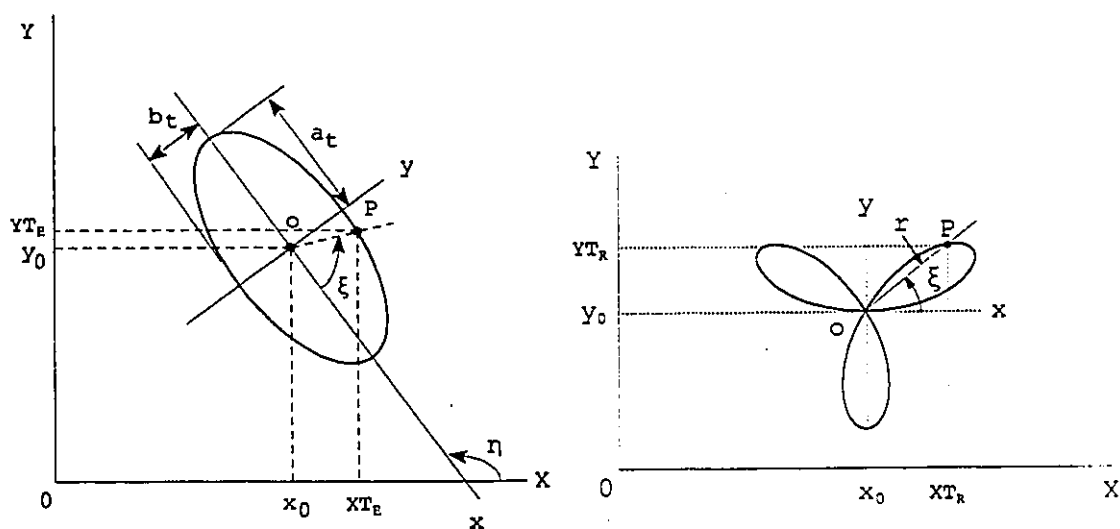

Figure 3.1: Strategy of NIT Control and its validation.
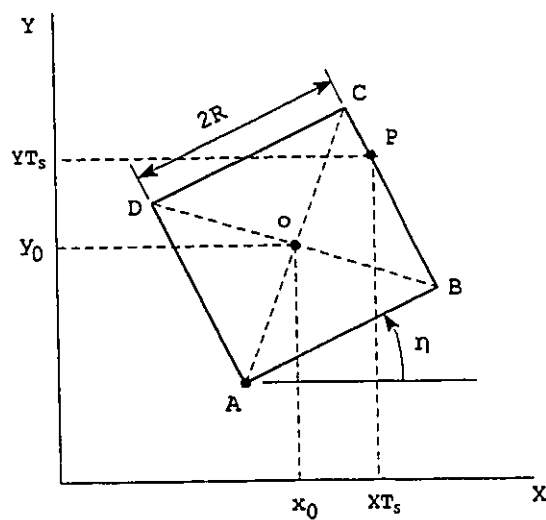
3.4 THE DESIRED TRAJECTORY

Three trajectories are selected to represent continuous and discontinuous paths. An ellipse, a three-leaved rose and a square are typical cases. The basic parameters for each are

as indicated in Figure (3.2).

(a) Ellipse

(b) Three-leaved rose

(c) Square

Figure 3.2: Desired trajectories.

The coordinates $(XT)_E$, $(YT)_E$ of a point P on the ellipse can be shown to be given by:

$$(XT)_E = x_0 + \frac{R}{\sqrt{2}} (\sin \xi + \cos \xi)$$

$$(YT)_E = y_0 + \frac{R}{\sqrt{2}} (\sin \xi - \cos \xi)$$

$$R = \frac{a_t \, b_t}{\sqrt{b_t^2 \cos^2 \xi + a_t^2 \sin^2 \xi}}$$

$$for \ 0 \leq \xi \leq 2 \pi \ and \ \eta = 3 \, \frac{\pi}{4} \tag{3.2.a}$$

x_0 and y_0 are the coordinates of the center of the ellipse. a_t and b_t are the semi major and semi minor axes respectively. η and ξ are angles as shown in Figure (3.2.a).

The coordinates $(XT)_R$, $(YT)_R$ of P on the three-leaved rose are given by:

$$(XT)_R = x_0 + r \cos \xi$$

$$(YT)_R = y_0 + r \sin \xi$$

$$r = R \cos (3 \, \xi)$$

$$for \ 0 \leq \xi \leq 2 \pi \ and \ R = constant \tag{3.2.b}$$

x_0 and y_0 are the coordinates of the center of the rose and ξ is an angle as shown in Figure (3.2.b).

The coordinates of $(XT)_S$, $(YT)_S$ of P on the square are obtained by using the following relations:

$$(XT)_S = x^* \cos \eta - y^* \sin \eta + x_0$$

$$(YT)_S = y^* \cos \eta + x^* \sin \eta + y_0 \tag{3.2.c}$$

where (x_0, y_0) are the coordinates of the center of the square and η is the tilt angle shown in Figure 3.2.c. The x^*, y^* are obtained as follows:

$$
\begin{aligned}
side \ \overline{AB} \ &: \ -R \leq x^* \leq +R \quad ; \quad y^* = -R \\
\overline{BC} \ &: \quad\quad x^* = R \quad ; \ -R \leq y^* \leq +R \\
\overline{CD} \ &: \ -R \leq x^* \leq +R \quad ; \quad y^* = R \\
\overline{DA} \ &: \quad\quad x^* = -R \quad ; \ -R \leq y^* \leq +R
\end{aligned}
\tag{3.2.d}
$$

3.5 THE INVERSE KINEMATICS PROBLEM

Step (b) in Figure (3.1) calls for the evaluation of the angles Ψ_1 and Ψ_2 when the coordinates (XT,YT) of the wrist point are known. The Denavit-Hartenberg (D-H) notations are adopted for our analysis and are as depicted in Figure 3.3 for a full 3-link elbow arm. Given the desired cartesian coordinates (X,Y,Z) of the wrist point, i.e. of the point O_3 in the world's coordinates, one can define the associated joint angles θ_1, θ_2 and θ_3 using the following relations [43]:
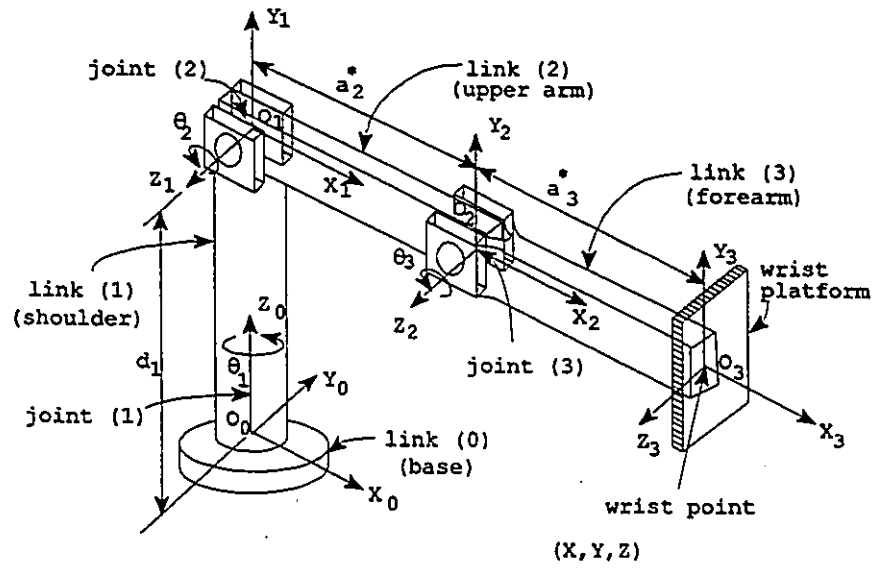
Figure 3.3: The D-H notations.

$$\theta_1 = \tan^{-1} (Y / X)$$

$$\theta_2 = \tan^{-1} \left\{ \left(\pm \frac{\beta_2}{\sqrt{\beta_1^2 - \beta_2^2 + Z^2}} \right) \right\} - \tan^{-1} \{ \beta_1 / Z \}$$

$$\theta_3 = \tan^{-1} \left\{ \frac{Z - a_2^{\cdot} s_2^{\cdot}}{\beta_1 - a_2^{\cdot} c_2} \right\} - \theta_2$$

$$\beta_1 = \sqrt{X^2 + Y^2} \ ; \ \beta_2 = \frac{\beta_1^2 + Z^2 + a_2^{\cdot 2} - a_3^{\cdot 2}}{2 \, a_2^{\cdot 2}}$$

$$c_2^{\cdot} = \cos \, \theta_2 \ ; \ s_2^{\cdot} = \sin \, \theta_2$$

where :

$$X = XT \ ; \ Y = 0 \ ; \ Z = YT$$

$a_2^{\cdot}$ *and* $a_3^{\cdot}$ *are as shown   in Fig* .(3.3).   (3.3)

Due to the absence of θ_1 in the elbow arm under study, it is obvious that Ψ_1 is equivalent to θ_2 and Ψ_2 to $(\theta_1 + \theta_2)$. The vectors Ψ_1 and Ψ_2 are evaluated using XT and YT of the desired trajectory and relations (3.3). The vectors Ψ_1 and Ψ_2 are stored in tabular form in arrays YY2(I) and YY4(I) respectively for I=1, 2, ...Np where Np is the number of points on the trajectory.

The coordinates of the desired trajectory, as obtained from the inverse kinematic solution, are denoted by XTT(I) and YTT(I) and are given by:

$$XTT(I) = a_1 \cos \Psi_1(I) + a_2 \cos \Psi_2(I)$$

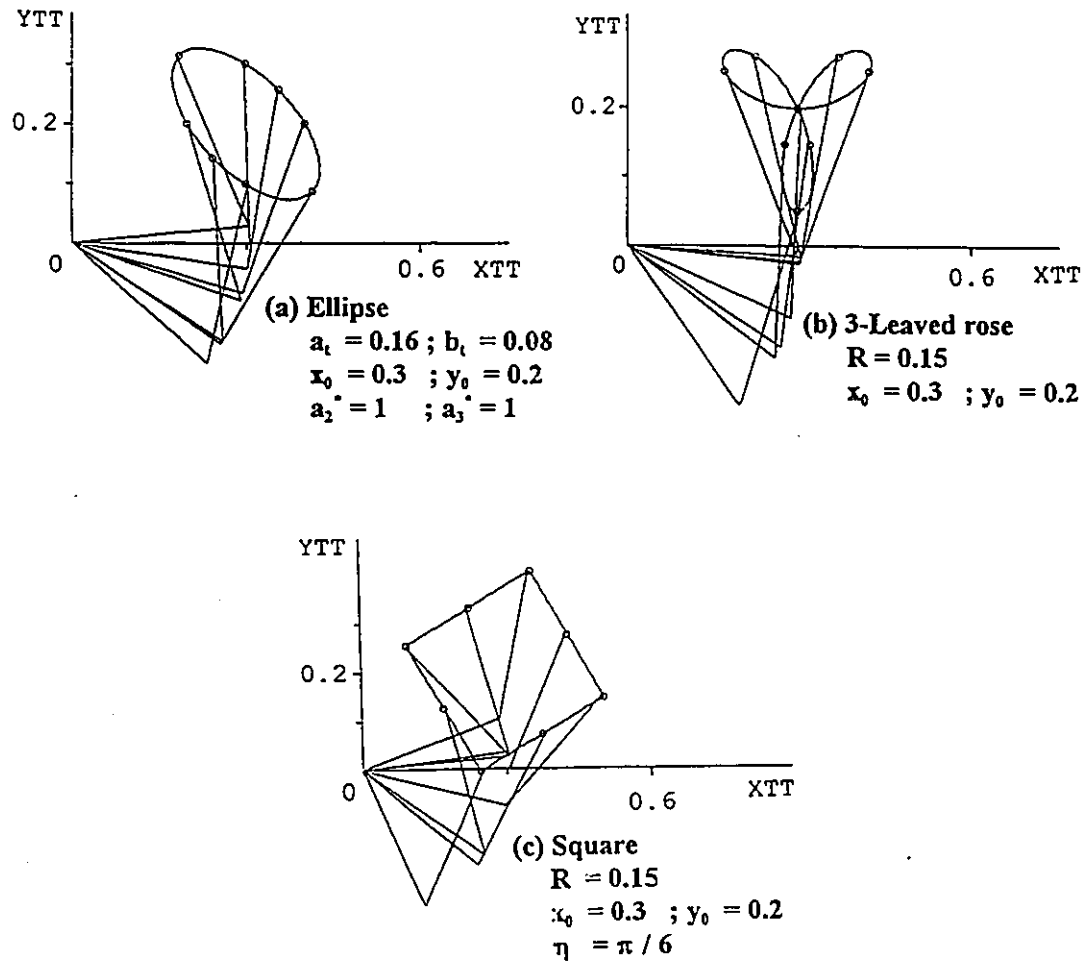$$YTT(I) = a_1 \sin \Psi_1(I) + a_2 \sin \Psi_2(I)$$

$$(3.4)$$

Figure (3.4) demonstrates the plots of (XT,YT) and (XTT,YTT) on top of each other for the ellipse, rose and square. The coordinates (XT,YT) and (XTT,YTT) are practically identical as expected.

3.6 TIME MARKERS

Step (c) in Figure (3.1) requires that dimensionless time (T) to be assigned to the trajectory points. A constant tracking velocity V along the trajectory, is assumed. One considers two consecutive points on the trajectory (i) and (i+1) which are associated with the times $(T)_i$ and $(T)_{i+1}$ respectively. One can thus write:

$$(T)_{i+1} = (T)_i + \left[\{ XT(I+1) - XT(I) \}^2 + \{ YT(I+1) - YT(I) \}^2 \right]^{1/2} / V$$

$$(3.5)$$

The reference point, i.e. position 1 is associated with T = 0.

(a) Ellipse
$a_t = 0.16$; $b_t = 0.08$
$x_0 = 0.3$; $y_0 = 0.2$
$a_2^{\cdot} = 1$; $a_3^{\cdot} = 1$

(b) 3-Leaved rose
$R = 0.15$
$x_0 = 0.3$; $y_0 = 0.2$

(c) Square
$R = 0.15$
$x_0 = 0.3$; $y_0 = 0.2$
$\eta = \pi / 6$

All coordinates above in meters.

Figure 3.4: Inverse Kinematics.

3.7 DERIVATIVES OF Ψ_1 AND Ψ_2 VECTORS

Step (d) in Figure (3.1) calls for the numerical evaluation of the first and second

derivatives of Ψ_1 and Ψ_2. To achieve this task with the minimum generation of numerical

noise, a cubic polynomial is fitted to every three consecutive points on the trajectory. The

parabola is used to extract information only at the middle point of the span. Figure (3.5)

shows the variables used to construct the algorithm.
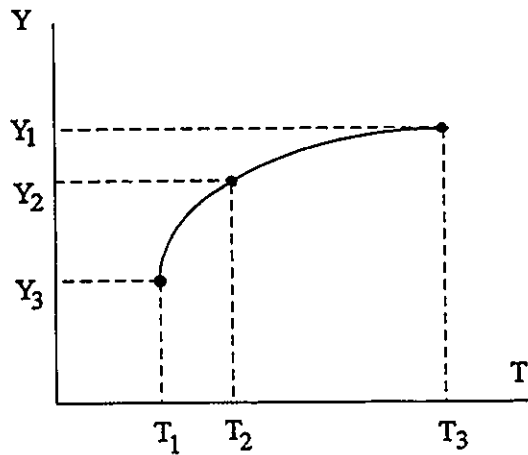

Figure 3.5: Cubic polynomial for derivatives.

A polynomial is assumed in the form:

$$Y^* = a_0 + a_1 T + a_2 T^2 \tag{3.6.a}$$

The coordinates (T1, Y_1^*), (T$_2$,Y$_2^*$) and (T$_3$,Y$_3^*$) have to satisfy (3.6.a). One can thus write:

$$\begin{bmatrix} a_0 \\ a_1 \\ a_2 \end{bmatrix} = \frac{1}{\sigma_1\,\sigma_2\,\sigma_3} \begin{bmatrix} T_2\,T_3\,\sigma_1 & -\,T_1\,T_3\,\sigma_2 & T_1\,T_2\,\sigma_3 \\ -\,(T_2 + T_3)\,\sigma_1 & (T_1 + T_3)\,\sigma_2 & -\,(T_1 + T_2)\,\sigma_3 \\ \sigma_1 & -\,\sigma_2 & \sigma_3 \end{bmatrix} \begin{Bmatrix} Y^{\cdot}_1 \\ Y^{\cdot}_2 \\ Y^{\cdot}_3 \end{Bmatrix}$$

where :

$$\sigma_1 = T_3 - T_2 \; ; \; \sigma_2 = T_3 - T_1 \; ; \; \sigma_3 = T_2 - T_1 \tag{3.6.b}$$

The derivatives of the middle point $(T_2, Y_2^{\cdot})$ are given by:

$$Y_2^{\prime} = a_1 + 2\,a_2\,T_2 \; ; \; Y_2^{\prime\prime} = 2\,a_2 \tag{3.6.c}$$

It should be noticed that the cubic curve fitting is not the only possible approach. One can use Chebyshev polynomials in the case of larger intervals between tabular points and the derivatives are evaluated directly from the resulting Chebyshev coefficients. For noisy data one can use Savitzky-Golay smoothing filters [59].

To assess the degree of smoothness of the algorithm proposed by relations (3.6), Figures (3.6), (3.7) and (3.8) are prepared for the ellipse, the rose and the square trajectories respectively for v = 0.3 m/s and ω_0=5.671 rad/s. It is noticed that numerical differentiation was achieved almost free of noise for the ellipse and the rose. Sharp spikes were noticed for the second derivatives in the case of the square. As expected, the spikes appear at the corner points of the square because of the associated sudden changes of the first derivatives of Ψ_1 and Ψ_2 at these points. As will be shown later, these spikes neither degrade the simulation for the rest of the points on the square path, nor degrade the quality of control of the tracking.
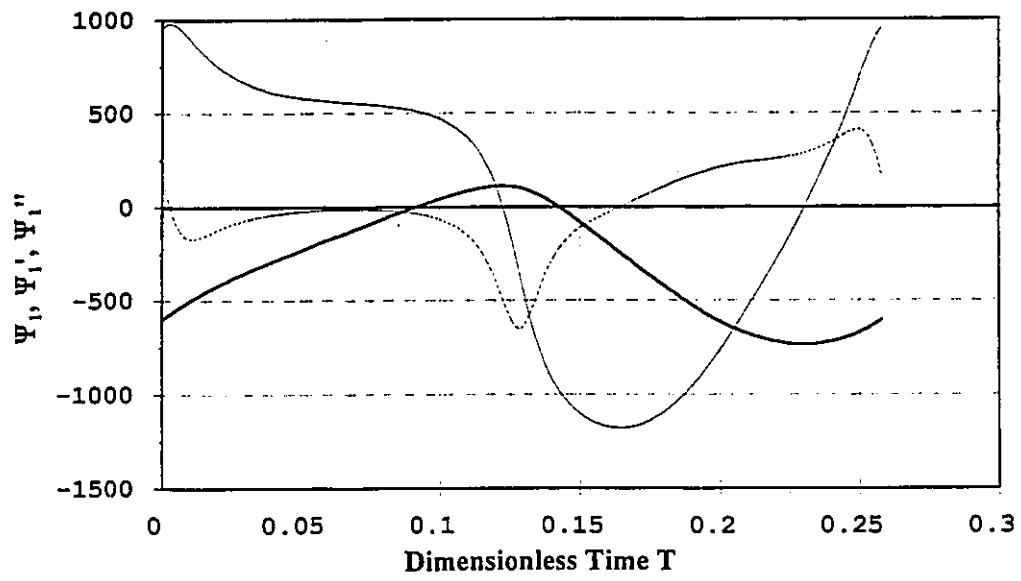
(a) — $\Psi_1 \times 1000$ — $\Psi_1' \times 100$ ----- Ψ_1''

(a) Ψ_1 and derivatives
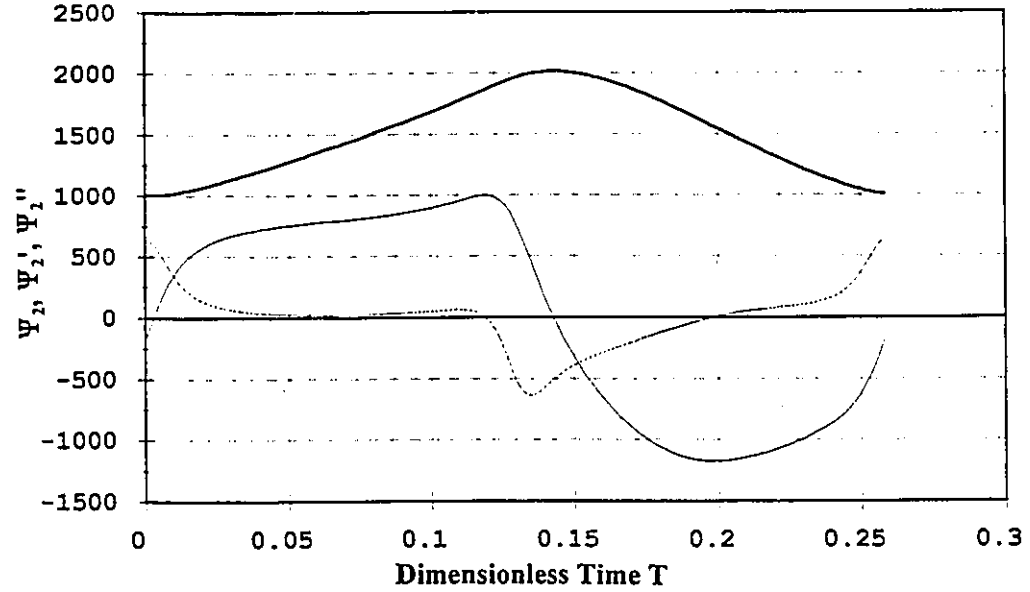
(b) — $\Psi_2 \times 1000$ — $\Psi_2' \times 100$ ----- Ψ_2''

(b) Ψ_2 and derivatives.

Figure 3.6: Ψ_1, Ψ_2 and derivatives (ellipse).

(a) Ψ_1 and derivatives.

(b) Ψ_2 and derivatives.

Figure 3.7: Ψ_1, Ψ_2 and derivatives (3-leaved-rose).

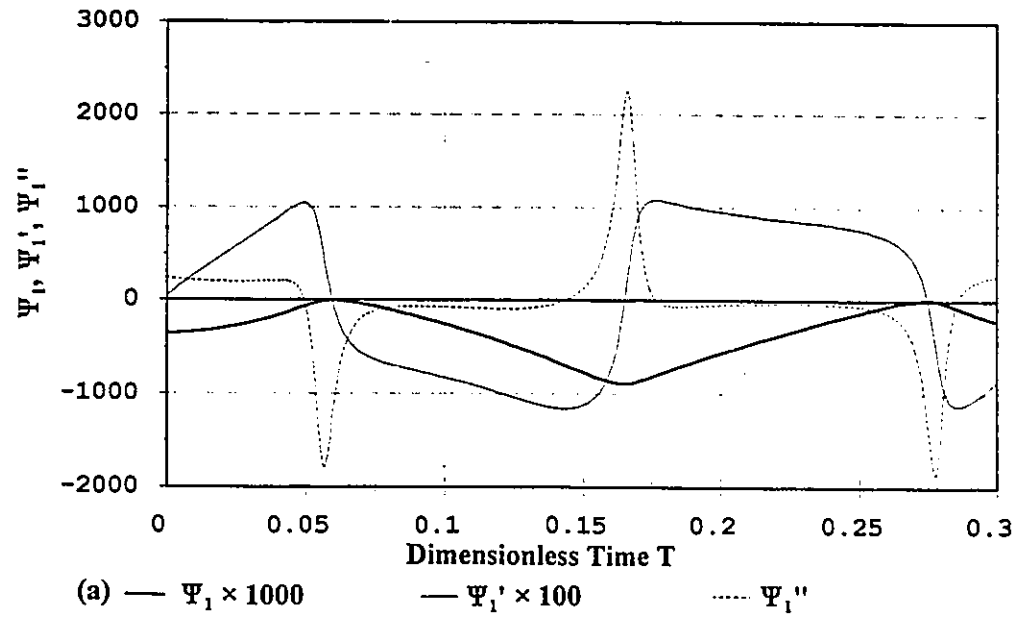(a) —— $\Psi_1 \times 10000$ —— $\Psi_1' \times 1000$ ----- Ψ_1''
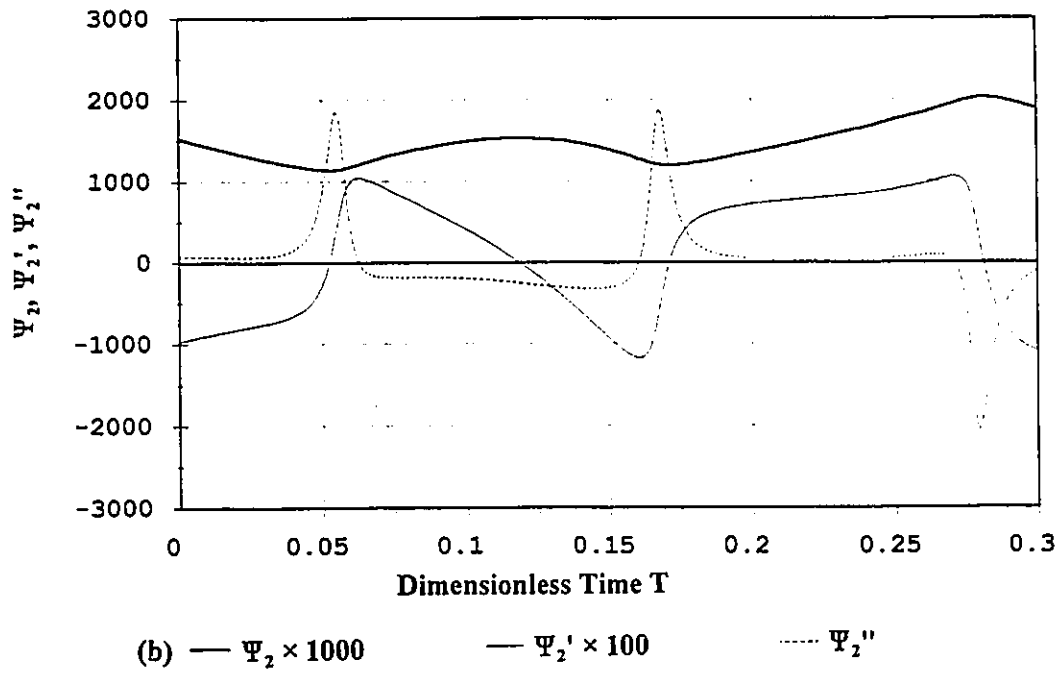
(a) Ψ_1 and derivatives.
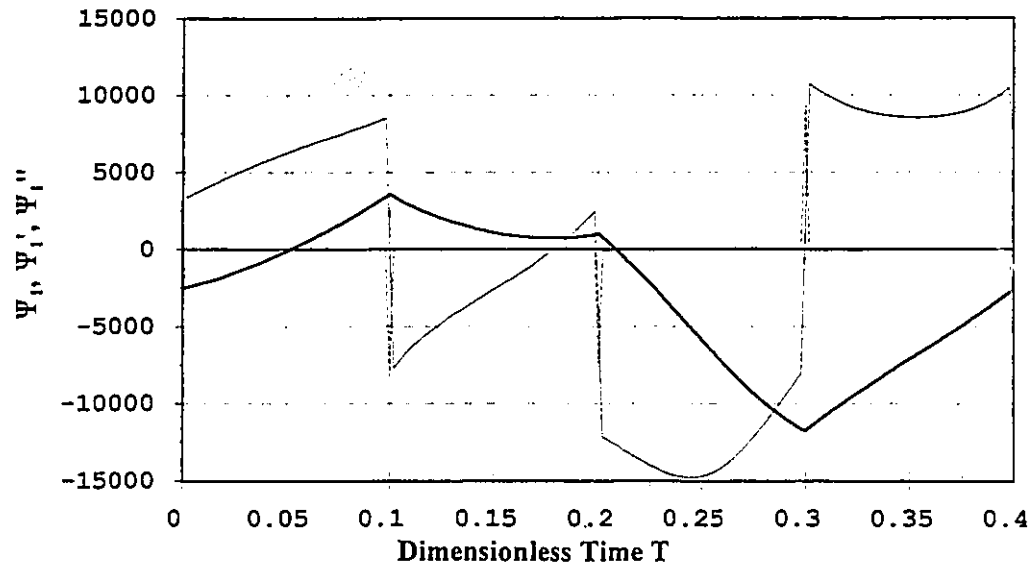

(b) —— $\Psi_2 \times 10000$ —— $\Psi_2' \times 1000$ ----- Ψ_2''

(b) Ψ_2 and derivatives.

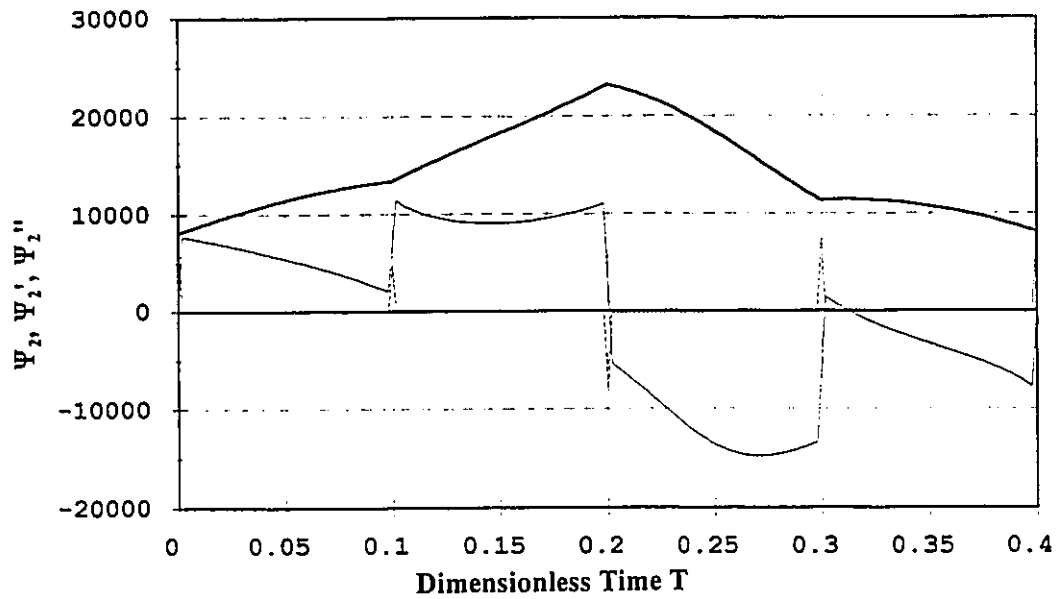Figure 3.8: Ψ_1, Ψ_2 and derivatives (square).

3.8 COMMAND VOLTAGES (NIT)

Step (e) calls for the evaluation of the command voltages.

(a) For the case of "RAM" given by equations (2.17), the command voltages u_1^* and u_2^*, i.e. NIT, are given by:

$$u_1^* = \frac{1}{\mu_1} \{\Psi_1'' + a_{11} \Psi_1' + a_{12} c_{21} \Psi_2'' - a_{12} s_{21} (\Psi_2')^2 + a_{13} c_1\}$$

$$u_2^* = \frac{1}{\mu_2} \{\Psi_2'' + a_{21} \Psi_2' + a_{22} c_{21} \Psi_1'' + a_{22} s_{21} (\Psi_1')^2 + a_{23} c_2\} \qquad \text{(3.7.a)}$$

Every quantity on the R.H.S. of the previous relations is known or has been evaluated in the previous step. One can thus use relations (3.7.a) to define u_1^* and u_2^* at every point on the trajectory. Figure (3.9) demonstrates the command voltages (NIT) required for tracking an ellipse, a rose and a square.

(b) For the case of the FJM given by (2.19) additional steps have to be executed before computing the command voltages. This is due to the appearance of ϕ_1 and ϕ_2 and their derivatives in the model. An examination of the model shows that ϕ_1 and ϕ_2 can be evaluated using:

$$\phi_1 = \frac{1}{b_{23}} \{\Psi_1'' + b_{21} \Psi_1' + \omega_2^2 \Psi_1 + b_{22} c_{21} \Psi_2'' - b_{22} s_{21} (\Psi_2')^2 + b_{24} c_1\}$$

$$\phi_2 = \frac{1}{b_{43}} \{\Psi_2'' + b_{41} \Psi_2' + \omega_4^2 \Psi_2 + b_{42} c_{21} \Psi_1'' + b_{42} s_{21} (\Psi_1')^2 + b_{44} c_2\} \qquad \text{(3.7.b)}$$
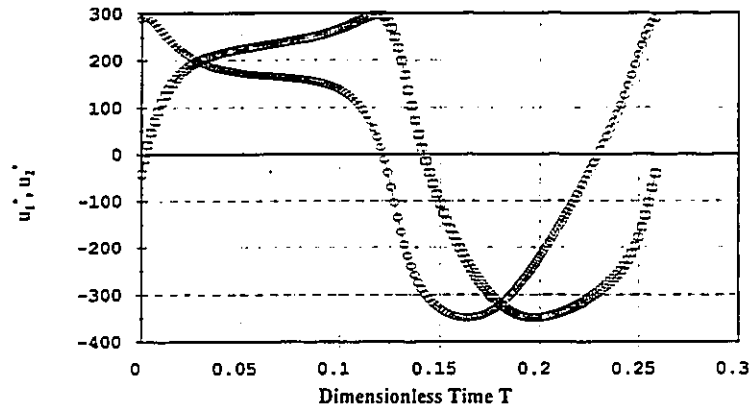
Every quantity on the R.H.S. of the previous relations is known or has been evaluated before. One can thus use (3.7.b) to define ϕ_1 and ϕ_2 at every point on the trajectory.

(a) Ellipse. $-\bullet-$ $u_1^{\bullet}$ $-\bullet-$ $u_2^{\bullet}$
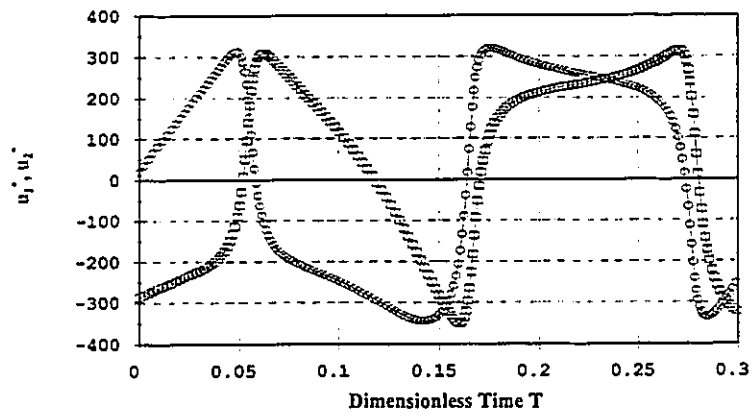
(b) Rose. $-\bullet-$ $u_1^{\bullet}$ $-\circ-$ $u_2^{\bullet}$
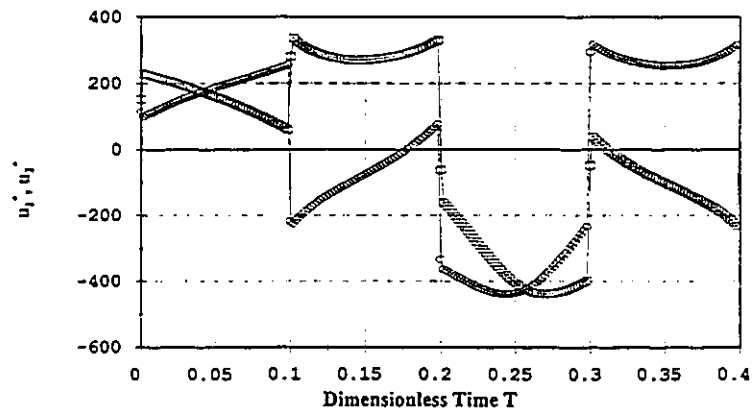
(c) Square. $-\bullet-$ $u_1^{\bullet}$ $-\bullet-$ $u_2^{\bullet}$

Figure 3.9: Command voltages (NIT) for (RAM).

The first and second derivatives of ϕ_1 and ϕ_2 can be obtained using cubic curve fitting.

With (ϕ_1, ϕ_1' and ϕ_1'') and (ϕ_2, ϕ_2' and ϕ_2'') available one can use relations (2.19.a) and (2.19.c) to evaluate the control voltages u_1^* and u_2^*, i.e. NIT, as follows:

$$u_1^{\cdot} = \frac{1}{\mu_1^c} \{\phi_1'' + b_{11} \phi_1' + \omega_1^2 \phi_1 - b_{12} \Psi_1\}$$

$$u_2^{\cdot} = \frac{1}{\mu_2^0} \{\phi_2'' + b_{31} \phi_2' + \omega_3^2 \phi_2 - b_{32} \Psi_2\} \tag{3.7.c}$$

Relations (3.7.c) are used to evaluate the command voltages at every point on the trajectory.

Figure (3.10.a) and (3.10.b) is a time history for ϕ_1 and ϕ_2 and their derivatives for an arm tracking an ellipse with flexibility in the joints. The higher derivatives are noticed to be contaminated with numerical noise. This is rather expected because they are the outcome of four successive numerical differentiations. In spite of the presence of this numerical noise, the associated command voltages, shown in Figure (3.10.c) are almost noise-free.

(c) For the case of "FLM", one can extend the previous strategies to extract the command voltages. The steps in this case are as follows:

    (i) The coordinates XT(I) and YT(I) of the points on the desired trajectory are essentially the state variables X3 and Y3 which appear in the FLM given by equation (2.37).
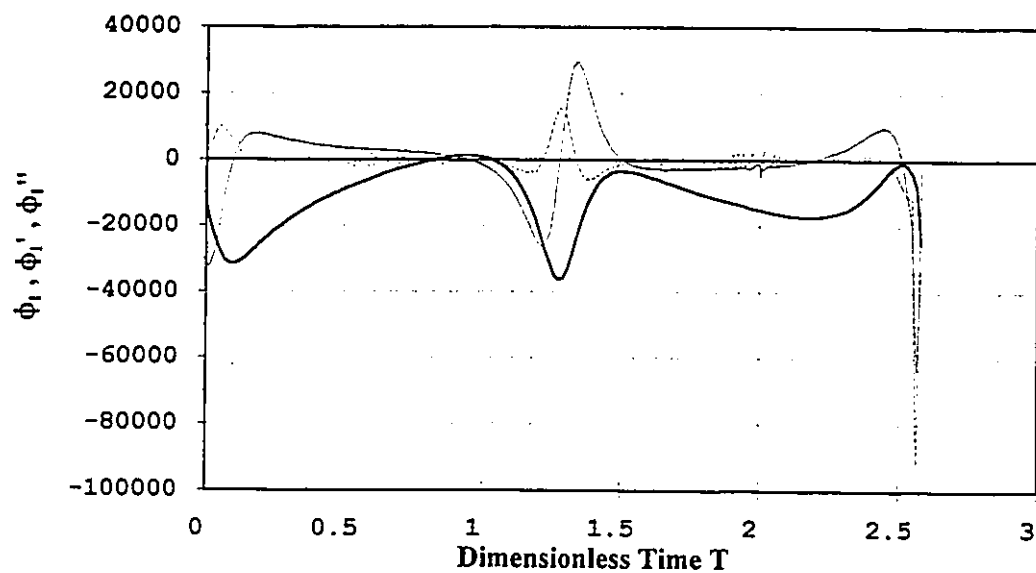
(a) —— $\phi_1 \times 500$ —— $\phi_1' \times 50$ ······ ϕ_1''
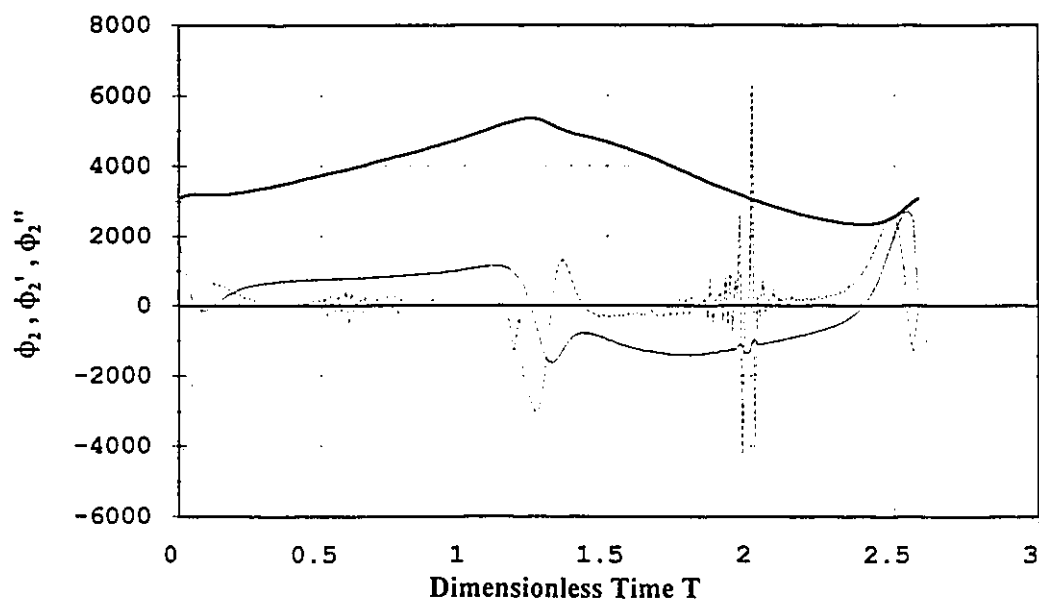
(b) —— $\phi_2 \times 25$ ——$\phi_2' \times 10$ ······ ϕ_2''

Figure 3.10: Ψ_1 and Ψ_3 command voltages (FJM) - ellipse.
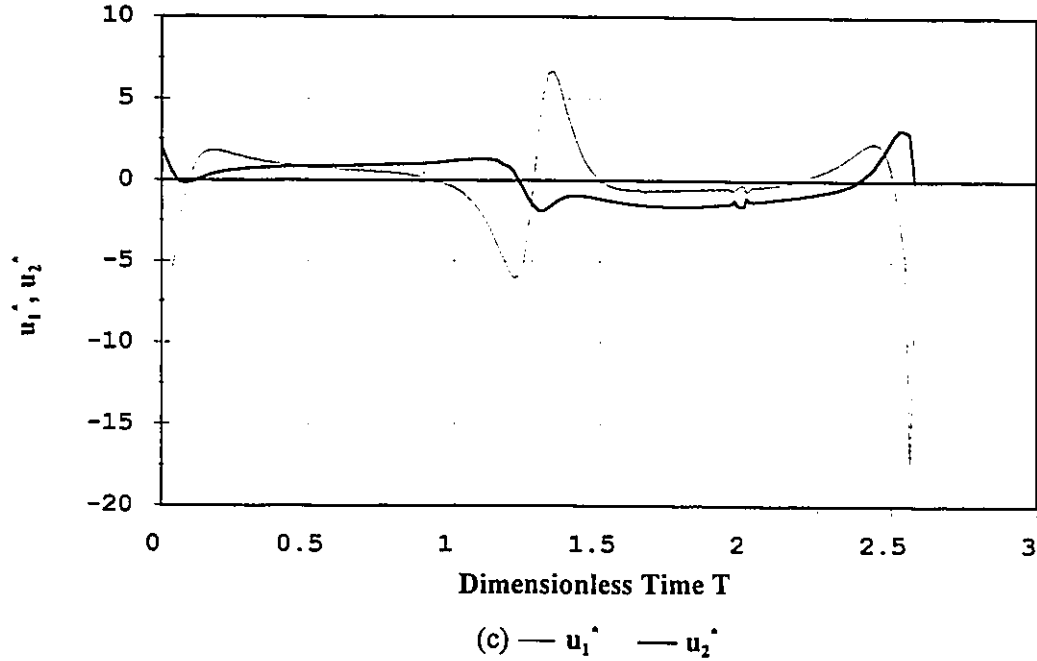
Figure 3.10: Ψ_1 and Ψ_3 command voltages (FJM) - ellipse.

(ii) Using the inverse kinematic algorithm (3.3), one can obtain Ψ_1 and Ψ_2 at every point on the trajectory.

(iii) The coordinates X_2, Y_2 of joint 2 can be obtained for every point on the trajectory using:

$$X_2 = a_1 \cos \Psi_1$$

$$Y_2 = a_1 \sin \Psi_1 \tag{3.8.a}$$

(iv) By now the following quantities are evaluated in tabular form:

Using cubic curve fitting one can evaluate the first and second derivatives of the previous variables at every point on the desired trajectory.

(v) An examination of the matrix relation given by (2.37) shows that only the first and fifth equations contain informations regarding u_1^* and u_2^*. Dropping these two equations from the FLM model and rearranging the remaining six equations, one obtains:

$$[A^0]\{\underline{\Psi}^0\} = \{\underline{b}^0\} \tag{3.8.b}$$

where $[A^0]$ is a (6×6) matrix and $\{\underline{b}^0\}$ is a (6×1) vector whose elements are already known as functions of:

$$[\Psi_1, X_2, Y_2, \Psi_2, X_3, Y_3]^T$$

and their derivatives. The $\{\Psi^0\}$ vector is defined as a (6×1) vector given by:

$$\underline{\Psi}^0 = [\Psi_1^*, \Psi_1^{*\prime}, \Psi_1^{*\prime\prime}, \Psi_2^*, \Psi_2^{*\prime}, \Psi_2^{*\prime\prime}] \tag{3.8.c}$$

(vi) Solving for $\{\underline{\Psi}^0\}$ using (3.8.b), one can evaluate the quantities $\Psi_2^*(I)$ and $\Psi_3^*(I)$ and their derivatives at every point on the trajectory.

(vii) Finally, one picks up the first and fifth equations in the model which have been dropped before to write NIT:

$$u_1^* = \frac{1}{r_1} \{[m_{11} \Psi_1'' + m_{12} X_2'' + m_{13} Y_2'' + m_{14} \Psi_2''] +$$

$$\left[\frac{N_1^2}{\omega_0^2}\left(b_{m,1} + \frac{b_{L,1}}{N_1^2} + \frac{K_{m,1}}{R_{a,1}}\right)\right]\Psi_1' + [k_{11} \Psi_1 + k_{12} X_2 + k_{13} Y_2 + k_{14} \Psi_2^*]\}$$

$$u_2^* = \frac{1}{r_2} \{[m_{25} X_2'' + m_{35} Y_2'' + m_{55} \Psi_2'' + m_{56} X_3'' + m_{57} Y_3'' + m_{58} \Psi_1''] +$$

$$\left[\frac{N_2^2}{\omega_0^2}\left(b_{m,2} + \frac{b_{L,2}}{N_2^2} + \frac{K_{m,2}}{R_{a,2}}\right)\right]\Psi_2' + [k_{25}X_2 + k_{35} Y_2 + k_{55} \Psi_2 + k_{56} X_3 + k_{57} Y_3 + k_{58} \Psi_3^*]\}$$

$$\tag{3.8.d}$$

All the quantities on the R.H.S. of (3.8.d) have been evaluated before.

3.9 DYNAMIC SIMULATOR: (NIT) FOR (RAM)

Relations (2.17) are integrated starting with a given initial point in the state space. In its canonic form, the mathematical model reads:

$$X_1' = X_2$$

$$X_2' = -a_{11} X_2 - a_{12} \cos(X_3 - X_1) X_4' + a_{12} \sin(X_3 - X_1) X_4^2 - a_{13} \cos X_1 + \mu_1 u_1^*$$

$$X_3' = X_4$$

$$X_4' = -a_{21} X_4 - a_{22} \cos(X_3 - X_1) X_2' - a_{22} \sin(X_3 - X_1) X_2^2 - a_{23} \cos X_3 + \mu_2 u_2^*$$

$$(3.9.a)$$

where the state vector $[\ \Psi_1, \Psi_1', \Psi_2, \Psi_2'\ ]^T$ is written as $[\ X_1, X_2, X_3, X_4\ ]^T$.

The model has the following features:

(a) It contains strong nonlinear terms:

$$\cos X_1, \cos X_3, \cos(X_3 - X_1), \sin(X_3 - X_1), X_2^2, X_4^2$$

(b) The explicit appearance of X_2' and X_4' on the R.H.S. of equations (3.9.a) can cause numerical problems.

(c) u_1^* and u_2^* are available only in tabular form. They are defined at instants which are not equidistant.

A number of explicit and implicit algorithms were considered for the RAM. The most appropriate was found to be a variable step Rung-Kutta. The adopted algorithm was found to be numerically stable and reasonably accurate at an acceptable computing cost.

Relations (3.9.a) are written in the conventional form:

$$X' = f(X) \ , \ X(0) = X_0 \tag{3.9.b}$$

The Rung-Kutta algorithm advances the solution X_n at $T=T_n$, to X_{n+1}, at $T=T_{n+1}$ where,

$$(T)_{n+1} - (T)_n = h$$

The algorithm reads:

$$X_{n+1} = X_n + \frac{h}{6} \left[K_1 + 2K_2 + 2 K_3 + K_4 \right]$$

where :

$$K_1 = f(X_n) \ ; \ K_2 = f(X_n + \frac{h}{2} K_1) \ ; \ K_3 = f(X_n + \frac{h}{2} K_2) \ ; \ K_4 = f(X_n + h K_3)$$

$$\tag{3.9.c}$$

h is the substep size which varies from one segment to the other as depicted in Figure (3.11). The flow diagram representation of the validation strategy is as shown in Figure 3.12. The basic strategy of simulation is summarized as follows:

(a) The time span between two consecutive positions, i.e. from $(T)_i$ to $(T)_{i+1}$ is divided into a number of equal substeps h. The substep size h varies from one span to the other.

(b) From the tabulated values of u_1^* and u_2^*, linear interpolation is used to update the value of the command voltages at the start of each substep h.

(c) At the start of each substep, the following quantities are updated and then held fixed
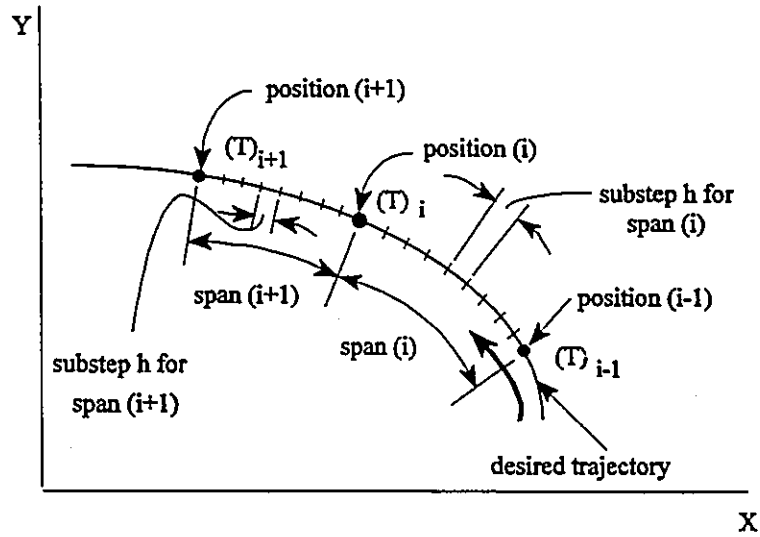
Figure 3.11: The substep h.

during the four function evaluations: $\underline{K}_1$, $\underline{K}_2$, $\underline{K}_3$ and $\underline{K}_4$. These quantities are:

$$\cos X_1, \; \cos X_3, \; \cos(X_3 - X_1), \; \sin(X_3 - X_1), \; X_2^2, \; X_4^2$$

(d) The terms X_2' and X_4' which appear in (3.9.a) are updated at the start of each substep using the backward differences of X_2 and X_4 as follows:

$$(X_2')_n = \left\{ \frac{(X_2)_n - (X_2)_{n-1}}{h} \right\} \; ; \; (X_4')_n = \left\{ \frac{(X_4)_n - (X_4)_{n-1}}{h} \right\} \qquad \textbf{(3.9.d)}$$

(e) To be able to use relations (3.9.d) recursively, one should evaluate X_2' and X_4', the first time, from another source. Combining the second and fourth relations in (3.9.a), one obtains:

start

```
read
fixed data
```

```
define trajectory
XT(KK),YT(KK)
```

KK=1,M

```
inverse
kinematics
$\Psi_1$(KK),$\Psi_2$(KK)
```

KK=1,M

```
first and second
derivatives of
$\Psi_1$(KK),$\Psi_2$(KK)
```

KK=1,M

```
NIT
$u_1^*$(KK),$u_2^*$(KK)
```

KK=1,M

```
set initial conditions
$X_0$(I)
```

I=1,4

```
Evaluate coefficients
$a_{11}$,$a_{12}$,$a_{13}$,$\mu_1$
$a_{21}$,$a_{22}$,$a_{23}$,$\mu_2$
```

```
Evaluate
H,$\Delta u_1^*$,$\Delta u_2^*$
$(u_1)_0(u_2)_0$
```

```
Update
$c_1$,$c_2$,$C_{21}$,$S_{21}$,$X_2^2$,$X_4^2$
$u_1^* = (u_1)_0 + \Delta u_1^*$
$u_2^* = (u_2)_0 + \Delta u_2^*$
```

```
Rung's vectors
using current values
of H Eq.(3.9)
```

N=1,4

```
Advance Solution
one substep H
$X_{N+1}$
replace
$X_N = X_{N+1}$
```

JJ=1,NS

```
Store X in XXX
Evaluate actual Trajectory
XTTT(KK),YTTT(KK)
```

KK=1,M

```
Evaluate
error percentage
```

KK=1,M

stop
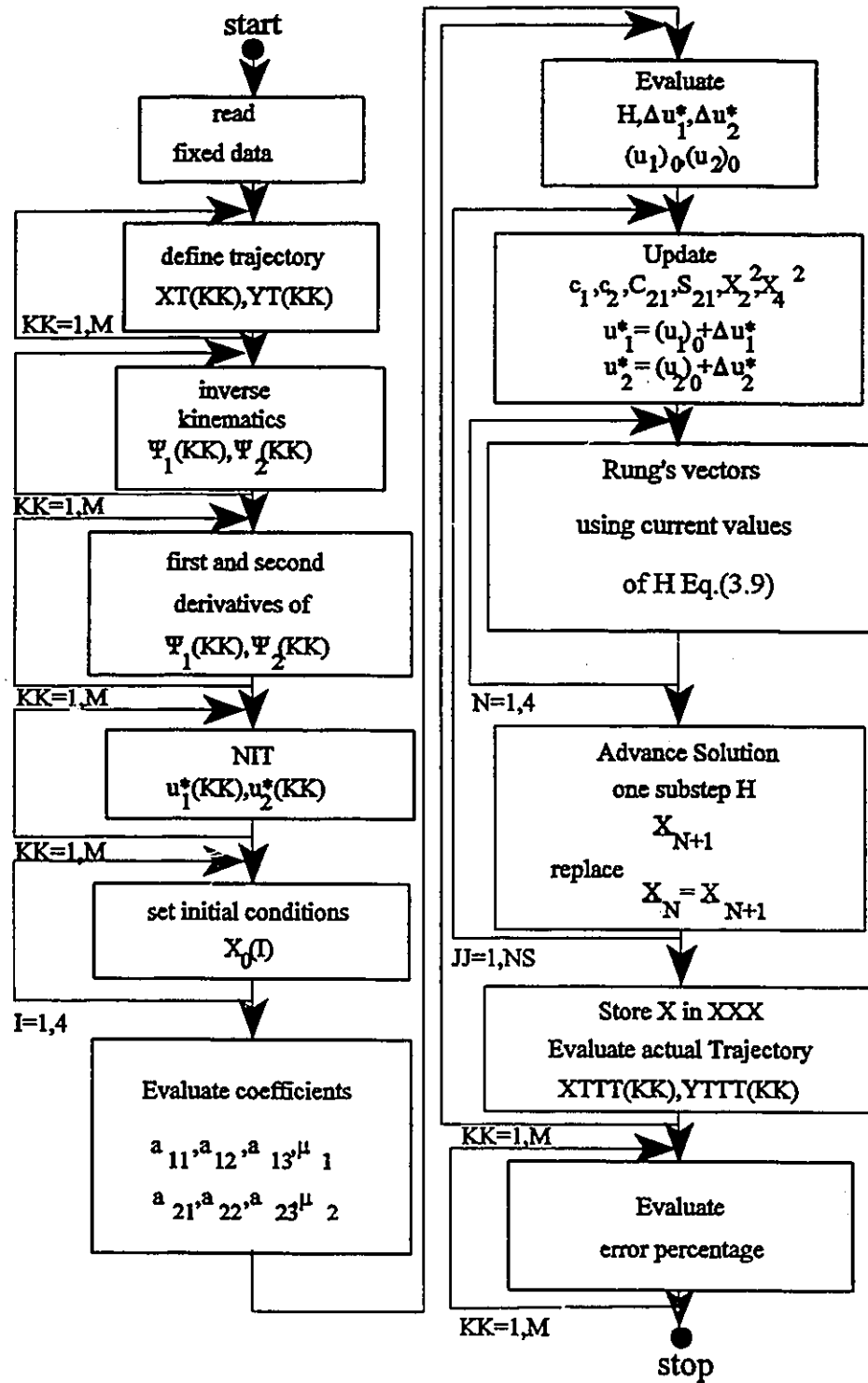
Figure 3.12: Validation (NIT) for (RAM).

$$X_2' = \frac{1}{1 - \rho_1\, a_{22}\, c_{21}} \left\{ - a_{11}\, X_2 + a_{12}\, s_{21}\, X_4^2 - a_{13}\, c_1 + \mu_1\, \dot{u}_1 + \right.$$

$$\left. \rho_1\, [a_{21}\, X_4 + a_{22}\, s_{21}\, X_2^2 + a_{23}\, c_2 - \mu_2\, \dot{u}_2] \right\}$$

$$X_4' = \frac{1}{1 - \rho_2\, a_{12}\, c_{21}} \left\{ - a_{21}\, X_4 + - a_{22}\, s_{21}\, X_2^2 - a_{23}\, c_2 + \mu_2\, \dot{u}_2 + \right.$$

$$\left. \rho_2\, [a_{11}\, X_2 - a_{12}\, s_{21}\, X_4^2 + a_{13}\, c_1 - \mu_1\, \dot{u}_1] \right\}$$

where :

$$c_1 = \cos(X_1) \; ; \; c_2 = \cos(X_3) \; ; \; c_{21} = \cos(X_3 - X_1) \; ; \; s_{21} = \sin(X_3 - X_1)$$

$$\rho_1 = a_{12}\, c_{21} \; ; \; \rho_2 = a_{22}\, c_{21}$$

$$\tag{3.9.e}$$

Relations (3.9.e) are used only once, at the beginning of the simulation.

A computer routine TRKRAM was developed to perform the simulation using the strategies previously presented. The coordinates XTT(I), YTT(I) of the desired trajectory were compared with XTTT(I), YTTT(I) of the actual trajectory. An almost perfect replica was noticed as shown in Figure (3.13) for the ellipse, the rose and the square. To assess the difference between the desired and the actual trajectories a performance index ε is defined as follows:

$$\varepsilon(I) = \frac{|Distance \quad from \quad desired \quad to \quad actual \quad points \quad |}{| \quad Distance \quad from \quad origin \quad to \quad desired \quad point \quad |} \times 100 \tag{3.10}$$

ε is essentially a measure of the deviation of the actual trajectory from the desired. The plots in Figure (3.14), with $\omega_0 = 5.67$ rad/sec, demonstrate the variation of ε over the entire path.
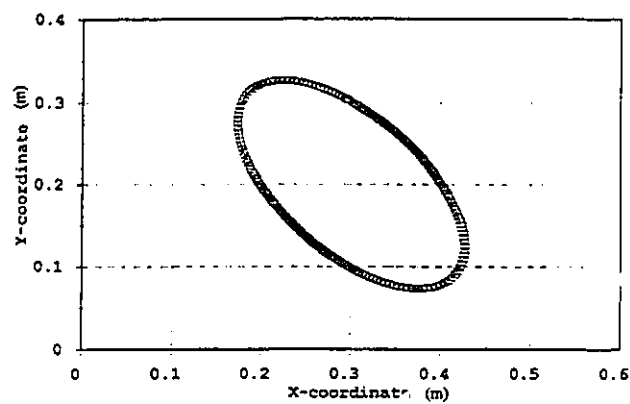
(a) Ellipse. ⊷ REFERENCE ⊶ ACTUAL
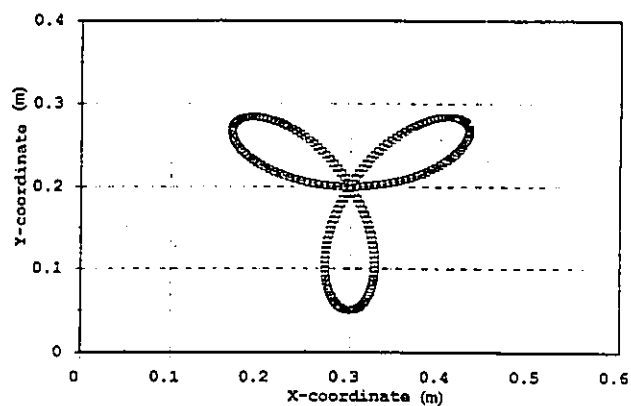
(b) Rose. ⊷ REFERENCE ⊶ ACTUAL
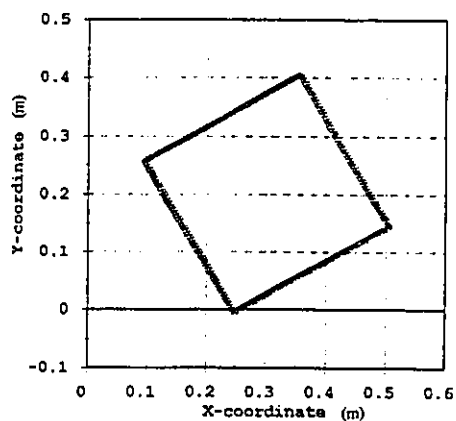
(c) Square. ⊷ REFERENCE ⊶ ACTUAL

Figure 3.13: Desired ⊖ and actual ⊟ trajectories (NIT) for (RAM).

(note the almost perfect tracking)
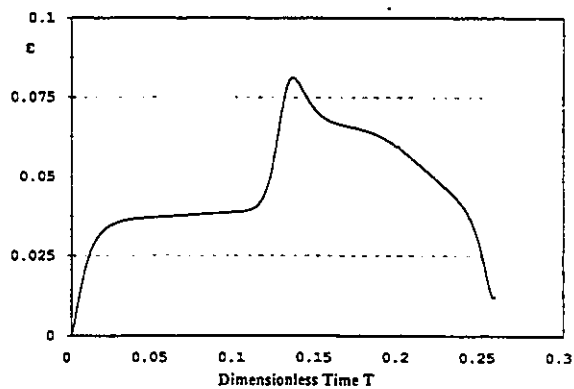
(a) Ellipse.
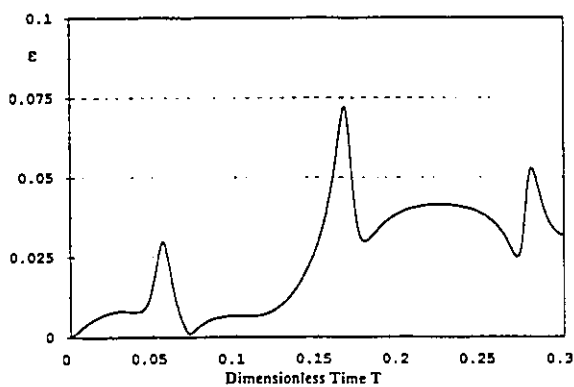
(b) 3-Leaved-rose.

(c) Square.

Figure 3.14: Performance index ε (NIT) for (RAM).

The highest percentage error is noticed in the case of tracking a square as expected.

Simulation of the full path, i.e. for $200 \times 50 = 10,000$ substeps, using the variable Rung-Kutta algorithm took less than one minute of computing time using a 50 Mhz - 486 PC.

The results presented in this section demonstrate that the NIT control is simple, accurate, reliable and can be extended for flexible arms as discussed in the following section.
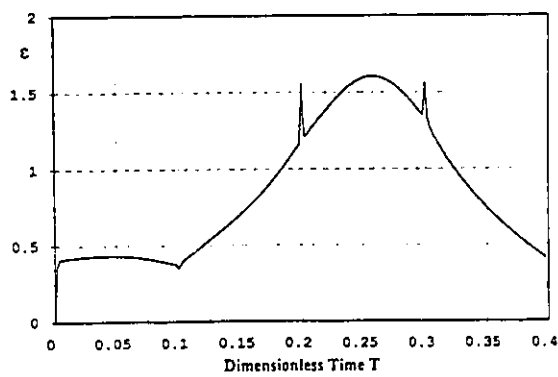
3.10 DYNAMIC SIMULATOR : (NIT) FOR (FJM)

To validate (NIT) for (FJM) we use relations (2.21.a) which can be rearranged in the form:

$$[M] \; X'' + [C] \; X' + [K] \; X = R \qquad (3.11.a)$$

where [M], [C] and [K]=[G] are (4×4) real matrices as defined by (2.21.b) and $\underline{R}$ is a (4×1) real vector given by:

$$R^T = [\; \mu_1^0 \, u_1^{\cdot} \; , \; - \, b_{24} \, c_1 \; , \; \mu_2^0 \, u_2^{\cdot} \; , \; - \, b_{44} \, c_2 \;]^T \qquad (3.11.b)$$

The state vector $\underline{X}$ is to be determined starting with the initial vector $\underline{X}_0$. An adaptation to the Newmark algorithm is used here to improve the efficiency and the numerical stability. This was deemed necessary because of the heavy coupling among the variables in the model.

The Newmark algorithm, similar to Rung-Kutta, considers two instants in time (n) and (n+1) separated by h such that:

$$h = (T)_{n+1} - (T)_n \qquad (3.11.c)$$

The algorithm allows one to predict ($\underline{X}_{n+1}$, $\underline{X}_{n+1}'$, $\underline{X}_{n+1}''$) if ($\underline{X}_n$, $\underline{X}_n'$, $\underline{X}_n''$) and the coefficients of the model given by (3.11.a), are all known at $(T)_n$. The Newmark's algorithm reads:

$$\underline{X}_{n+1}' = \underline{X}_n' + h\,(1 - \delta)\,\underline{X}_n'' + h\,\delta\,\underline{X}_{n+1}''$$

$$\underline{X}_{n+1} = \underline{X}_n + h\,\underline{X}_n' + h^2\left(\frac{1}{2} - \alpha\right)\underline{X}_n'' + h^2\,\alpha\,\underline{X}_{n+1}''$$

$$[M]\,\underline{X}_{n+1}'' + [C]\,\underline{X}_{n+1}' + [K]\,\underline{X}_{n+1} = \underline{R}_{n+1} \qquad\qquad \textbf{(3.12.a,b,c)}$$

where α and δ are parameters that are chosen to obtain the desired integration stability and accuracy. When $\alpha=1/6$; $\delta=1/2$ the algorithm is described as the "linear acceleration" method. When $\alpha=1/4$; $\delta=1/2$ one obtains the "trapezoidal rule". h is the time step size.

One can rearrange (3.12.b) to express $\underline{X}_{n+1}''$ in terms of $\underline{X}_{n+1}$ as follows:

$$\underline{X}_{n+1}'' = \frac{1}{h^2\alpha}\left\{\underline{X}_{n+1} - \underline{X}_n - h\,\underline{X}_n' - h^2\left(\frac{1}{2} - \alpha\right)\underline{X}_n''\right\} \qquad \textbf{(3.12.d)}$$

Substituting (3.12.d) and (3.12.a) in (3.12.c), one obtains:

$$\left(\frac{1}{h^2\alpha}\right)[M]\left\{\underline{X}_{n+1} - \underline{X}_n - h\,\underline{X}_n' - h^2\left(\frac{1}{2} - \alpha\right)\underline{X}_n''\right\} + [C]\left\{\underline{X}_n' + h\,(1 - \delta)\,\underline{X}_n'' + \right.$$

$$\left. \frac{\delta}{h\,\alpha}\left[\underline{X}_{n+1} - \underline{X}_n - h\,\underline{X}_n' - h^2\left(\frac{1}{2} - \alpha\right)\underline{X}_n''\right]\right\} + [K]\,\underline{X}_{n+1} = \underline{R}_{n+1}$$

$$\left[ZZ1 \ [M] + ZZ2 \ [C] + [K] \right] \underline{X}_{n+1} = \underline{R}_{n+1} + \left[ZZ1 \ [M] + ZZ2 \ [C] \right] \underline{X}_n +$$

$$\left[ZZ3 \ [M] + ZZ4 \ [C] \right] \underline{X}_n' + \left[ZZ5 \ [M] + ZZ6 \ [C] \right] \underline{X}_n''$$

where :

$$ZZ1 = \frac{1}{h^2 \alpha} \quad ; ZZ2 = \frac{\delta}{h\alpha} \quad ; ZZ3 = \frac{1}{h\alpha}$$

$$ZZ4 = \frac{\delta - \alpha}{\alpha} \quad ; ZZ5 = \frac{1 - 2\alpha}{2\alpha} \quad ; ZZ6 = \frac{h(\delta - 2\alpha)}{2\alpha} \qquad \textbf{(3.13.a)}$$

Relation (3.13.a) can be written in the compact form:

$$[Q] \ \underline{X}_{n+1} = \underline{Z} \qquad\qquad \textbf{(3.13.b)}$$

which has a solution:

$$\underline{X}_{n+1} = [Q]^{-1} \ \underline{Z} \qquad\qquad \textbf{(3.13.c)}$$

for [Q] nonsingular.

Once $\underline{X}_{n+1}$ is obtained using (3.13.c), one can evaluate $\underline{X}_{n+1}''$ using (3.12.d) which

can be written in the following form:

$$\underline{X}_{n+1}'' = ZZ1 \ \{\underline{X}_{n+1} - \underline{X}_n\} - ZZ3 \ \underline{X}_n' - ZZ5 \ \underline{X}_n'' \qquad \textbf{(3.13.d)}$$

$\underline{X}_{n+1}'$ can be evaluated using (3.12.a) which can be written in the following form:

$$\underline{X}_{n+1}' = \underline{X}_n' + ZZ7 \ \underline{X}_n'' + ZZ8 \ \underline{X}_{n+1}''$$

where :

$$ZZ7 = h \ (1 - \delta) \ ; \ ZZ8 = h \ \delta \qquad\qquad \textbf{(3.13.e)}$$

Normally $\underline{X}_0$ and $\underline{X}_0'$ are readily available at T=0. To be able to use the Newmark

algorithm it is necessary to evaluate $\underline{X}_0''$ as well. This is achieved by using (3.11.a) to write:

$$X_0'' = [M]^{-1} \left\{ R_0 - [C] \, X_0' - [K] \, X_0 \right\} \qquad (3.13.f)$$

To advance the solution one step h in time, the Newmark algorithm calls for an inversion of a (4×4) matrix [Q] as depicted by equation (3.13.c). An efficient Gauss-Jordan algorithm with pivotal condensation is used to achieve the inversion. [Q] is reassembled and inverted on top of itself in each step of the solution.

The algorithm given by (3.13.a), (3.13.d), (3.13.e) are implemented in a computer routine TRKFJM to simulate FJM. The algorithm is adapted to account for:

(a) The variable substep size h calls for updating of some of the ZZ's which appear in (3.13.a) and (3.13.e).

(b)The [M], [C] and [K] matrices have to be updated every step, because of their dependence on the variables $\underline{X}$ and $\underline{X}'$.

(c) Linear interpolation for $\underline{u}_1^*$ and $\underline{u}_2^*$ since these are available in tabular form.

The Newmark's algorithm, similar to Rung's took less than one minute of computing time using the 50 Mhz - 486DX PC. The flow diagram of the simulation is shown in Figure (3.15). The (NIT) for (FJM) is as depicted in Figure (3.16) with $\omega_0 = 7.317$ rad/sec. δ_1 and δ_2 refer to the deflection ($\Psi_1 - \phi_1 / N_1$) and ($\Psi_2 - \phi_2 / N_2$) across harmonic drives 1 and 2 respectively. The max. deviation is found to be 2.13%.

start

Read Data
Define Trajectory
XT , YT

Inverse Kinematics
Ψ_1 , Ψ_2 and
derivatives

ϕ_1 , ϕ_2
Eq.(3.7.b)

Command voltages
u_1^* , u_2^*
Eq.(3.7.c)

Set initial conditions
X_0 , X_0' , X_0''
using Eq.(3.13.f)

Evaluate
b_{11} , ω_1^2 , b_{12} , μ_1^0
b_{21} , ω_2^2 , b_{22} , b_{23} , b_{24}
b_{31} , ω_3^2 , b_{32} , μ_2^0
b_{41} , ω_4^2 , b_{42} , b_{43} , b_{14}
Basic Fixed Elements of
[M] , [C], [K] , R

Evaluate
H , Δu_1^* , Δu_2^* ,
$(u_1)_0$, $(u_2)_0$

Update
c_1, c_2 , c_{21} , s_{21} , ZZ's
$u_1^* = (u_1)_0 + \Delta u_1^*$
$u_2^* = (u_2)_0 + \Delta u_2^*$
[M] , [C] , [K] , R
using Eq.(2.21.b)
Construct [Q] , {Z}
using Eq.(3.13.a)

Invert [Q]
Solve for:
X_{n+1} : Eq.(3.13.c)
X''_{n+1} : Eq.(3.13.d)
X'_{n+1} : Eq.(3.13.e)

Advance solution one step
replace
X_n , X'_n , X''_n by
X_{n+1} , X'_{n+1} , X''_{n+1}

JJ=1, NS

Store X in XXX
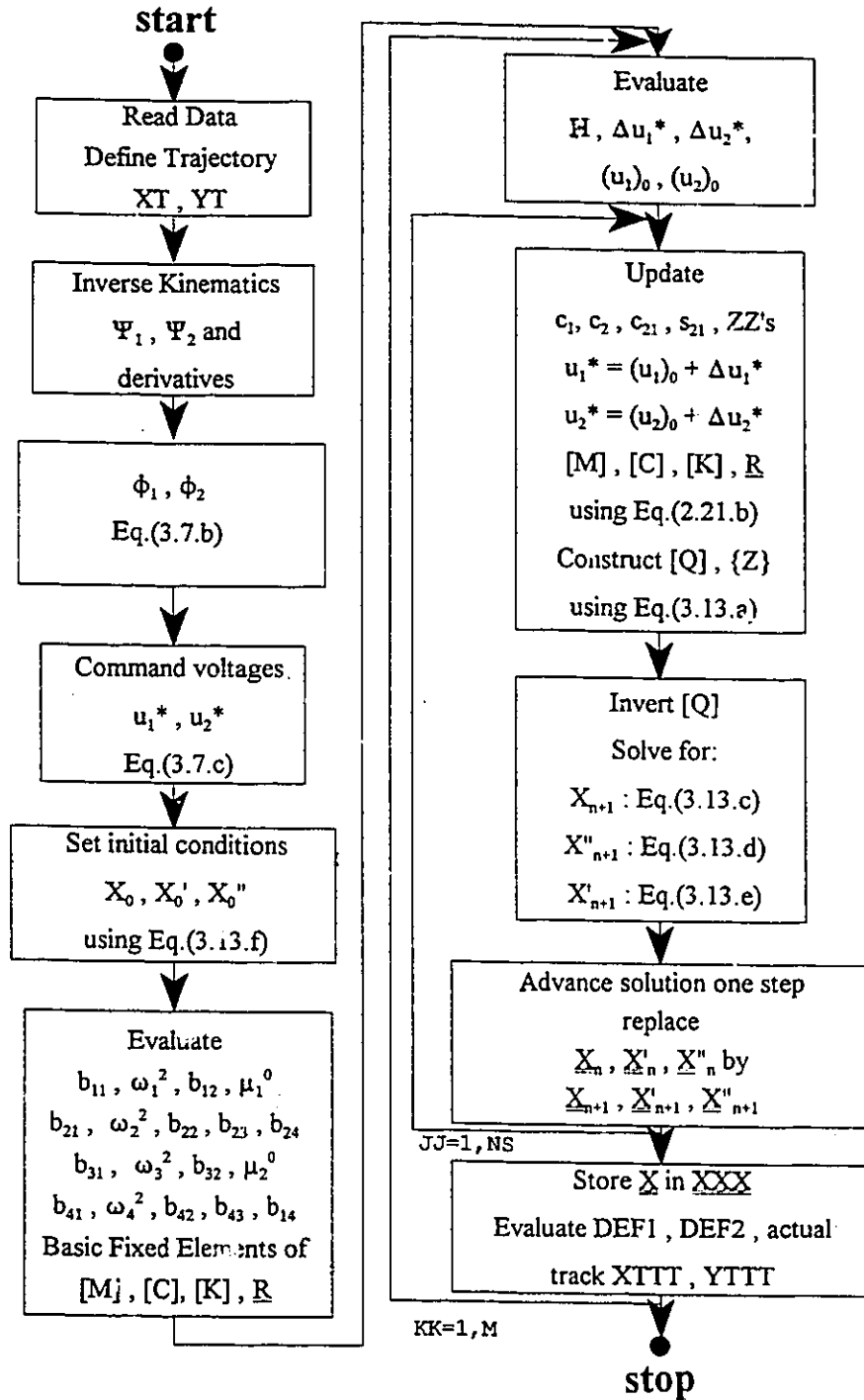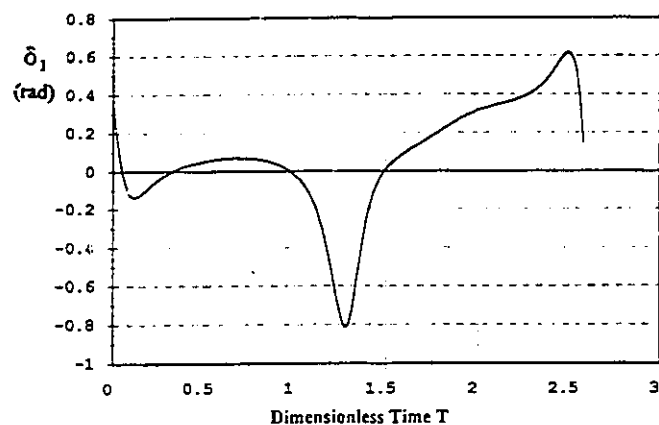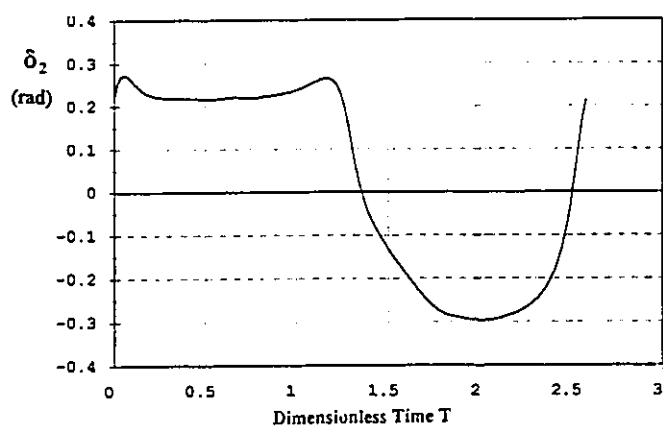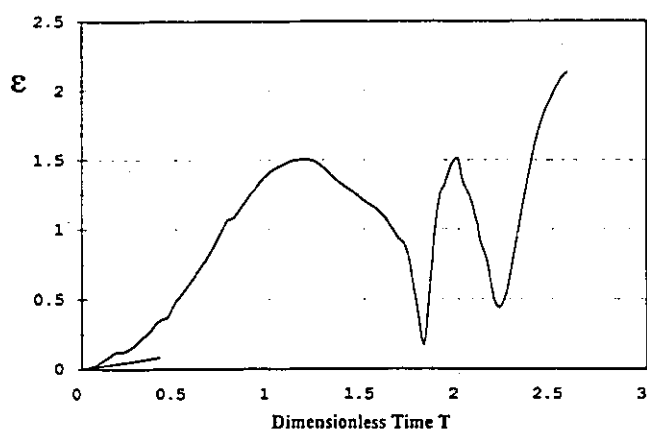Evaluate DEF1 , DEF2 , actual
track XTTT , YTTT

KK=1, M

stop

Figure 3.15: Validation (NIT) for (FJM).

(a) Deflection of harmonic drive 1.

(b) Deflection of harmonic drive 2.

(c) Performance index.

Figure 3.16: Validation of (NIT) for (FJM) (Tracking an ellipse).

3.11 TRANSIENT RESPONSE OF WRIST POINT

The transient response of the wrist point is assessed here by considering the case when brakes are applied to bring the motors to a sudden stop during tracking. The arm is considered to have compliant joints in the revolutes.

The model (2.19), describing the elbow arm has to be modified and interpreted in a different manner. In fact, the dynamics of the actuators, represented by (2.19.a) and (2.19.c) are suppressed since ϕ_1 and ϕ_2 are suddenly held fixed at some prescribed values. Consequently $\phi_1',\phi_1'',\phi_2',\phi_2''$ are all zero for T>0. In other words (2.19.a) and (2.19.c) serve only to furnish the values of u_1^* and u_2^* during the time the brakes are applied. This amounts to saying that the governing equations, for T>0, are given by (2.19.b) and (2.19.d). These equations can be exchanged for equations (2.15) with τ_1^* and τ_2^* given by:

$$\tau_1^{\cdot} = \frac{N_1 \, K_{h1}}{m_1 \, g \, a_1} \left(\phi_1 - N_1 \, \Psi_1 \right) \quad ; \quad \tau_2^{\cdot} = \frac{N_2 \, K_{h2}}{m_2 \, g \, a_2} \left(\phi_2 - N_2 \, \Psi_2 \right)$$

$$\begin{bmatrix} 1 & \alpha_1^{\cdot} c_{21} \\ \alpha_2^{\cdot} c_{21} & 1 \end{bmatrix} \left\{ \begin{matrix} \psi_1'' \\ \psi_2'' \end{matrix} \right\} + \begin{bmatrix} 0 & -\alpha_1^{\cdot} s_{21} \, \psi_2' \\ \alpha_2^{\cdot} s_{21} \, \psi_1' & 0 \end{bmatrix} \left\{ \begin{matrix} \psi_1' \\ \psi_2' \end{matrix} \right\} +$$

$$\begin{bmatrix} \gamma_1^{\cdot\cdot} \, K_{h1} & 0 \\ 0 & \gamma_2^{\cdot\cdot} \, K_{h2} \end{bmatrix} \left\{ \begin{matrix} \psi_1 \\ \psi_2 \end{matrix} \right\} + \left\{ \begin{matrix} \beta_1^{\cdot} \, c_1 \\ \beta_2^{\cdot} \, c_2 \end{matrix} \right\} = \left\{ \begin{matrix} \gamma_1^{\cdot\cdot} \, \phi_1 \\ \gamma_2^{\cdot\cdot} \, \phi_2 \end{matrix} \right\}$$

where :

$$\gamma_1^{\cdot\cdot} = (\gamma_1^{\cdot} \, N_1 \, K_{h1}) \, / \, (m_1 \, g \, a_1) \quad ; \quad \gamma_2^{\cdot\cdot} = (\gamma_2^{\cdot} \, N_2 \, K_{h2}) \, / \, (m_2 \, g \, a_2)$$

(3.14.a)

A computer routine DYNFJM was developed to solve (3.14.a) Figures.(3.17) and (3.18) are typical simulation-results for the FJM. The initial conditions are chosen as follows:

$$(\Psi_1)_0 = 0.8727 \ rad \qquad ; \ (\Psi_2)_0 = 0.3491 \ rad$$

$$(\Psi'_1)_0 = 0.15 \ rad/s \qquad ; \ (\Psi'_2)_0 = 0.15 \ rad/s$$

$$(\Psi''_1)_0 = 0.001 \ rad/s^2 \ ; \ (\Psi''_2)_0 = 0.001 \ rad/s^2$$

$$\omega_0 \qquad = 4.372 \ rad/s$$

The remaining parameters are as defined by relations (3.1).

Figure (3.17) shows the phase plane trajectories as well as the time-domain history of $(\delta_1 = \Psi_1 - \phi_1 / N_1)$; $(\delta_2 = \Psi_2 - \phi_2 / N_2)$.

ϕ_1 and ϕ_2 are assumed frozen during braking at the values $(\phi_1)_0$ and$(\phi_2)_0$ respectively. The plots show that the equilibrium point is not coinciding with the origin of the phase plane because of the presence of the D.C. components $(\beta_1 \, ^\bullet c_1)$ and $(\beta_2 \, ^\bullet c_2)$ in relations which are a consequence of the effect of the gravitational field on the two links.

Figure (3.18.a) represents the positions of the two links during the application of the brakes in the global frame. Figure (3.18.b) shows the path of the wrist point, during that period as viewed by an observer located at the would-be equilibrium point (x*, y*) given by:

$$x^\bullet = a_1 \cos (\Psi_1)_0 + a_2 \cos (\Psi_2)_0$$

$$y^\bullet = a_1 \sin (\Psi_1)_0 + a_2 \sin (\Psi_2)_0 \qquad\qquad (3.14.b)$$
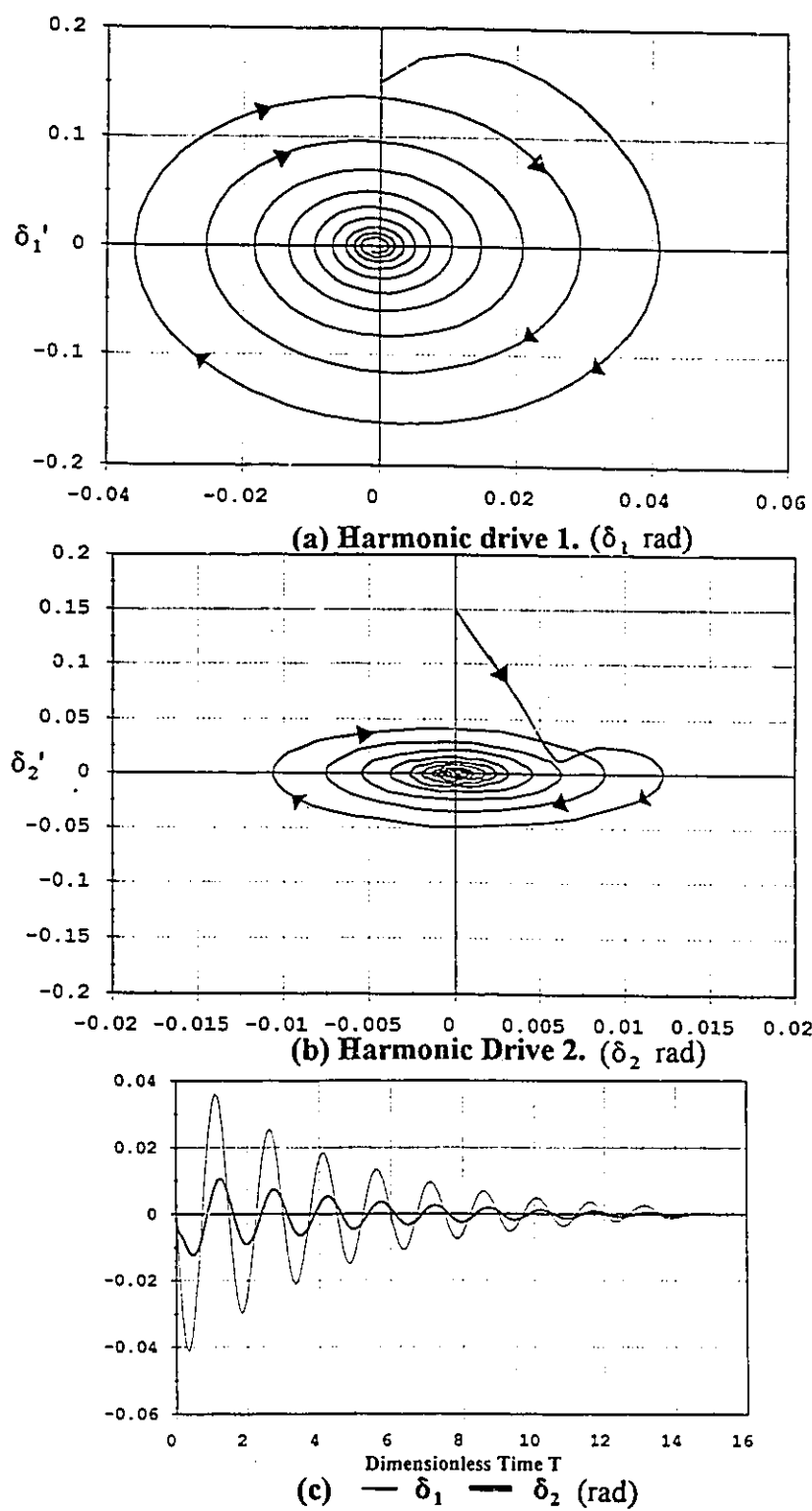
Figure 3.17: Deflections of harmonic drives (Brake Test).
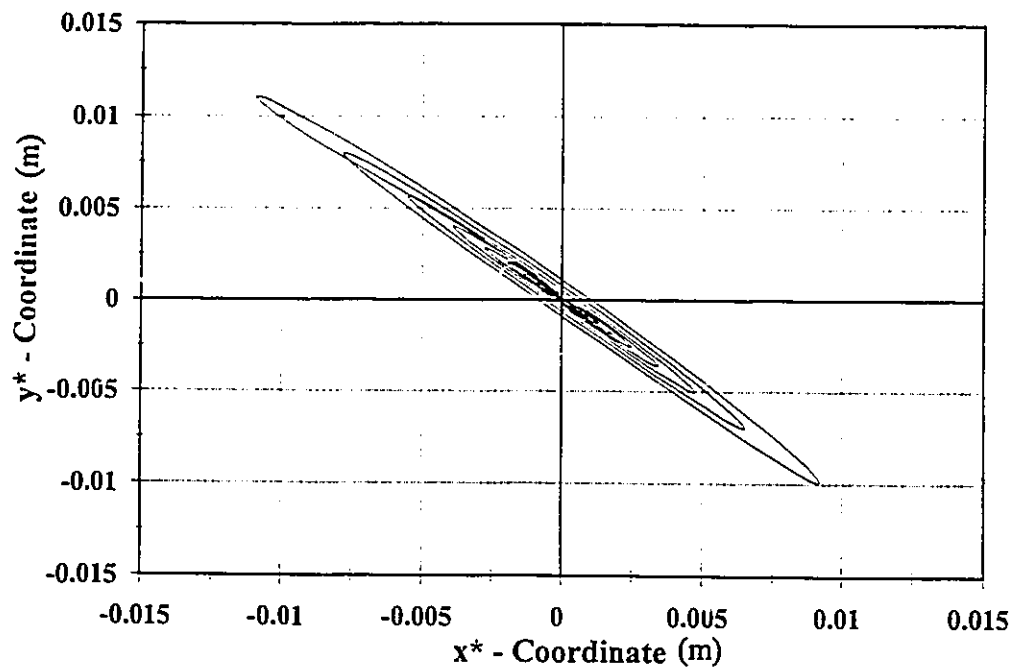
(a) Positions of joints during brake.
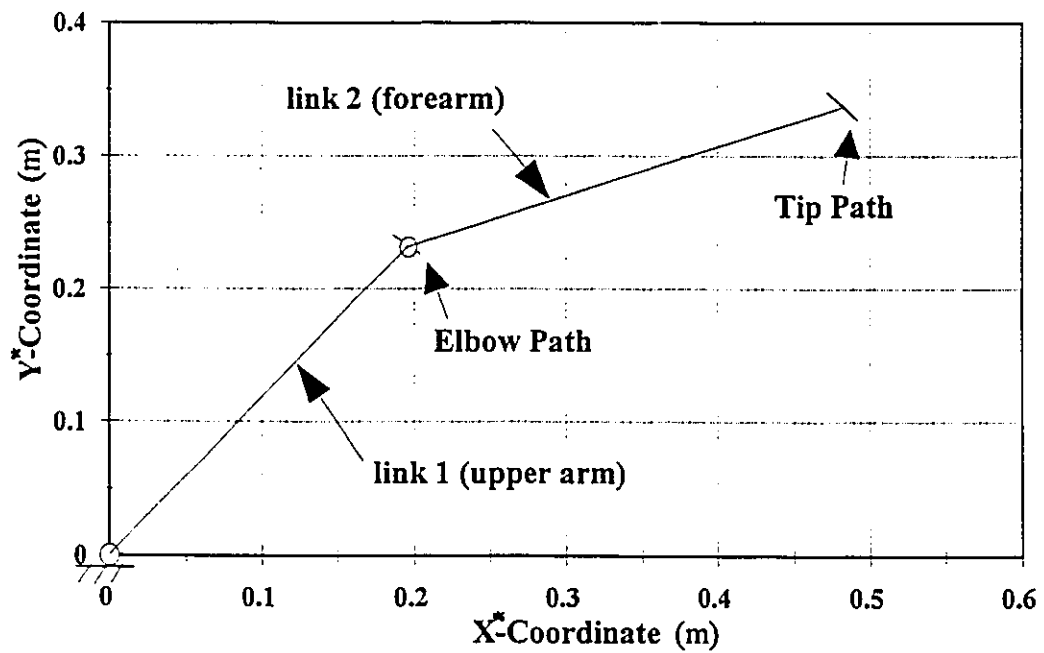
(b) Movement of wrist point during brake.

Figure 3.18: Joints during brake.

3.12 SUMMARY OF CHAPTER 3

In this chapter, a new strategy is developed for the definition of the command voltages which are necessary to track a given trajectory. The strategy uses stable algorithms which are applied to the realistic dynamic models developed in the previous chapter. The smoothness of the predicted commands was assessed and found adequate. The strategy is the heart of the Nonlinear Integrated Tabular "NIT" control which is also validated.

The transient response of the elbow arm, after applying the brakes, was also obtained for the FJM. The theoretical prediction of the transient response compared with the experimental findings in Chapter 7 of this thesis.

CHAPTER 4

NIT VERSUS CONVENTIONAL CONTROLS

4.1 OBJECTIVES

The objective of this chapter is to compare the "Nonlinear Integrated Tabular", NIT control developed in the previous chapter with other conventional controls. The evaluations and assessments are made for the elbow arm for tracking continuous and discontinuous trajectories. Rigid and compliant arms are considered. Comparisons are based on the following criteria:

(a) The maximum of the percentage error "ε", as defined by Eq.(3.10).

(b) The smoothness of the actual trajectory and its freedom from spikes.

(c) The oscillatory nature of the command voltages.

(d) The maximum levels attained by the command voltages.

Conventional controls investigated in this chapter are:

* Proportional + derivative + gravity   : PDG control.

* Feedback linearization   : FBL control.

* Variable structure (sliding mode)   : SLM control.

4.2 STATE SPACE REPRESENTATION OF THE RAM

The governing relations for the RAM are given by (2.17) and can be written in the following form:

$$q_1'' + a_{11} q_1' + a_{12} c_{21} q_2'' - a_{12} s_{21} q_2'^2 + a_{13} c_1 = \mu_1 u_1^{\cdot}$$

$$q_2'' + a_{21} q_2' + a_{22} c_{21} q_2'' - a_{22} s_{21} q_2'^2 + a_{23} c_2 = \mu_2 u_2^{\cdot} \qquad (4.1)$$

where the Ψ's are replaced by q's:

$$q_i = \Psi_i \ ; \ i = 1,2$$

The coefficients in (4.1) are as defined by (2.18) and (2.13.e). Equations (4.1) can be written in the following matrix form:

$$[D(q)] \ q'' + \{c \ (q \ , \ q')\} + \{b \ (q)\} + \{h \ (q')\} = \{\tau\} \qquad (4.2)$$

where:

$$[D(q)] = \begin{bmatrix} d_{11} & d_{12} \\ d_{21} & d_{22} \end{bmatrix} = \begin{bmatrix} 1 & a_{12}c_{21} \\ a_{22}c_{21} & 1 \end{bmatrix} \quad ; \ q = \begin{Bmatrix} \Psi_1 \\ \Psi_2 \end{Bmatrix} = \begin{Bmatrix} q_1 \\ q_2 \end{Bmatrix}$$

$$\{c \ (q \ , \ q')\} = \begin{Bmatrix} - a_{12} s_{21} q_2'^2 \\ a_{22} s_{21} q_1'^2 \end{Bmatrix} \quad ; \ \{b \ (q)\} = \begin{Bmatrix} a_{13} c_1 \\ a_{23} c_2 \end{Bmatrix}$$

$$\{h \ (q')\} = \begin{Bmatrix} a_{11} q_1' \\ a_{21} q_2' \end{Bmatrix} \quad ; \ \{\tau\} = \begin{Bmatrix} \mu_1 u_1^{\cdot} \\ \mu_2 u_2^{\cdot} \end{Bmatrix} = \begin{Bmatrix} \tau_1 \\ \tau_2 \end{Bmatrix}$$

$$(4.3.a)$$

It should be noticed that [D(q)] is invertible and its inverse is written in the following form:

$$[D(\underline{q})]^{-1} = [\ d_{ij}\ ]$$

where :

$$d_{11} = \frac{1}{\sigma} \quad d_{12} = \frac{-\ a_{12}\ c_{21}}{\sigma} \qquad ;\ d_{21} = \frac{-\ a_{22}\ c_{21}}{\sigma}$$

$$d_{22} = \frac{1}{\sigma} \qquad\qquad\qquad ;\ \sigma = 1 - a_{12}\ a_{22}\ c_{21}^{2} \qquad\qquad \text{(4.3.b)}$$

The state representation of RAM is given by:

$$\underline{q}' = \underline{v}$$

$$\underline{v}' = [D]^{-1}\ \{\ \underline{\tau} - \underline{c}\ (\underline{q}\ ,\ \underline{v}) - \underline{b}\ (\underline{q}) - \underline{h}\ (\underline{v})\ \} \qquad\qquad \text{(4.4)}$$

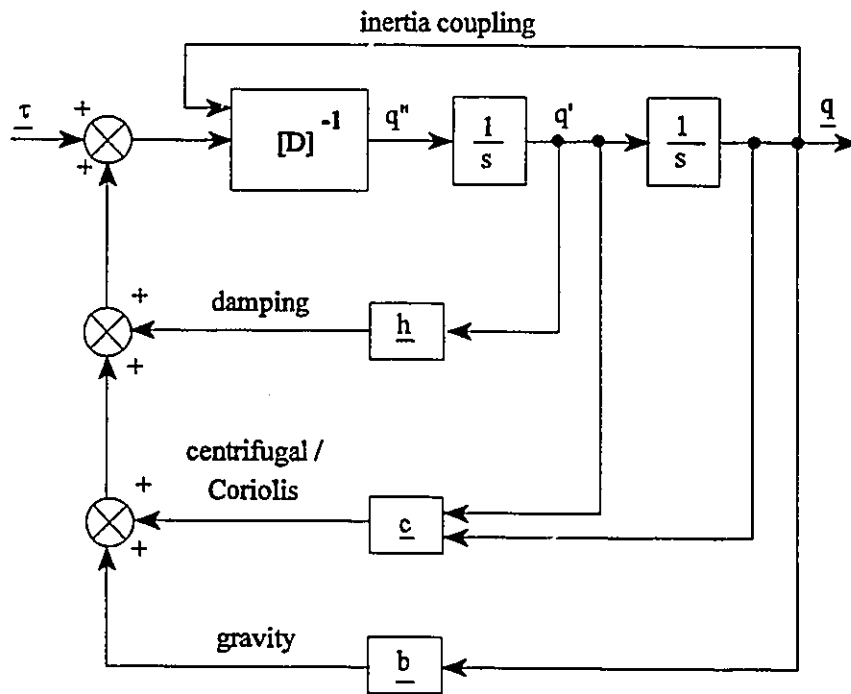and its block diagram is as depicted in Figure 4.1.

Figure 4.1: State space representation of elbow arm.

The central problem is essentially that of choosing $\underline{\tau}$ in equation (4.4) such that $\underline{q}$ follows a prescribed vector $\underline{r}$ at all times. In the case of "RAM", $\underline{r}$ is given by $[\Psi_1, \Psi_2]^T$ which is evaluated from the inverse kinematic problem of the arm at unequally spaced discrete points on the desired trajectory. The first and second derivatives of $\underline{r}$, i.e. $\underline{r}'$ and $\underline{r}''$ can also be evaluated at these discrete points.

The state space representation of the "RAM" as given by (4.4) consists of 4 (four) first order differential equations which can be written in the canonic form:

$$\underline{X}' = \underline{f}(X, X') \quad \text{where} \quad \underline{X}^T = [\ \Psi_1, \Psi'_1, \Psi_2, \Psi'_2] \tag{4.5}$$

4.3 "PDG" CONTROL FOR RAM

The proportional + derivative + gravity control (PDG) is widely used in practice due to its simplicity. The error signal $\underline{e}$ and the control law $\underline{\tau}$ in this case are chosen in the form:

$$\underline{e} = \underline{r} - \underline{q}$$

$$\underline{\tau} = [K_p]\ \underline{e}\ +\ [K_d]\ \underline{e}'\ +\ \underline{b}\ (\underline{q}) \tag{4.6}$$

where:

$[K_p]$ = a diagonal (2 x 2) position gain matrix.

$[K_d]$ = a diagonal (2 x 2) velocity gain matrix.

$\underline{r}, \underline{q}$ = (2 x 2) vectors for the desired and actual positions of the wrist point.

Substituting (4.6) in equations (4.4), one obtains:

$$q' = \underline{v}$$

$$\underline{v}' = [D(\underline{q})]^{-1} \{ [K_p] (\underline{r} - \underline{q}) + [K_d] (\underline{r}' - \underline{v}) - \underline{c} (\underline{q}, \underline{v}) - \underline{h} (\underline{v}) \} \tag{4.7}$$

The state vector $[q^T, \underline{v}^T]^T$ is denoted by $\{\underline{X}\}^T$.

One can show that:

(i)   The mathematical model (4.7) represents a closed-loop system which has one equilibrium point:

(ii)   The equilibrium point is asymptotically stable in the sense of Liapunov.

(iii)   The domain of attraction of $\{\underline{X}\}$ encompasses the entire state space.

The PDG control strategy, as given by (4.7), is depicted in the block diagram of Figure 4.2.
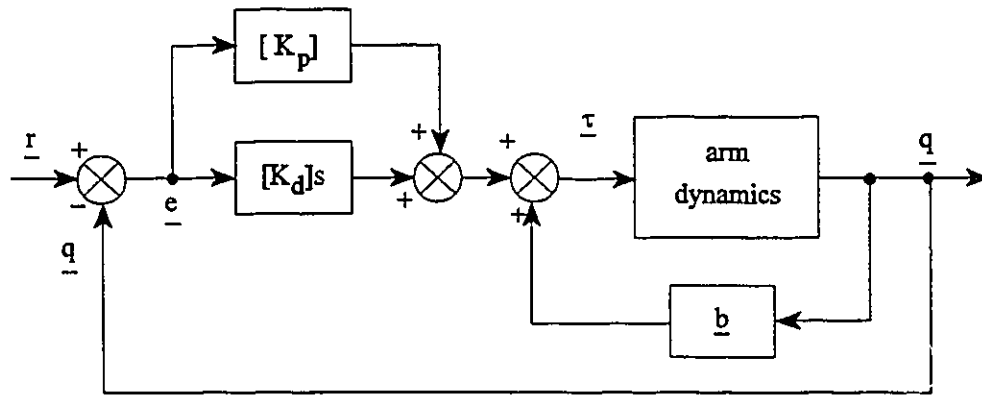

Figure 4.2: PDG Control for RAM.

The variable step Rung-Kutta algorithm is used for the computer simulation of the PDG control for RAM. The strategy of simulation is implemented in a computer routine

PDGRAM as depicted in Figure (4.3). The number of points on the desired trajectory is denoted by M and the number of substeps by NS. The constant linear velocity along the path is denoted by V.

At the start of each substep, the $\underline{r}$ and $\underline{r}'$ vectors are updated using linear interpolation. The coefficients in the $[D(\underline{q})]$ matrix and the $\underline{c}$, $\underline{h}$, $\underline{b}$ vectors are updated each substep using the current values of the state vector.

To investigate the role played by the gains $[K_p]$ and $[K_d]$, an elbow arm is considered with parameters as given by relations (3.1). The following additional parameters are also used:

$$V = 3 \text{ m/s} \; ; \; \omega_0 = 56.7 \text{ rad/s} \; ; \; NS = 80$$

Figure 4.4 shows the desired trajectory superimposed on the actual path of the wrist point with the following gains:

$$k_{p1} = k_{p2} = 0.1 \times 10^6 \; ; \; k_{d1} = k_{d2} = 0.1$$

It is obvious that the choice of the gains is poor and no meaningful tracking is obtained.
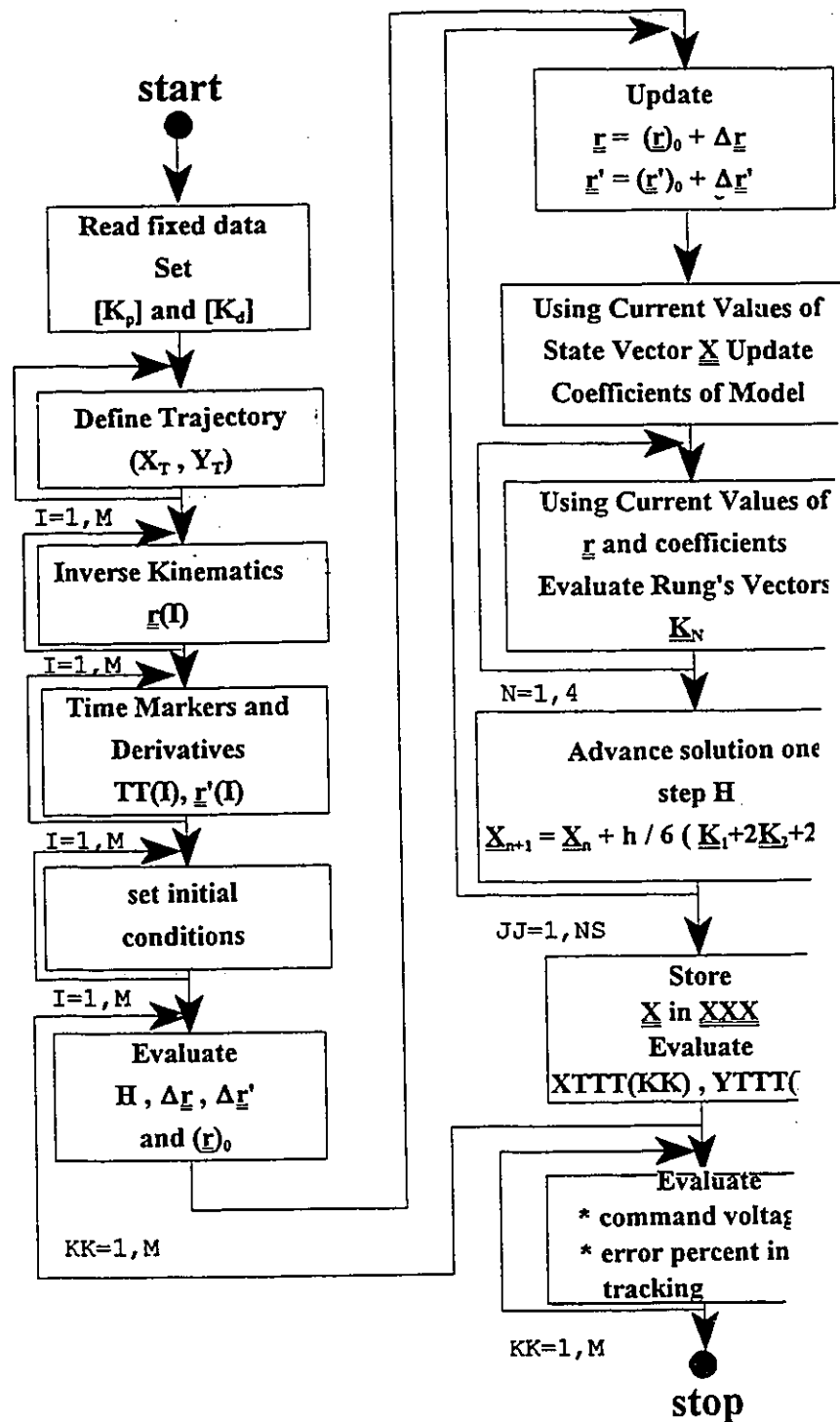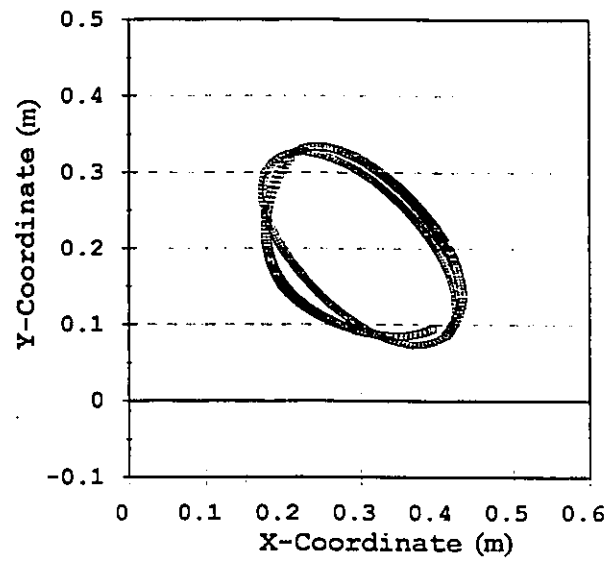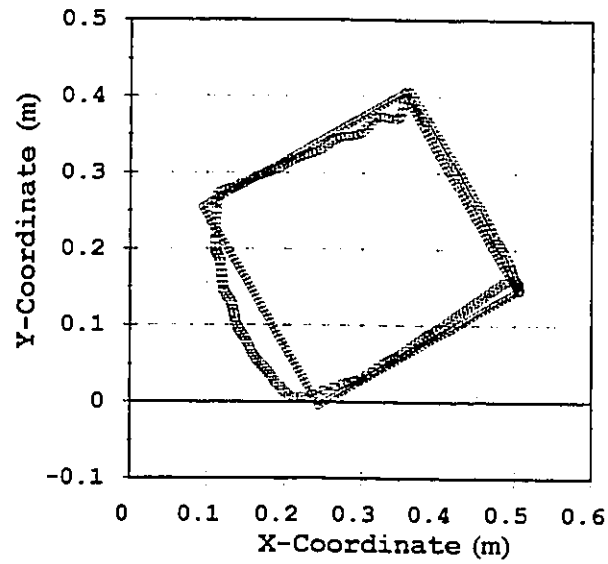
start

Read fixed data
Set
$[K_p]$ and $[K_d]$

Define Trajectory
(X_T, Y_T)

I=1,M

Inverse Kinematics
$\underline{r}(I)$

I=1,M

Time Markers and
Derivatives
$TT(I), \underline{r}'(I)$

I=1,M

set initial
conditions

I=1,M

Evaluate
H, $\Delta\underline{r}$, $\Delta\underline{r}'$
and $(\underline{r})_0$

KK=1,M

Update
$\underline{r} = (\underline{r})_0 + \Delta\underline{r}$
$\underline{r}' = (\underline{r}')_0 + \Delta\underline{r}'$

Using Current Values of
State Vector $\underline{X}$ Update
Coefficients of Model

Using Current Values of
$\underline{r}$ and coefficients
Evaluate Rung's Vectors
$\underline{K}_N$

N=1,4

Advance solution one
step H
$\underline{X}_{n+1} = \underline{X}_n + h/6 (\underline{K}_1 + 2\underline{K}_2 + 2$

JJ=1,NS

Store
$\underline{X}$ in $\underline{XXX}$
Evaluate
$XTTT(KK)$, $YTTT($

Evaluate
* command voltag
* error percent in
tracking

KK=1,M

stop

Figure 4.3: PDGRAM routine.

(a) Ellipse.   — REFERENCE —◻— ACTUAL

(b) Square.   — REFERENCE —◦— ACTUAL

Figure 4.4: PDGRAM (poor choice of gains).

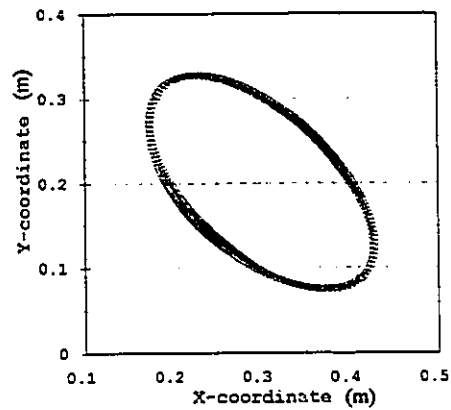$k_{p1}=k_{p2}=0.1\times10^6$; $k_{d1}=k_{d2}=0.1$; V=3 m/s ; $\omega_0=56.7$ rad/s

Figures (4.5) to (4.7) show the performance of the same elbow arm after changing k_{p1} and k_{p2} from (0.1×10^6) to (0.5×10^6). Tracking qualities improved but were still considered poor because the errors are inacceptable in practice and the command voltages are noticed to be oscillatory.

It is interesting to notice that the actual trajectories of the ellipse and the rose, are relatively smooth in this case in spite of the fact that their associated command voltages u_1^* and u_2^* are oscillatory.

Acceptable tracking with smoother controller performance is possible through the use of higher gains. The price is paid through higher command voltages. For example, using:

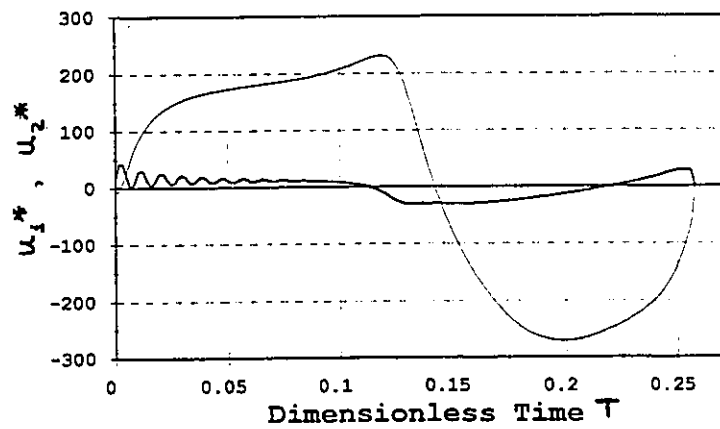$$k_{p1} = k_{p2} = 0.3 \times 10^6 \; ; \; k_{d1} = k_{d2} = 0.1 \times 10^5$$

the (u_1^*, u_2^*) plots become smoother as shown in Figure (4.8). The errors improved a great deal. It dropped from (2.76 to 0.459%) for the ellipse, from (2.84 to 0.451%) for the rose and from (4.65 to 0.958%) for the square. However the level of the command voltages is still considered high. Other control strategies are sought to lower these levels.
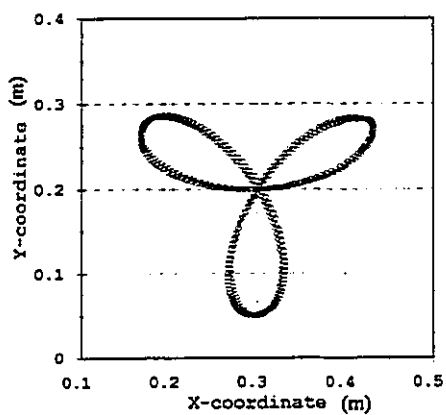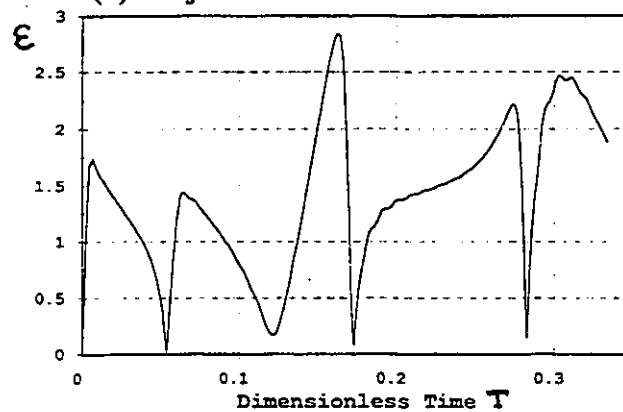
(a) Trajectories. — REFERENCE —○— ACTUAL
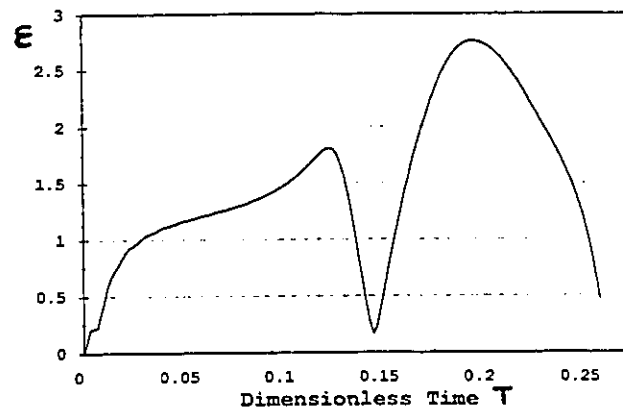
(b) Error ε.

(c) Command voltages. — u1· — u2·

Figure 4.5: Poor tracking PDGRAM -ellipse

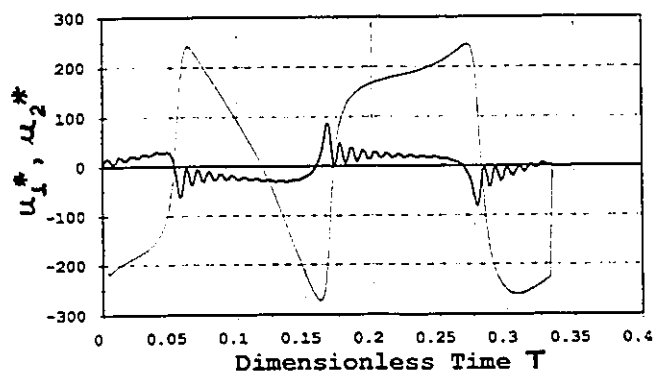$k_{p1}=k_{p2}=0.1\times10^6$; $k_{d1}=k_{d2}=0.1$; V=3 m/s ; $\omega_0=56.7$ rad/s
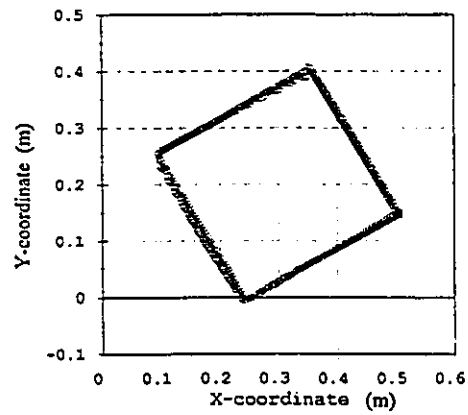
(a) Trajectories. — REFERENCE — ACTUAL

(b) Percentage error.

(c) Control voltages. — u1* — u2*

Figure 4.6: Poor tracking PDGRAM - rose

$k_{p1}=k_{p2}=0.5\times10^6$; $k_{d1}=k_{d2}=0.1$; V=3 m/s ; $\omega_0=56.7$ rad/s

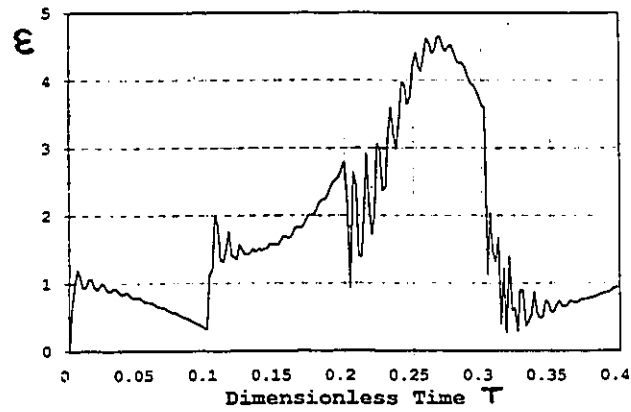**(a) Trajectories.** — REFERENCE — ACTUAL

(b) Percentage error.
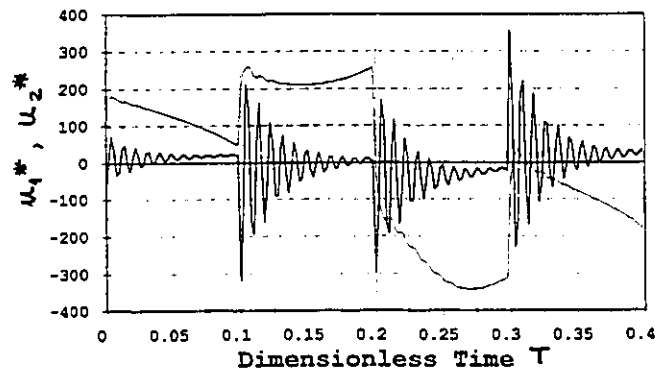
(c) Command voltages. — u1* — u2*

Figure 4.7: Poor tracking PDGRAM - square

$k_{p1} = k_{p2} = 0.5 \times 10^6$; $k_{d1} = k_{d2} = 0.1$; $V = 3$ m/s ; $\omega_0 = 56.7$ rad/s
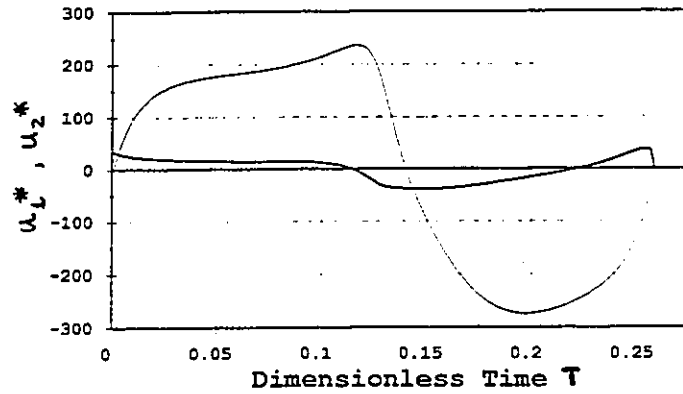
(a) Ellipse $(\varepsilon)_{max}=0.459\%$ — u1* — u2*
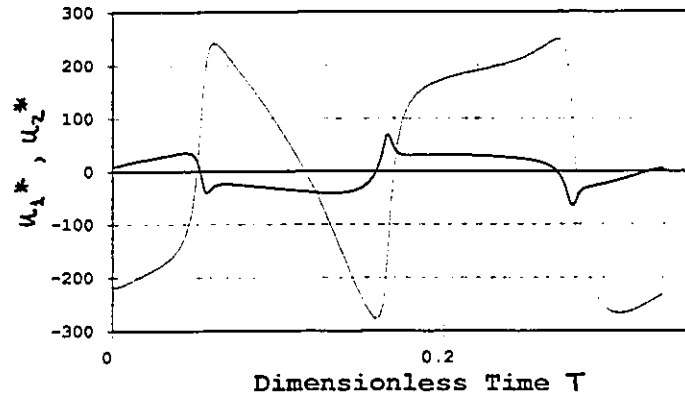
(b) 3-Leaved rose $(\varepsilon)_{max}=0.451\%$ — u1* — u2*
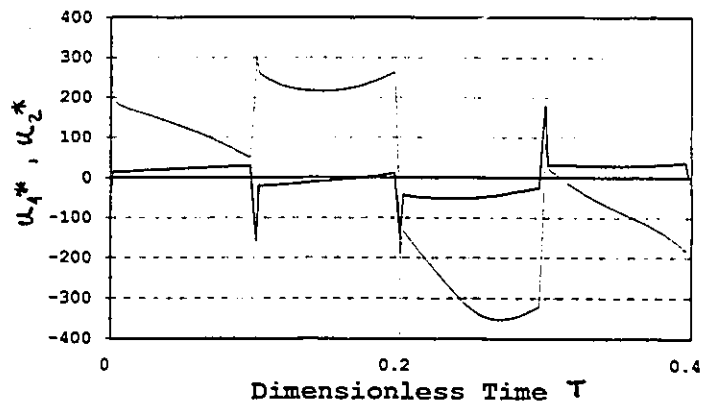
(c) Square $(\varepsilon)_{max}=0.958\%$ — u1* — u2*

Figure 4.8: Acceptable tracking PDGRAM command voltages

$k_{p1}=k_{p2}=0.3\times10^{7}$; $k_{d1}=k_{d2}=0.1\times10^{5}$; V=3 m/s ; $\omega_{0}=56.7$ rad/s

4.4 PDG CONTROL FOR FJM

The model describing the dynamics of FJM is given by (2.19). The governing

relations of PDG control for FJM can be written in the following form:

$$[M^\cdot] \; X'' + [C^\cdot] \; X' + [K^\cdot] \; X = R^\cdot$$

where :

$$[M^\cdot] = \begin{bmatrix} 1 & 0 & 0 & 0 \\ 0 & 1 & 0 & b_{22} \; c_{21} \\ 0 & 0 & 1 & 0 \\ 0 & b_{42} \; c_{21} & 0 & 1 \end{bmatrix} \;;$$

$$[C^\cdot] = \begin{bmatrix} b_{11} + k_{d1} & 0 & 0 & 0 \\ 0 & b_{21} & 0 & -b_{22} \; s_{21} \; X_4' \\ 0 & 0 & b_{31} + k_{d3} & 0 \\ 0 & b_{42} \; s_{21} \; X_2' & 0 & b_{41} \end{bmatrix} \;;$$

$$[K^\cdot] = \begin{bmatrix} \omega_1^2 + k_{p1} & -b_{12} & 0 & 0 \\ -b_{23} & \omega_2^2 & 0 & 0 \\ 0 & 0 & \omega_3^2 + k_{p3} & -b_{32} \\ 0 & 0 & -b_{43} & \omega_4^2 \end{bmatrix} \;;$$

$$R^\cdot = \begin{Bmatrix} k_{p1} \; r_1 + k_{d1} \; r_1' \\ 0 \\ k_{p3} \; r_3 + k_{d3} \; r_3' \\ 0 \end{Bmatrix} \;; \; X = \begin{Bmatrix} \phi_1 \\ \Psi_1 \\ \phi_2 \\ \Psi_2 \end{Bmatrix}$$

where :$c_1 = \cos X_2$; $c_2 = \cos X_4$; $c_{21} = \cos(X_4 - X_2)$; $s_{21} = \sin(X_4 - X_2)$ (4.8)

The remaining coefficients in (4.8) are defined in (2.20). The $\underline{r}$ and $\underline{r}'$ refer to the desired trajectory and its derivative. The k_p's and k_d's are the position and velocity gains in the PDG control law.

As mentioned before, r_2 and r_4 in the $\underline{r}$ vector are evaluated by solving the inverse kinematic problem. Their associated first and second derivatives, i.e. r_2', r_2'', r_4' and r_4'' are obtained through parabolic fitting as was explained in Section 3.7.

The variables (r_1 and r_3) in the $\underline{r}$ vector are obtained by using the second and fourth relations of (2.19). They are given by:

$$r_1 = \frac{1}{b_{23}} \left[r_2'' + b_{21} \, r_2' + \omega_2^2 \, r_2 + b_{22} \, c_{21} \, r_4'' - b_{22} \, s_{21} \, (r_4')^2 + b_{24} \, c_1 \right]$$

$$r_3 = \frac{1}{b_{43}} \left[r_4'' + b_{41} \, r_4' + \omega_4^2 \, r_4 + b_{42} \, c_{21} \, r_2'' + b_{42} \, s_{21} \, (r_2')^2 + b_{44} \, c_2 \right] \qquad (4.9)$$

The derivatives r_1', r_1'', r_3' and r_3'' are obtained through parabolic fitting. Thus one can consider that $\underline{r}$, $\underline{r}'$ and $\underline{r}''$ are all known in advance for every point on the desired trajectory. It should be noticed that the representation given by (4.8) is based on the following control law:

$$\mu_1^0 \, u_1^{\cdot} = k_{p1} \, e_1 + k_{d1} \, e_1' \quad ; \quad \mu_2^0 \, u_2^{\cdot} = k_{p3} \, e_3 + k_{d3} \, e_3'$$

$$where : e_i = r_i - X_i \; ; \; i= 1 \, , 3 \qquad (4.10)$$

and the command voltages ($u_1^{\cdot}$ and $u_2^{\cdot}$) are evaluated using relations (3.7.b) and (3.7.c). As noticed, the choice of the error signals e_1 and e_2 is based on the fact that they are easy to measure in practice.

4.5 PDG CONTROL FOR FLM

The model in this case is given by (2.37) and the PDG control law can be implemented as discussed in the FJM case. The $\underline{r}$ is an (8×1) vector $[r_1, r_2 ... r_8]^T$ given by:

$$\underline{r} = [\ \Psi_1\ ,\ X_2\ ,\ Y_2\ ,\ \Psi_2^{\cdot}\ ,\ \Psi_2\ ,\ X_3\ ,\ Y_3\ ,\ \Psi_3^{\cdot}\ ]^T$$

It is noticed that (r_1, r_5) are obtained by solving the inverse kinematic problem. The quantities (r_2, r_3) and (r_6, r_7) are obtained using the following relations:

$$r_2 = a_1\, c_1 \qquad\qquad ;\ r_3 = a_1\, s_1$$

$$r_6 = a_1\, c_1 + a_2\, c_2 \qquad ;\ r_7 = a_1\, s_1 + a_2\, s_2 \qquad\qquad \textbf{(4.11.a)}$$

The remaining quantities $(r_4,\ r_8)$ are obtained by rearranging rows 2,4,6,and 8 of relations (2.37) in the form

$$[A]\ \{Z\}\ =\ \{\underline{b}\}$$

where

$$\{Z\}\ =\ [\ r_4''\ ,\ r_4\ ,\ r_8''\ ,\ r_8\ ]^T \qquad\qquad \textbf{(4.11.b)}$$

and [A] is a (4×4) matrix and $\{\underline{b}\}$ is a(4×1) vector whose elements are all known in terms of r_1, r_2, r_3, r_5, r_6 and r_7 and their derivatives.

Solving (4.11.b) one can define all elements of $\underline{r}$, $\underline{r}'$ and $\underline{r}''$ completely at every point on the described trajectory.

The strategies discussed in this section are implemented in a computer routine, PDGFLX for the tracking of an elbow arm with flexibility in the joints. Typical results are presented in the following section.

4.6 SIMULATION OF PDG FOR FJM

The variable step Newmark algorithm, with $\alpha=1/6$ and $\delta=1/2$, is used to perform tracking using an elbow arm with the same parameters as given by relations (3.1). Simulation was performed using $\omega_0 = 5.671$ rad/s, $V = 0.3$ m/s, $k_{p1} = k_{p3} = 0.01$ and the number of substeps=20. The gains K_{d1} and K_{d3} were allowed to vary to satisfy Equation (4.10).

Figure 4.10 shows the results of simulation for an elliptical path using PDG control with a maximum percentage error of 0.974%. The control voltages u_1^* and u_2^* were found to be relatively smooth as seen in Figure 4.9.c. The time history for k_{d1} and k_{d3} are given in Figure 4.10 which shows oscillations and spikes. These are attributed to numerical noise. It is obvious that the noise is filtered out by the dynamics and has little effect on the final tracking performance of the elbow arm.

Figure 4.11 shows the results of the "PDGFLX" for the tracking of a rose. Numerical noise and sharp spikes contaminate the velocity gains. However tracking is achieved with a maximum percentage error of 3.4%.

It is noticed that the performance of the PDG control for FJM is highly sensitive to the choice of the position and velocity gains. In spite of the adaptive approach employed for adjusting the gains during tracking, there does not exist a simple rule for the selection of the fixed gains, i.e. k_{p1} and k_{p3}.
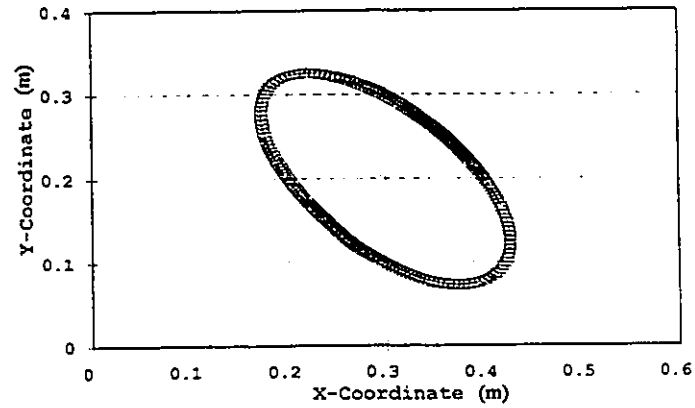
(a) Trajectories. ← DESIRED ← ACTUAL
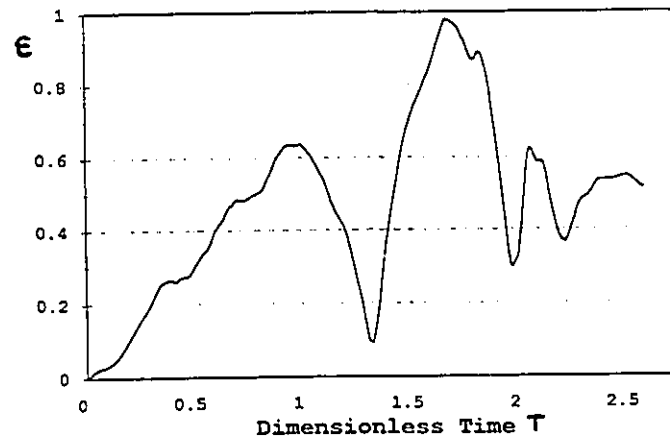
(b) Percentage error.
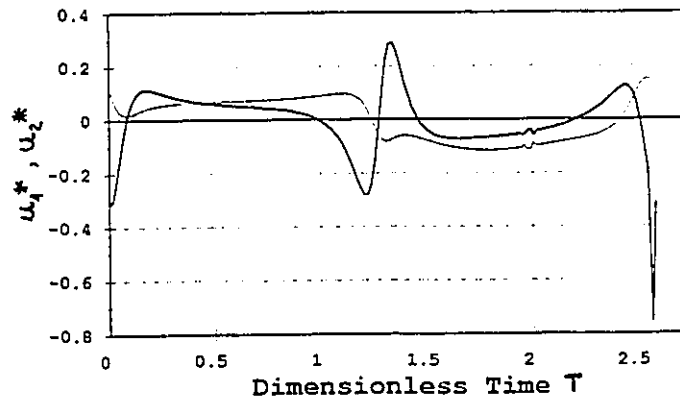
(c) Control voltages. — u1· — u2·

Figure 4.9: PDG for FJM (ellipse) - ε and u*.

$(k_{p1}=k_{p3}=0.01; \omega_0=5.671 \text{ rad/s}; V=0.3 \text{ m/s})$
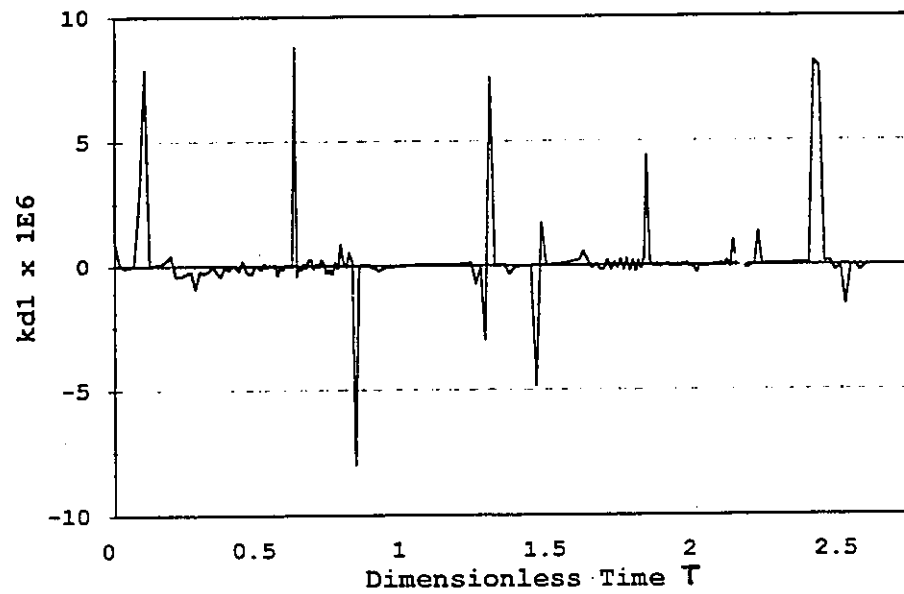
(a) Velocity gain k_{d1}.
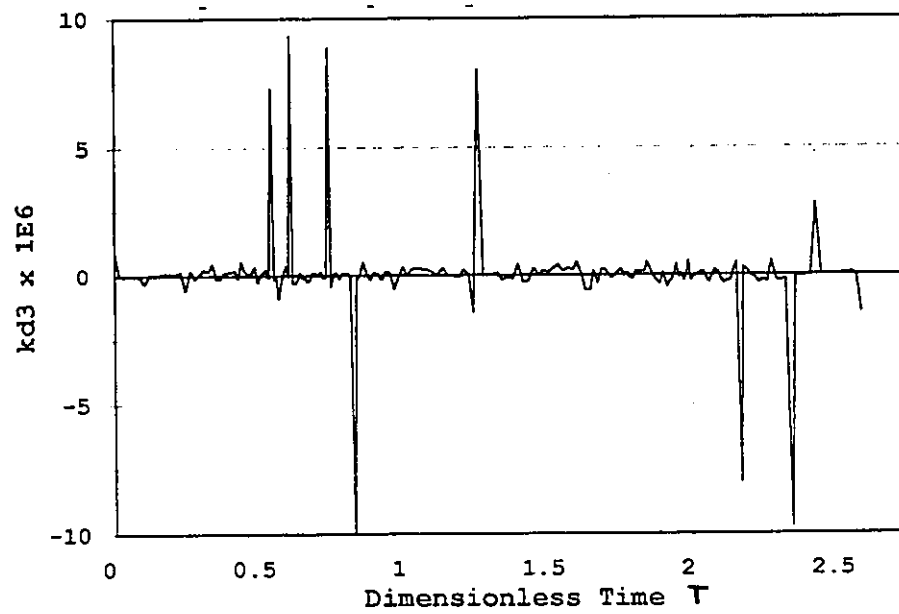
(b) Velocity gain k_{d3}.

Figure 4.10: PDG for FJM - k_{d1} and k_{d2}.

($k_{p1} = k_{p3} = 0.01$; $\omega_0 = 5.671$ rad/s ; V = 0.3 m/s)
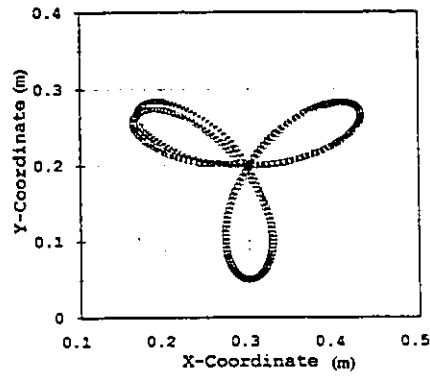
(a) Trajectories (max. ε=3.4%). — REFERENCE — ACTUAL
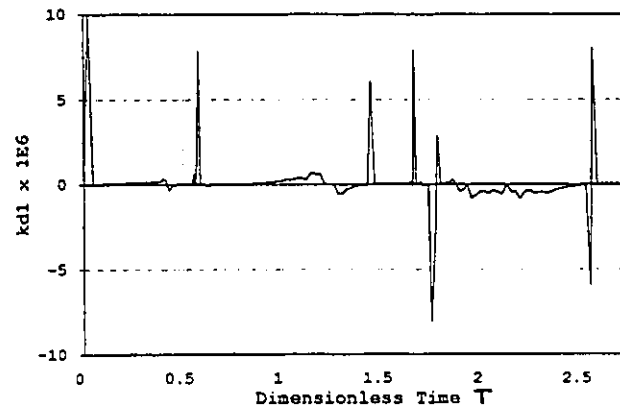
(b) Velocity gain k_{d1}.
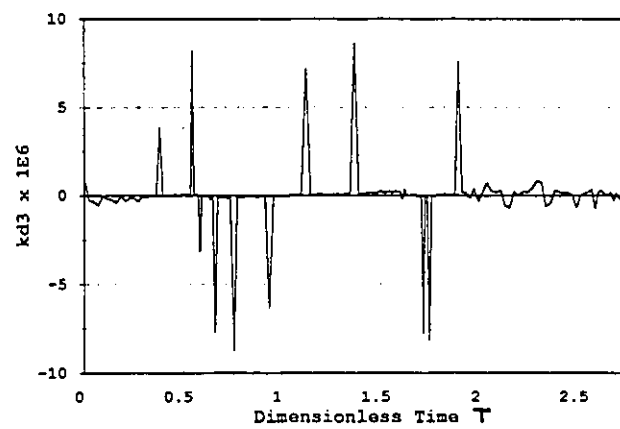
(c) Velocity gain k_{d3}.

Figure 4.11: PDG for FJM (rose) - k_{d1} and k_{d3}.

$(k_{p1} = k_{p3} = 0.01$; $\omega_0 = 5.671$ rad/s ; $V = 0.3$ m/s$)$

4.7 FEEDBACK LINEARIZATION CONTROL

This strategy is known in the literature under different names and with slight variations. It is known as the "Inverse Dynamics Control" or the "Computed Torque Control" when applied to manipulators with rigid links. The strategy assumes that the reference trajectory is smooth and has first and second derivatives.

The approach makes direct use of the complete model describing the dynamics of the elbow arm to cancel not only the effects of gravity, but also the centrifugal force, Coriolis forces if present, friction and the manipulator's inertia tensor. Using (2.18), one can write:

$$[D(\underline{q})] \; \underline{q}'' + \underline{c} \; (\; \underline{q},\underline{q}') + \underline{b} \; (\underline{q}) + \underline{h} \; (\underline{q}') = \{\underline{\tau}\} \qquad (4.12.a)$$

The control law to be used for "feedback linearization" is referred to have as FBL, and is given by:

$$\underline{\tau} = [D(\underline{q})] \; \underline{v} + \underline{c} \; (\underline{q} \; , \; \underline{q}') + \underline{b} \; (\underline{q}) + \underline{h} \; (\underline{q}') \qquad (4.12.b)$$

where $\underline{v}$ is chosen in the following form:

$$\underline{v} = [K_p] \; \{\underline{r} - \underline{q}\} + [K_d] \; \{\underline{r}' - \underline{q}'\} + \underline{r}'' \qquad (4.12.c)$$

where $[K_p]$, $[K_d]$ and $\underline{r}$ are as defined before in connection with equation (4.6). To verify that the control law guarantees asymptotic stability, one substitutes (4.12.b) in (4.12.a) to obtain:

$$[D(\underline{q})] \; \underline{q}'' - [D(q)] \; \underline{v} = \underline{0}$$

which yields

$$\underline{q}'' - [K_p] \; \{ \; \underline{r} - \underline{q} \; \} + [K_d] \; \{ \; \underline{r}' - \underline{q}' \; \} - \underline{r}'' = 0 \qquad (4.12.d)$$

Recalling that the error $\underline{e}$ is defined as:

$$\underline{e} = \underline{r} - \underline{q} \qquad\qquad (4.12.e)$$

then relation (4.12.d) reads:

$$\underline{e}'' + [K_d]\, \underline{e}' + [K_p]\, \underline{e} = \underline{0} \qquad\qquad (4.12.f)$$

Since $[K_p]$ and $[K_d]$ are positive definite then the tracking error $\underline{e}$ converges to zero exponentially. It is possible to choose

$$[K_p] = \begin{bmatrix} \nwarrow & & \\ & \lambda_i^2 & \\ & & \searrow \end{bmatrix} \quad ; \quad [K_d] = \begin{bmatrix} \nwarrow & & \\ & 2\,\lambda_i & \\ & & \searrow \end{bmatrix} \qquad (4.12.g)$$

where λ is a positive number. This implies a critically damped system which converges without oscillation. The closed loop system, using the FBL control law, can be represented by the block diagram shown in Figure 4.13.

The inner loop attempts to cancel the undesired nonlinear dynamics while the outer loop inserts the desired linear dynamics. If $[K_p]$ and $[K_d]$ are diagonal, the closed loop equations of motion are not only linear but are also uncoupled.
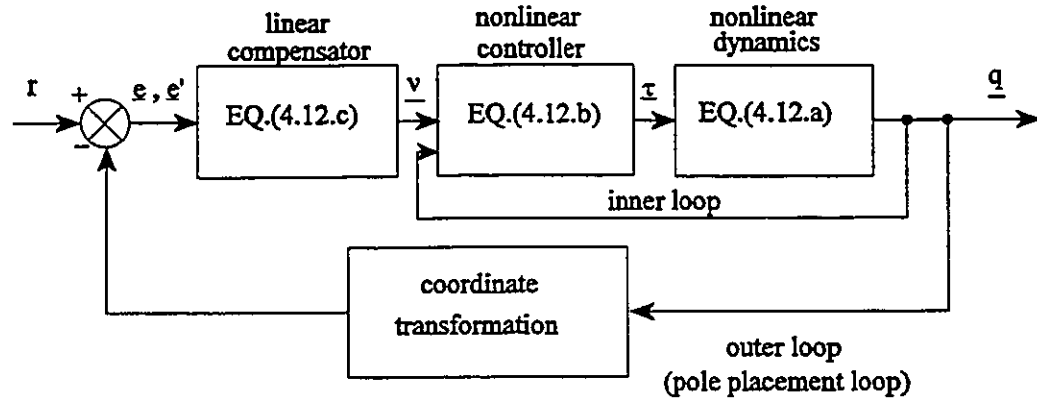
Figure 4.12: Architecture of feedback linearization.

For computer simulation, relations (4.12) can be rearranged to read:

$$\underline{q}' = \underline{v}$$

$$\underline{v}' = [D]^{-1} \{ \underline{\tau} - \underline{c} (\underline{q}, \underline{v}) - \underline{b} (\underline{q}) - \underline{h} (\underline{v}) \}$$

$$\underline{e} = \underline{r} - \underline{q}$$

$$\underline{\tau} = \underline{c} + \underline{b} + \underline{h} + [D] \left\{ [K_p] \{\underline{r} - \underline{q}\} + [K_d] \{\underline{r}' - \underline{q}'\} \underline{r}'' \right\} \tag{4.13}$$

4.8 FBL CONTROL FOR RAM

The feedback linearization is applied here to the RAM and the results are compared with the PDG control. Equations (4.13) are written in an expanded form as follows:

$$
\begin{Bmatrix} q_1' \\ q_2' \end{Bmatrix} = \begin{Bmatrix} v_1 \\ v_2 \end{Bmatrix}
$$

$$
\begin{Bmatrix} v_1' \\ v_2' \end{Bmatrix} = \begin{bmatrix} k_{p1} & 0 \\ 0 & k_{p2} \end{bmatrix} \begin{Bmatrix} r_1 - q_1 \\ r_2 - q_2 \end{Bmatrix} + \begin{bmatrix} k_{d1} & 0 \\ 0 & k_{d2} \end{bmatrix} \begin{Bmatrix} r_1' - q_1' \\ r_2' - q_2' \end{Bmatrix} + \begin{Bmatrix} r_1'' \\ r_2'' \end{Bmatrix}
$$

$$(4.14.a)$$

Denoting $X_1 = q_1$, $X_2 = q_1'$, $X_3 = q_2$, $X_4 = q_2'$ the required equations for computer simulation read:

$$
X_1' = X_2
$$

$$
X_2' = k_{p1} \ (r_1 - X_1) + k_{d1} \ (r_1' - X_2) + r_1''
$$

$$(4.14.b)$$

$$
X_3' = X_4
$$

$$
X_4' = k_{p2} \ (r_2 - X_3) + k_{d2} \ (r_2' - X_4) + r_2''
$$

The torques in this case are evaluated using:

$$
\tau_1 = c_1 + b_1 + h_1 + d_{11} \ U_1 + d_{12} \ U_2
$$

$$
\tau_2 = c_2 + b_2 + h_2 + d_{21} \ U_1 + d_{22} \ U_2
$$

where

$$
U_1 = k_{p1} \ (r_1 - X_1) + k_{d1} \ (r_1' - X_2) + r_1''
$$

$$
U_2 = k_{p2} \ (r_2 - X_3) + k_{d2} \ (r_2' - X_4) + r_2''
$$

$$(4.14.c)$$

The quantities (c_1, c_2), (b_1, b_2), (h_1, h_2) and $(d_{11}, d_{12}, d_{21}, d_{22})$ are all as defined in relations (4.3.a) and (4.3.b).

Relations (4.14.b) and (4.14.c) are implemented in a computer routine FBLRAM

to study the tracking aspects of the elbow arm using feedback linearization. Typical results are shown in Figure 4.13 for tracking a rose and Figure 4.14 for tracking a square. Almost perfect tracking is obtained. The accuracy of tracking is high and the control voltages vary smoothly during tracking, i.e. they are free from noise.

The maximum percentage of the error is down to 0.0156% for the rose and down to 0.273% for the square. It was impossible to reach these levels with any combination of gains in the PDG case.

It should be noticed that the governing relations of the elbow arm contain strong nonlinearities which manifest themselves in terms such as $\sin(q_2-q_1)$, $\cos(q_2-q_1)$, $\cos(q_1)$, $\cos(q_2)$, $(q_1'^2)$ and $(q_2'^2)$. One cannot generalize or extrapolate the findings of one case to predict another. However, judging from the very large number of simulation cases which were performed, it was consistently found that the feedback linearization, for the same gains, gave much higher accuracy and slightly higher torques in comparison with the PDG control. The torques for the FBL were also found to be much smoother. The fact that the torques were found to be consistently higher for the FBL in comparison with the PDG can be explained by comparing the expressions for the torques τ for the two regimes, i.e. equations (4.6) and (4.14.c).

Some unusual and unexpected results were encountered during simulation. The results were repeatable and consistent for numerous simulations using different position and velocity gains for both the PDG and the FBL. The following is a short list for our observations:

(a) Trajectories. — REFERENCE -o- ACTUAL

(b) Percentage error.

(c) Command voltages. — u1* — u2*

Figure 4.13: Feedback linearization-RAM (rose).

-almost perfect tracking($k_{p1}=k_{p2}=0.3\times10^{7}$; $k_{d1}=k_{d2}=0.1\times10^{5}$; V=3 m/s ; ω_0=5.671 rad/s)

(a) Trajectories. — REFERENCE —•— ACTUAL
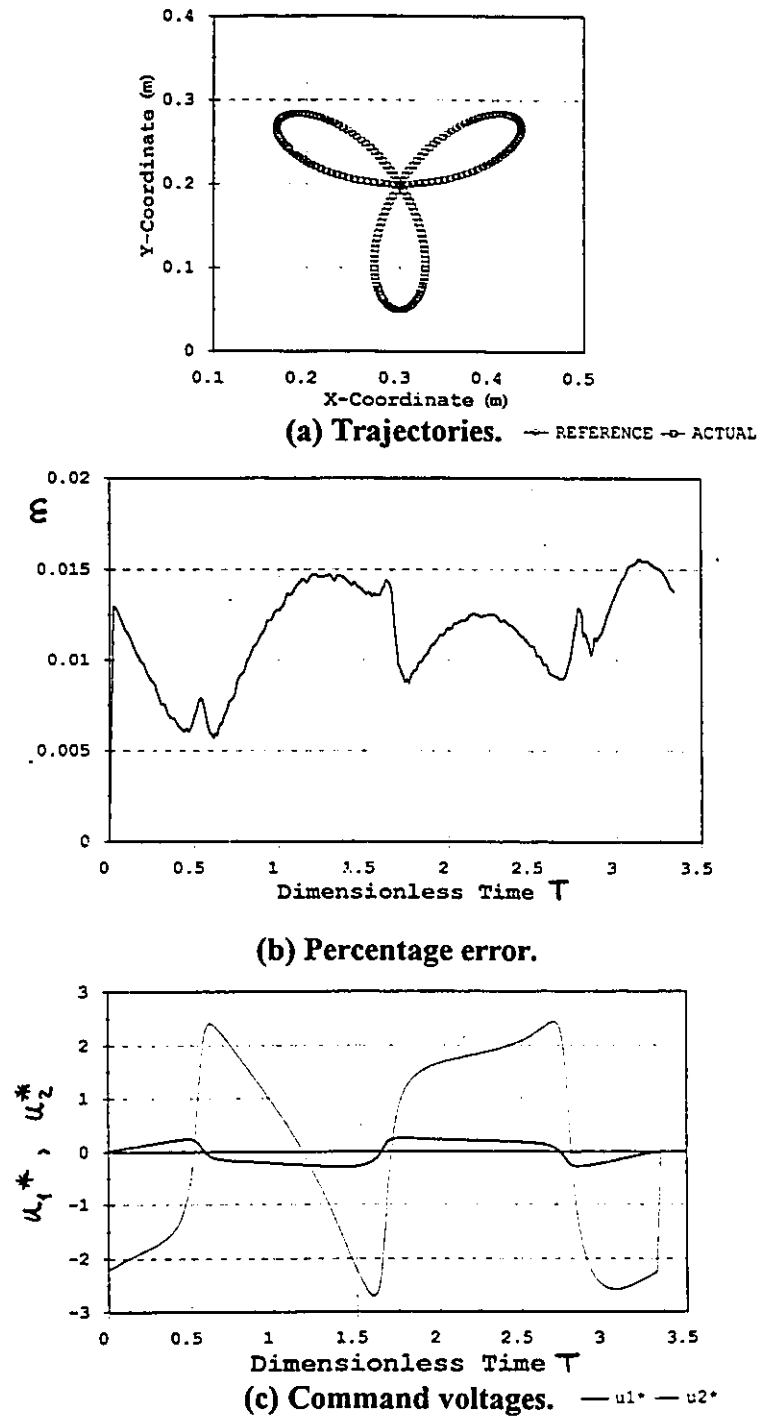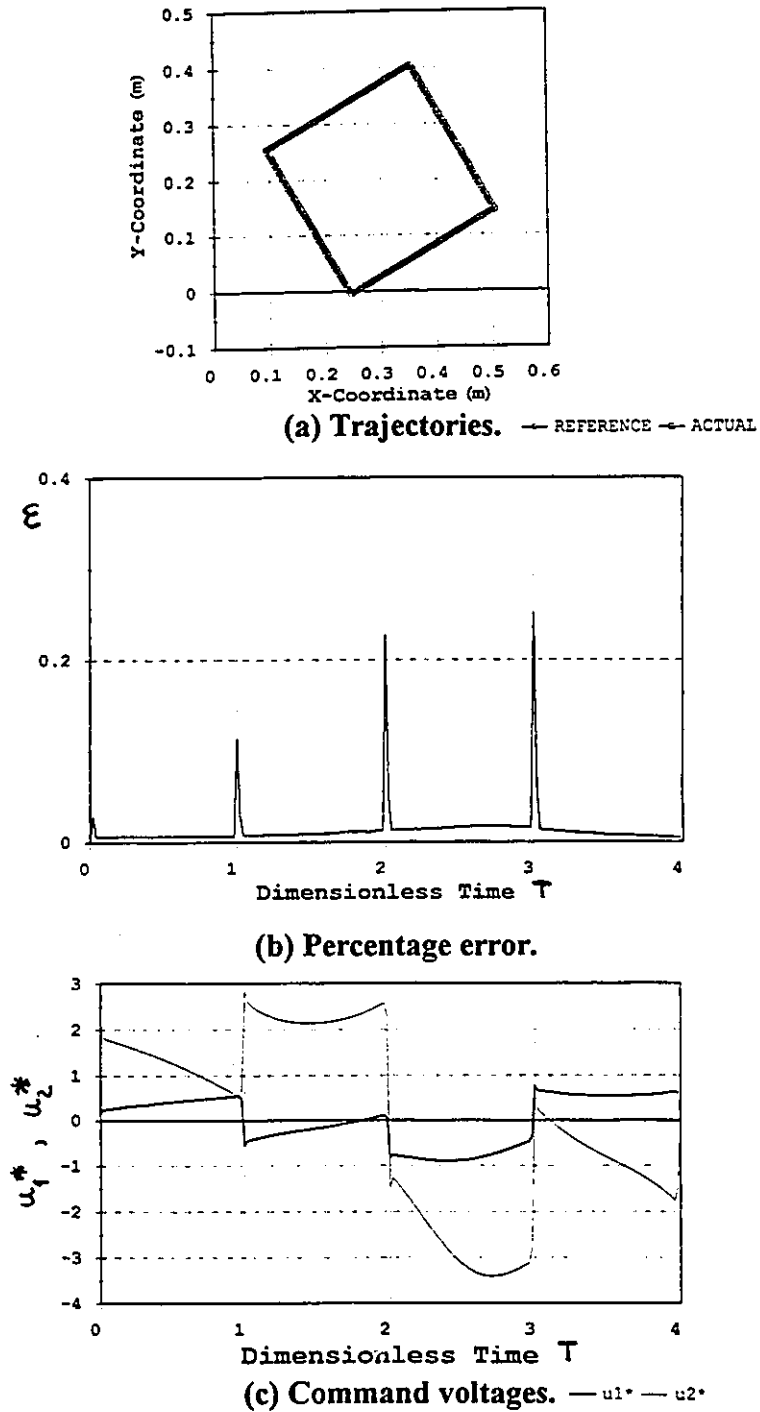
(b) Percentage error.

(c) Command voltages. — u1• — u2•

Figure 4.14: Feedback linearization - RAM (square)

- almost perfect tracking(k_{p1}=k_{p2}=0.3×10^7; k_{d1}=k_{d2}=0.1×10^5 ; V=3 m/s ; ω_0=5.671 rad/s) .

(a)   Many sets of gains failed to yield successful tracking using PDG. The same sets when used with FBL gave almost perfect tracking.

(b)   Violent oscillations and sharp spikes in the command voltages are generally filtered out by the dynamics, specially with FBL, and are never felt in the actual tracking.

(c)   There exists sets of gains which can give optimum tracking, i.e. with the lowest possible percentage error for the lowest possible command voltages. These are hard to define analytically. They are obtained here, for the simulation, by a trial-and-error approach.

(d)   The FBL is indeed a robust control. The gains were brought down from $(0.3 \times 10^7, 0.1 \times 10^5)$ for k_p and k_d to $(0.3 \times 10^5, 0.1)$. Tracking for the rose and the square was still possible and was smooth and acceptable with a maximum percentage error equal to 0.0356% for the rose and 2.31% for the square. The only thing that suffered was the command voltages which exhibited violent oscillations as shown in Figure 4.15. In spite of the oscillatory nature of the command signals, the smoothness of the actual tracking was not affected too much.

(e)   The PDG control was found to be super sensitive to the variations of the parameters of the system and to the choice of gains.
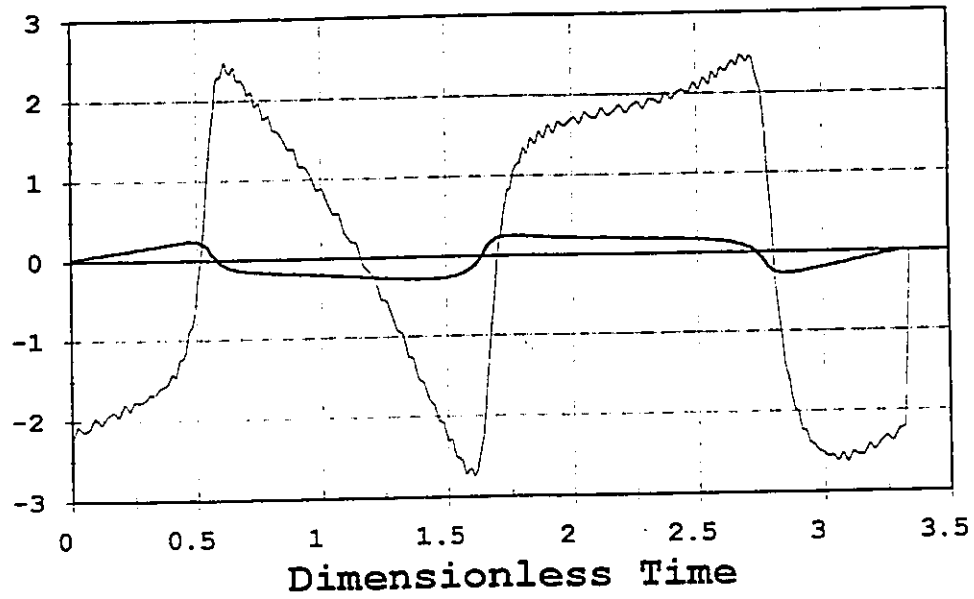
(a) Rose (max. ε = 0.0356%). —— u1* —— u2*
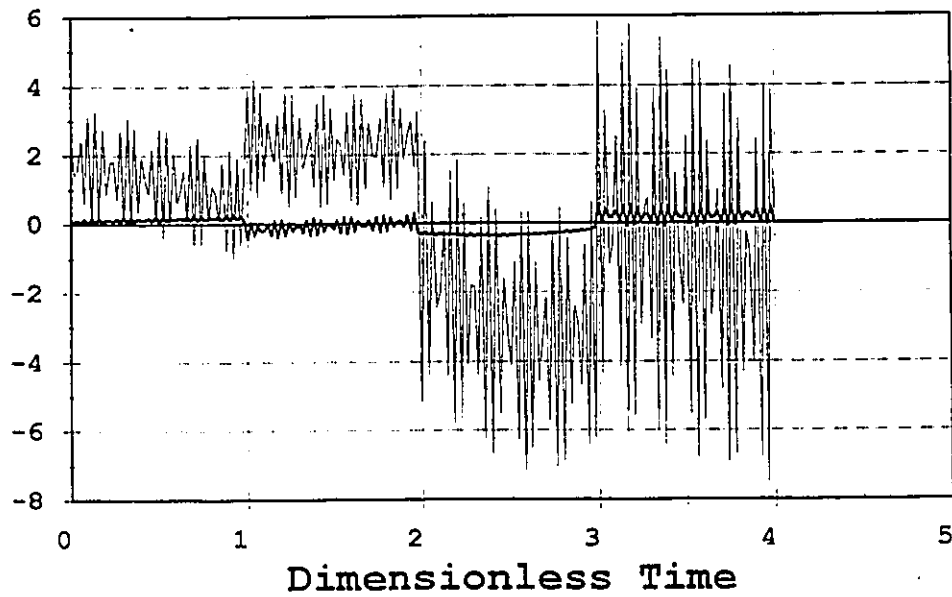
(b) Square (max ε = 2.31%). —— u1* —— u2*

Figure 4.15: The FBL - RAM is indeed a ROBUST CONTROL.

(gains changed drastically) ($k_{p1}=k_{p2}=0.3\times10^7$; $k_{d1}=k_{d2}=0.1$; V=3 m/s ; $\omega_0=5.671$ rad/s)

4.9 FBL CONTROL FOR FJM

The FJM is written in the form:

$$[M] \; \underline{X}'' + [C] \; \underline{X}' + [G] \; \underline{X} + \underline{h} = \underline{\tau} \tag{4.15.a}$$

where:

$\underline{X} = [\phi_1, \Psi_1, \phi_2, \Psi_2]^T$ and [M], [C], [G] and $\underline{h}$ are as defined by relations (2.21.b).

$$\tau = [\; \tau_1 \; , \; 0 \; , \; \tau_2 \; , \; 0 \;]^T = [\; \mu_1^0 \, u_1^* \; , \; 0 \; , \; \mu_2^0 \, u_2^* , \; 0 \;]^T$$

with μ_1^0, μ_2^0, u_1^*, u_2^* as defined by (2.4) and (2.9).

For feedback linearization, one makes use of the error vector $\underline{e}$ given by:

$$\underline{e} = \underline{r} - \underline{X} \tag{4.15.b}$$

where $\underline{r}$ and $\underline{x}$ are the desired and the actual position vectors for every point on the trajectory. $\underline{\tau}$ in (4.15.a) is chosen in the following form:

$$\underline{\tau} = [M] \; \underline{v} + [C] \; \underline{X}' + [G] \; \underline{X} + \underline{h} \tag{4.15.c}$$

where:

$$\underline{v} = [K_p] \; \underline{e} + [K_d] \; \underline{e}' + \underline{r}'' \tag{4.15.d}$$

$[K_p]$ = An all-zero (4×4) position gain matrix except for $(k_p)_{1,1} = k_{p1}$; $(k_p)_{3,3} = k_{p3}$

$[K_d]$ = An all-zero (4×4) velocity gain matrix except for $(k_d)_{1,1} = k_{d1}$; $(k_d)_{3,3} = k_{d3}$

Substituting (4.15.c), (4.15.d) in (4.15.a) one obtains:

$$[M] \; \underline{X}'' + [C] \; \underline{X}' + [G] \; \underline{X} + \underline{h} = [C] \; \underline{X}' + [G] \; \underline{X} + \underline{h} + [M] \; \{[K_p] \; \underline{e} + [K_d] \; \underline{e}' + \underline{r}''\}$$

which yields

$$X'' + [K_d] \, X' + [K_p] \, X = [K_p] \, \underline{r} + [K_d] \, \underline{r}' + \underline{r}'' \qquad (4.16)$$

Simulation in this case is performed using relation (4.16), where the R.H.S. is known for every point on the trajectory.

$$\underline{\tau} = [C] \, X' + [G] \, X + \underline{h} + [M] \left\{ [K_p] \, \underline{e} + [K_d] \, \underline{e}' + \underline{r}'' \right\}$$

Using relations (2.21.b) one writes the first and third relations of the previous matrix equation in the following expanded form:

$$\mu_1^0 \, \dot{u}_1 = b_{11} \, X_1' + \omega_1^2 \, X_1 - b_{12} \, X_2 + k_{p1} \, (r_1 - X_1) + k_{d1} \, (r_1' - X_1') + r_1''$$

$$\mu_2^0 \, \dot{u}_2 = b_{31} \, X_3' + \omega_3^2 \, X_3 - b_{32} \, X_4 + k_{p3} \, (r_3 - X_3) + k_{d3} \, (r_3' - X_3') + r_3''$$

$$(4.17.a)$$

One can select fixed values for (k_{p1}, k_{p3}) and evaluate (k_{d1}, k_{d3}) using:

$$k_{d1} = [\, \mu_1^0 \, \dot{u}_1 - (b_{11} \, X_1' + \omega_1^2 \, X_1 - b_{12} \, X_2) - k_{p1} \, (r_1 - X_1) - r_1'' \,] \, \Big/ \, (r_1' - X_1')$$

$$k_{d3} = [\, \mu_2^0 \, \dot{u}_2 - (b_{31} \, X_3' + \omega_3^2 \, X_3 - b_{32} \, X_4) - k_{p3} \, (r_3 - X_3) - r_3'' \,] \, \Big/ \, (r_3' - X_3')$$

$$(4.17.b)$$

The previous strategy is implemented in a computer routine FBLFLX using the Newmark algorithm. Several cases were simulated using different gains, integration steps and parameters.

Typical results are shown in Figure 4.16 for an elbow arm tracking an ellipse. The parameters of the elbow arm are as given by Equation (3.1). The following additional parameters are also used:

$\omega_0 = 5.67$ rad/s ; $V = 0.3$ m/s ; no. of points = 395;

no. of intermediate steps = 3 ; $\alpha = 1/6$; $\delta = 1/2$

$k_{d1} = 10$; $k_{d3} = 10$

In all the simulations, the controller was found to be robust as expected. The response was found to be insensitive to small deviations in the parameters and gains. However, the accuracy of tracking was found unacceptable for the majority of the cases simulated. The maximum error percentage for Figure (4.16) was found to be 8.45%. The command voltages, as shown in Figure (4.16.b) and the position gains as in Figure (4.16.c), were found oscillatory. However, these oscillations did not affect the smoothness of the tracking.

The feedback linearization control is judged to be inefficient in the presence of compliance in the elbow arm.
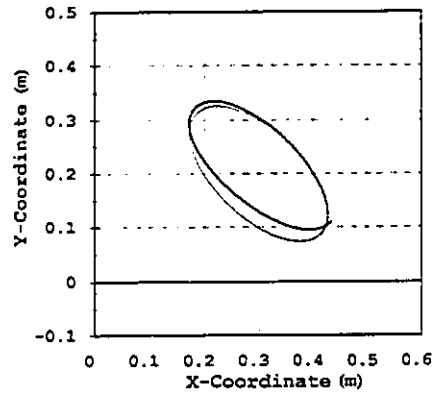
(a) Trajectories. ---- REFERENCE ---- ACTUAL
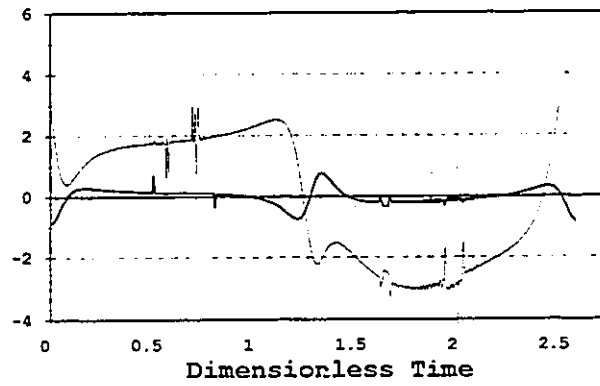
(b) Command voltages. — u1* — u2*
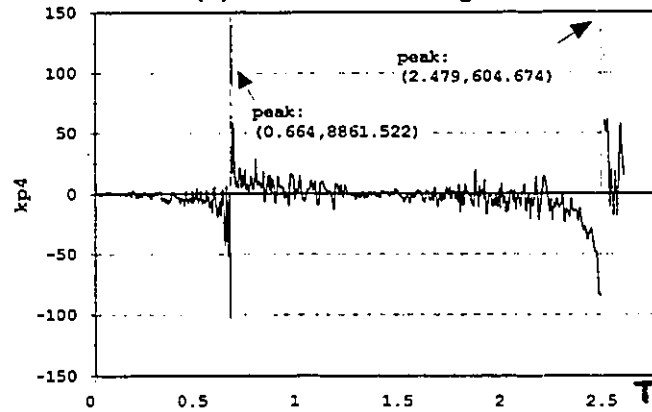
(c) Position gain k_{p3}.

Figure 4.16: The FBL-FJM is indeed a robust control but poor tracking.

($k_{d1} = 10$, $k_{d3} = 10$; $\omega_0 = 5.67$ rad/s ; V = 0.3 m/s)

4.10 VARIABLE STRUCTURE CONTROL

In this strategy, the control voltage is switched from a + ã to - ã and vice versa according to a prescribed criterion. Figure 4.17 demonstrates the basic blocks which form the "variable structure" control as applied to a tracking elbow arm.
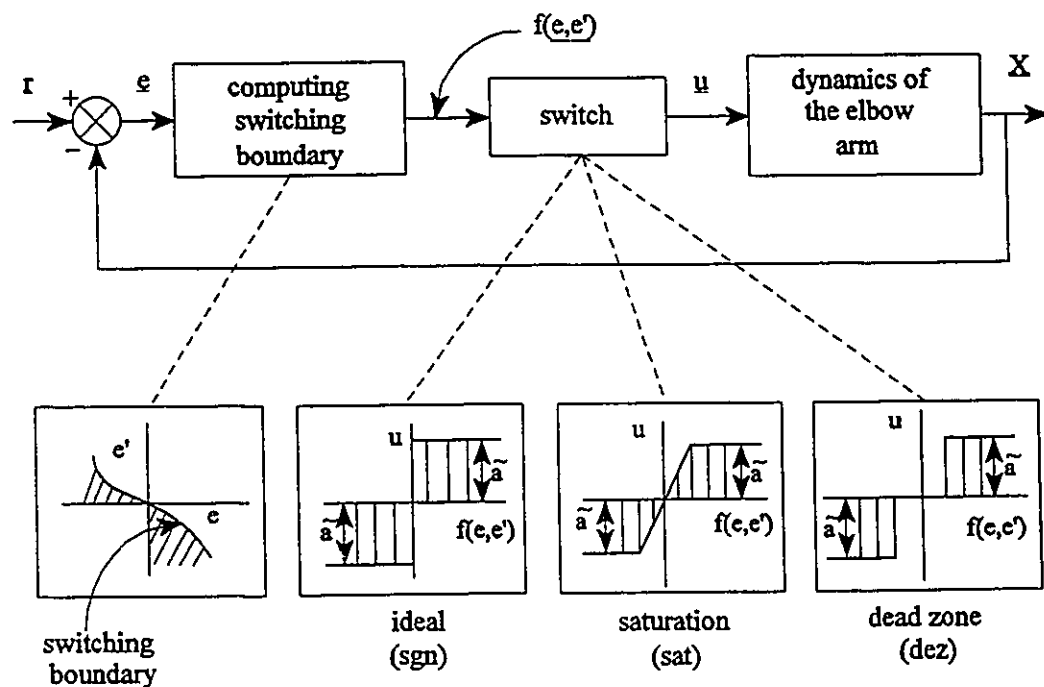
Figure 4.17: Variable structure control.

The signal f(e,e') obtained from the "computing switching boundary" block is applied to a switch which can be any one of the following types:

* An ideal relay: "SGN".

* A relay with a narrow linear band around the origin, i.e. saturation: "SAT".

* A relay with a dead zone: "DEZ".

The "SAT" and the "DEZ" types are used to introduce smoothness in the command voltages during switching.

The "Variable Structure Control" has several advantages. The most important one is attributed to the fact that it is essentially a "robust controller", i.e. a control system which is not sensitive to modelling errors. To implement variable structure control, one does not have to use the exact parameters. Only upper and lower bounds of these parameters are required. The approach is normally adequate as long as the variable bounds are reliable. To formulate a "variable structure control" law, one has to set the dynamic model of the system in terms of the error signal $\underline{e}$ and its derivatives. The "variable structure control" is known in practice under different names and variations. The "ON-OFF", the "bang-bang" and the "sliding control" are just a few. The strategy is essentially a minimum-time control problem. Pontryagin's minimum principle can be used to show that this type of control is an admissible class which achieves the transition from an initial state to a target set in the state space in the shortest time.

Here we develop the strategy for the control of a rigid single link manipulator. The system is essentially a single degree of freedom positioning servo. One can use relation (2.2.d) for the actuator to write:

$$N \, J_m \, \ddot{x} + N \left(b_m + \frac{b_L}{N^2} + \frac{k_b \, k_m}{R_a} \right) \dot{x} = \left(\frac{k_m}{R_a} \right) u^0 - \frac{1}{N} \tau^0 \quad \textbf{(4.18.a)}$$

where the coefficients in (4.18.a) are as defined before in Chapter 2. Referring to Figure 4.18, one can write the following relation for the dynamics of the link:

$$\tau^0 = I \; \ddot{x} + m \; a_c^2 \; \ddot{x} + m \; g \; a_c \; \cos \; x \qquad\qquad \textbf{(4.18.b)}$$
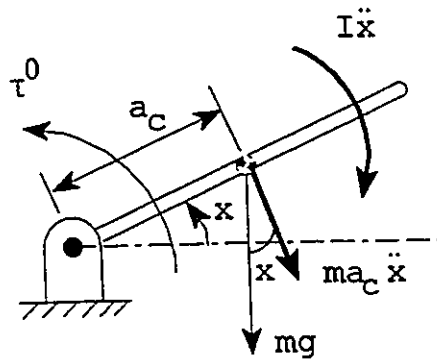
Figure 4.18: External forces and torques on link.

where I, m and a_c are the mass-moment of inertia, the mass and the distance from the motor

to the center of mass of the link respectively.

Eliminating τ^0 between (4.18.a) and (4.18.b) and introducing the dimensionless time

T defined by (2.3) one obtains:

$$X'' + (\tilde{k}) \; X' + \tilde{b} \; \cos \; X = \tilde{\mu} \; \tilde{u} \qquad\qquad \textbf{(4.19)}$$

where:

$$\tilde{k} = \left\{ \frac{N^2 \; b_m + b_L + \left(N^2 \; k_b \; \dfrac{k_m}{R_a} \right)}{\omega_0 \; (\; N^2 \; J_m + I + m \; a_c^2 \;)} \right\} \qquad ; \; \tilde{b} = \frac{m \; g \; a_c}{\omega_0^2 \; (\; N^2 \; J_m + I + m \; a_c^2 \;)}$$

$$\tilde{\mu} = \frac{N \; k_m \; E_0}{R_a \; \omega_0^2 \; (\; N^2 \; J_m + I + m \; a_c^2 \;)} \qquad ; \; \tilde{u} = \frac{u^0}{E_0} \qquad\qquad \textbf{(4.20)}$$

Primes refer to differentiation with respect to the dimensionless time T.

The mathematical model given by (4.19) can be further simplified by dropping the term ($\check{b}$ cos X) which implies that the link is now operating in a horizontal plane. The system becomes linear and is described by:

$$X'' + \tilde{k} \, X' = u \qquad\qquad \textbf{(4.21.a)}$$

where u(T) is an unknown control command which is required to drive the state vector from its initial position to its required target position in the state space in the shortest possible time. Adopting the "SGN" control law, one can construct the block diagram shown in Figure 4.19 where b is a feedback gain.
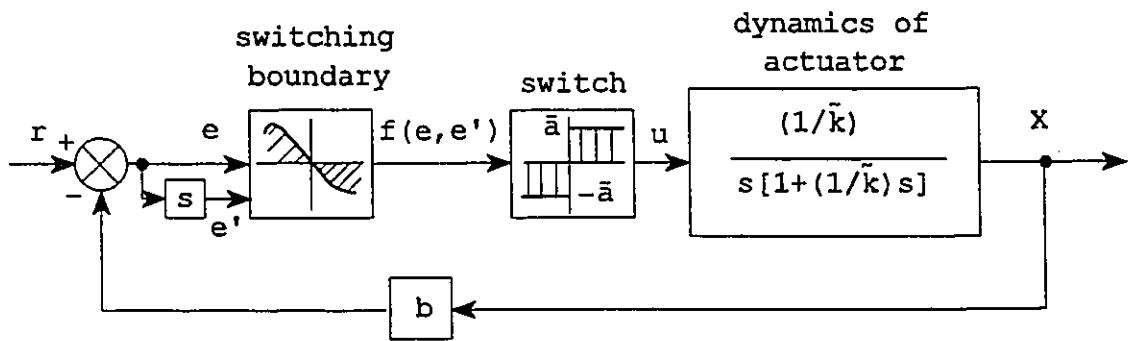
Figure 4.19: Variable Structure Control for a Single Link.

One can define

$$e = r - b \, X \; ; \; e' = r' - b \, X' \; ; \; u = \tilde{a} \; sgn \; [\, f \, (e, e') \,] \qquad\qquad \textbf{(4.21.b)}$$

where sgn(η) is a function which is defined as follows:

$$sgn(\eta) \quad = \quad 1 \text{ for } \eta > 0$$

$$= \text{-1 for } \eta < 0$$

$$= \quad 0 \text{ for } \eta = 0$$

r(T) is assumed to be a step demand given by:

$$r\ (T)\ =\ A_s\ U_0\ (T)\ ;\ r'\ (T)\ =\ 0$$

where: A_s = Step height (constant) ; $U_0(T)$ = Unit step at $\lambda = 0$

Using equations (4.21.b) one can express the relation which governs the single link actuator

in terms of e and its derivatives as follows:

$$e'' + \tilde{k}\ e' + \bar{b}\ sgn\ [f(e,e')] = 0 \qquad\qquad (4.22)$$

where:

$$\tilde{b} = b\ \tilde{a}$$

For f(e,e') > 0, the previous relation has an exact solution. The phase plane

trajectory in this case can be shown to be given by

$$e\ =\ A_s\ -\ \left(\ \frac{1}{\tilde{k}}\ \right)\ e'\ +\ \left(\ \frac{\tilde{b}}{\tilde{k}^2}\ \right)\ \ln\ \left[\ 1\ +\ \left(\ \frac{\tilde{k}}{\tilde{b}}\ \right)\ e'\ \right] \qquad (4.23.a)$$

which represents a family of trajectories which cover the e-e' phase plane with A_s as a

parameter. It is noticed that as $T \to \infty$, e' approaches a limiting value $(- \tilde{b} / \tilde{k})$ and e approaches $-\infty$. When plotted in the phase plane, the trajectories appear as distorted parabolas with their branches pointing in the direction of the negative e-axis as shown in Figure (4.20.a).

The case of $f(e,e') < 0$ is associated with the trajectories given by:

$$e = A_t - \left(\frac{1}{\tilde{k}} \right) e' - \left(\frac{\tilde{b}}{\tilde{k}^2} \right) \ln \left[1 - \left(\frac{\tilde{k}}{\tilde{b}} \right) e' \right] \qquad (4.23.b)$$

They appear as shown in Figure (4.20.b).

The phase plane portrait of the single link manipulator is as shown in Figure 4.20.c. The representative point is confined to move along one of these trajectories at a time. When $f(e,e')$ is positive, the movement takes place along a trajectory marked with (0). When $f(e,e')$ is negative, the movement is confined along a trajectory marked with an (X). Switching from one family to the other occurs whenever $f(e,e')$ is zero.

One is free to select the switching boundary $f(e,e')$ which has to pass by the origin of the phase plane. A simple choice for $f(e,e')$ is a straight line given by:

$$f(e \ e') = e' + v \ e \qquad (4.24)$$

where v is a positive constant. This is not the best choice since the system takes a longer time to reach its equilibrium state. Multiple switching and chatter are inevitable. The upper part of the trajectory for $f(e,e') > 0$ which passes through the origin and the lower part of the trajectory for $f(e,e') < 0$ which also passes through the origin furnish an optimum switching boundary. That boundary guarantees one switching and smooth sliding to the equilibrium state in the shortest possible time.
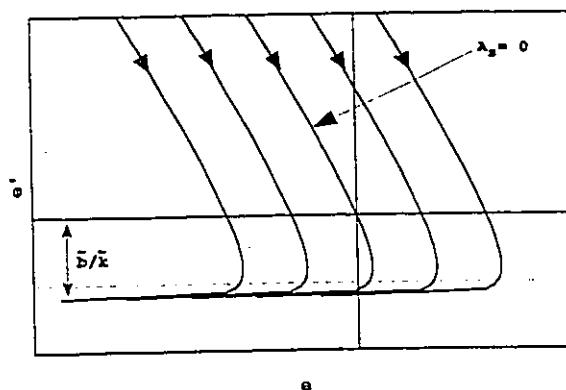
(a) Case f(e,e') > 0.
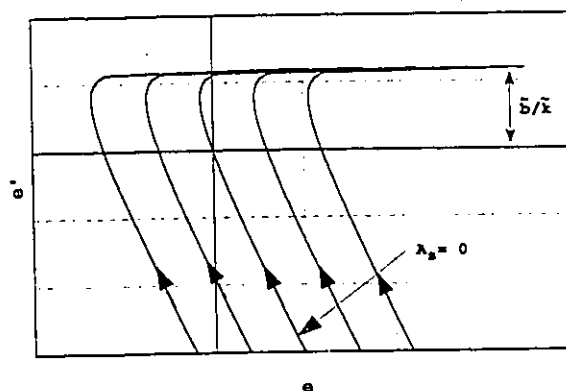
(b) Case f(e,e') < 0.
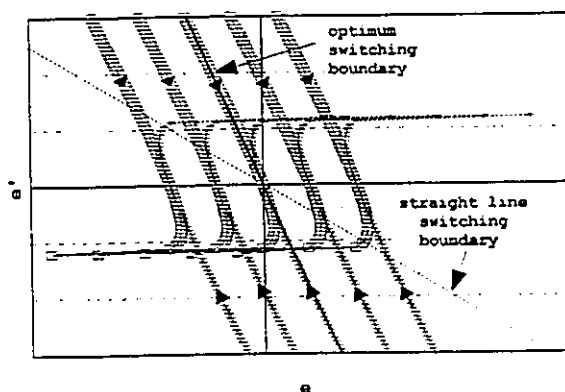
(c) Phase plane portrait.

Figure 4.20: Step response of a single link manipulator.

To facilitate the implementation of the previous strategy in practical systems, one drops the damping term $\tilde{k}$ from equation (4.22). One can show that the phase plane portrait in this case is given by:

$$e\,'' + \left(\frac{1}{2\tilde{b}^{\,2}} \right) (e\,')^2 = A_s \qquad \text{for } f(e,e\,') > 0$$

$$e\,'' - \left(\frac{1}{2\tilde{b}^{\,2}} \right) (e\,')^2 = A_s \qquad \text{for } f(e,e\,') < 0 \tag{4.25}$$

These represent two families of symmetric parabolas in the phase plane as shown in Figure (4.21).

Figure 4.21: Phase plane portrait for $\tilde{k} = 0$.

The optimum switching boundary is formed by the upper part of the parabola through the origin for $f(e, e') > 0$ and the lower part of the parabola through the origin for $f(e, e') < 0$ as shown in Figure (4.21). The governing relation of the optimum switching boundary can be shown to be given by:

$$e + v \quad e' \, |e'| = 0 \qquad\qquad (4.26)$$

where $v = (1 / 2\tilde{b}^2)$.

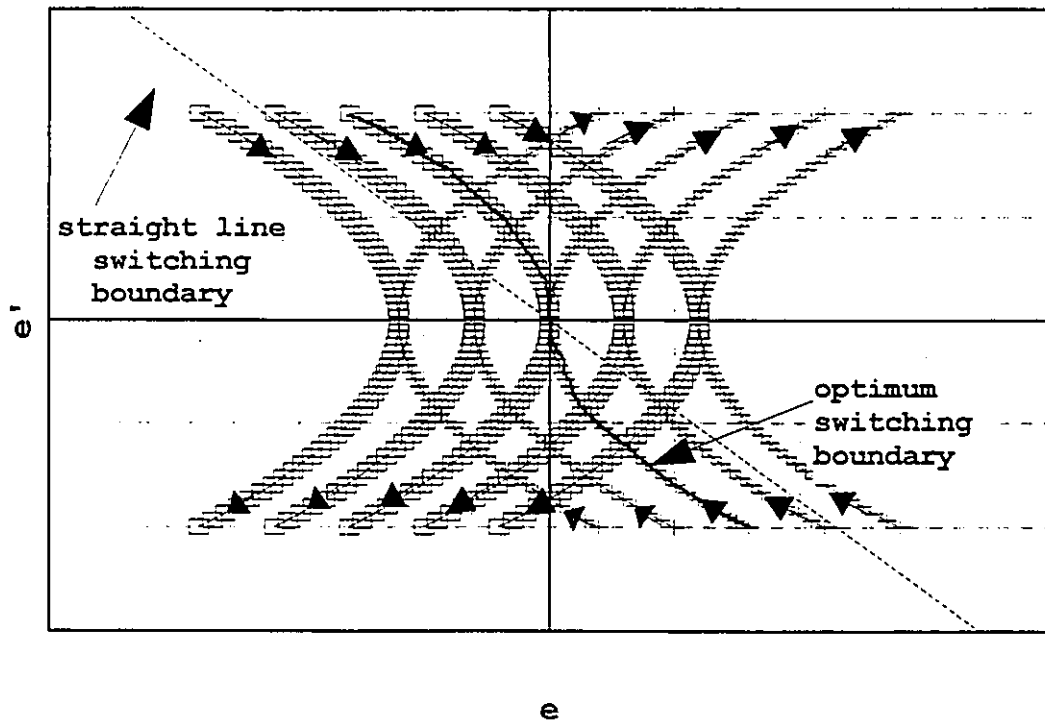This switching boundary is referred to as the VEE-MOD-VEE control. The name is selected because of the presence of the term $e'|e'|$, i.e. velocity-modulus-velocity of error.

Figure 4.22 shows typical step responses for the single link manipulator using a straight line switching boundary. The parameters of the motor and links are as given by relation (3.1). The slope v of the straight line was selected to be equal to 1.

It is noticed that the trajectories for $A_s = 12$ and -8 are associated with more than one switching. The trajectory which pertains to $A_s = 6$ is unique. It is the only case in all possible positive values of A_s where only one switching is obtained followed by a direct movement along the only parabola that passes through the origin, i.e. without sliding along the switching boundary. The trajectory associated with $A_s = -2$ will have one switching followed by a sliding mode towards the origin. The sliding mode in this case, although appears as a smooth movement along the straight line boundary, is normally accompanied by CHATTER. These are rapid and somewhat violent reversals of the command voltage as shown in Figure (4.22.b) for the case $A_s = -2$. Figure (4.22.c) shows the responses of the single link manipulator for four different sizes of the step input.

The behaviour of the same system is shown in Figure 4.23 under the same inputs when a VEE-MOD-VEE control is used. One notices a drastic improvement in the response in spite of the fact that an approximate VEE-MOD-VEE switching boundary is used in place of the exact one given by relations (4.23.a) and (4.23.b). Only one switching occurs regardless of the step size. Comparing Figures (4.23.b) with (4.22.b), one notices that the chatter almost vanished in the sliding mode when the VEE-MOD-VEE control is used.
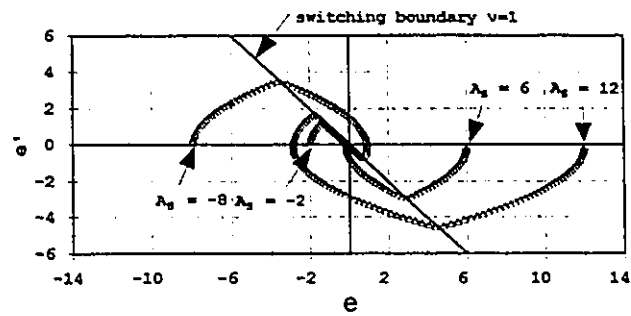
(a) Trajectories and switching boundary.
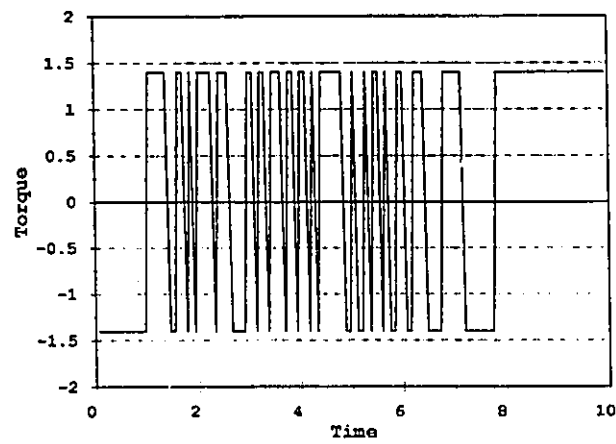
(b) Command voltages for A_s=-2.
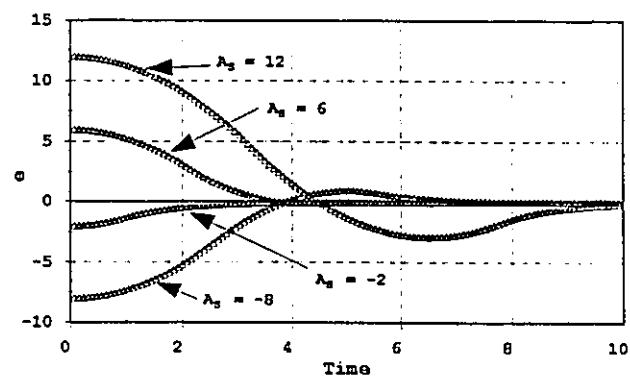
(c) Time response.

Figure 4.22: Straight line switching boundary (Step Response).

(Single link ω_0=0.45×10^4 rad/s)
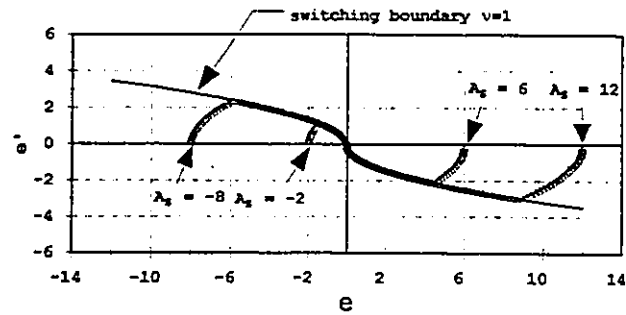
(a) Trajectories and switching boundary.
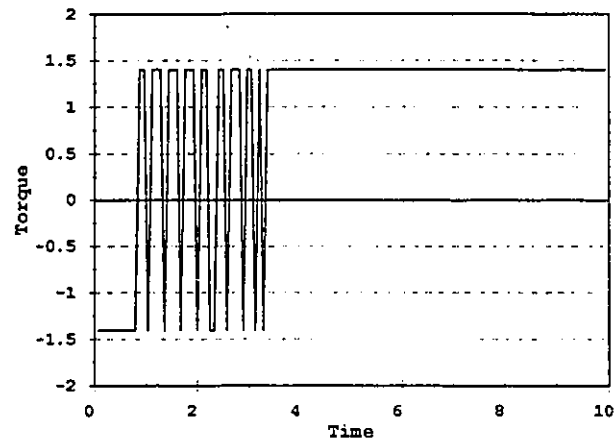
(b) Control voltages for A_s=-2.
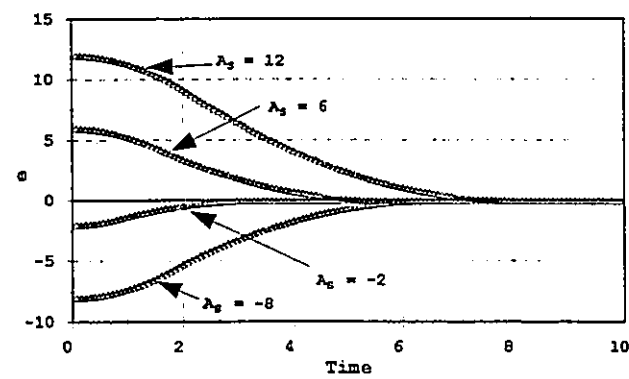
(c) Time response for different step inputs.

Figure 4.23: VEE-MOD-VEE control (Step response).(Single link ω_0=0.45×10^4 rad/s)

4.11 SLIDING CONTROL FOR RAM

The equations governing the RAM are given by (4.2) which reads:

$$[D(\underline{q})] \; \underline{q}'' + \{ \underline{c} \; (\; \underline{q} \; , \; \underline{q}' \;)\} + \{ \underline{b} \; (\underline{q}) \; \} + \{ \underline{h}(\underline{q}) \} = \{\underline{\tau}\} \qquad (4.27.a)$$

where

$\underline{q} = [\Psi_1, \Psi_2]^T$. The elements of $[D]$, $\underline{c}$, $\underline{b}$ and $\underline{h}$ given are as defined by (4.3.a) and (4.3.b). $\underline{\tau}$ is an unknown control command, yet to be determined, such that the wrist of the elbow arm is guaranteed to track a prescribed reference vector $\underline{r}(T)$ which is known together with its derivatives at any instant in time.

The model in (4.27.a) can be expressed in terms of the error vector $\underline{e}$ where:

$$\underline{e} = [\; e_1 \; , \; e_2 \;]^T = \underline{r} - \underline{q}$$

to obtain:

$$\underline{e}'' = \underline{r}'' - [D]^{-1} \{ \; \underline{\tau} - \underline{c} - \underline{b} - \underline{h} \; \} \qquad (4.27.b)$$

Let $\underline{x}$ be the state vector of the system where

$$\underline{x} = [\; e_1 \; , \; e_1' \; , \; e_2 \; , \; e_2' \;]^T = [\; x_1 \; , \; x_2 \; , \; x_3 \; , \; x_4 \;]^T$$

Relations (4.27.b) can be written in the following expanded form:

$$x_1' = x_2 \; ; \; x_2' = (\; \overline{\sigma} \; r_1'' - \omega_1 + \beta_1 \; \omega_2 \;) \Big/ \; \overline{\sigma}$$

$$x_3' = x_4 \; ; \; x_4' = (\; \overline{\sigma} \; r_2'' + \beta_2 \; \omega_1 - \omega_2 \;) \Big/ \; \overline{\sigma} \qquad (4.27.c)$$

where

$$\omega_1 = \hat{\tau}_1 - \alpha_{11} - \alpha_{12}\ (\ r_1' - x_2\ ) + \alpha_{13}\ (\ r_2' - x_4\ )^2$$

$$\omega_2 = \hat{\tau}_2 - \alpha_{21} - \alpha_{22}\ (r_2' - x_4\ ) + \alpha_{23}\ (\ r_1' - x_2\ )^2$$

$$\alpha_{11} = a_{13}\ \bar{c}_1 \qquad ;\ \alpha_{12} = a_{11} \qquad ;\ \alpha_{13} = a_{12}\ \bar{s}_{21}$$

$$\alpha_{21} = a_{23}\ \bar{c}_2 \qquad ;\ \alpha_{22} = a_{21} \qquad ;\ \alpha_{23} = a_{22}\ \bar{s}_{21}$$

$$\beta_1 = a_{12}\ \bar{c}_{21} \qquad ;\ \beta_2 = a_{22}\ \bar{c}_{21}$$

$$\bar{\sigma} = 1 - a_{12}\ a_{22}\ \bar{c}_{21}^{2}$$

$$\bar{c}_1 = \cos\ (\ r_1 - x_1\ )\ ;\ \bar{c}_2 = \cos\ (\ r_2 - x_3\ )$$

$$\bar{c}_{21} = \cos\ [(\ r_2 - x_3\ ) - (\ r_1 - x_1\ )]$$

$$\bar{s}_{21} = \sin\ [(\ r_2 - x_3\ ) - (\ r_1 - x_1\ )] \qquad\qquad (4.27.c)$$

The a_{ij}'s are as defined by (2.18).

The objective now is to find a control law, i.e. select $= [\tau_1\ \tau_2]^T$ as a function of $\underline{x}$ such that tracking is achieved with the minimum possible deviation from the reference vector $\underline{r}(T)$.

A switching boundary $\underline{S}(\underline{x})$ is chosen in the form of a hypersurface to perform the same task as that of the straight line switching boundary discussed in the previous section. $\underline{S}(\underline{x})$ is essentially a linear decoupled combination of $\underline{e}$ and $\underline{e}'$ in the following form:

$$\underline{S}\ (\underline{x}) = \begin{Bmatrix} S_1 \\ S_2 \end{Bmatrix} = \begin{bmatrix} K_1 & 0 \\ 0 & K_2 \end{bmatrix} \begin{Bmatrix} x_1 \\ x_3 \end{Bmatrix} + \begin{Bmatrix} x_2 \\ z_4 \end{Bmatrix} \qquad (4.27.d)$$

when K_1 and K_2 are any two positive numbers. The diagonal matrix [K] is known as the sliding mode gain matrix. $\underline{\tau}$ is chosen to drive the system towards the chosen switching

surface in a finite time after which the system is confined to slide on the surface towards the equilibrium position. The last state is referred to as the "SLIDING MODE".

In the "sliding mode", the following condition is satisfied:

$$\underline{S} \ (\underline{x}) = 0 \qquad\qquad (4.27.e)$$

An examination of (4.27.d) and (4.27.e) shows that the error, in the SLIDING mode, is independent of the parameters of the elbow arm. It is solely dependent on the [K] matrix which controls the slope of the switching surface and consequently controls the "rate" at which the error decreases. Since the solution of (4.27.e) is totally independent of the parameters of the elbow arm, the SLIDING mode is ROBUST. Of course this is only true when one has a smooth operation which does not excite the higher modes.

The desired control law, i.e. the definition of $\underline{\tau}$, is achieved by considering a Liapunov function $V(\underline{x})$ for the system. A natural choice is given by

$$V(\underline{x}) = \frac{1}{2} \ \underline{S} \ (\underline{x})^T \ \underline{S} \ (\underline{x}) \qquad\qquad (4.28.a)$$

It is obvious that $V(\underline{x})$ satisfies the conditions

$$V(\underline{x}) \geq 0 \ ; \ V \ (\underline{x}) = 0 \qquad only \ \ if \ \ \underline{S}(\underline{x}) = \underline{0}$$

It remains to enforce the condition required for negative slopes for $V(\underline{x})$. For convergence to the equilibrium position, the following inequalities have to be satisfied:

$$S_1 S_1' < 0 \ ; \ S_2 \ S_2' < 0 \qquad\qquad (4.28.b)$$

To guarantee that the representative point approaches and reaches the switching

surface in a finite time $(T)_{switch}$, one should find two positive numbers, η_1 and η_2, which satisfy the following inequalities:

$$S_1 \, S_1' < - \eta_1 \mid S_1 \mid \; ; \; S_2 \, S_2' < - \eta_2 \mid S_2 \mid \qquad \textbf{(4.28.c)}$$

If η_1 and η_2 are found, then $(T)_{switch}$ is given by:

$$(T)_{switch} = \max \left(\frac{|S_1|}{\eta_1} \; ; \; \frac{|S_2|}{\eta_2} \right) \qquad \textbf{(4.28.d)}$$

To construct the control law, one must first establish bounds on the robot's parameters including $\underline{r}'$ and $\underline{r}''$. One can thus assume:

$$\bullet \; 0 < \sigma_L < \overline{\sigma} < \sigma_U \qquad ; \; |r_i'| \leq \rho_i^* \quad (i = 1,2)$$

$$\bullet \; |r_i''| \leq \nu_i^* \; ; \; i = 1,2 \qquad ; \; |\alpha_{ij}| \leq \alpha_{ij}^* \quad (i = 1,2), \; (j = 1,2)$$

$$\bullet \; |\beta_i| \leq \beta_i^* \; ; \; i = 1,2 \qquad\qquad\qquad\qquad\qquad \textbf{(4.29.a)}$$

where the subscripts L and U refer to lower and upper bounds and the bar above the variable refers to an average value.

Using relations (4.27.c), (4.27.e), (4.28.b), and (4.29.a) one can construct the control law in a direct manner as follows:

$$S_1 \, S_1' = S_1 \, (K_1 \, x_1' + x_2')$$

$$= S_1 \left(K_1 \, x_2 + \left\{ \overline{\sigma} \, r_1'' - \omega_1 + \beta_1 \, \omega_2 \right\} / \, \overline{\sigma} \right)$$

$$= \frac{S_1}{\overline{\sigma}} \left[K_1 \, \overline{\sigma} \, x_2 + \overline{\sigma} \, r_1'' - \tau_1 + \alpha_{11} + \alpha_{12} \, (r_1' - x_2) \right.$$

$$\left. - \alpha_{13} \, (r_2' - x_4)^2 + \beta_1 \, \tau_2 - \beta_1 \, \alpha_{21} - \beta_1 \, \alpha_{22} \, (r_2' \cdot x_4) - \beta_1 \, \alpha_{23} \, (r_1' - x_2)^2 \right]$$

$$= \frac{S_1}{\overline{\sigma}} \left(- \tau_1 + \beta_1 \, \tau_2 \right) + S_1 \left\{ K_1 \, x_2 + r_1'' + [(\alpha_{11} - \beta_1 \, \alpha_{21}) + \alpha_{12} \, (r_1' - x_2) - \right.$$

$$\left. \beta_1 \, \alpha_{23} \, (r_1' - x_2)^2 - \beta_1 \, \alpha_{22} \, (r_2' - x_4) - \alpha_{13} \, (r_2' - x_4)^2 \,] / \, \overline{\sigma} \right\}$$

From the previous relation one can write:

$$S_1 \, S_1' \le \frac{S_1}{\overline{\sigma}} \left(- \tau_1 + \beta_1 \, \tau_2 \right) + |S_1| \cdot \left| K_1 \, x_2 + r_1'' + [\, (\alpha_{11} - \beta_1 \, \alpha_{21}) + \alpha_{12} \, (r_1' - x_2) - \right.$$

$$\left. \beta_1 \, \alpha_{23} \, (r_1' - x_2)^2 - \beta_1 \, \alpha_{22} \, (r_2' - x_4) - \alpha_{13} \, (r_2' - x_4)^2 \,] / \, \overline{\sigma} \right|$$

$$\le \frac{S_1}{\overline{\sigma}} \left(- \tau_1 + \beta_1 \, \tau_2 \right) + | \, S_1 \, | \circ \left[\, \left| \, K_1 \, x_2 \, \right| + \left| \, r_1'' \, \right| + \left| \, \frac{(\alpha_{11} - \beta_1 \, \alpha_{21})}{\overline{\sigma}} \, \right| + \right.$$

$$\left| \, \frac{\alpha_{12} \, (r_1' - x_2)}{\overline{\sigma}} \, \right| + \left| \, \frac{\beta_1 \, \alpha_{23} \, (r_1' - x_2)^2}{\overline{\sigma}} \, \right| + \left| \, \frac{\beta_1 \, \alpha_{22} \, (r_2' - x_4)}{\overline{\sigma}} \, \right| +$$

$$\left. \left| \, \frac{\alpha_{13} \, (r_2' - x_4)^2}{\overline{\sigma}} \, \right| \, \right]$$

$$\leq \frac{S_1}{\bar{\sigma}}\left(-\tau_1 + \beta_1^{\cdot}\tau_2\right) + |S_1| \cdot \left\{ K_1\ |x_2| + v_1^{\cdot} + \left[\ (\alpha_{11}^{\cdot} + \beta_1^{\cdot}\ \alpha_{21}^{\cdot}) + \alpha_{12}^{\cdot}\ (\rho_1^{\cdot} + |x_2|\ ) + \right.\right.$$

$$\left.\left. \beta_1^{\cdot}\ \alpha_{21}^{\cdot}\ (\rho_1^{\cdot} + |x_2|\ )^2 + \beta_1^{\cdot}\ \alpha_{22}^{\cdot}\ (\rho_2^{\cdot} + |x_4|\ ) + \alpha_{13}^{\cdot}\ (\rho_2^{\cdot} + |x_4|\ )^2 \Big/\ \sigma_L\ \right]\right\}$$

$$\therefore\ S_1 S_1' \leq \frac{S_1}{\bar{\sigma}}\left(-\tau_1 + \beta_1^{\cdot}\tau_2\right) + |S_1| \cdot (\ \mu_{11} + \mu_{12}\ x_2^2 + \mu_{13}\ x_4^2\ ) +$$

$$\mu_2\ |\ S_1\ x_2\ | + \mu_3\ |\ S_1\ x_4\ |$$

where:

$$\mu_{11} = v_1^{\cdot} + \left[\ (\alpha_{11}^{\cdot} + \beta_1^{\cdot}\ \alpha_{21}^{\cdot}) + \alpha_{12}^{\cdot}\ \rho_1^{\cdot} + \beta_1^{\cdot}\ \alpha_{23}^{\cdot}\ \rho_1^{\cdot 2} + \beta_1^{\cdot}\ \alpha_{22}^{\cdot}\ \rho_2^{\cdot} + \alpha_{13}^{\cdot}\ \rho_2^{\cdot 2} \Big/\ \sigma_L\ \right]$$

$$\mu_{12} = \beta_1^{\cdot}\ \alpha_{23}^{\cdot} \Big/\ \sigma_L \qquad\qquad ;\quad \mu_{13} = \alpha_{13}^{\cdot} \Big/\ \sigma_L$$

$$\mu_2 = K_1 + \left[\ (\alpha_{12}^{\cdot} + 2\ \beta_1^{\cdot}\ \alpha_{23}^{\cdot}\ \rho_1^{\cdot})\ \Big/\ \sigma_L\ \right] \quad ;\quad \mu_3 = (\ \beta_1^{\cdot}\ \alpha_{22}^{\cdot} + 2\ \alpha_{13}^{\cdot}\ \rho_2^{\cdot})\ \Big/\ \sigma_L$$

$$\text{(4.29.b)}$$

The μ_{ij}'s and μ_i's are all known quantities in terms of the bounds given in (4.29.a). The coefficient of $(S_1/\bar{\sigma})$ in inequality (4.29.b) can be written in the form

$$-\tau_1 + \beta_1^{\cdot}\ \tau_2 = \Psi_1$$

where

$$\Psi_1 = - [\ k_{11}\ sgn\ (S_1) + k_{12}\ sgn\ (\ S_1\ x_2\ ) + k_{13}\ sgn\ (\ S_1\ x_4\ )\ ] \qquad\qquad \text{(4.29.c)}$$

where the k_{ij}'s are constants to be determined. Substituting (4.29.c) in (4.29.b) and making

use of the relation

$$\eta \, sgn(\eta) = |\eta|$$

one obtains:

$$S_1 S_1' \leq - \frac{S_1}{\sigma} [\, k_{11} \, sgn \, (S_1) + k_{12} \, sgn \, (\, S_1 \, x_2 \,) + k_{13} \, sgn \, (\, S_1 \, x_4 \,) \,] +$$

$$|S_1| \cdot (\, \mu_{11} + \mu_{12} \, x_2^2 + \mu_{13} \, x_4^2 \,) + \mu_2 \, | \, S_1 \, x_2 \, | + \mu_3 \, | \, S_1 \, x_4 \, |$$

$$\leq - \frac{k_{11}}{\sigma} \, |S_1| - \frac{k_{12}}{\sigma} \, | \, S_1 \, x_2 \, | - \frac{k_{13}}{\sigma} \, | \, S_1 \, x_4 \, | +$$

$$|S_1| \cdot (\, \mu_{11} + \mu_{12} \, x_2^2 + \mu_{13} \, x_4^2 \,) + \mu_2 \, | \, S_1 \, x_2 \, | + \mu_3 \, | \, S_1 \, x_4 \, |$$

$$S_1 \, S_1' \leq \left(\, \mu_{11} + \mu_{12} \, x_2^2 + \mu_{13} \, x_4^2 - \frac{k_{11}}{\sigma} \, \right) \, |S_1| + \left(\, \mu_2 - \frac{k_{12}}{\sigma} \, \right) \, | \, S_1 \, x_2 \, | +$$

$$\left(\, \mu_3 - \frac{k_{13}}{\sigma} \, \right) \, | \, S_1 \, x_4 \, |$$

<div align="right">(4.29.d)</div>

The previous inequality can be satisfied by choosing large gains for k_{11}, k_{12}, k_{13} in specific, these should satisfy:

$$k_{11} > \overline{\sigma} \left[\, \mu_{11} + \mu_{12} \, (x_2)_{max}^2 + \mu_{13} \, (x_4)_{max}^2 \, \right] \; ; \; k_{12} > \overline{\sigma} \, \mu_2 \; ; \; k_{13} > \overline{\sigma} \, \mu_3$$

<div align="right">(4.29.f)</div>

It is obvious that a reasonable estimate for $(x_2)_{max}$ and $(x_4)_{max}$ is necessary to define the k_{ij} gains.

A similar treatment for the second inequality in (4.28.b) yields:

$$S_2\, S_2' \le \frac{S_2}{\sigma} \left(\beta_2^{\cdot} \tau_1 - \tau_2 \right) + |S_2| \cdot \left(\mu_{21} + \mu_{22}\, x_2^2 + \mu_{23}\, x_4^2 \right) + \mu_2\, |\, S_2\, x_2\, | +$$

$$\mu_3\, |\, S_2\, x_4\, |$$

where:

$$\mu_{21} = v_2^{\cdot} + \left(\alpha_{21}^{\cdot} + \beta_2^{\cdot}\, \alpha_{11}^{\cdot} + \beta_2^{\cdot}\, \alpha_{12}^{\cdot}\, \rho_1^{\cdot} + \beta_2^{\cdot}\, \alpha_{13}^{\cdot}\, \rho_2^{\cdot 2} + \alpha_{22}^{\cdot}\, \rho_2^{\cdot} + \alpha_{23}^{\cdot}\, \rho_1^{\cdot 2} \right) \Big/ \sigma_L$$

$$\mu_{22} = \alpha_{23}^{\cdot} \Big/ \sigma_L \qquad\qquad ; \quad \mu_{23} = \left(\beta_2^{\cdot}\, \alpha_{13}^{\cdot} \right) \Big/ \sigma_L$$

$$\mu_4 = \left(\beta_2^{\cdot}\, \alpha_{12}^{\cdot} + 2\, \alpha_{23}^{\cdot}\, \rho_1^{\cdot} \right) \Big/ \sigma_L \quad ; \quad \mu_5 = K_2 + \left(\alpha_{22}^{\cdot} + 2\, \beta_2^{\cdot}\, \alpha_{13}^{\cdot}\, \rho_2^{\cdot} \right) \Big/ \sigma_L$$

$$\text{(4.30.a)}$$

All the μ_{ij}'s and the μ_i's are known quantities. One can introduce

$$\beta_2^{\cdot}\, \tau_1 - \tau_2 = \Psi_2$$

where

$$\Psi_2 = - \left[\, k_{21}\, sgn\, (S_2) + k_{22}\, sgn\, \left(S_2\, x_2 \right) + k_{23}\, sgn\, \left(S_2\, x_4 \right) \,\right]$$

$$\text{(4.30.b)}$$

where the k_{ij}'s are constants to be determined. Substituting (4.30.b) in (4.30.a) one obtains

the following inequalities which have to be satisfied:

$$k_{21} > \overline{\sigma} \left[\mu_{21} + \mu_{22} \, (x_2)^2_{max} + \mu_{23} \, (x_4)^2_{max} \right]$$

$$k_{22} > \overline{\sigma} \, \mu_4$$

$$k_{23} > \overline{\sigma} \, \mu_5 \tag{4.30.c}$$

Solving for τ_1 and τ_2 using (4.29.c) and (4.30.b) one finally obtains:

$$\tau_1 = - \frac{\Psi_1 + \beta_1^*}{1 - \beta_1^* \, \beta_2^*} \quad ; \quad \tau_2 = - \frac{\Psi_2 + \beta_2^*}{1 - \beta_1^* \, \beta_2^*} \tag{4.31}$$

The previous strategy can be implemented in a computer routine to simulate the tracking problem for RAM using SLIDING MODE control.

4.12 SUMMARY OF CHAPTER 4

A number of conventional strategies were developed for the control of the RAM and the FJM for elbow arms. Some were simulated and gave satisfactory results in terms of accuracy, smoothness of traced trajectory and the levels of the command signals. However the majority showed an oscillatory response for the command voltages.

The NIT control developed in the previous chapter compares very well with the best performance obtained so far in terms of accuracy, smoothness and cost of computing time. It may be only next to the "sliding mode" control in terms of response time.

CHAPTER 5

EXPERIMENTAL SETUP

5.1 OBJECTIVES

The objectives here are to build an experimental setup to validate some of the control strategies which were developed in the previous chapter. The experimental setup is referred to as "**FLEXROD**" for "Flexible Robot Device". FLEXROD was designed, manufactured, assembled and debugged in the Laboratories of the department of Mechanical Engineering at McMaster University. It was designed in a modular form to facilitate its adaptation and extension to perform other future research activities in this area.

AUTOCAD was used to prepare the final drawings for the parts of FLEXROD. "Harmonic drives" were used for speed reduction. "Transputers" were employed for computer hardware. Timing belts with steel cable as core were used for power transmission.

FLEXROD as it stands today consists of an "upper" and a "lower" arm complete with their actuators, controllers and sensors. The setup can be easily extended in the future to include a "shoulder" for azimuth rotation and a "hand" for pitch and roll movements. In other words "FLEXROD", when reaches maturity, will be a five-degrees-of-freedom experimental manipulator which will serve a wide spectrum of research activities because of its built-in modularities. It will then have the following characteristics:

141

Payload 1.5 kg ;   reach 0.6 m

linear speed 0.6 m/s ;   repeatability ± 0.08 mm

A brief description of FLEXROD is given in the following sections. The architecture of the associated software is covered in the next chapter.

5.2 GENERAL LAYOUT

Figure 5.1 shows the general layout of FLEXROD. Joints (1) and (2) are equipped with harmonic drives as speed reducers. Any or all of the links can be rigid or flexible as required. Strain gauges and accelerometers can be attached to link 2. Figure 5.2 shows the assembly of the upper and lower arms of FLEXROD. The assembly in Figure 5.2 consists of:

ITEM NO.	DESCRIPTION	NO. OFF
1	Base plate	(1)
2	Fixed shoulder (two channels)	(1)
3	DC motors complete with their encoders	(2)
4	Motor supports	(2)
5	Flexible couplings to connect motors to respective axles	(2)
6	Power-off brake	(2)
7	Axles for joint 1	(2)

Figure 5.1: General layout of FLEXROD.

link 2

spacer and bearing-housing

pulley and timing belt

harmonic drive

axle for joint 2

link 1

spider coupling

shoulder

motor support

motor and encoder

power-off brake

flexible coupling

base

1035

690

Dimensions in mm.
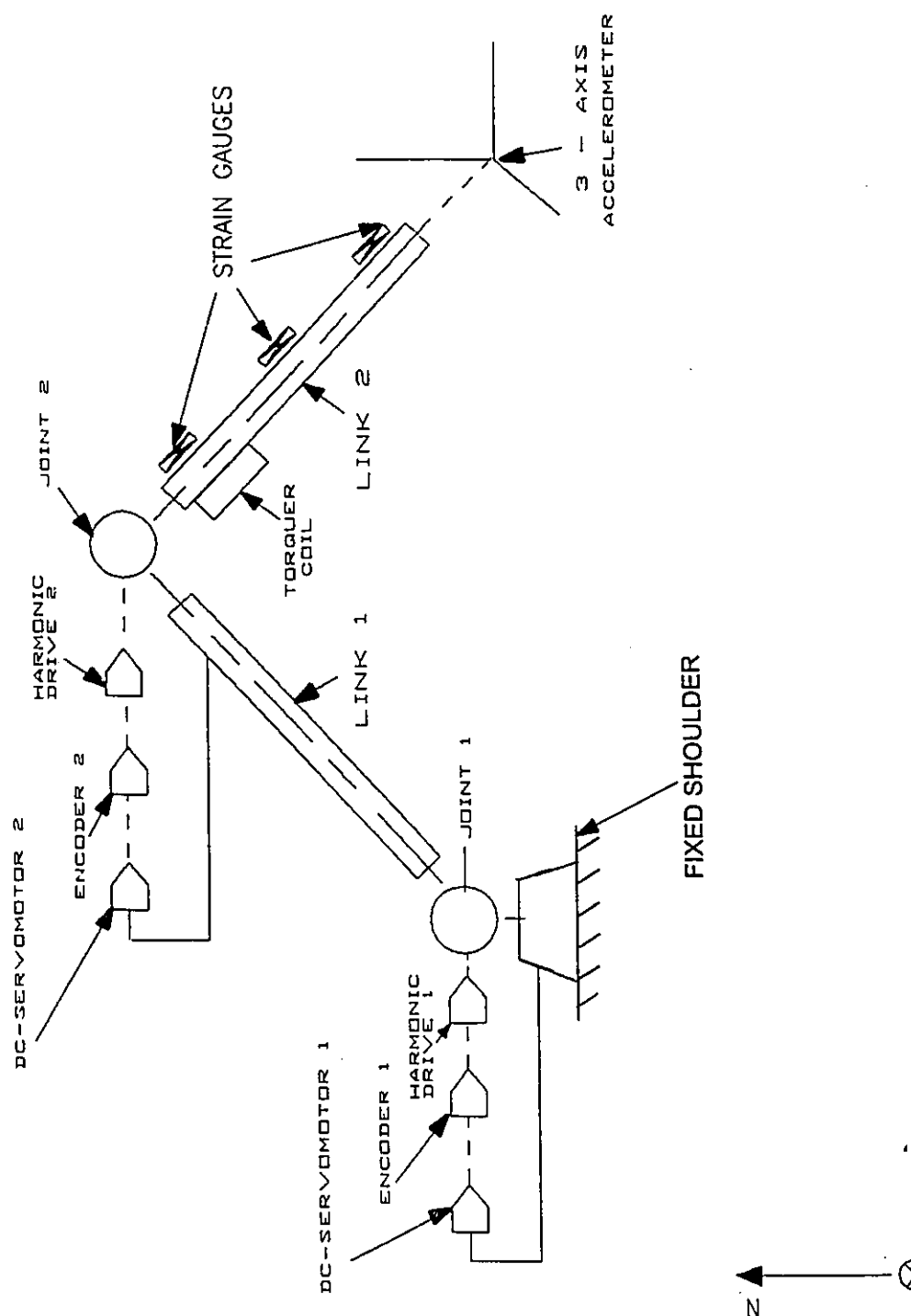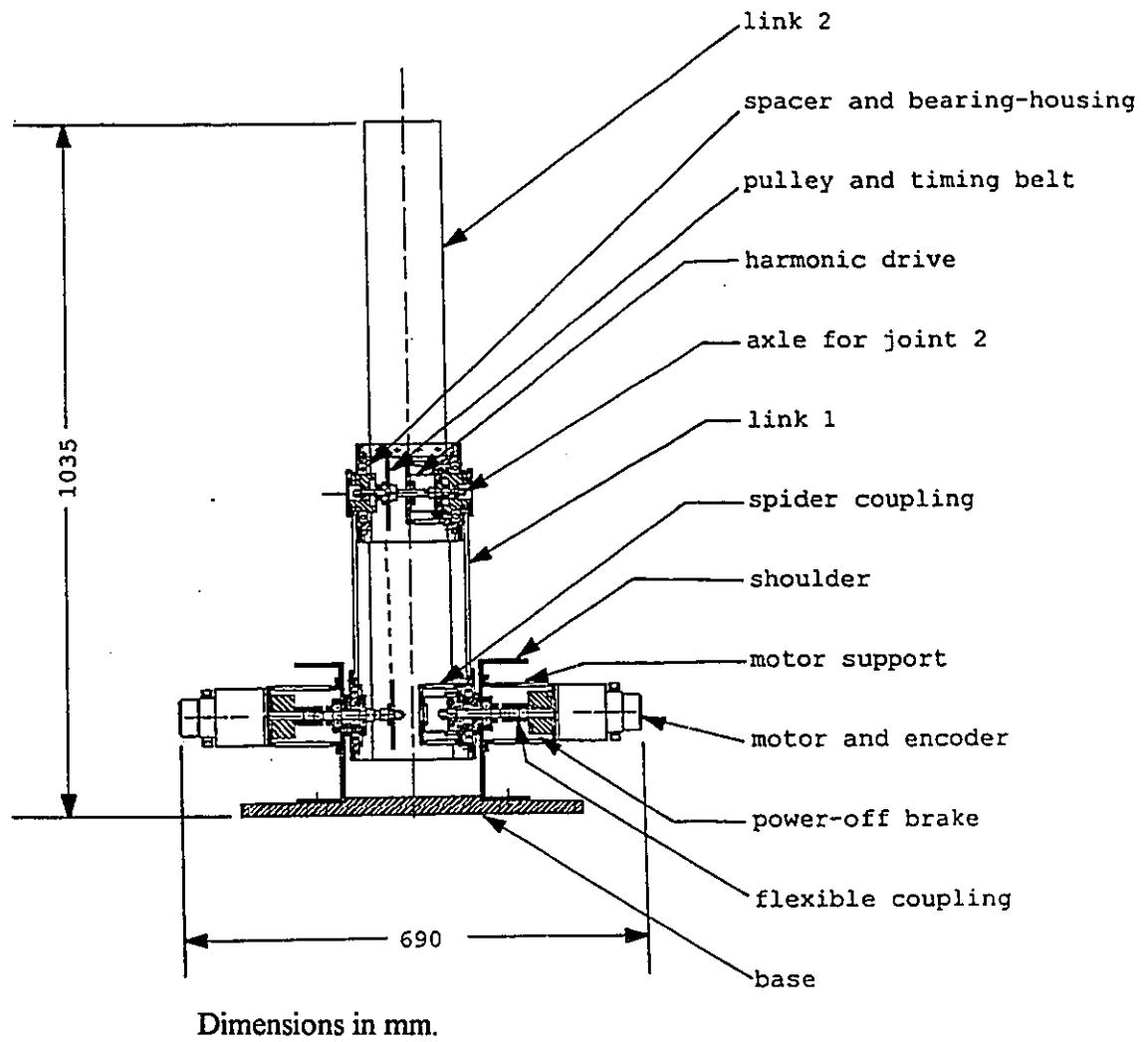
Figure 5.2: Assembly of upper and lower arms of FLEXROD.

ITEM NO.	DESCRIPTION	NO. OFF
8	Axle for joint 2	(1)
9	Harmonic drive	(2)
10	Spider coupling between flexspline and link	(2)
11	Spacers and bearing housing	(4)
12	Ball bearings	(10)
13	Links	(2)
14	Pulley and timing belt transmission	(1)

5.3 SUBASSEMBLIES FOR JOINTS 1,2 AND LINK 1

Figures (5.3),(5.4) and (5.5) show the details of the assemblies of joints 1, 2 and link 1 respectively. They are drawn to scale. The following is a list of parts:

PART NO	DESCRIPTION
1	D.C. motor complete with encoder.
2	Harmonic drive 1: three parts; wave generator (WG), flex spline (FS) and circular spline (CS).
3	Pulley and timing belt transmission.
4	Hub to accommodate pulley.
5	Right spacer and bearing housing for joint 1.
6	Spider coupling to connect (FS) of harmonic drive 1 to link 1.

PART NO	DESCRIPTION
7	Right axle for joint 1.
8	Securing nut for pulley at joint 1.
9	Adaptor ring for (FS) of harmonic drive 1.
10	Securing nut for outer bearings of the axles of joint 1.
11	Securing nut for spacer and bearing-housing for joint 1.
12	Left spacer and bearing-housing for joint 1.
13	Ball bearing housing for spacer at joint 1.
14	Left axle for joint 1.
15	Housing for axles of joint 1.
16	Motor support.
17	Fixed shoulder.
18	Lateral walls of link 1 at joint 1.
19	Lateral walls of link 1 at joint 2.
20	Axial angles of link 1.
21	Axial angles of link 1.
22	Window with dowels for link 1.
23	Lateral bars for link 1.
24	Flexible coupling.
25	Washers for axles of joint 1.
26	Right spacer and bearing-housing for joint 2.

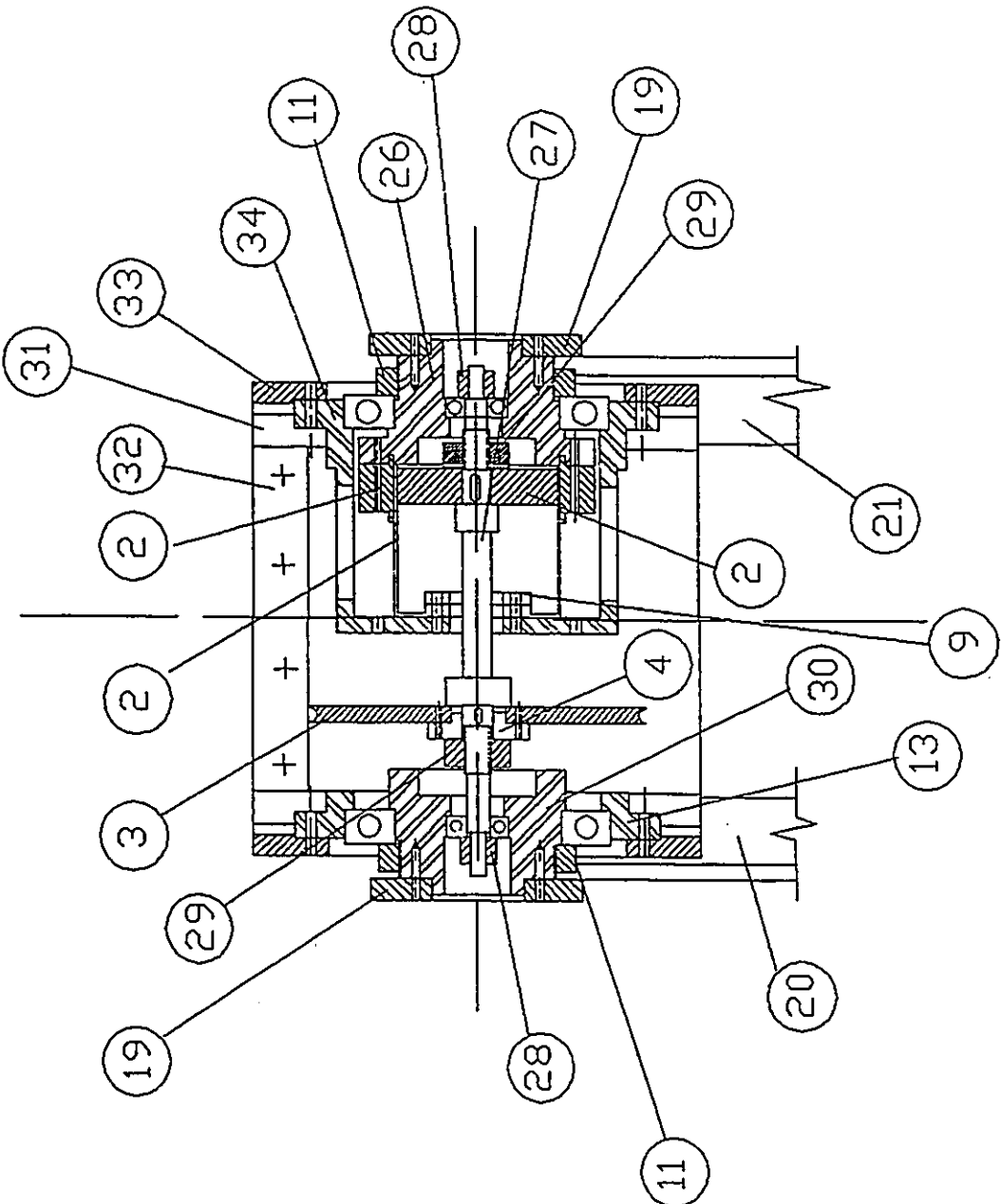| PART NO	DESCRIPTION
27	Axle for joint 2.
28	Securing nut for outer bearing of axle 2.
29	Securing nut for pulley at joint 2.
30	Left spacer and bearing-housing for joint 2.
31	Axial angle of link 2.
32	Lateral angle of link 2.
33	Lateral walls of link 2.
34	Spider coupling for joint 2.
35	Base.
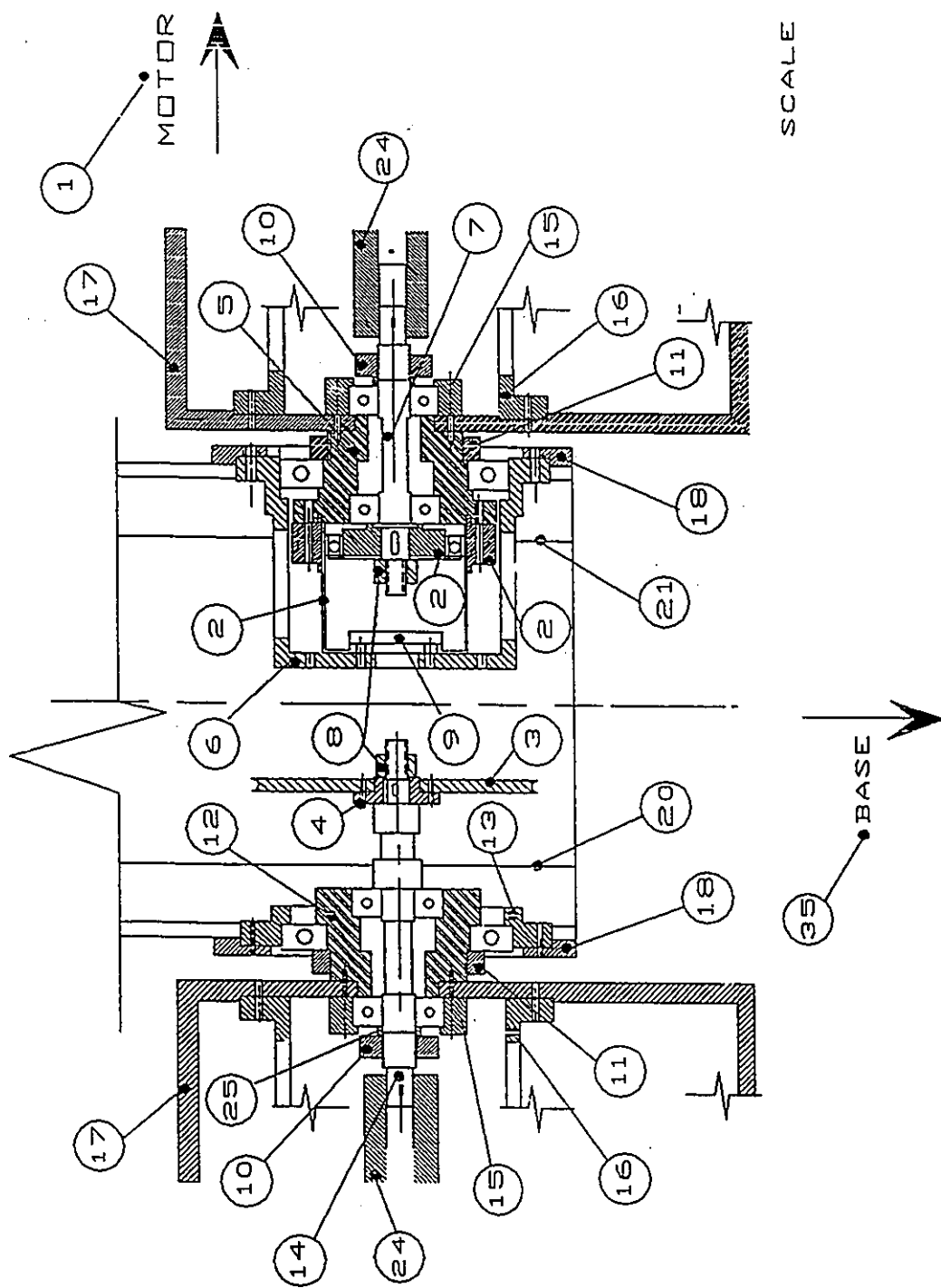
Figure 5.3: Assembly of joint 1.
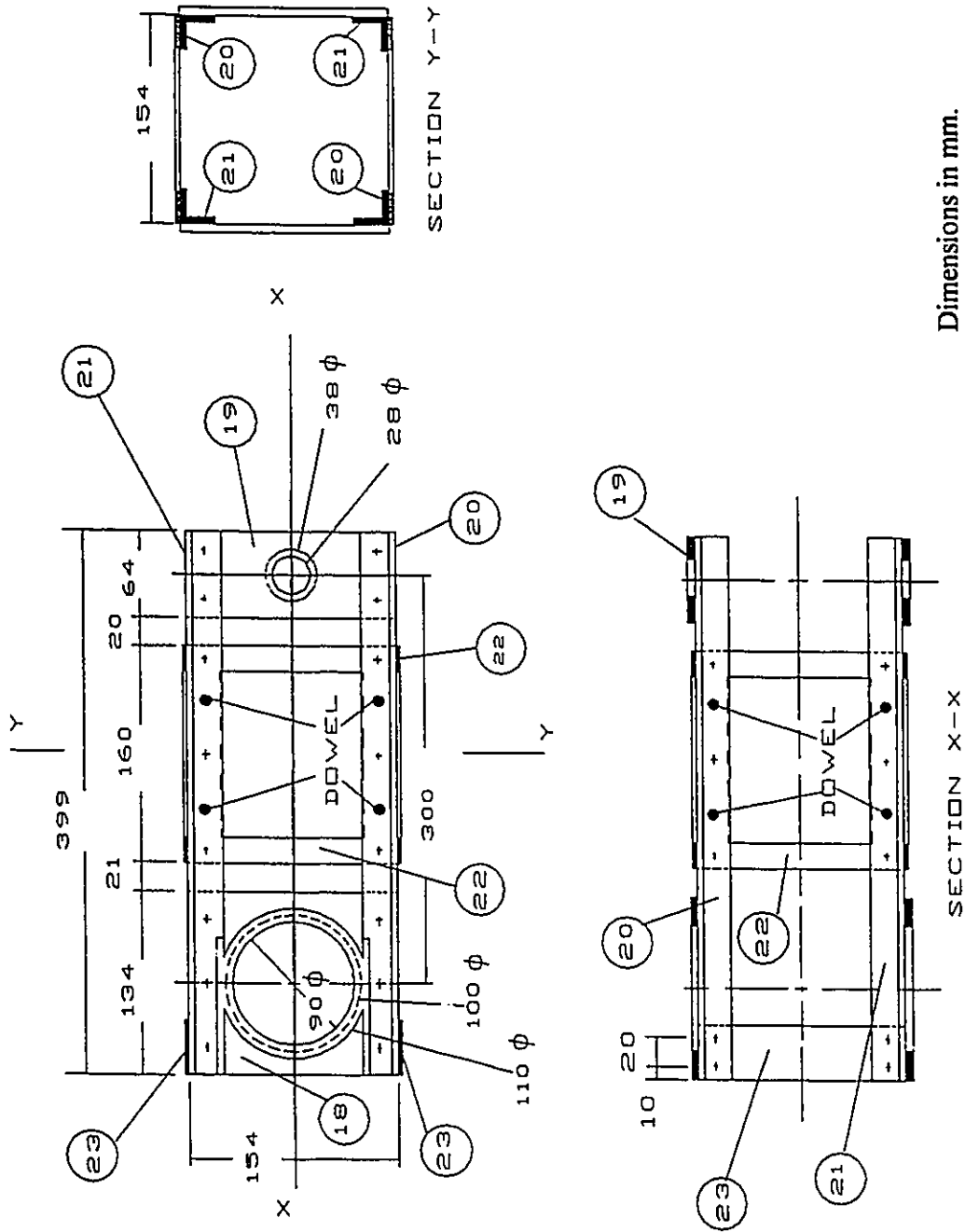
Figure 5.4: Assembly of joint 2.

Dimensions in mm.

Figure 5.5: Assembly of link 1.

The detailed workshop drawing of each part was prepared using AUTOCAD. Typical drawings for parts 5 and 6 are shown in Figures 5.6 and 5.7.

The following remarks shed some light on FLEXROD:

a)   All parts, except for the axles and washers, are machined from stock using ALUMINUM 6061-T6.

b)   Dowels are used in the assembly and mounting of the windows and lateral strips of links to ensure mechanical integrity and dimensional stability.

c)   The base, machined of a heavy steel plate is anchored to a seismic concrete foundation to isolate FLEXROD from unwanted ground excitation.

The remaining sections of this chapter deal with parts of FLEXROD which were acquired from reliable manufacturers.
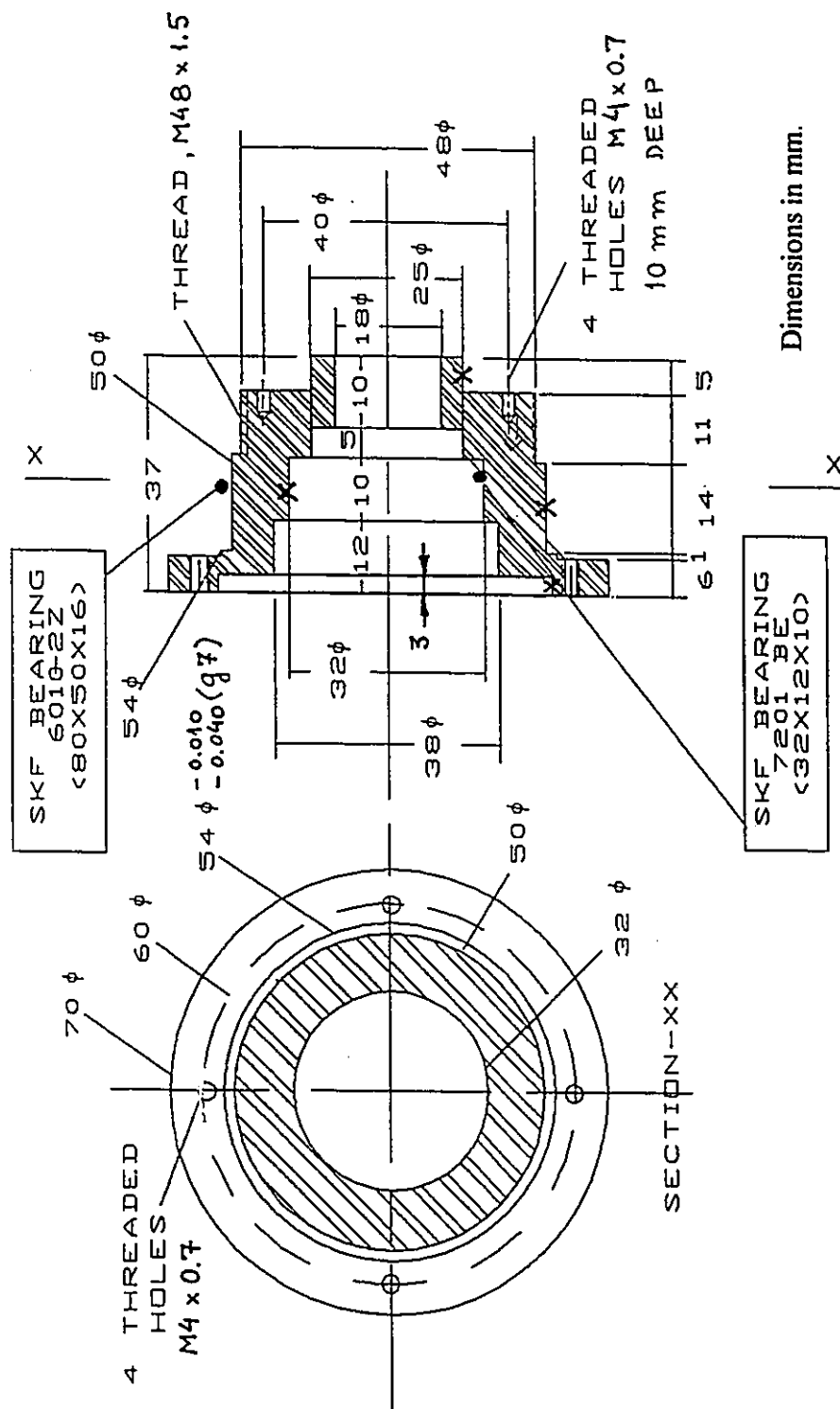
Figure 5.6: Part no.5 – Right spacer and bearing housing for joint 1

SKF BEARING
6010-2Z
<80X50X16>

THREAD, M48 x 1.5

4 THREADED
HOLES M4 x 0.7
10 mm DEEP

Dimensions in mm.

SKF BEARING
7201 BE
<32X12X10>

4 THREADED
HOLES
M4 x 0.7

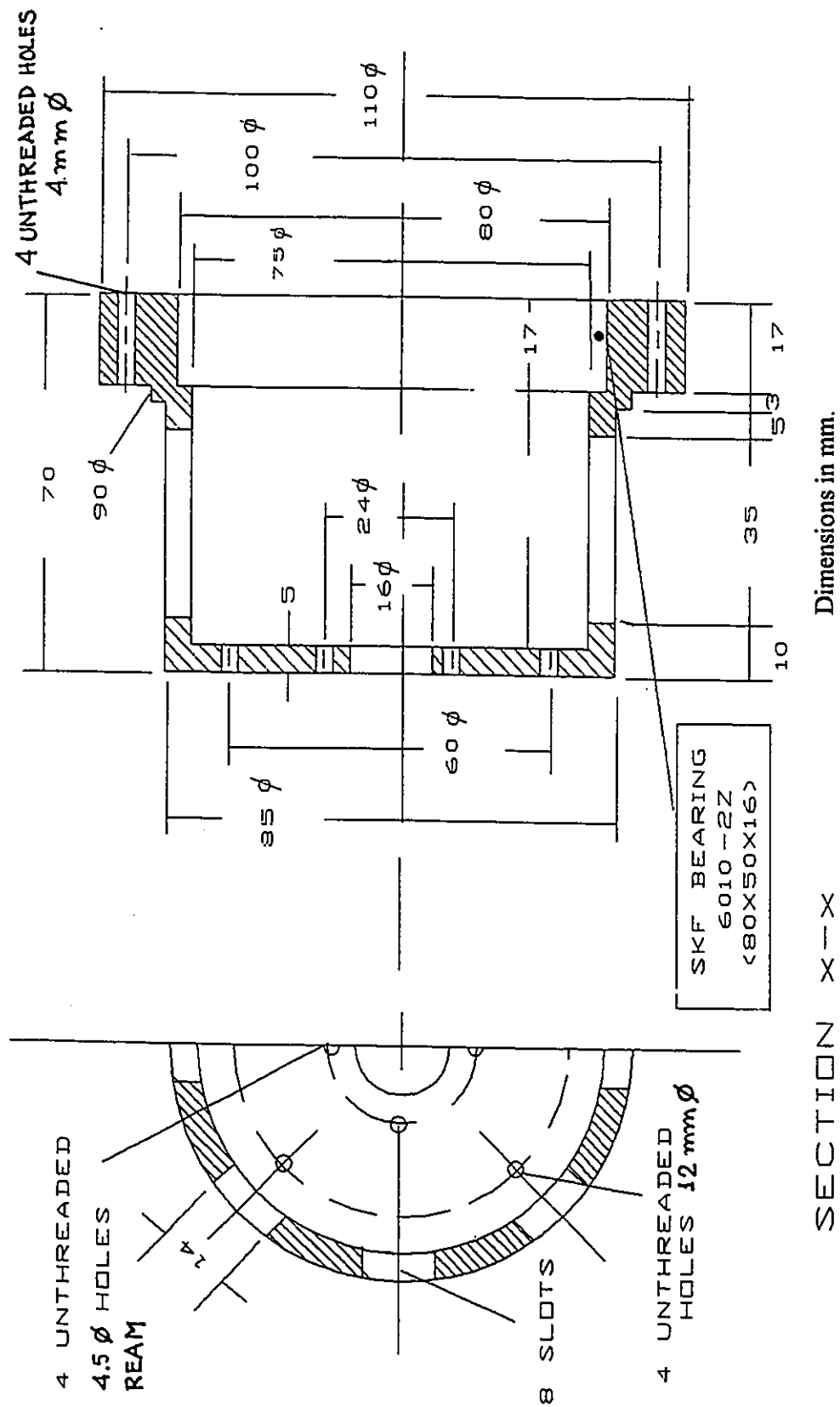SECTION-XX

SECTION X—X

Dimensions in mm.

Figure 5.7: Part no.6 – Spider Coupling.

5.4 THE ACTUATORS

Two identical DC servomotors are used to drive the upper and lower arms. The technical specifications of each motor are as given after:

Servomotor	M3515B - CRS PLUS
Rated power	0.195 HP = 148 W
Acceleration	79,500 rad/s^2
Outer diameter of body of motor	85.7 mm
Axial length of motor less spin axis	127 mm
Diameter of spin axis	11 mm ϕ
Weight	2.3 kgf
Mass moment of inertia	0.7 × 10^4 kg.m^2
Viscous friction constant	0.01 N.m/kRPM
Stiction friction torque	0.04 N.m
Max.RPM	3000 RPM
Peak torque	6.35 N.m
Continuous torque	0.73 N.m
Time constant	3.9 msec
Armature resistance	0.84 ohms
Volts at peak torque(stall)	5.81 Vdc
Amps. at peak torque	44.6 amps.
Back e.m.f. voltage	14.9 Volt/kRPM

(cont.)

Motor torque constant   0.143 N.m/amp.

Encoder type   1000 lines differential

Amplifier   PWM

5.5 THE HARMONIC DRIVE

Two identical harmonic drives are used as speed reducers to step down the speed

from the actuator to the associated link. The harmonic drive consists of three basic elements

as shown in Figure 5.8, namely,

*   A Wave Generator (WG) in the form of an elliptic steel ball bearing assembly.

*   A Flexspline (FS) in the form of a thin wall steel cup with external spline teeth.

*   A Circular Spline (CS) which is essentially a thick wall ring with internal spline

teeth.

One of the three elements mentioned above has to be held fixed in inertial space.

An element is to be attached to the input axis and another to the output axis. For the elbow

arm, the input is imparted through the wave generator (WG) which is driven by the associated

motor through a flexible coupling. The output is tapped from the flexspline (FS) which is

coupled to the associated link through a spider cage. The circular spline (CS) of the harmonic

drive is held fixed to the housing of the input shaft. The technical specifications of each

harmonic drive are given after.
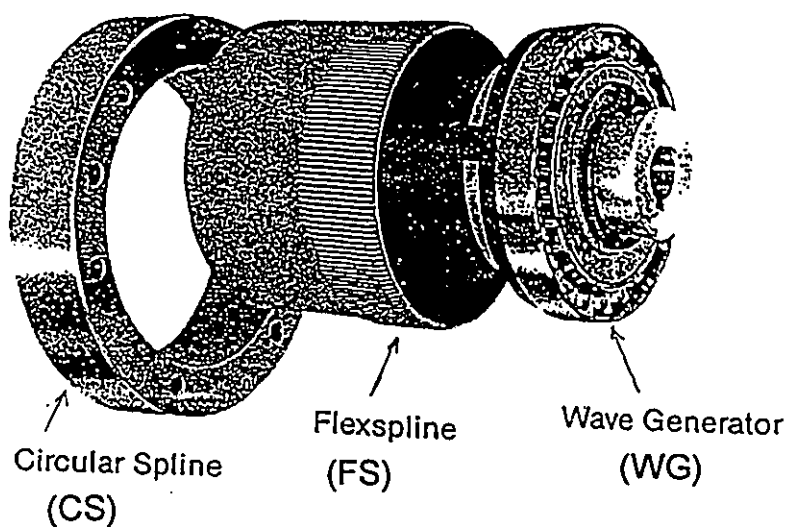
Figure 5.8: Harmonic Drive.

Harmonic drive	HDUC-20
Rated speed ratio	100
Input speed	500-3600 RPM
Tabulated output torque	30-36 N.m
Max. output torque	54 N.m
Moment of inertia	0.14×10^{-4} kg.m^2
Tabulated average spring rate	1.318×10^4 N.m/rad
Lubrication	Harmonic Grease SK-1A

Figure (5.9) shows the schematics of a typical load deflection curve for the harmonic drive. The curve is furnished by the supplier. The curve is obtained with the input shaft locked. The tabulated load as well as the tabulated average spring rate are as given in the list of specifications.

Tabulated Load

+

Tabulated Average
Spring Rate
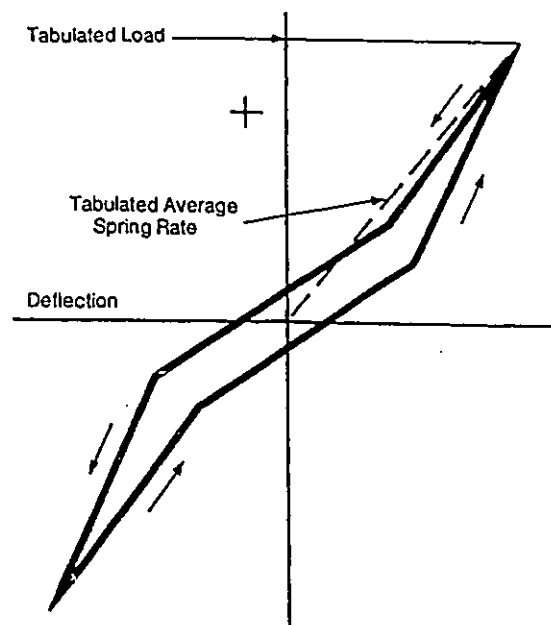
Deflection

Figure 5.9: Schematics of load deflection characteristics of a harmonic drive.

In this thesis a linear spring is assumed in all models. The inclusion of hysteresis and the nonlinear characteristics of the drive are possible but are considered out of the scope of this work.
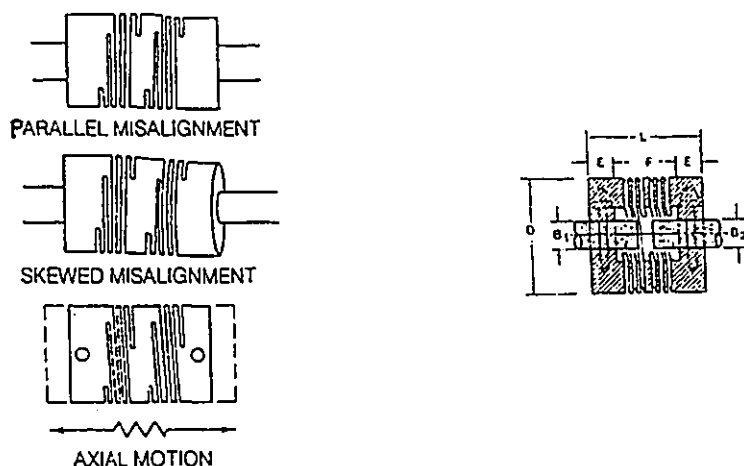
5.6 THE COUPLING

A flexible coupling is used to connect the output shaft of the DC motor to the axle which drives the wave generator (WG) of the harmonic drive. The coupling is used to

accommodate parallel misalignment, skewed misalignment as well as the axial motion as shown in Figure (5.10).

The used coupling is a monobloc which is carved in a way to contain multi-overlapping curved beams. The specifications of the coupling are as given after.

Coupling   ROCOM with six short curved beams

Part no   BL0100-C10MM-C10MM

Material   QQA225/6-2024-T3.51 Aluminum with

                    MIL-A8625   black anodized

Misalignment   parallel offset 0.01",

                    skewed offset = 5°, axial motion 0.01"

Max.torque rating   6.25 N.m

Life tests   in accordance with MIL-HDBK-5A

Dimensions   (see Figure 5.10):

                    $D = 1"$; $L = 1"$; $E = 0.28"$; $F = 0.41"$

                    $B1 = 0.375"$; $B2 = 0.375"$

PARALLEL MISALIGNMENT

SKEWED MISALIGNMENT

AXIAL MOTION

Figure 5.10: The coupling.

5.7 - THE POWER-OFF BRAKE

Each D.C. motor is equipped with a power-off brake which is activated when the

power is turned off. The schematics of the brake are as shown in Figure 5.11. It consists of

a coil field assembly, a friction disc and a pressure plate. The specifications are as follows:

Power-off brake   INERTIA DYNAMICS INC.

Type   FSBR007

Steady torque   0.79 N.m

Electrical   Volt=24 dc ; Amps = 0.247 ; ohms = 97.3

Dimensions (see Figure 5.11)

$$A = 1.4" ; B = 1.2" ; C = 1.255" ; D = 0.722"$$

$$E = 2.465" ; G = 0.781" ; \varepsilon = 0.01"$$
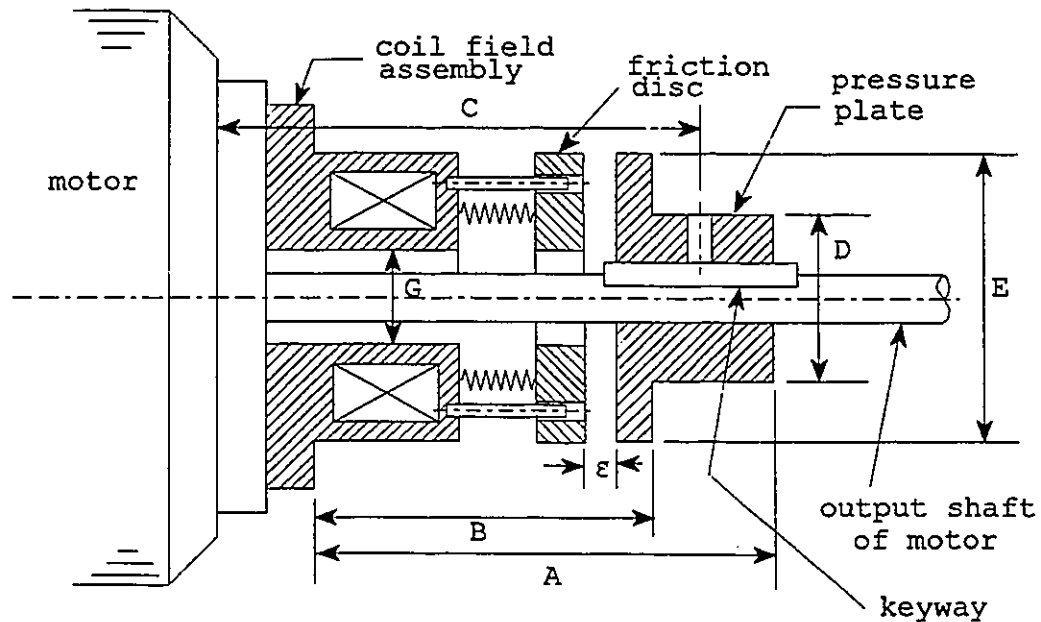
Figure 5.11: Schematics of power-off brake.

5.8 THE TIMING BELT AND PULLEY

The lower arm is driven by a D.C. motor which is attached to the shoulder of FLEXROD. This calls for a power transmission of the belt-pulley type. The transmission has to guarantee the "NO-SLIP" and "zero backlash" requirements. A timing endless belt and two pulleys are used. The schematics of the parts are as shown in Figure 5.12. The specifications are as follows:

Gear drive	BERG-B8

Belt   endless molded with steel cable as core. Strength 20 lbf ; hardness

90A; DURO; weight 0.11 oz/ft ; width 13/64"

Pulley   E-Z ENTRY-32D4-128

Pitch diameter 4" ; outside diam. 4.062" ; No. of teeth 128

Dimensions are as shown in Figure 5.12.

Figure 5.12: Timing belt and pulleys.

5.9 PARTS AND SUBASSEMBLIES OF FLEXROD

Figs. (5.13) to (5.24) show close ups to demonstrate the details of the parts and subassemblies described before. Figure (5.13) shows the assembled Harmonic drive. Figures
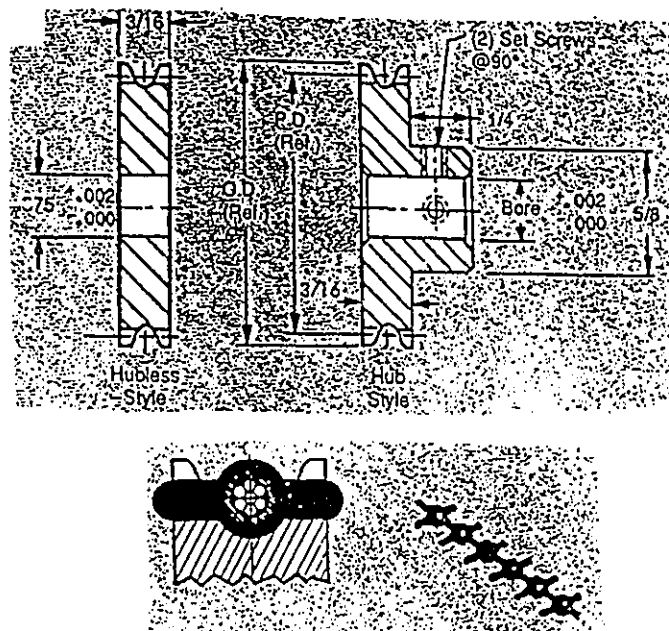
(5.14) to (5.16) show the average wave generator, the flexspline and the circular spline respectively.

Figures (5.17) and (5.18) are close ups for joint 2 and its parts. They show the harmonic drive, the spider and the time-belt.

Figure (5.19) is a close up of the D.C. motor and its support cage. The figure shows the C-channel used for the fixed shoulder and shows the encoder. Figure (5.20) is a close up for joint 1 and shows the two motors mounted to the two channels forming the fixed shoulder.

Figure (5.21) is a close up showing the mounting to the seismic block. Figure (5.22) demonstrates the assembled FLEXROD with the auxiliary equipment for its controls.

Figure (5.23) is a close up for an Industrial controller acquired from CRS-plus for the investigation. Figure (5.29) shows FLEXROD during an investigation where link 2 was assumed possible.

Figure 5.13: Harmonic Drive.
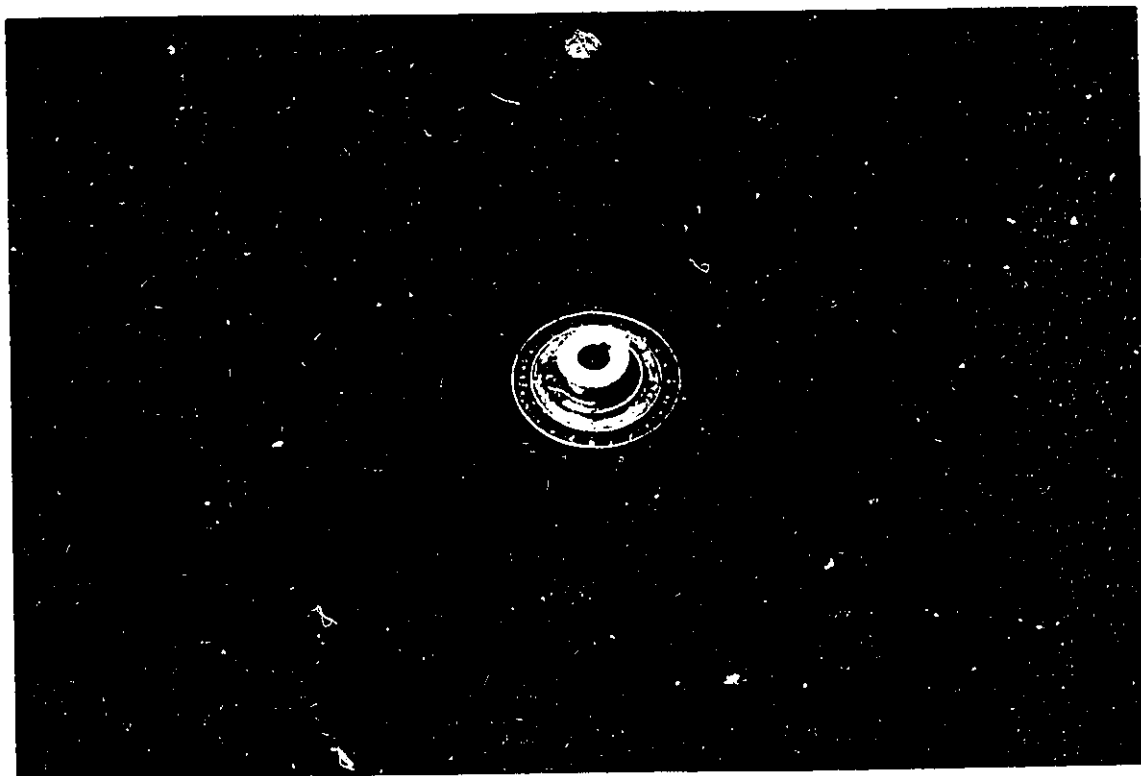
Figure 5.14: Wave Generator.
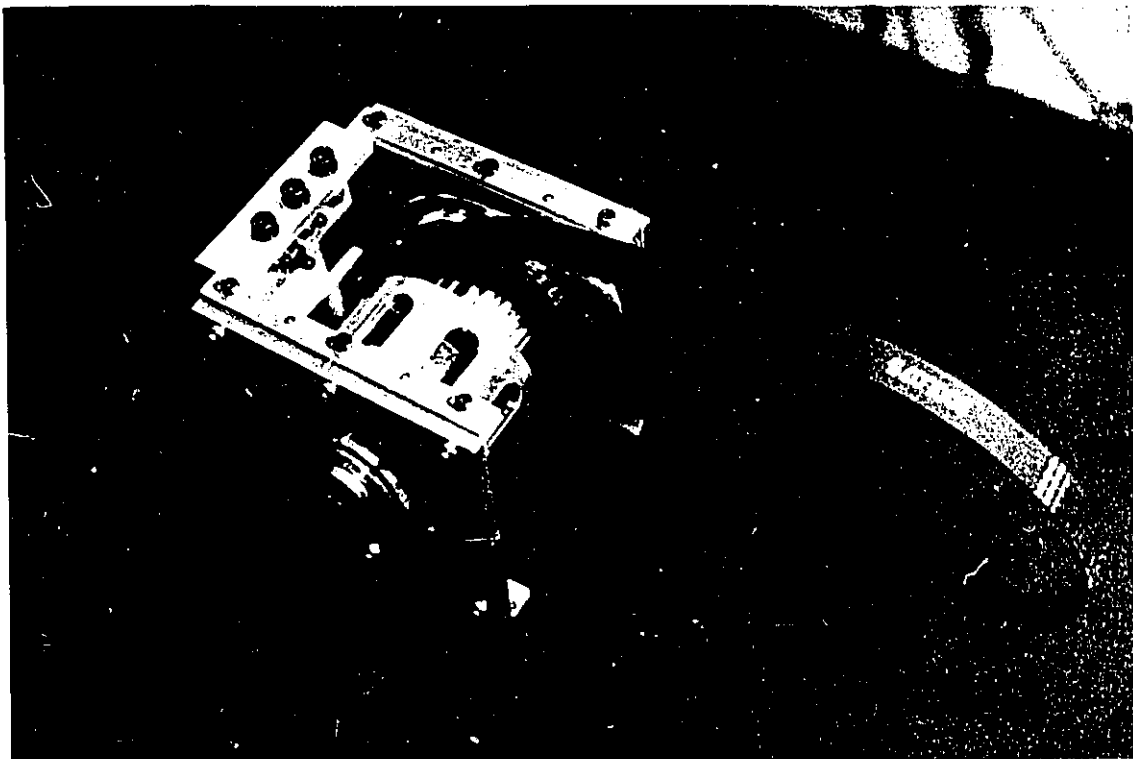
Figure 5.15: Flexspline.
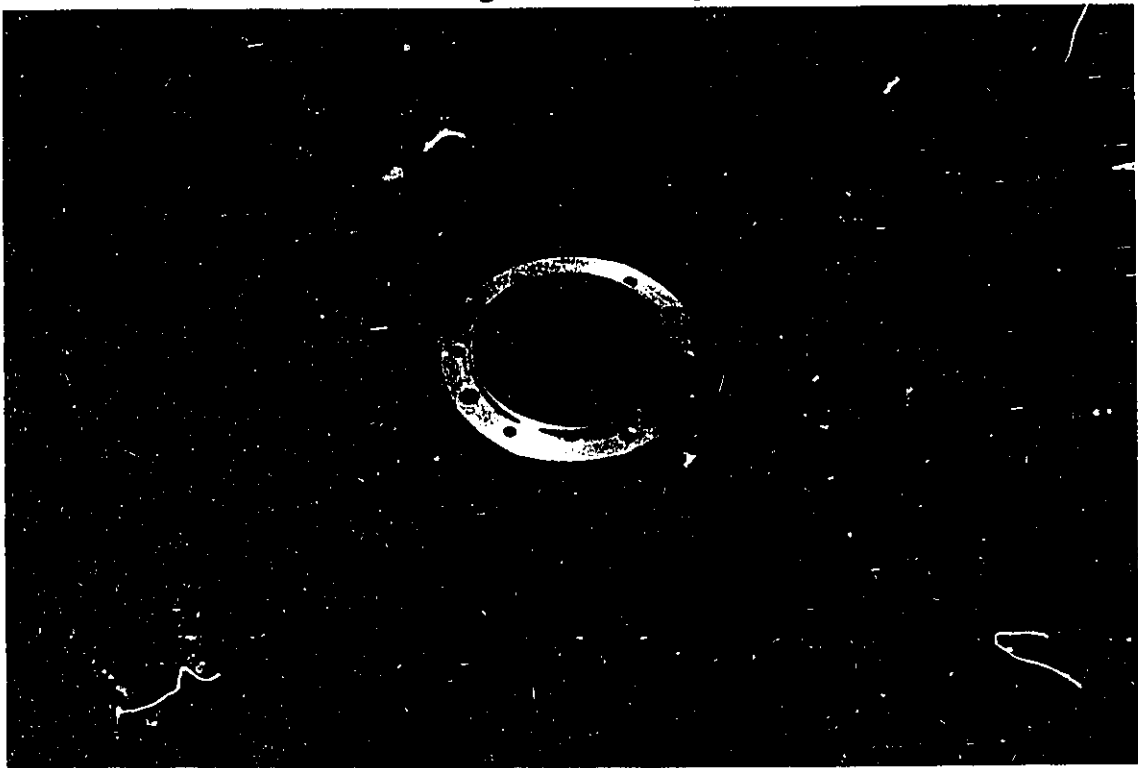
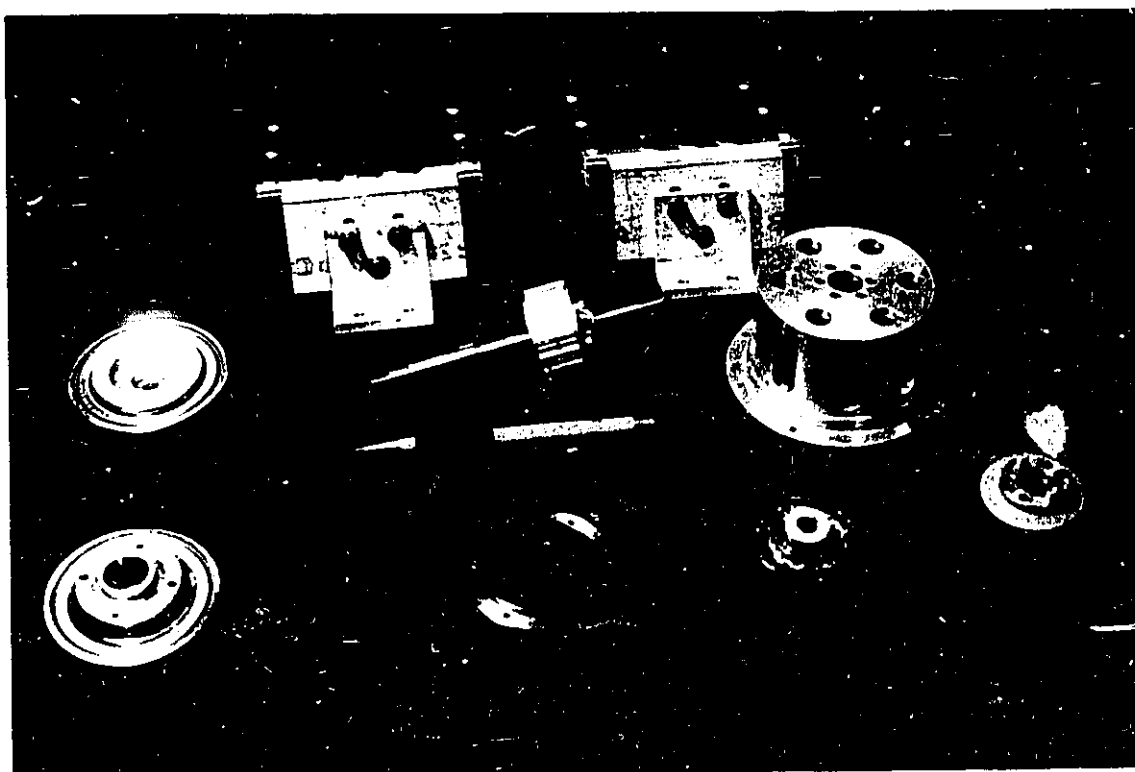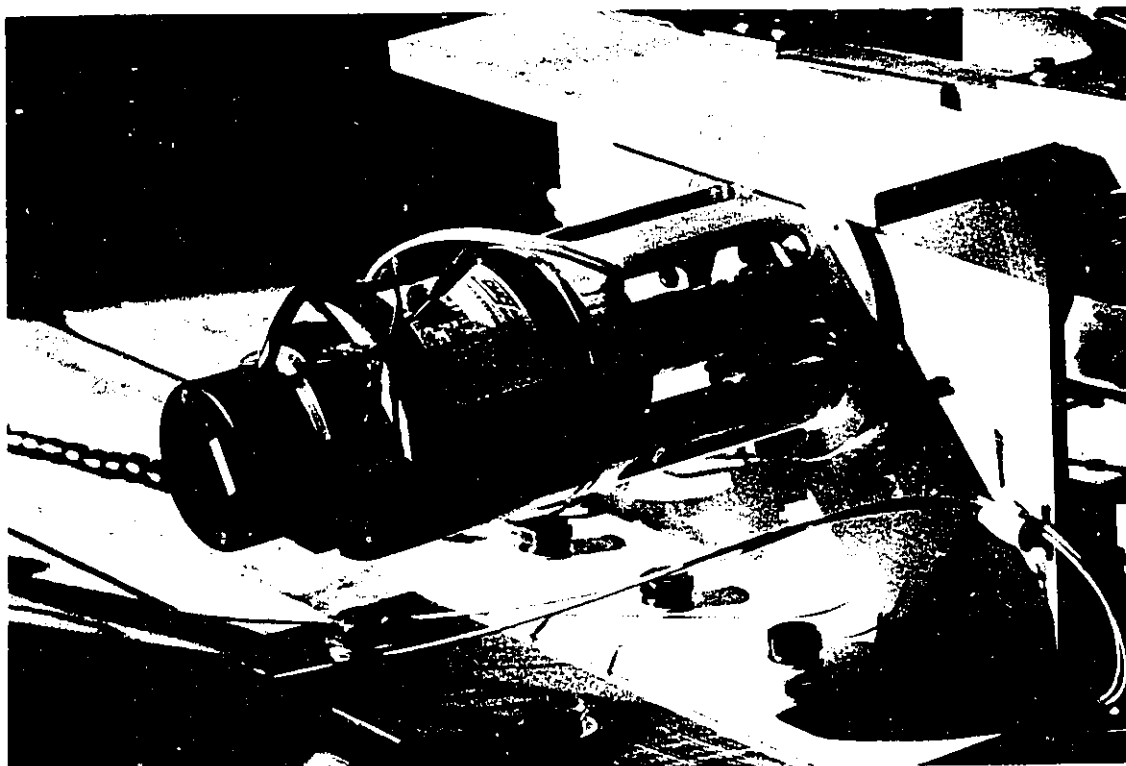**Figure 5.16: Circular Spline.**
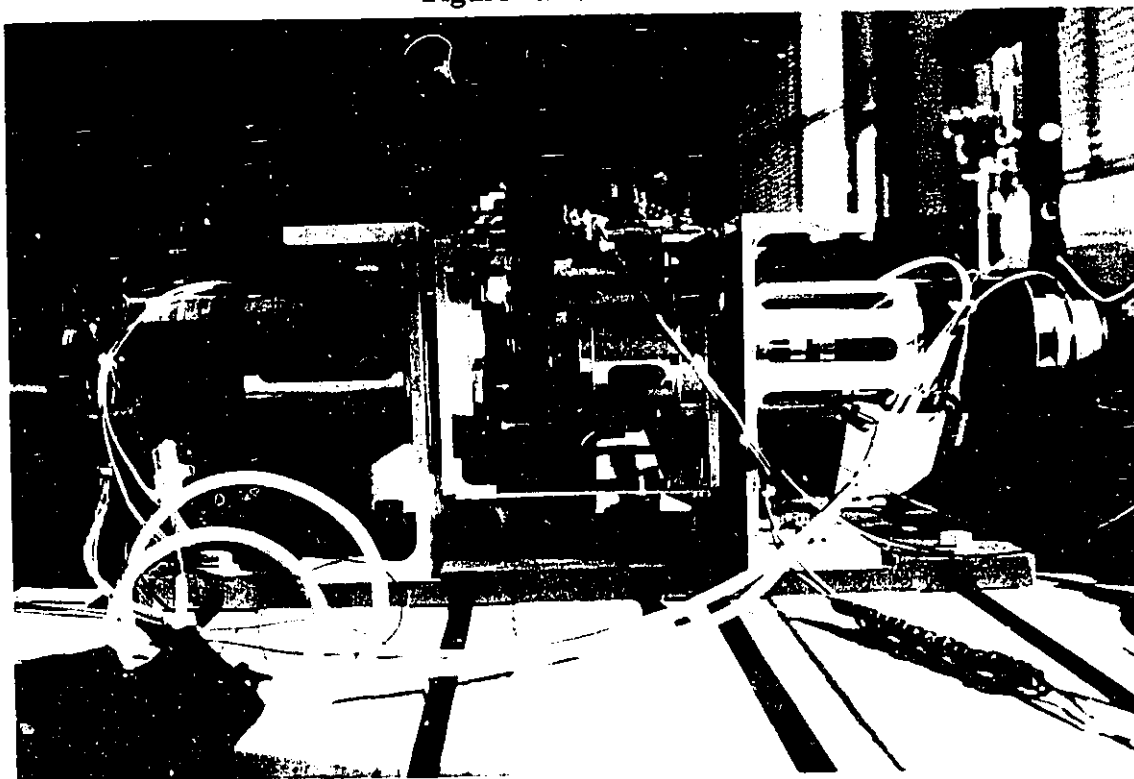
Figure 5.17: Joint 2.

Figure 5.18: Parts of joint 2
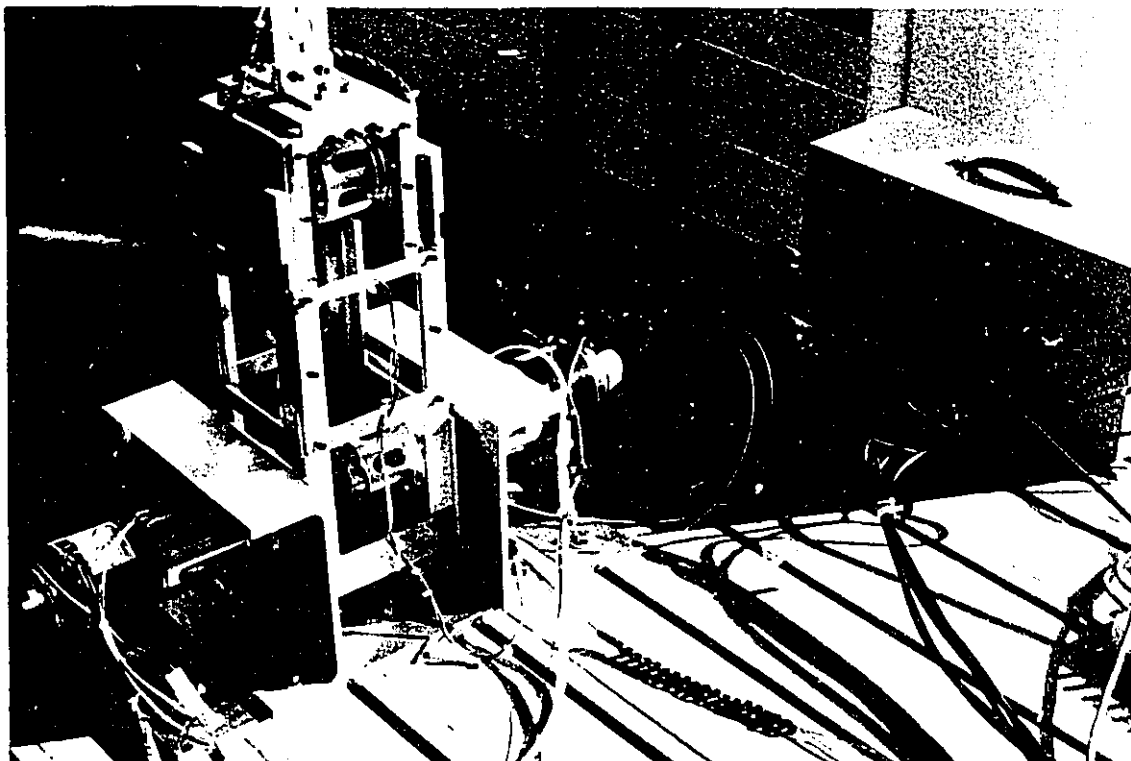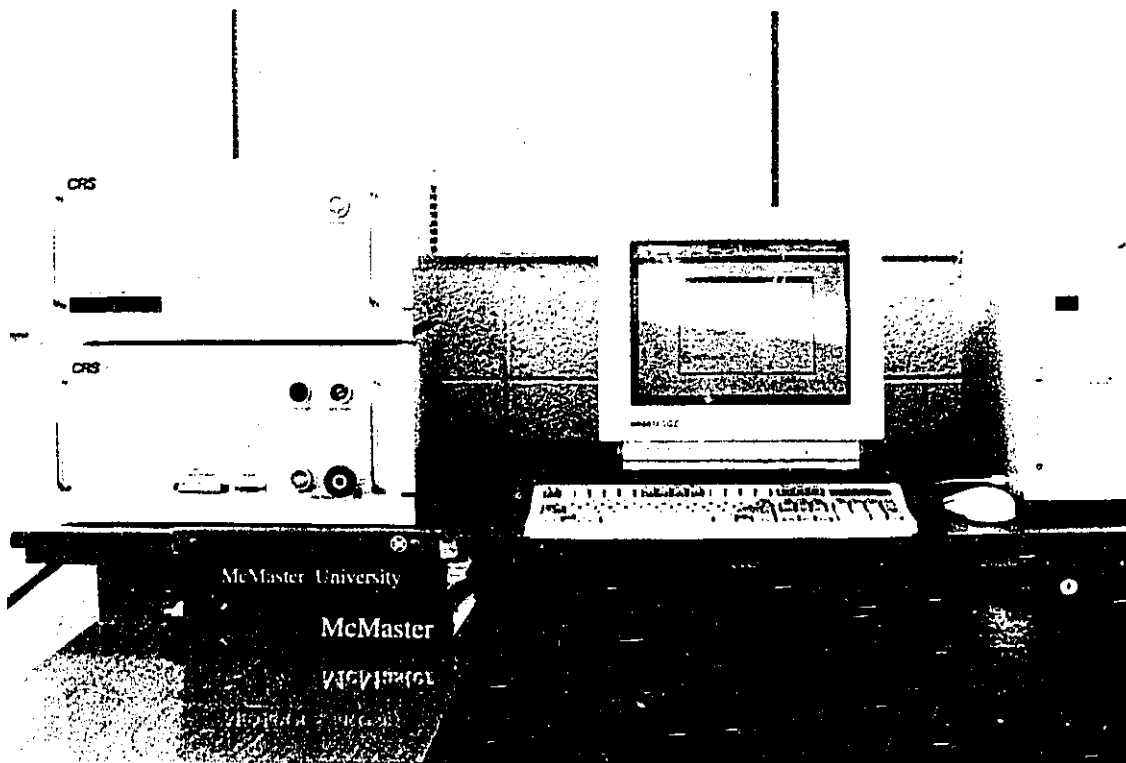
Figure 5.19: DC-Servomotor.

Figure 5.20: Shoulder joint.
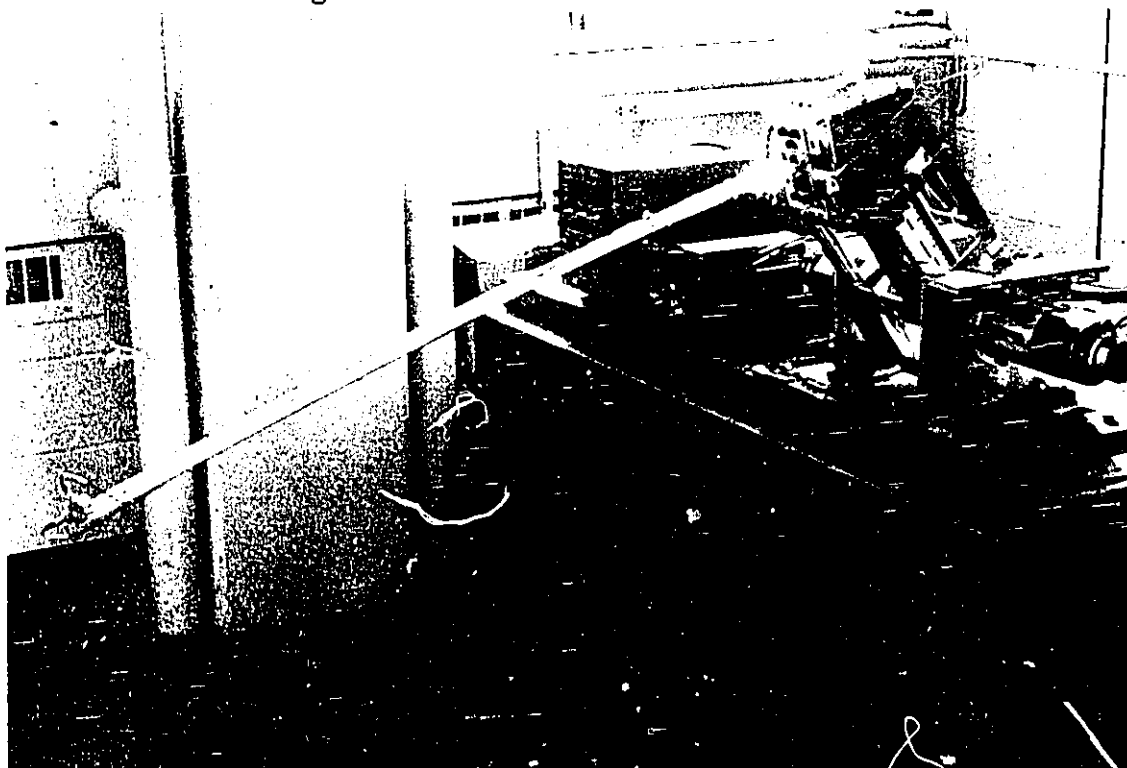
Figure 5.21: Seismic Platform.

Figure 5.22: Assembled FLEXROD.

Figure 5.23: Industrial Controller for FLEXROD.

Figure 5.24: "FLEXROD" with flexible lin...

5.10 SUMMARY OF CHAPTER 5

The mechanical setup was described in this chapter. The design, manufacture, assembly and debugging were all made in the Laboratories of McMaster. The setup is designed carefully in a modular form to allow for the investigators to be carried on for this thesis and for future ones. The state of the art technology is used in its development.

CHAPTER 6

EXPERIMENTAL RESULTS

6.1 OBJECTIVES

In this chapter we start by a brief review of the controller's hardware and its architecture. This is followed by a description of the development of the interface between the sensors and the controller. Typical test results are reported and analysed. These tests have the following objectives:

a)   Checking the data acquisition system and the developed interface units to assess their accuracy and limitations. To that end, FLEXROD was equipped with 50 mm by 3.2 mm of length 1000 mm flexible forearm which was adequately equipped with sensors to measure the deflections at some selected points. The output signals from the sensors were fed to the controller for processing. The experimental results were compared with the analytical solutions using an available Finite Element package.

b)   Comparing the path of the wrist point when brakes are applied to the motors with the analytical prediction.

6.2 CONTROLLER HARDWARE AND ARCHITECTURE

An industrial robot controller was acquired from CRS PLUS. It is known as the ALPHA C500 transputerized controller. This model was selected because of its open architecture which allows the implementation of the proposed controls for the elbow arm. The ALPHA C500 has a host PC and two transputers known as T400 and T805 from INMOS. These transputers allow the algorithms that control the motion and task execution to be changed easily. One transputer is known as the "Kinematic Transputer" and the other as the "Servo Transputer". The first executes kinematics calculations during the motion of the elbow arm and also can perform force-adaptive control. The second transputer executes a Proportional plus Derivative plus Integral local joint control. The ALPHA C500 has the capacity to handle six robot axes and can accommodate two additional signals. The controller has a parallel architecture which allows two tasks to be executed by different processors independently. This parallelism is termed parallel pipeline system in computer literature.

The pipeline architecture is shown in Figure (6.1) and is interpreted as a computer inside another computer. Further details regarding the transputers are furnished by the manuals from INMOS. Figure (6.2) shows the data paths between the individual units of the T805.

PARALLEL C from "Logical Systems" was the language which was used throughout this investigation. This choice was a consequence of the fact that the software package which is already residing in the controller was coded in PARALLEL C. This language provides vast options for compiling the programs through the "makefiles" and real-
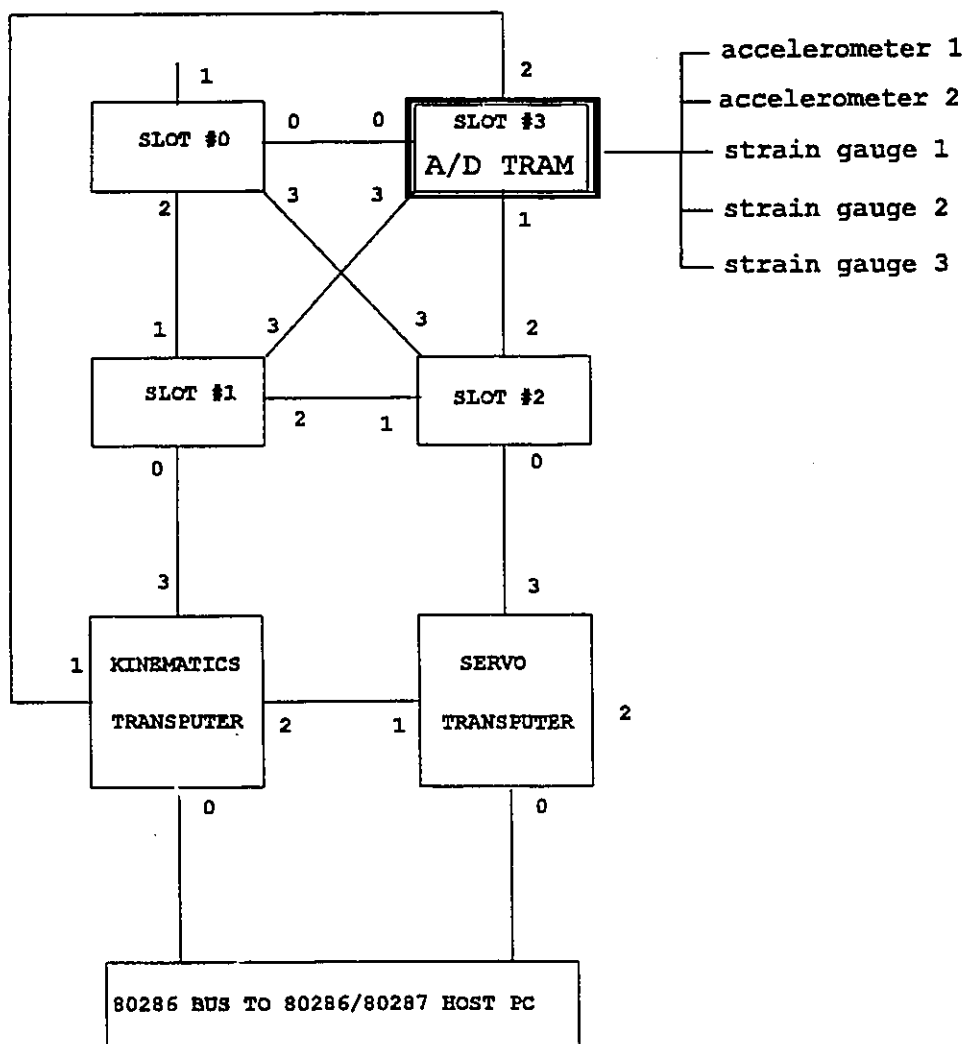
time controls through several commands.

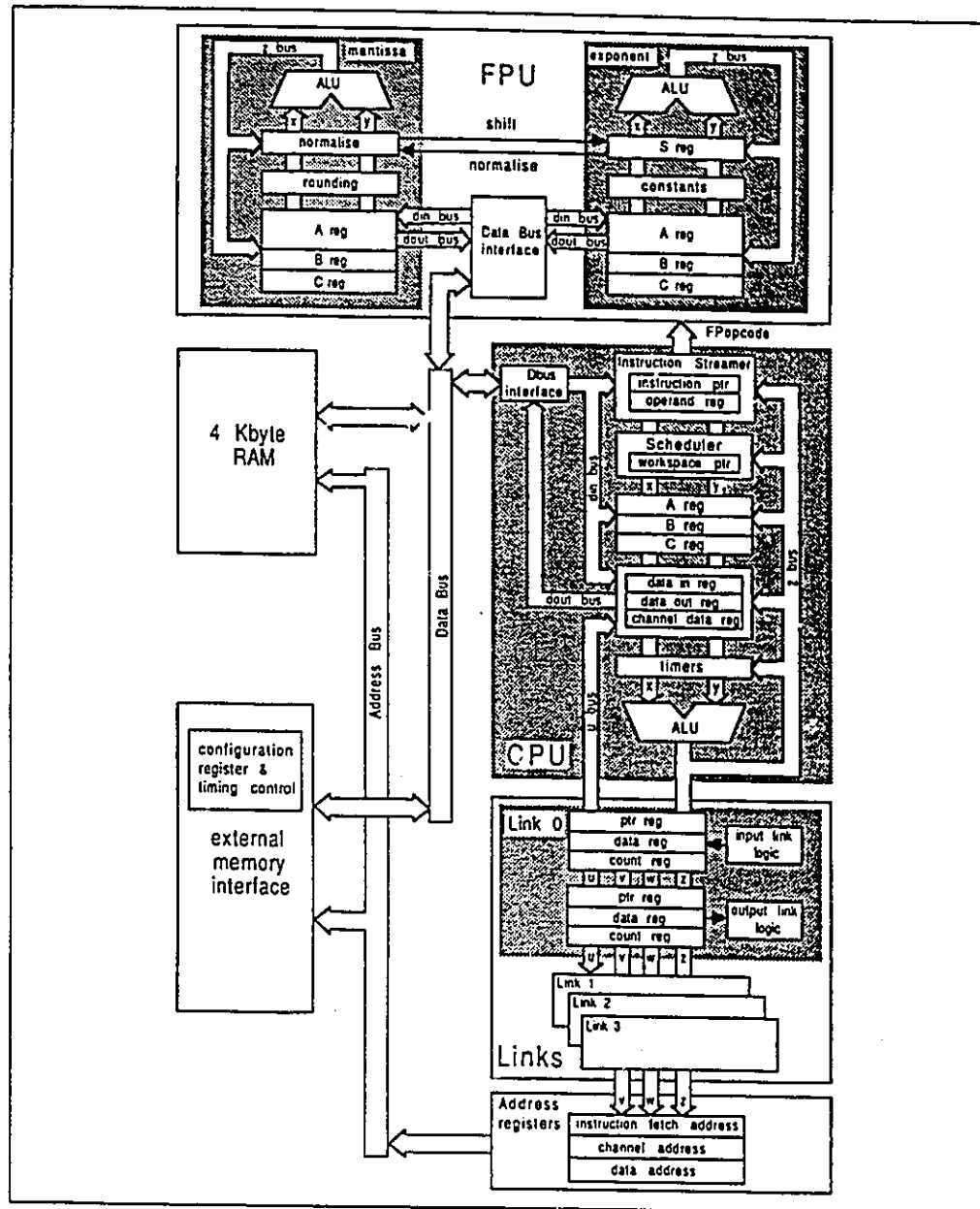Figure 6.1: Parallel pipeline architecture of the controller.

Figure 6.2: INMOS T805: internal data paths (SOURCE: INMOS [61]).

6.3 DEVELOPMENT OF THE INTERFACE UNIT BETWEEN SENSORS AND CONTROLLER

A three-axis accelerometer and three quarter-bridge strain gauges were installed on the flexible link of FLEXROD. That prompted the need to develop an interface that allows the controller to communicate with its sensors. A conventional A/D converter will not solve the problem because it is supposed to interface with serial microprocessors. A Transputer Module ADT108, known as A/D TRAM, is implemented in the controller. Real-time subroutines for the A/D TRAM were developed to perform the network communication protocol as depicted in the architecture shown in Figure (6.1). Great care was taken in writing the protocols to preserve the levels of priority of execution. Figure (6.3) shows the ADT108 A/D TRAM architecture.
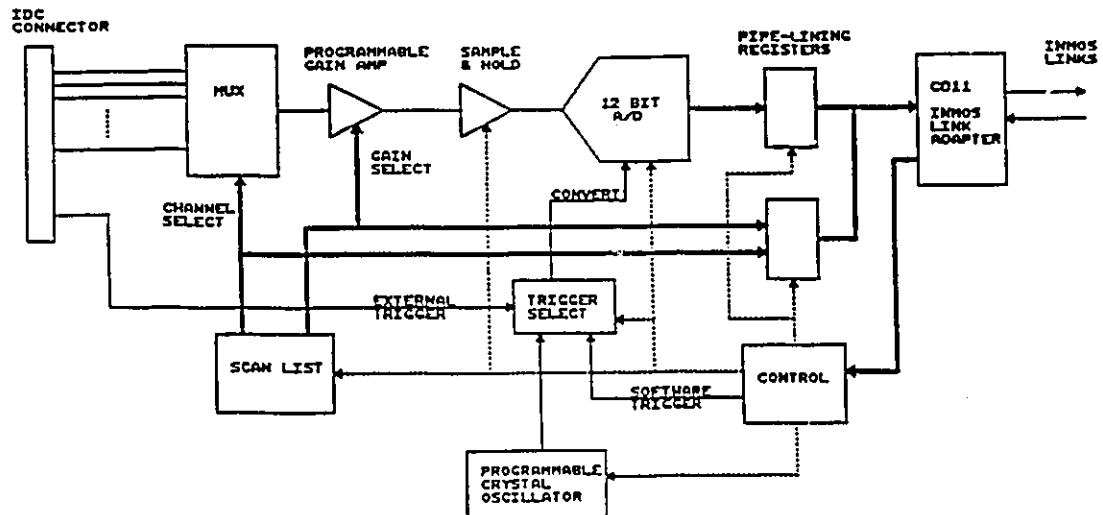

Figure 6.3: A/D TRAM ADT108 architecture (source: Sunnyside [60]).

6.4 CHECKING DATA ACQUISITION AND INTERFACE UNIT

Programs "IT" and "IT902X" were written in RAPL-II, the robot language, to make the arm execute a series of movements as shown in Figure (6.4), and Figure (6.5). The HP dynamic analyser was connected to the rig and data from the strain gauges and the accelometer were collected over a period of 48 s. The sensors were calibrated using a Nicolet oscilloscope before the test. The experimental setup is shown in Figure (6.6).

Objectionable noise was observed and its source was traced to the PWM modules of the DC-servomotors. The software filter which is available in the dynamic analyser was reprogrammed and the problem was solved.

The following series of tests were conducted:

(a) Time history of the deflections of the flexible link and the accelerations at the wrist point.

(b) Power spectrum analysis of the captured signals received from the sensors.

The signals were directed as follows:

channel 1:   tangential component of acceleration

channel 2:   radial component of acceleration

channel 3:   middle span strain gauge

channel 4:   root strain gauge

Figures (6.7) to (6.10) show typical results of the Lower spectrum of the 4 channels for the IT and the IT902X programs is a plot of the first five mode-shapes. Figure (6.11) of the flexible link as obtained from Finite Element analysis.

PROGRAM "IT"

1: SPEED 10
2: MI 2.5,-1.25
3: MI -2.5,1.25
4: RETURN
5:$

Figure 6.4: Program "IT".

```
PROGRAM "IT902X"

1: SPEED 10
2: MI 0.8,-1.25
3: MI 0.8,1.25
4: MI -0.8,-1.25
5: MI -0.8,1.25
6: RETURN
7:$
```
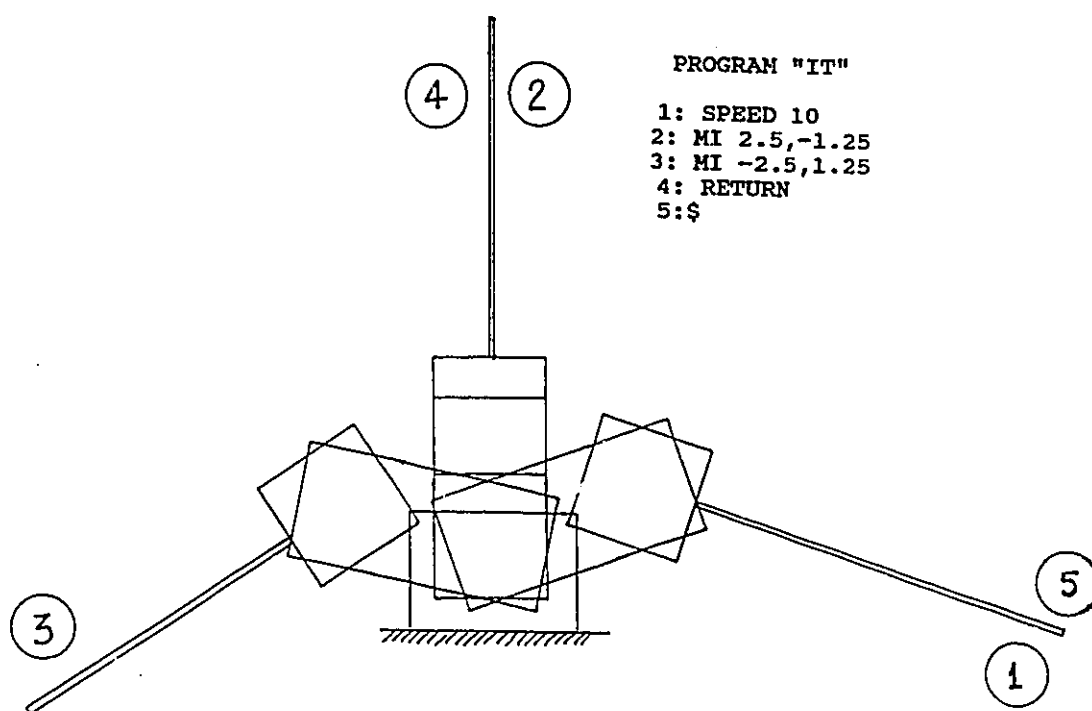
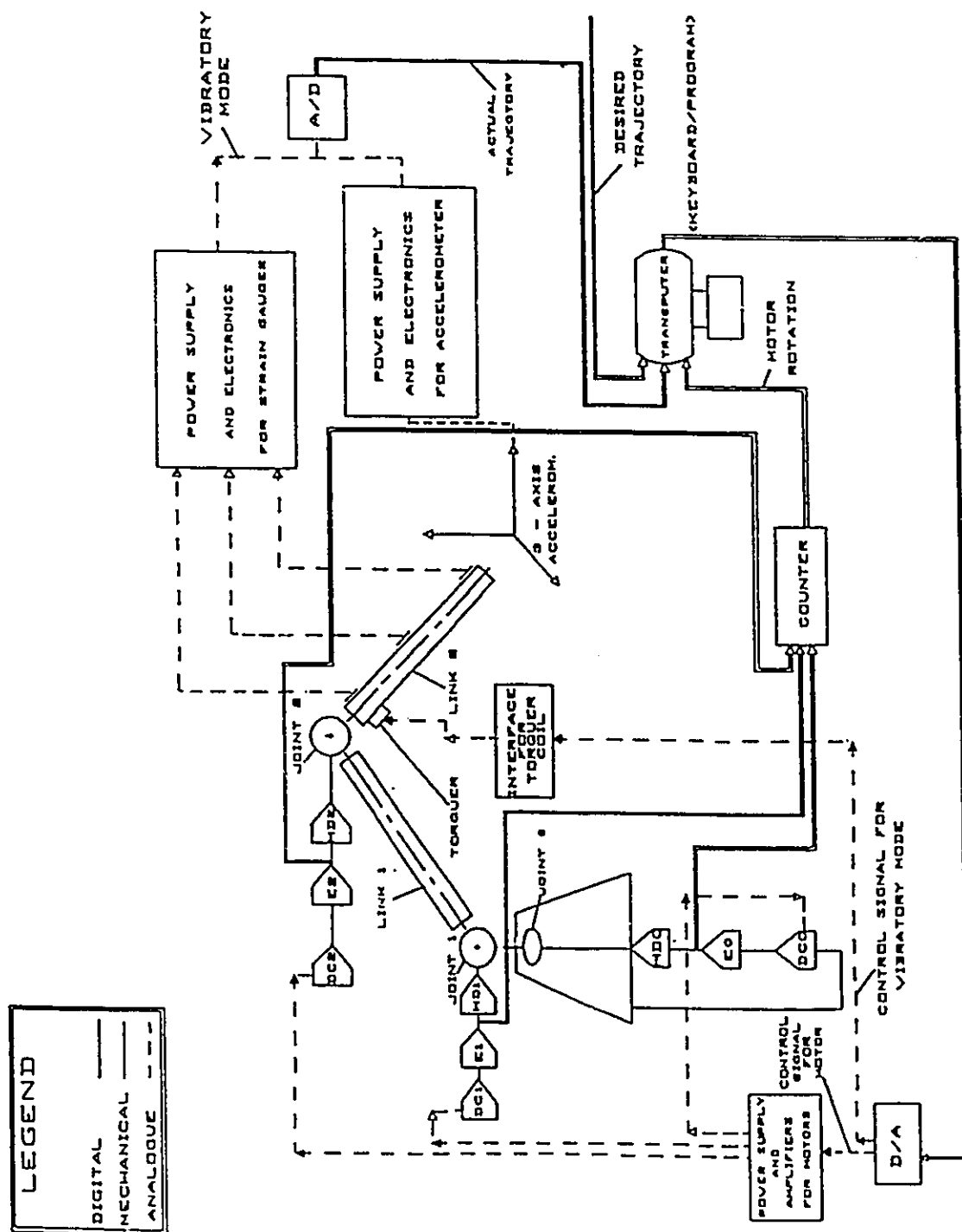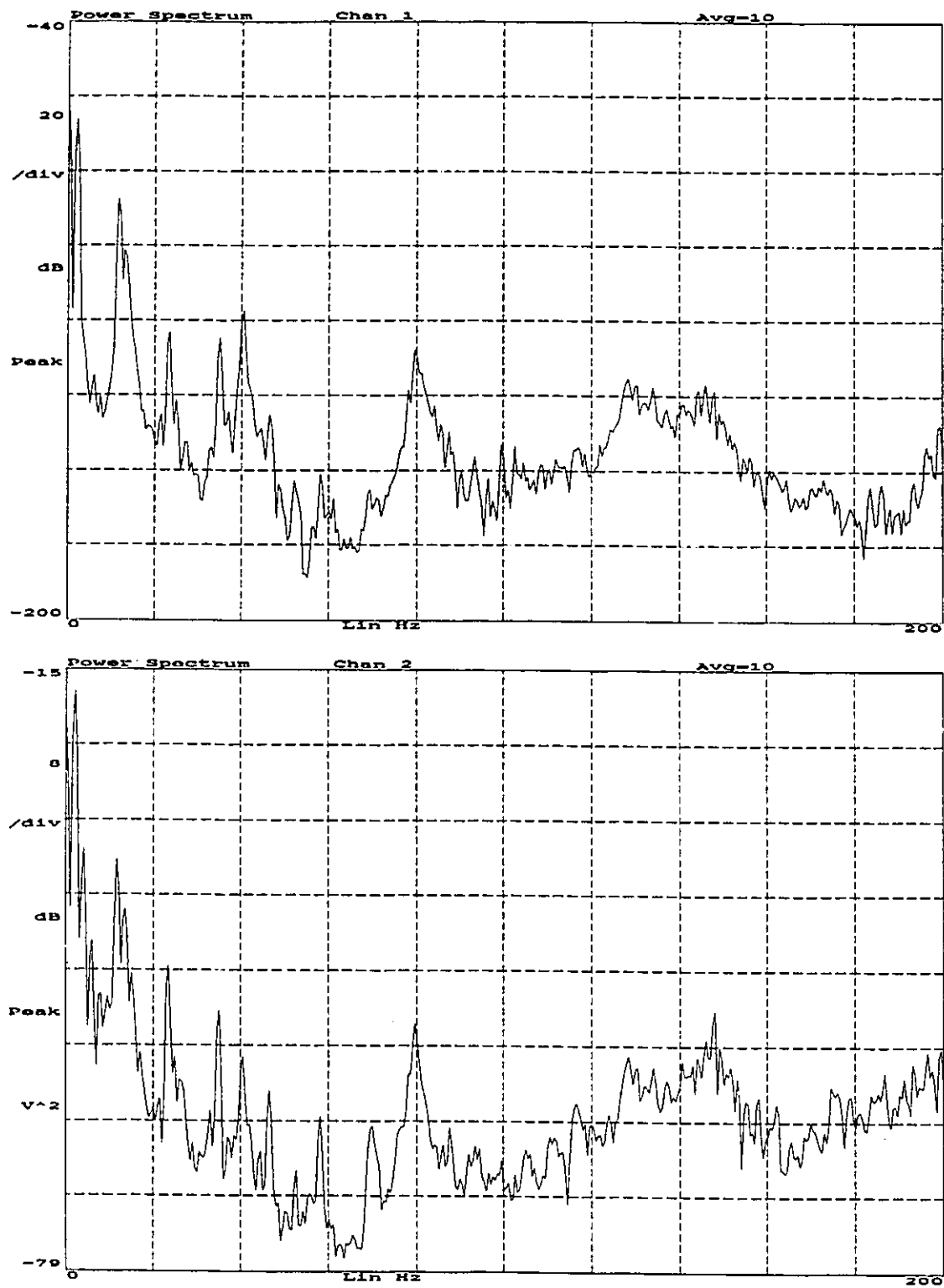Figure 6.5: Program "IT902X".

Figure 6.6: Experimental setup.

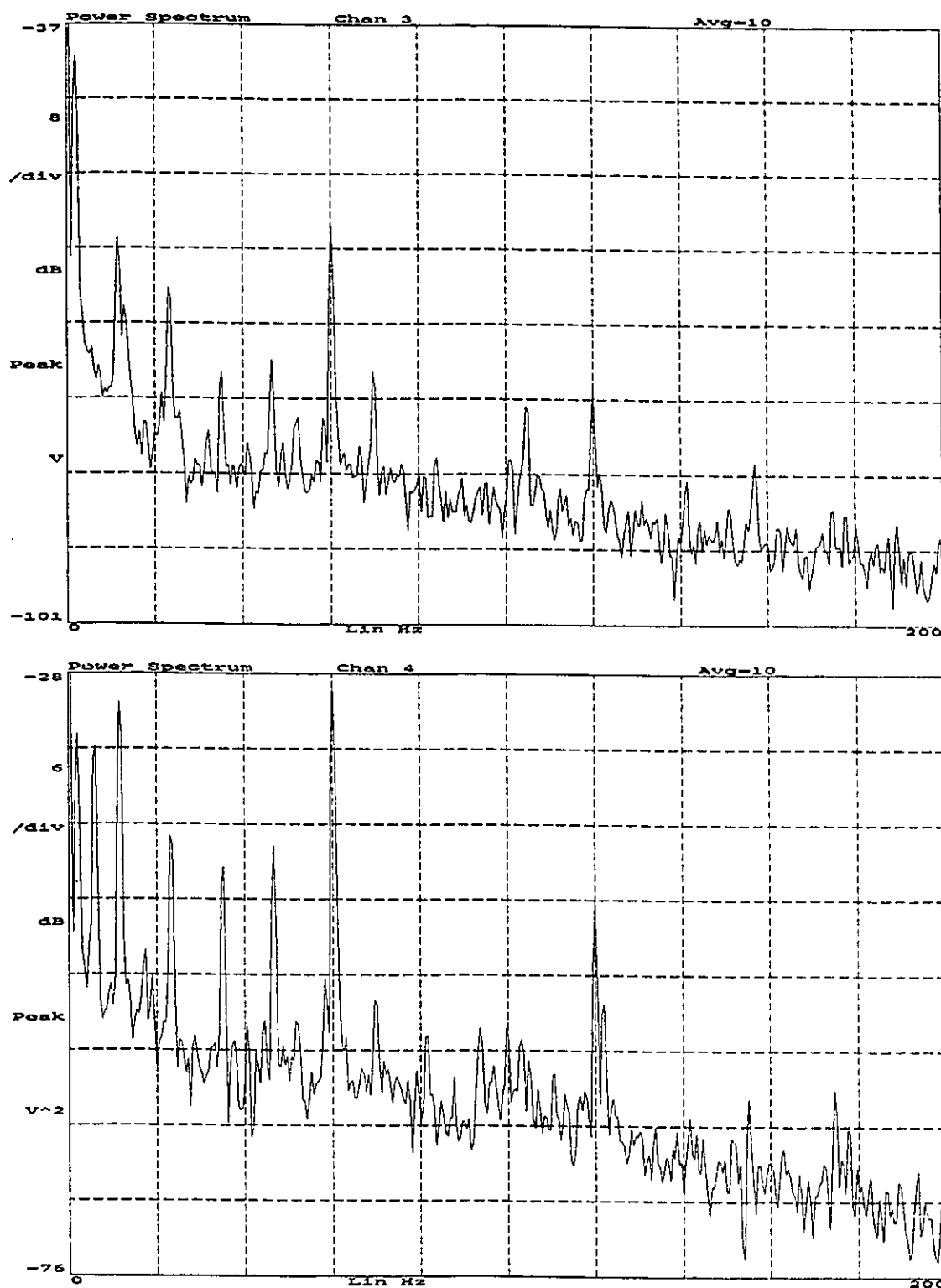**Figure 6.7: Power spectrum from channels 1 and 2 for "IT".**

Figure 6.8: Power spectrum from channels 3 and 4 for "IT".
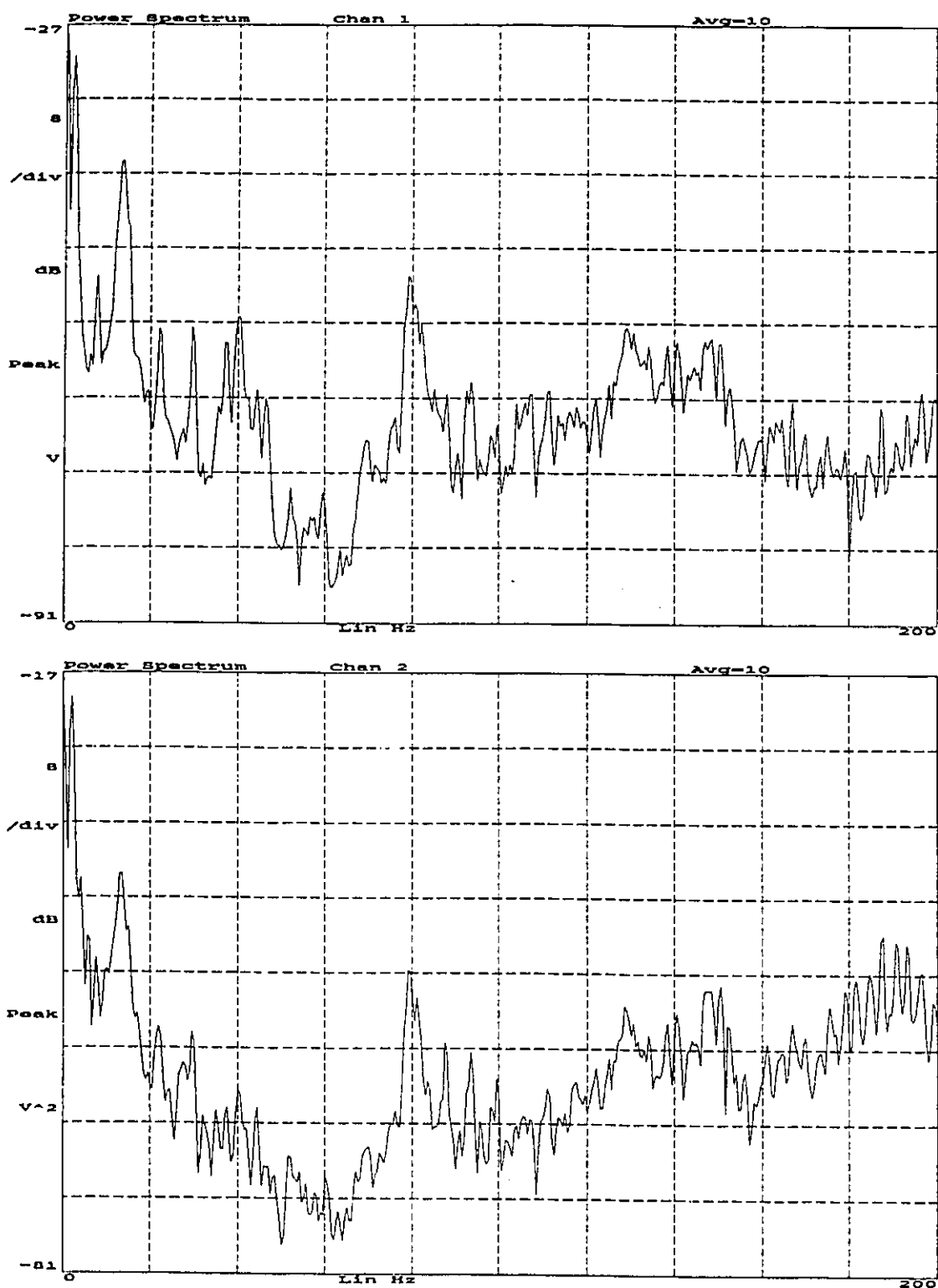
Figure 6.9: Power spectrum from channels 1 and 2 for "IT902X".
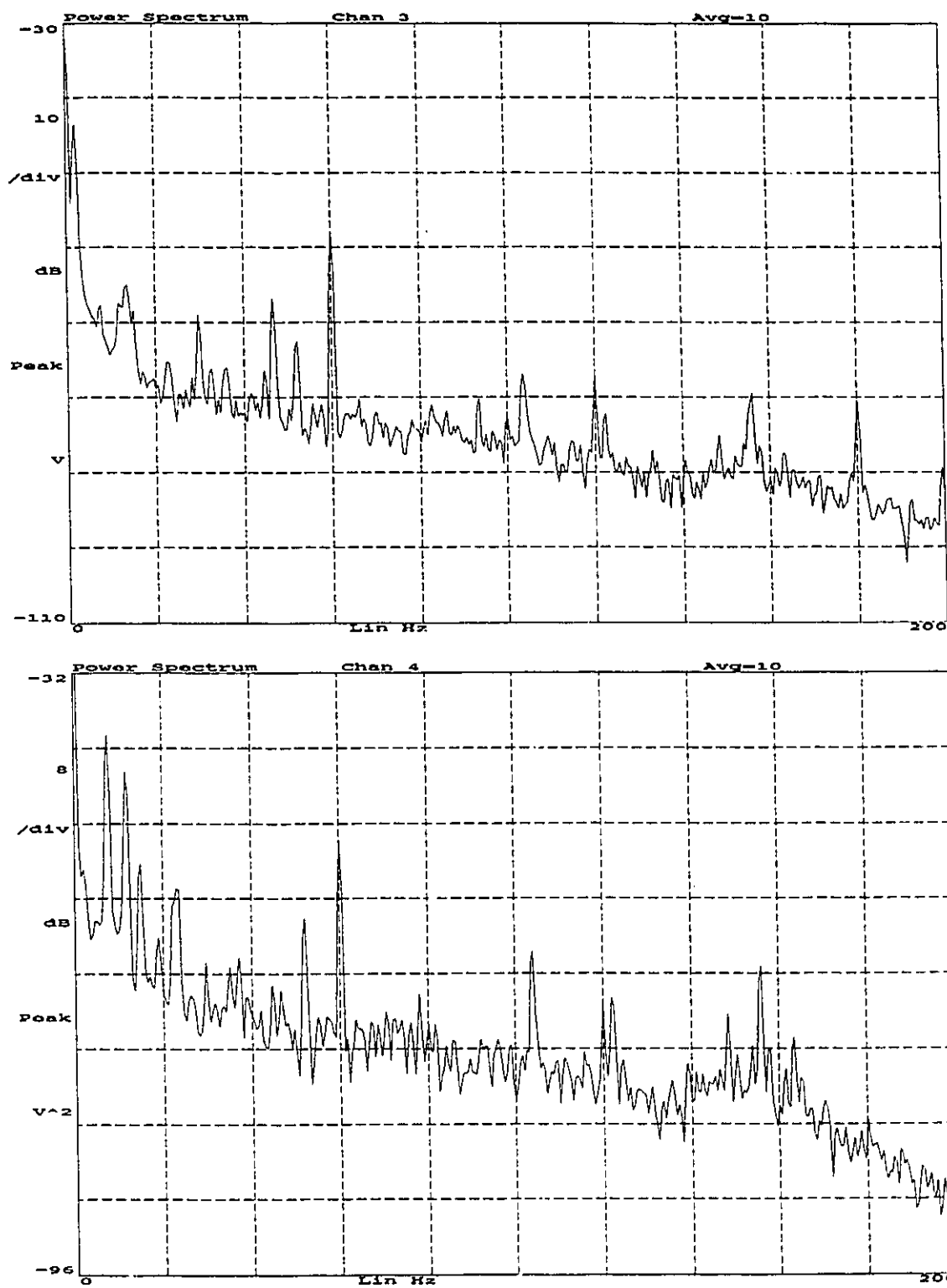
Figure 6.10: Power spectrum from channels 3 and 4 for "IT902X".
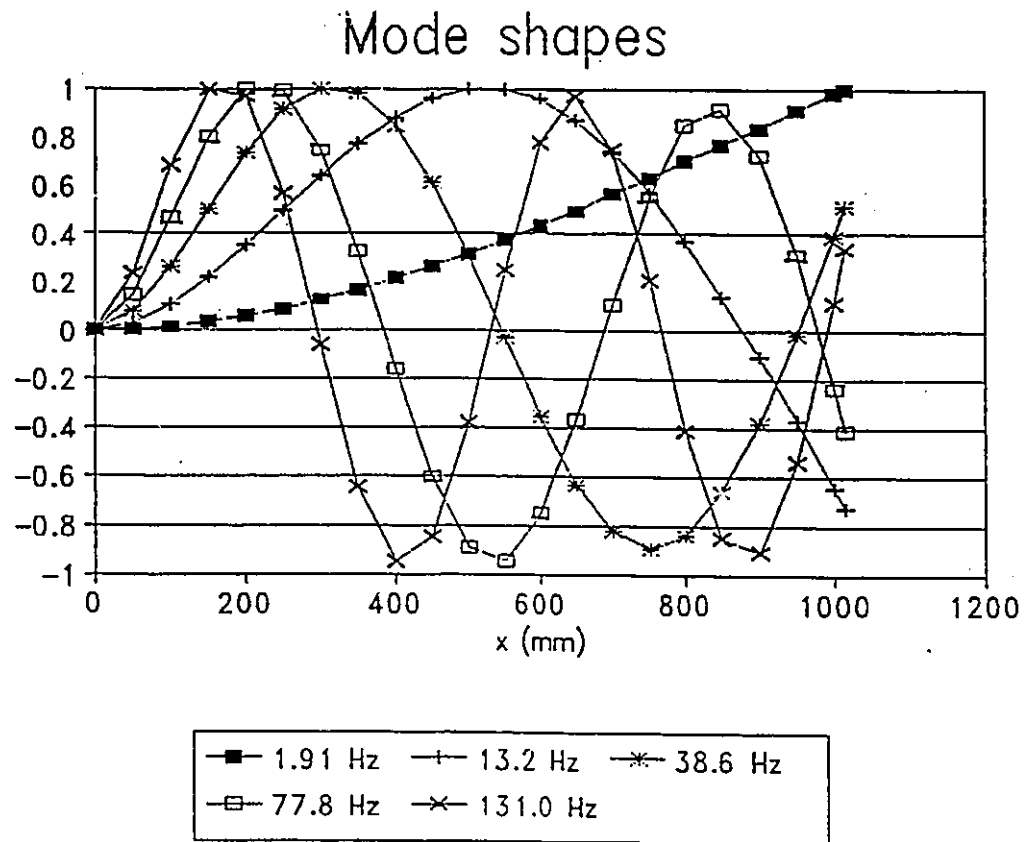
Figure 6.11: Mode shapes of flexible link Finite Element Analysis.

One can draw the following remarks:

(a)   The power spectrum of the signals showed that the peaks correspond to the natural

frequencies. These are listed in Table 6.1 together with the Finite Element results.

Deviations attributed to the different configurations assumed by the link in space.

TABLE 6.1 – EXPERIMENTAL AND ANALYTICAL FREQUENCIES

MODE	EXPERIMENTAL		FEM
	Hz	σ^2	
1	2.31	0.27	1.91
2	12.58	1.5	13.2
3	23.34	0.58	na
4	32.82	2.62	na
5	43.56	3.49	38.6
6	50.63	2.56	na
7	70.02	0.56	na
8	79.79	0.66	77.8
9	124.26	4.57	131.0
10	147.34	6.39	na

(b)   Small amplitude high frequency oscillations were detected. These are attributed to the harmonic drives and the associated gear train.

(c)   It was observed that the amplitudes of vibration decrease as the arm stretches and increase as the arm retracts..

(d)   The frequencies obtained from the experimental setup are in close agreement with the FEM analysis, as shown in Table 6.1, in spite of the fact that the FE analysis is a crude approximation of the actual link.

## 6.5 COMPARING PATH OF WRIST POINT WITH ANALYTICAL PREDICTION

The signals generated by the 3-Axis accelerometer are acquired together with the signals from the strain gauges placed on the flexible forearm. The strain gages used are quarter bridges. The acceleration components are first transformed from the local frame to the world frame then integrated twice using a simple trapezoidal rule with a time step in the order of 1 msec. Using D-H inverse matrices one obtains the position of the tip at every one msec. The developed parallel controller is able to sample at a remarkable speed of 1000 Hz. Higher sampling frequencies are not possible at this stage of research because of the calculations that the controller has to perform during the operation of the elbow arm. Another limitation is also due to the 100 Hz clock cycle of the host processor which is considered low for this type of application. However, the devised scheme proved to be very efficient in evaluating the position of the tip in real-time and also in providing most of the sensory information that the flexible robot needs.

To transform the readings of the accelerometer at the wrist point to the world frame we had to use the coordinate systems shown in Figure (6.12) with the proper D-H transfer matrices. Flexibility of the links has to be taken into account.

One can isolate the second link and use the undamped vibrations solution of the Euler-Bernoulli beam with clamped -free boundary conditions. This reads:

$$\eta(\xi,t) = \left\{ A \ (\cosh \ \beta \xi - \cos \ \beta \xi) + B \ (\sinh \beta \xi - \sin \beta \xi) \right\} \sin \omega \, t \qquad (6.1)$$

where ξ and η are the longitudinal coordinates and lateral deflections of a point on the centre level beam. A and B are coefficients to be determined from the boundary conditions and
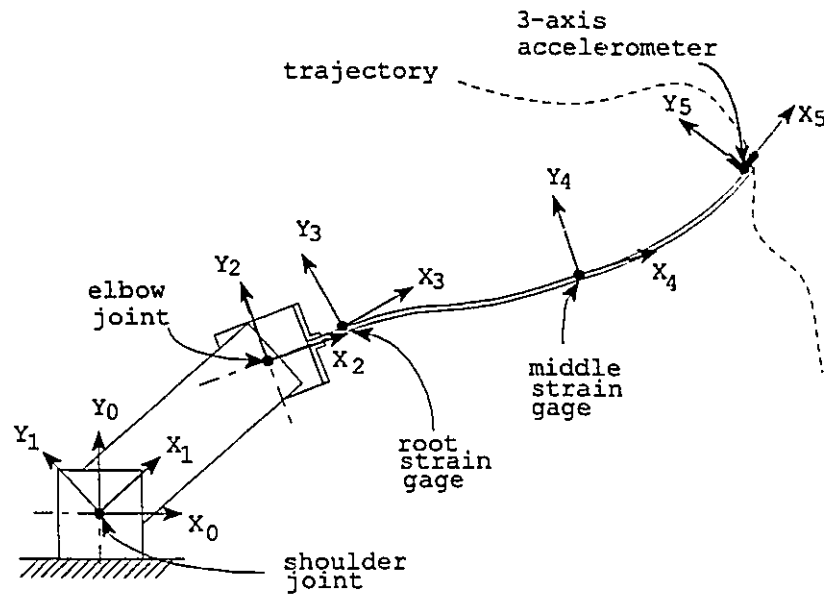
Figure 6.12: Coordinate Systems for the Flexible Forearm.

the constant β is given by:

$$\beta = \sqrt[4]{\frac{\rho \, \omega^2}{EI}}$$

where ρ is the mass per unit length, E and I are Young's modulus and the area moment of

inertia of the cross section respectively. In order to construct a simple solution only the first

fundamental mode ω is considered. From the definition of Young's modulus, one can write:

$$M = \frac{2 \, \varepsilon \, E \, I}{b} \tag{6.4}$$

where b is the thickness of the beam and ε is the reading of the strain gauge. The chain slope

$\Delta\theta$ between two points at ξ_1 and ξ_2 on the beam is given by:

$$\Delta\theta = \int_{\xi_1}^{\xi_2} \frac{M}{E\,I}\,dx \qquad (6.3)$$

Integrating $M = EI\,d^2\eta\,/\,d\xi^2$ and using (6.1) one obtains:

$$\Delta\theta(\xi,t) = \beta\left\{ A\,[\sinh\beta\xi + \sin\beta\xi] + B[\cosh\beta\xi - \cos\beta\xi\,]\right\}\sin\omega_r t \qquad (6.4)$$

The strain is expressed in a similar form using (6.4) and the relation $M = EI\,d^2\eta\,/\,d\xi^2$ to

obtain:

$$\varepsilon = \frac{2\,\beta^2}{b}\left\{ A\,[\cosh\beta x + \cos\beta x\,] + B\,[\sinh\beta x + \sin\beta x]\right\}\sin\omega_r t \qquad (6.5)$$

Relations (6.5) and (6.4) can be rearranged in the form:

$$\left\{ \begin{array}{c} \varepsilon \\ \Delta\theta \end{array} \right\} = \left[\begin{array}{cc} K_{11} & K_{12} \\ K_{21} & K_{22} \end{array} \right] \left\{ \begin{array}{c} A \\ B \end{array} \right\}$$

where the k_{ij}'s are functions of $\beta\xi$. One can express A and B in terms of ε and $\Delta\theta$ as follows:

$$\left\{ \begin{array}{c} A \\ B \end{array} \right\} = \left[\begin{array}{cc} K_{11}^{\cdot} & K_{12}^{\cdot} \\ K_{21}^{\cdot} & K_{22}^{\cdot} \end{array} \right] \left\{ \begin{array}{c} \varepsilon \\ \Delta\theta \end{array} \right\}$$

Finally, one can write

$$\eta = [\,(K_{11}^{\cdot}\,\varepsilon + K_{12}^{\cdot}\,\Delta\theta)\cdot(\cosh\beta\xi - \cos\beta\xi) +$$

$$(K_{21}^{\cdot}\,\varepsilon + K_{22}^{\cdot}\,\Delta\theta)\cdot(\sinh\beta\xi - \sin\beta\xi)\,]\sin\omega t \qquad (6.5)$$

The signal from the accelerometer can be integrated after transformation to the world frame.

The above model was encoded in a real-time subroutine FLXTRF written in C++

to be integrated in the parallel network of FLEXROD. The parallel computer writes the

sensor outputs to a datafile FLXTRF. The interface that saves the data was developed and encoded using the parallel network and the A/D TRAM from Sunnyside Systems Inc.

Figure (6.13) shows the dynamic response of an elbow arm with flexibility in the joint and another with flexibility in the link. They are staggered for clarity. The brakes were applied for ($\theta_1 = 50^0$, $\theta_2 = 20^0$) for the first and were applied for ($\theta_1 = 48^0$, $\theta_2 = 20^0$) for the second. Notice the length of the arch traced by the wrist point in each case.
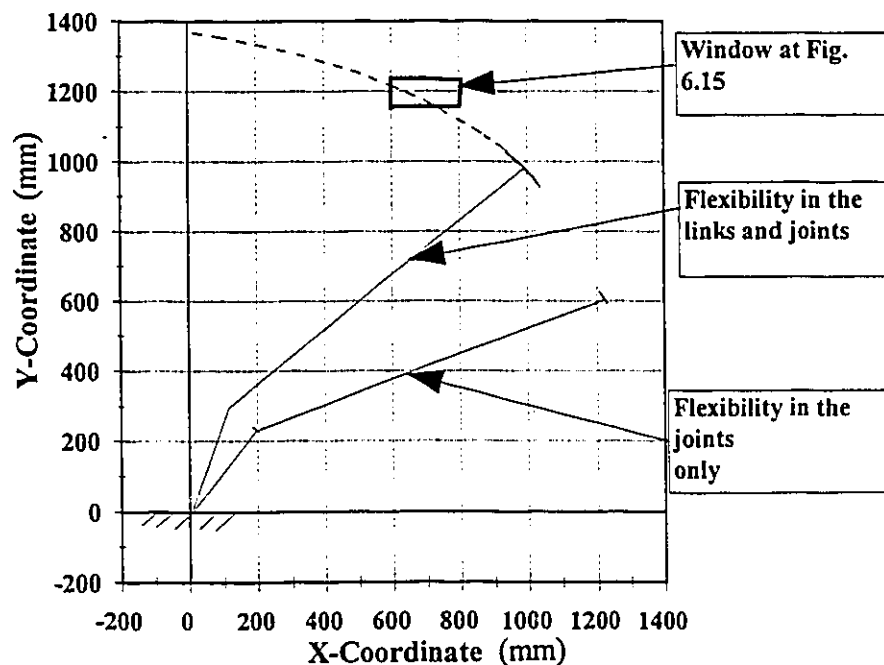
Figure 6.13: Dynamic response for the elbow arm with flexibility in the joint (analytical) and an elbow arm with flexibility in the forearm (experimental).

It is important to notice that the experimental results in Figure (6.13) are performed on an elbow arm with flexibility in the joints and the forearm. The analytical prediction is made for an elbow arm with exaggerated flexibility in the joints. If the trajectories shown in Figure (6.13) are windowed and amplified one see a series of lobes as depicted by Figures (6.14) and (6.15) the lobes dampen out. Figure (6.16) shows the window of the theoretical tip trajectory. Again the agreement is reasonable taking into account the presence of flexibility in the arm in the experimental setup. A damping assessment was done in Figure (6.17) and its window on Figure (6.19). The structural damping of the flexible link was found to be 0.078 as expected.
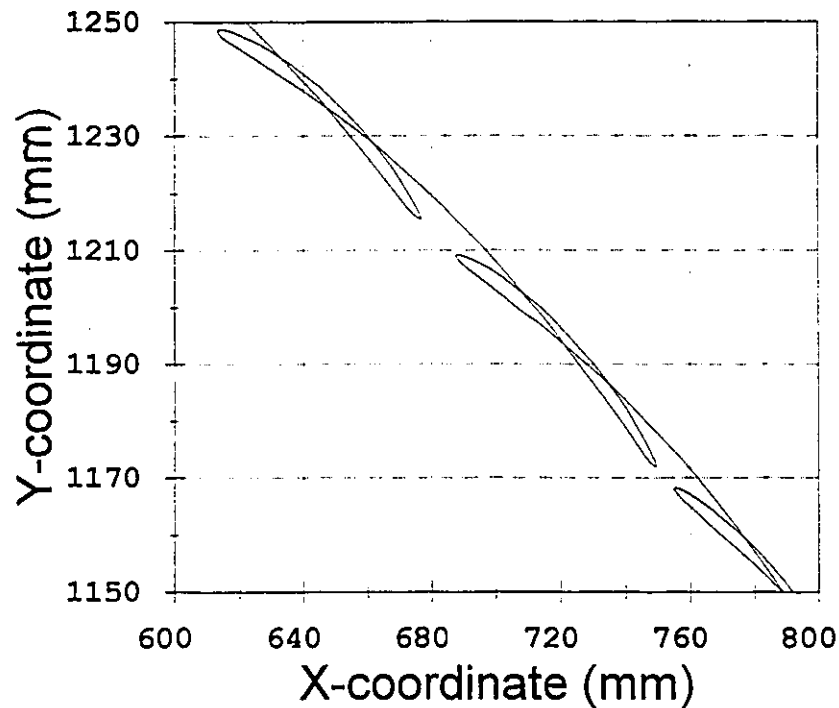
Figure 6.14: Trajectory of tip of flexible robot in its path to stop position.
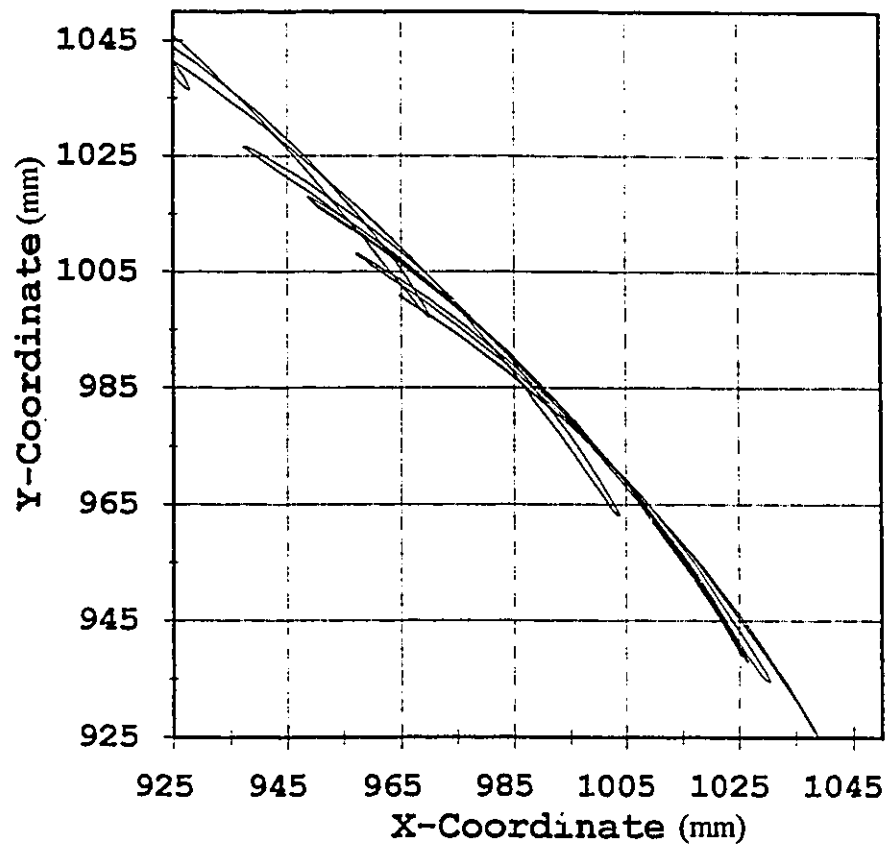
Figure 6.15: Tip trajectories after applying the brake (experimental).
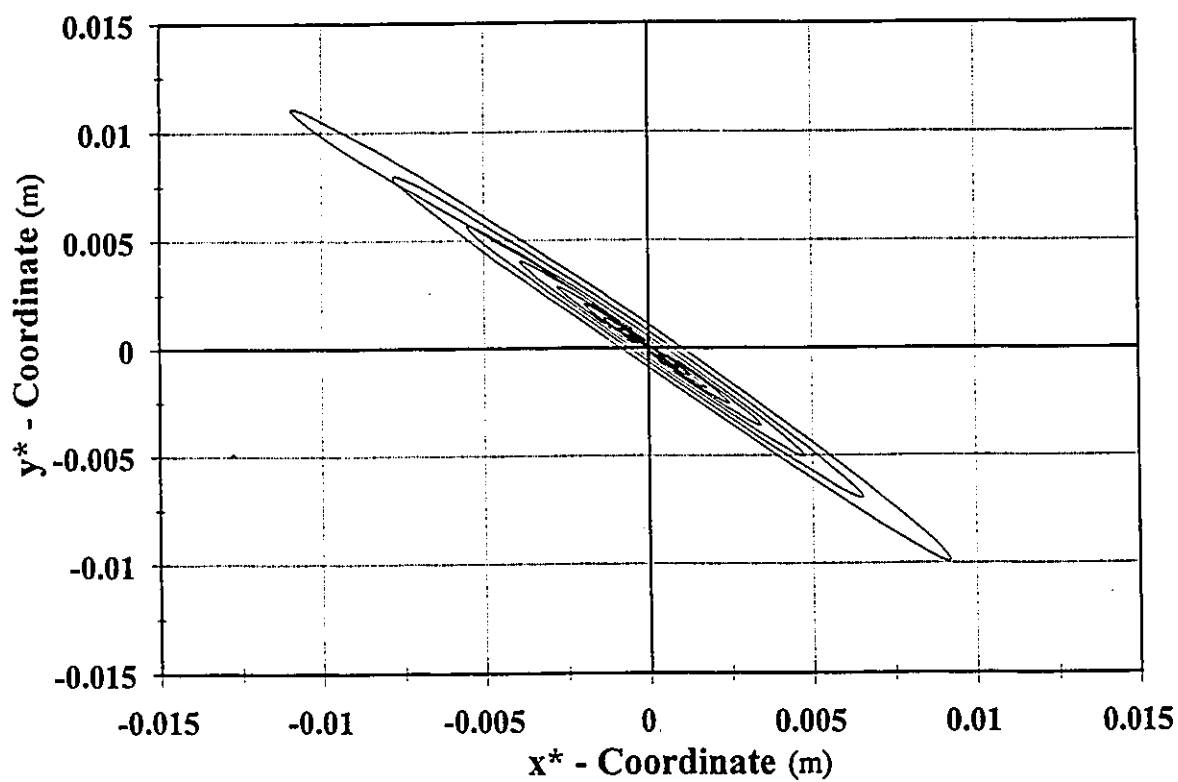
Figure 6.16: Tip Trajectories Window immediately after applying the brake. X*, Y*

measured from equilimrium point (analytical).
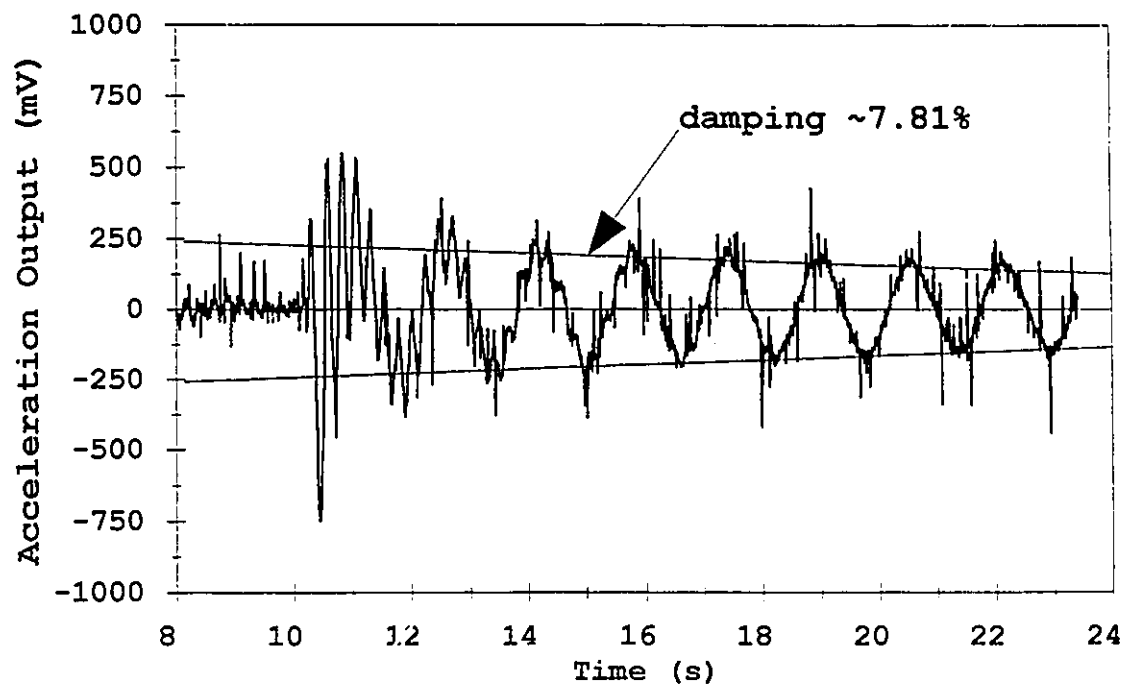
Figure 6.17: Tangential Acceleration showing a 0.078 damping ratio for the flexible arm (experimental).

Figure 6.18: Window for Tangential Acceleration of previouis record (experimental).

6.6 SUMMARY OF CHAPTER 6

Experiments were constructed using FLEXROD to check the data acquisition system as well as the sensors attached to the different points of the elbow arm to ensure freedom of the data from noise and distortions. The output signals, after their capture by the controller, were processed to predict the natural frequencies and modes of vibrations of the elastic forearm. The experimental results were found to compare reasonably well with the finite element solution.
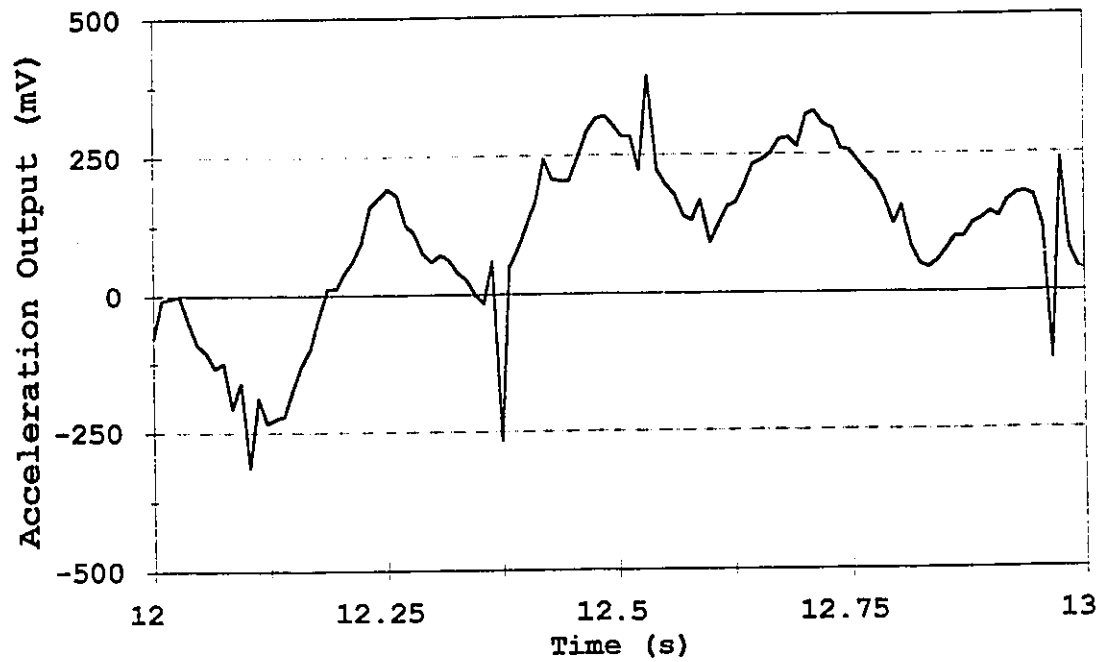
Another set of experiments were conducted to validate the dynamical models derived earlier. The readings of the accelometer and the strain gauges were processed to predict the motion of the wrist point immediately after the sudden application of the brakes to the two motors. It was found that the amplitudes of vibration for the experimental setup are higher than the theoretical prediction as expected. This is attributed to the presence of the additional elasticity on the forearm in the experimental setup.

The setup serves to conduct further experiments for the implementation of NIT and other control strategies for comparisons. This was considered outside the scope of objectives of the present work.

CHAPTER 7

CONCLUSIONS

1. Adequate mathematical models have been developed to describe the dynamics of a two link elbow arm with rigid links (RAM), with flexibility in the joints (FJM) and with flexibility in the links (FLM). The majority of the reported work in the literature is confined to one link.

2. A powerful algorithm; the nonlinear integrated tabular (NIT), was developed for the tracking of prescribed trajectories by the wrist point. Numerous simulations and evaluations were conducted to assess its feasibility, limitations for tracking smooth and discontinuous trajectories.

3. Conventional controls for the flexible elbow arm were developed, simulated and compared with NIT. Among the conventional strategies which were investigated are the "proportional plus derivative plus gravity", the "feedback linearization" as well as the "variable structure" controls. It was found that NIT compares well with all of them in terms of smoothness of tracking and computing cost in real time.

4. The Sliding Control was found to be a promising approach and the chatter problem can be easily resolved if one uses the (SAT) function or (DEZ) function with proper modifications.

5. The VEE-MOD-VEE, can be easily extended to handle higher order systems.

6. The experimental part consisted of the design, manufacture, assembly and debugging of the hardware of a two link elbow arm using the up-to-date technology available in terms of speed reducers and transputers. The design is modular allowing further additions and adaptations to be introduced to the set up to conduct further investigations.

7. The software of the controller was streamlined and an interface unit was developed to act as a mechanism to acquire data from the sensors to be processed by the transputers. The experimental set up was used to check the dynamic models developed in earlier sections. Reasonable agreement was found between the experimental findings and the theoretical predictions.

8. The parallel network that was developed proved to be efficient and computationally adequate for performing up to 1000 samples/sec. Also, it proved to be suitable for the inclusion of new processors that are eventually

needed.

SUGGESTIONS FOR FUTURE WORK

1. Full implementation of NIT in FLEXROD and in depth comparisons of its performance with the conventional controls.

2. Simulation and implementation of NIT for FLM.

3. The feasibility of applying sliding mode control for elbow arms with flexibility in the links.

4. Advanced designs for compliant grippers and their controls to meet the challenge posed by cooperative robots.

REFERENCES

[1]   Alves, D.S.R.; Kasper, K.; Mitchell, G.P.; Owen, D.R.J." A Multi-Processor Implementation for Elasto-plastic Finite Element Calculations". In: Proceedings 2nd International Conference On Computational Plasticity, pp. 199-212, Pineridge Press, Swansea 1989.

[2]   Balas, M.J. "Feedback Control of Flexible Systems", IEEE Transactions on Automatic Control, vol. AC. 23, no. 4 , pp. 673-679, 1978.

[3]   Bathe, K.-J. "Numerical Methods in Finite Element Analysis", Englewood Cliffs, N.J.; Prentice-Hall, 1984.

[4]   Bathe, K.-J.; Bolourchi, S. "Large Displacement Analysis of Three-Dimensional Beam Structures", International Journal for Numerical Methods in Engineering, vol. 14, pp. 961-986, 1979.

[5]   Berkkan, K. "A Solution Method for Nonlinear Contact Problems, Ph.D Thesis, McMaster University, Dept. Mech. Eng., 1988.

[6]   Book, W.J.; Maizza-Neto, O.; Whitney, D.E. "Feedback Control of a Two Beam , Two Joint Systems with Distributed Flexibility", Transactions of the ASME, Journal of Dynamic Systems, Measurement and Control, pp. 424-431, 1975.

[7]   Carrara, A.R.S. "Design of a Servo-Drive Pointing Mechanism to move a Sun Simulator", in Portuguese, M.Sc. Thesis, Brazilian Institute for Space Research (INPE), Sao José dos Campos, SP, Brazil, 1989.

[8]   Carusone, J.; D'Eleuterio, G.M.T. "Tracking Control for End-Effector Position and Orientation of Structurally Flexible Manipulators", Journal of Robotic Systems 10(6), pp. 847-870, 1993.

[9]   Cetinkunt, S.; Book, W.J. "Symbolic Modeling and Dynamic Simulation of Robotic Manipulators with Compliant Links and Joints", Robotics & Computer-Integrated Manufacturing, vol. 5, no. 4, pp. 301-310, 1989.

[10]   Cetinkunt, S.; WU, S. "Tip Position Control of a Flexible One-Arm Robot with Predictive Adaptive Output Feedback Implemented with Lattice Filter Parameter Identifier", Computers & Structures, vol. 36, no. 10, October 1991.

[11]   Chang, L.-W. and Hamilton, J.F. "The Kinematics of Robotic Manipulators With Flexible Links Using an Equivalent Rigid Link System (ERLS) Model", Transactions of the ASME, Journal of Dynamic Systems, Measurement and Control, vol. 113, pp. 48-53, March 1991.

[12]   Chang, L.-W. and Hamilton, J.F. "Dynamics of Robotic Manipulators With Flexible Links", Transactions of the ASME, Journal of Dynamic Systems, Measurement and Control, vol. 113, pp. 54-59, March 1991.

[13]   Dado, M.H.; Soni, A.H. "A Dynamic Analysis Tool for Flexible Robotic Manipulators", Proceedings of the USA-Japan Symposium on Flexible Automation, Minneapolis, Minnesota, pp. 399-405, 1988.

[14]   DE Luca A. "Dynamic Control of a Robot with Joint Elasticity", In: IEEE International Conference on Robotics and Automation, Philadelphia, PA, 1988.

[15]   Gandhi, M.V.; Thompson, B.S. "The Finite Element Analysis of Flexible Components of Mechanical Systems Using a Mixed Variational Principle", In: Design Engineering Technical Conference, ASME paper 80-det-64, 1981.

[16]   Good, M.C.; Sweet, L.M.; Strobel, K.L. "Dynamic model for Control System Design of Integrated Robot and Drive Systems", Transactions of the ASME, Journal of Dynamic Systems, Measurements and Control, vol. 107, pp. 53-59, 1985.

[17]   Hallauer Jr., W.L.; Waggie, D.A. "An Inexpensive Experiment for Undergraduates on Active Control of Structure Vibrations", In: 1989 ASEE Annual Conference Proceedings, pp. 433-435, 1989.

[18]   Hastings, G.G.; Book, W.J. "A Linear Dynamic Model for Flexible Robotic Manipulators", IEEE Control Systems Magazine, pp. 61-64, 1987.

[19]   Hewit, J.R. "Twin Active Force Control for Robots with Flexible Transmissions", Robotics & Computer - Integrated Manufacturing, vol. 5, no. 2/3, pp. 119-122, 1989.

[20]   Hollerbach, J.M. and Sahar, G. "Wrist-Partitioned, Inverse Kinematic Accelerations and Manipulator Dynamics", The International Journal of Robotics Research, vol. 2, No. 4, pp. 61-76, 1983.

[21]   Hsiao, K.M.; Jang, J,-Y. "Dynamic Analysis of Planar Flexible Mechanisms by Co-Rotational Formulation", Computer Methods in Appl. Mechanics and Engineering 87, pp. 1-14, 1991.

[22]   Hsiao, K.M.; Yang, R.T.; Lee, A.C. "A Consistent Finite Element Formulation for Non-Linear Dynamic Analysis of Planar Beam", International Journal of Num. Methods in Engineering, vol. 37, pp. 75-89, 1994.

[23]   Hurty, W.C. "Dynamic Analysis of Structural Systems Using Component Modes", AIAA Journal, vol. 3 , no. 4, pp. 678-685, 1965.

[24]   Khorrami, F.; Jain, S. "Nonlinear Control with End-Point Acceleration Feedback for a Two-Link Flexible Manipulator: Experimental Results", Journal of Robotic Systems 10(4), pp. 505-530, 1993.

[25]   Koivo, A.J. "Control of Robotic Manipulators", Wiley and Sons, 1990.

[26]   Lin, S.-H.; Tosunoglu, S.; Tesar, D. "Control of a Six-Degree-of-Freedom Flexible Industrial Manipulator", IEEE Control Systems Magazine , pp. 24-30, April 1991.

[27]   Low, K.H. "Formulation and Computer Simulation of the Dynamic Equations of Flexible Robots", In: Proceedings Of The Second International Symposium On Robotic And Manufacturing: Research Education And Applications, 1988.

[28]   Luecke, G.R. and Gardner, J.F. "Local Joint Control in Cooperating Manipulator Systems - Force Distribution and Global Stability", Robotica, vol. 11, pp. 111-118, 1993.

[29]   Luh, J.Y.S.; Walker, M.W.; Paul, R.P.C. "On-line Computational Scheme for Mechanical Manipulators", Transactions of ASME, Journal of Dynamic Systems, Measurements and Control, vol. 102 , pp. 69-76, 1980.

[30] Maizza-Neto, O.M. "Model Analysis and Control of Flexible Manipulators Arms", Ph.D. Thesis, Mech. Eng. Dept. MIT, 1974.

[31] Marilier, T.; Richard, J.A. "Non-Linear Mechanic and Electric Behaviour of a Robot Axis with a Harmonic-Drive' Gear", Robotics & Computer - Integrated Manufacturing, vol. 5, no. 2/3, pp. 129-136, 1989.

[32] Matsuno, F.; Sakawa, Y. "A Simple Model of Flexible Manipulators with Six Axes and Vibration Control by Using Accelerometers", Journal of Robotics Systems, 7(4), pp. 575-597, 1990.

[33] Mattiasson, K.; Bengtsson, A.; Samuelsson, A. "On the Accuracy and Efficiency of Numerical Algorithms for Geometrically Nonlinear Structural Analysis", In: Finite Element Methods for Nonlinear Problems Symposium, Trondheim, Normay proceedings, 1986.

[34] Meirovitch, L.; Baruh, H.; Oz, H. "A Comparison of Control Techniques for Large Flexible Systems", Journal of Guidance, vol. 6, no. 4, pp. 302-310, 1983.

[35] Meirovitch, L.; Kwak, M.K. "Convergence of the Classical Rayleigh-Ritz Method and the Finite Element Method", vol. 28, no. 8, pp. 1509-1516, 1990.

[36] Naganathan, G.; Soni, A.H. "Coupling Effect of Kinematics and Flexibility in Manipulators", The International Journal of Robotics Research, vol. 6, no. 1, pp. 75-84, 1987.

[37]   Naganathan, G.; Soni, A.H. "Non-Linear Flexibility Studies for Spatial Manipulators", In: IEEE International Conference on Robotic and Automation, San Francisco, CA, pp. 373-378, 1986.

[38]   Nathan, P.J.; Singh, S.N. "Sliding Mode Control and Elastic Mode Stabilization of a Robotic Arm with Flexible Links", Transactions of the ASME, Journal of Dynamic Systems, Measurement and Control, vol. 113, pp. 669-676, 1991.

[39]   Nicosia, S.; Tomei, P. "Design of Global Tracking Controllers for Flexible-Joint Robots", Journal of Robotic Systems 10(6), pp. 835-846, 1993.

[40]   Nikolic, Ilija. "Determination of Elastodynamic Errors in Joints of Industrial Robots", Robotica, vol. 6, pp. 213-219, 1988.

[41]   Pfeiffer, F.; Gebler, B. "A Multistage Approach to the Dynamics and Control of Elastic Robots", Proceedings of the IEEE International Conference On The Robotic And Automation, Philadelphia, PA, pp.2-8, 1988.

[42]   Singer, N.C.; Seering, W.P. "Controlling Vibrations in Remote Manipulators" In: ASME Design Technology Conferences - The Design Automation Conference, vol. 2, pp. 11-15, 1987.

[43]   Spong, M.W.; Vidyasagar, M. "Robots Dynamics and Control", John Wiley & Sons, 1989.

[44]   Sunada, W.H. "Finite Element Dynamic Analysis of Flexible Spatial Mechanisms and Manipulators", Ph.D. Thesis, School of Engineering and Applied Science, University of California, Los Angeles, CA, 1980.

[45]   Sunada, W.H.; Dubowsky, S. "On the Dynamic Analysis and Behaviour of Industrial Robotic Manipulators with Elastic Members", Transactions of the ASME, Journal of Mechanics, Transmissions and Automation in Design, vol. 105, pp. 42-51, 1983.

[46]   Sunada, W.H.; Dubowsky, S. "The Application of Finite Element Methods of the Dynamic Analysis of Flexible Spatial and Co-Planar Linkage Systems", Transactions of the ASME, Journal of Mechanical Design, vol. 103, pp. 643-651, 1981.

[47]   Takegaki, M. and Arimoto, S. "A New Feedback Method for Dynamic Control of Manipulators", Transactions of the ASME, Journal of Dynamic Systems, Measurement and Control, vol. 102, pp. 119-125, 1981.

[48]   Thompson, B. S.; Gandhi, M.V. "The Finite Element Analysis of Mechanism Components Made From Fiber Reinforced Materials", In: Design Engineering Technical Conference, ASME paper 80-DE-63, 1981.

[49]   Tomei, P. "A Simple PD Controller for Robot with Elastic Joints "Transactions of the IEEE, IEEE Transactions on Automatic Control, vol. 36, no. 10, 1991.

[50]   Tzes, A.P.; Yurkovich, S. "A Frequency Domain Identification Scheme for Flexible Structure Control", Transactions of the ASME , Journal of Dynamic Systems Measurement and Control, vol. 112, pp. 427-434, 1990.

[51]   Tzou, H.S.; Wan, G.C. "Structural Dynamics and Distributed Visco-elastic Actuator-I", Components & Structures, vol. 35, No. 6, pp. 669-677, 1990.

[52]   Tzou, H.S.; Wan, G.C. "Distributed Structural Dynamics Control of Flexible Manipulators - II. Distributed Sensor and Active Electromechanical Actuator", Computers & Structures, Vol. 35, No. 6, pp. 679-687, 1990.

[53]   Utkin, V.I. "Variable Structure Systems with Sliding Modes", IEEE Transactions on Automatic Control, vol. AC-22, no. 2, pp. 212-222, 1977.

[54]   Wells, R.L.; Schueller, J.K.; Tlusty, J. "Feedforward and Feedback Control of a Flexible Robotic Arm", IEEE Control Systems Magazine, 1990.

[55]   Yang, G.-B.; Donath, M. "Dynamic Model of a One-Link Robot Manipulator with Both Structural and Joint Flexibility", In: Proceedings of 1988 IEEE International Conference on Robotics and Automation, Philadelphia, PA, 1988.

[56]   Yeung, K.S.; Chen, Y.P. "A New Controller Design for Manipulators Using the Theory of Variable Structure Systems", IEEE Transactions on Automatic Control, vol. 33, no. 2, 1988.

[57]   Young, K.-K.D. "Controller Design for Manipulator Using the Theory of Variable Structure Systems", Transactions of the IEEE, IEEE Transactions on Systems, Man, Cybernetics, vol. SMC-8, no. 2, pp. 101-109, 1978.

[58]   Yurkovich, S.; Pacheco, F.E.; Tzes, A.P. "On-line Frequency Domain Information for Control of a Flexible-Link Robot with Varying Payload", IEEE Transactions on Automatic Control, vol. 34, no. 12, pp. 1300-1304, 1989.

[59] Press, W.H.; Teukolsky, S.A.; Vetterling, W.T.; Flannery, B.P. "Numerical Recipes in FORTRAN: The Art of Scientific Computing", 2nd.ed., Cambridge Univ. Press, 1992.

[60] Sunnyside Systems ltd. "adt108 A/D TRAM USER'S MANUAL", Sunnyside Systems Ltd., 1991.

[61] INMOS "The Transputer Databook", 2nd. ed., INMOS, 1989.